Unravelling sediment transport driven by a multimodal wind-wave spectrum

FINAL REPORT
C. D. HOOGERVORST

Unraveling sediment transport driven by a multimodal wind-wave spectrum

By

Christiaan Dominique Hoogervorst

In partial fulfillment of the requirements for the degree of

Master of Science,
in Civil Engineering

At the Delft University of Technology,
to be defended publicly on Friday, June 24, 2022, at 13:00 hr.

Thesis committee:

Dr. J.A.Á. Antolínez	TU Delft
Prof. dr. i.r. S.G.J. Aarninkhof	TU Delft
Dr. M. Tissier	TU Delft
Dr. J. Portilla-Yandún	Escuela Politecnica Nacional, Equador

Preface

The last part of my Hydraulic Engineering track at the Civil Engineer faculty at TU is Delft is being completed through this thesis. The Coastal Engineering and Environmental Fluid mechanics specializations requirements are fulfilled and nicely represented in this thesis. The study was made during a period when the world was plagued by a corona pandemic, in which the work mainly took place at home due to lockdowns. The support from many people has contributed to successfully finishing this report, which I would like to thank.

First of all, I would like to thank my daily supervisor José A.Á. Antolínez, who gave me the opportunity to go into this topic and gave me various tools for my research, such as outcomes of an ESTELLA model, digital bathymetric nearshore data, organized weather data, and introduced me to different machine learning techniques. Our cooperation was enjoyable, and I look back on it with great pleasure.

The nearshore spectral data was simulated in SWAN by George Lavidas, which was essential for this study. Calculating, storing, and working with wave frequency spectral data with high resolution is very computationally demanding and time-consuming, so my thanks are great.

I would also like to thank Jesus Portilla-Yandún, who gave me the offer to perform an analysis on the nearshore data generated by George Lavidas. The formation of wave partitions and wave families on nearshore data was not yet performed, so we were curious about the results and the application possibilities. The explanation of the defined parameters was very useful and gave me some ideas tested in this research.

Furthermore, I have had pleasant talks about estimating sediment transport with Amin R. Zarifsanayei. It is a complicated topic, and it was beneficial to discuss ideas and problems I encountered with somebody with experience in multiple sediment transport concepts and models.

Last but not least, I would like to thank Stefan G.J. Aarninkhof and Marion F.S. Tissier, members of the assessment committee, who gave me nice feedback. During the progress meetings, I presented complex results at a fast pace. It was challenging to explain everything digitally, but the results and plans were pleasantly thought through every time.

Table of contents

Glossary

This chapter contains the relevant terminology in this study in alphabetical order.

Cluster:	A group of similar data.
Frequency-directional spectrum:	A discretized energy density spectrum that describes the energy within the specific frequency and directional bands.
Kmean clustering algorithm:	A machine learning technique that classifies data based on their similarity.
Principal Component Analysis (PCA):	A machine learning technique that defines new parameters, called Principal Components.
Maximum Dissimilarity Analysis (MDA):	A machine learning technique that is used to reduce the number of data points that show high similarity.
Multimodal wave spectrum:	A wave field in which at least two wave trains can be recognized.
Sea State:	A characteristic wave condition that is based on the energy density in the frequency-directional spectrum. It describes and relates wind, wave, and sediment transport.
Unimodal wave spectrum:	A wave field in which only one wave train occurs.
Wave family:	A specific part of the frequency-directional spectrum. It describes wave characteristics within its domain. A wave family is related to one or multiple wave systems.
Wave train:	An arbitrary group of coexisting waves that have a similar wave period and propagation direction.
Wave partition:	A part of an arbitrary wave frequency-directional spectrum. It is related to one wave train.
Wave system:	Consistently occurring wind-induced waves generated at a specific location and can be related to one or multiple specific forcing conditions.
Weather Type:	A characteristic wind condition, it describes the magnitude and positioning of high and low-pressure systems. It describes and relates wind, wave, and sediment transport.
Wave field:	A description of all the waves that are occurring, including their height, period, and propagation direction.
Wind field:	The direction and strength of the wind at all the locations within the considered spatial domain.

List of symbols

The used symbols in formulations and graphs are listed in this chapter.

a Reference height

$c(z)$ Sediment mass concentration at any depth

c_a Representative concentration at a specified reference height (a)

C   Covariance matrix

d Water depth

D   Wave train propagation direction, or bearing of the not most energetic wave train

D_0 Wave train propagation direction, or bearing of the most energetic wave train

D_s Diameter of suspended sediment

D_{50} Median grain size

D_{90} 90% cumulative mass passing diameter

E Energy inside the considered frequency-directional spectrum (domain)

f Wave frequency.

H_s Significant wave height

k_i Wave number, which could be related to their direction with the index "i"

L Wave length

λ Eigenvalue

MDA   Maximum Dissimilarity Analysis

m_n Moments of the wave frequency-directional spectrum.

m_0 The variance of the water surface elevation, the zero-moment of the wave spectrum

P Probability of occurrence of a specific condition

PC   Principal Component

ϕ Wave propagation direction or bearing

σ^2 The variance of the data

R_c Current related roughness height

R_w Wave related roughness height

s Standard deviation

V Eigenvector

X Standardized matrix

Abstract

Changing (wind) climate will significantly influence the magnitude, direction, and frequency of wave systems (Lobeto et al., 2021). The changes might significantly impact coastal wave-driven sediment transport processes and, consequently, the coastal evolution (Antolínez et al., 2018; Murray & Antolínez, 2019). Generalized wave parameters are commonly used in climate change assessments but significantly underestimate the future wind-driven changes in wave climate and sediment transport (Lobeto et al., 2021). Performing, analyzing, and comparing the impact of various climate scenarios on morphodynamics is complex and time-consuming (Ranasinghe, 2016; Zanifsanayei et al., 2022b). Uncertainties in (wind) climate and modeling affect the usability of sandy coastal maintenance, like (mega) nourishments, and thus the decision-making of long-term, multidecadal, coastal strategies (Ministerie van Verkeer en Waterstaat, 2020; Rijksoverheid, 2013), which uses the Building with Nature concept (de Vriend et al., 2015).

This thesis analyses the importance and application of considering multiple coexisting wave trains in sediment transport predictions. The wave trains at offshore and nearshore locations are analyzed by wave spectral partitions (Portilla at el., 2009). The temporal variability of consistently occurring wave trains can be analyzed through so-called wave families (Portilla et al., 2015). The wave partitions show that a unimodal wave spectrum occurs 35% of the time in front of the coast of the province of North Holland in the Netherlands. This means an error is introduced 65% of the time as unimodal spectra are assumed in traditional methods that use generalized wave parameters to estimate sediment transport. When the wave field is not unimodal, the angle between wave trains is considerable. Only 39% of the time is the angle between a wave train and the most energetic wave train smaller than 60°. For 43% of the time, the angle is between 60° and 120°. The remaining 17% are wave trains propagating in opposite directions. The difference in wave angle is half of the time larger than 50° when a threshold of one meter of deepwater significant wave height over the whole spectrum, defined by Holthuijsen (2007), is used.

Unsupervised machine learning techniques Principal Component Analysis, Maximum Dissimilarity Analysis, and the kmean clustering algorithm are used to group similar wave spectrums over time, spatially group wave families, analyze the wave climate's spatial-temporal variability, relate wave - and weather conditions, and assess their impact on wave-driven potential sediment transport. The Principal Component Analysis is used as a dimensionality reduction technique. This study shows the physical meaning of the Principal Components and their temporal variability in the wave frequency-directional spectrums, where Principal Components describe wave energy in each frequency-directional bin. The kmean clustering algorithm groups similar wave spectrums over time and gives insight into wave conditions, like calm and stormy conditions, called Sea States. The Maximum Dissimilarity Technique changes the focus between common conditions or extreme events. The wave partitions, wave families, and Principal Components give additional insight into the Sea States.

Potential sediment transport estimations are made by traditional methods that use a representative wave frequency and direction and through vectorizing and superpositioning the estimations by wave partitions and wave families. The outcomes show that it is challenging to predict sediment transport for multimodal wave conditions with state-of-the-art sediment transport formulations and models. The results show that the wave period significantly impacts sediment transport. The sediment transport for coexisting wave trains causes about 58% of the time more sediment transport than traditional methods. Here the not considered interaction between wave trains on bedload and sediment suspension will enhance sediment transport. Furthermore, the sediment transport estimations give insight into the wavefield and weather conditions that contribute most to the yearly wind-wave induced potential sediment transport caused by high energetic or consistently occurring conditions.

1 Introduction

1.1 Background

Global and regional climate changes affect sea level, waves, storm surges, and tides and threaten coastal areas worldwide (IPCC, n.d.; Toimil et al., 2020). Changing (wind) climate will significantly influence the magnitude, direction, and frequency of wave systems and their impacts (Lobeto et al., 2021). The changes might significantly impact coastal wave-driven sediment transport processes and, consequently, the coastal evolution (Antolínez et al., 2018; Murray & Antolínez, 2019).

In generalized wave parameters is the energy of all the waves is attributed to one representative wave component with its frequency and propagation direction (Holthuijsen, 2007). These parameters are currently commonly used in climate change assessments due to their extensive application in formulations that describe coastal processes and the vast storage capacity demand of the wave spectrum. However, these models significantly underestimate the future wind-driven changes in wave climate and their effect (Lobeto et al., 2021). From the significant wave height, mean wave period, and (mean) wave direction will probably two change for approximately 40% of the world's coast for high-emissions scenarios (Morim et al., 2019). Even if the generalized parameters are constant, the distribution of wave energy over the frequencies and directions impacts sediment transport (Divinsky & Kosyan, 2019). The error in wave energy can be reduced when the different groups of waves, or wave trains, are described separately (Portilla-Yandún et al., 2015) or if the wave frequency-directional spectrum is used (Lobeto et al., 2021). Another downside of models with generalized wave parameters is that they cannot distinguish wave systems, which are wave trains generated at different locations (Lobeto et al., 2021; Pérez et al., 2014). This distinction is necessary to analyze the forcing mechanisms (Portilla-Yandún et al., 2015).

A local study is required to assess the impact of climate change since site-specific geomorphic features and the coastline orientation and exposure have a high effect on coastal evolution. Here, stormy conditions, combined with sea-level rise, cause various temporal and spatial fluctuations on the shoreline. These fluctuations could lead to an unforeseen long-term shoreline evolution if these are not considered (Stive et al., 2002, Ranasinghe, 2016; Toimil et al., 2020). Since the future wave climate is highly uncertain (Morim et al., 2019), many simulations must be made to analyze possible effects on coastal evolution (Kroon et al., 2020). Performing, analyzing, and comparing the impact of various climate scenarios on morphodynamics is complex and time-consuming (Ranasinghe, 2016; Zanifsanayei et al., 2022b). Here, uncertainties in boundary conditions and from modeling should be considered to avoid overconfidence in the forecast (Zanifsanayei et al., 2022a).

A broad investigation of the impacts of climate change on various climate scenarios is valuable for regions with a low uncertainty tolerance in the long-term coastal management, like the Netherlands. Here, flood protection is designed for events that occur up to once in a hundred thousand years (Haasnoot et al., 2020). This coastal area protects the low-lying polders in the hinterland, where approximately nine million people live. The shore has a crucial role in sustaining an ecological system and accommodates many local functions, like housing and busyness. Tides, waves, and wind affect the coastal system and cause temporal - and spatial-dependent erosion or sedimentation that leads to coastal evolution. The water- and shore policy focuses on the Building with Nature concept, where natural processes in the sandy coastal maintenance, like nourishments, are used to make a flexible yet resilient shore (Ministerie van Verkeer en Waterstaat, 2020; Rijksoverheid, 2013). This concept can improve the ecosystem, offer additional functionalities, and often has a lower cost than traditional methods (de Vriend et al., 2015). One example of a successful design and implementation of Nature-based solutions is the Sand Motor (Stive et al., 2013). Uncertainties in (wind) climate and modeling affect the usability of these soft solutions and thus the decision-making of long-term, multidecadal, coastal strategies (Ministerie van Verkeer en Waterstaat, 2020; Rijksoverheid, 2013).

1.2 Problem statement

Simplifications of parameters in classic models lead to uncertainties in sediment transport fluxes and coastal evolution. These models use generalized wave parameters, like the (total) significant wave height, to obtain the main characteristics of the flow and wavefield, like bed shear stress and orbital velocities. In these models, the energy flux or sediment transport within the wave spectrum is attributed to only one direction and frequency, like the direction and frequency described with the significant wave height or the mean wave direction. This generalization is valid for narrow banded wave spectrums (Bosboom & Stive, 2015; Holthuijsen, 2007, XBeach, 2020) but not for multimodal wave spectrums where multiple wave trains, groups of waves with similar lengths and propagation direction, can be recognized (Portilla et al., 2009). The generalization of the wavefield causes misalignment in the resultant energy flux (Hegermiller et al., 2017; Lobeto et al., 2021) and sediment transport flux. The simplification of multimodal wave spectrums causes wave trains to be considered as one wave train (Bosboom & Stive, 2015). Both the error in direction and the frequency lead to a miscalculation of the sediment transport (van Rijn, n.d.).

Investigating how the full wavefield, or wave frequency-directional spectrum, can be related to sediment transport and the large-scale wind climate can lead to more robust and time-efficient modeling and more insight into the consequences of a changing (wind) climate on wave-climate and sediment transport.

1.3 Objective and scope

This research aims to analyze the importance and application of accounting for coexisting wave trains with different propagation directions and frequencies while estimating potential sediment transport rather than generalized wave parameters used by the traditional methods. Another objective is to analyze how the wind-generated waves can be related to the large-scale wind climate, the atmospheric synoptic situation, and if more robust parameters or methods can be related to the wave-driven sediment transport. These parameters are wave partitions and wave families defined by Portilla-Yandún et al. (2009, 2015). The new method uses the machine learning techniques Principal Component Analysis, Maximum Dissimilarity Analysis, and the kmean clustering algorithm to group similar wavefields. Challenges can be recognized in this study, and suggestions for further improvements can be made to make the models that predict sediment transport and coastal evolution more accurate and confined in the long run.

The main research questions will be:
1. **What is the relation between large-scale atmospheric patterns, the wind-wave frequency-directional spectrum, and potential sediment transport in the nearshore of the Netherlands?**
2. **Can wave partitions, wave families, groups of similar wave frequency-directional spectrums, and characteristic weather conditions be used to predict potential sediment transport by waves?"**

The importance and application of accounting for coexisting wind-driven groups of waves, or wave trains, on sediment transport will be analyzed in this study. It will not focus on accurately predicting potential sediment transport by waves. The sediment transport along the Dutch coast is driven by the peak tidal velocities, density – and wind-driven residual flows, and waves, according to Grasmeijer et al. (2022). The various forcing mechanism and sediment transport restricting mechanism, like armoring, makes it very complex to verify the outcomes of the wind-wave-driven sediment transport predictions with measurements.

The preference goes to relative contributions rather than absolute quantifications when comparing the potential sediment transport since uncertainties arise for state-of-the-art methods due to their assumptions and parameterization.

This research focuses only on currently existing weather conditions and thus not on hypothetical situations that could occur. The expectation is that including these non-existing conditions would require large-scale high-resolution hydrodynamic modeling of nearshore waves, which is highly computational demanding and time-consuming, or a method that extrapolates trends, which might be less robust since it cannot account for changes in the system that affect the trend itself.

For this research is assumed that both hydrodynamic and (generalized) sediment transport models are accurate enough to assess trends in sediment transport and that there is no uncertainty arising from the lack of knowledge, which might not be the case.

1.4 Methodology

This subchapter elaborates on how the two main research questions in chapter 1.3 are answered. The first main research question will be answered by splitting it into the sub-questions: "What is the relation between large-scale atmospheric patterns and the wind-wave frequency-directional spectrum" and "What is the relation between the wave frequency-directional spectrum and potential sediment transport?". The second main research question will be answered by analyzing the applicability of the used parameters and techniques in this study.

The steps to answer the two subquestions and the main research questions are explained in this section. The methodology is simplified in Figure 1. Here each block consists of one or more steps that affect each other. All the steps within the methodology are depicted in Figure 2.
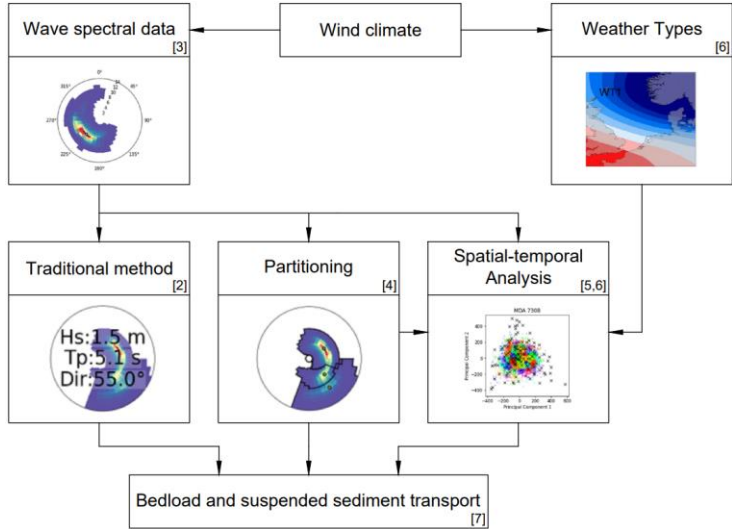
Figure 1: Simplified methodology, each block contains one or multiple steps. The numbers refer to chapters that elaborate on the content of each block.

The starting point of this study is that the wind climate is the driving mechanism for the wave field and can be simplified to a number of characteristic weather conditions called Weather Types. The wind also generates waves. The wave field is analyzed through three different techniques in this study. The traditional method describes the frequency-directional wave spectrum with one representative wave height, a peak period, and a peak direction. Secondly, a technique that uses the energy peak in the wave spectrum, which is related to each wave train, to partition the wave spectrum. Here temporal statistics are used to form so-called wave families that describe wave trains propagating in specific directions and within certain frequency bounds. A third more complex

technique uses various machine learning techniques in a spatial-temporal analysis wherein similar wavefields are grouped to the so-called Sea States. These Sea States describe various calm and high energetic wave conditions. This analysis, combined with results of wave partitions and wave families, gives a broad overview of wave statistics, like the number of coexisting wave trains, main wave propagation direction, and relevant wave generation areas.

A relation between Sea States and Weather types is expected since they are both based on wind data. This relation and the spatial-temporal analysis are used to answer the first sub research question, which focuses on the relation between wind and the wave frequency-directional spectrum.

The last block in this research analyzes the potential impact of changing the wave field description between one representative wave, wave partitions, and wave families on sediment transport. Furthermore, the dominant Sea States and Weather Types in regard to potential wave-driven sediment transport are analyzed. Comparing the outcomes of the various wave field descriptions gives insight into the relation between the wave frequency-directional spectrum and potential sediment transport, the second sub research question. The similarities in potential sediment transport between Sea States and Weather Types are used to substantiate the relation between Sea States and Weather Types.
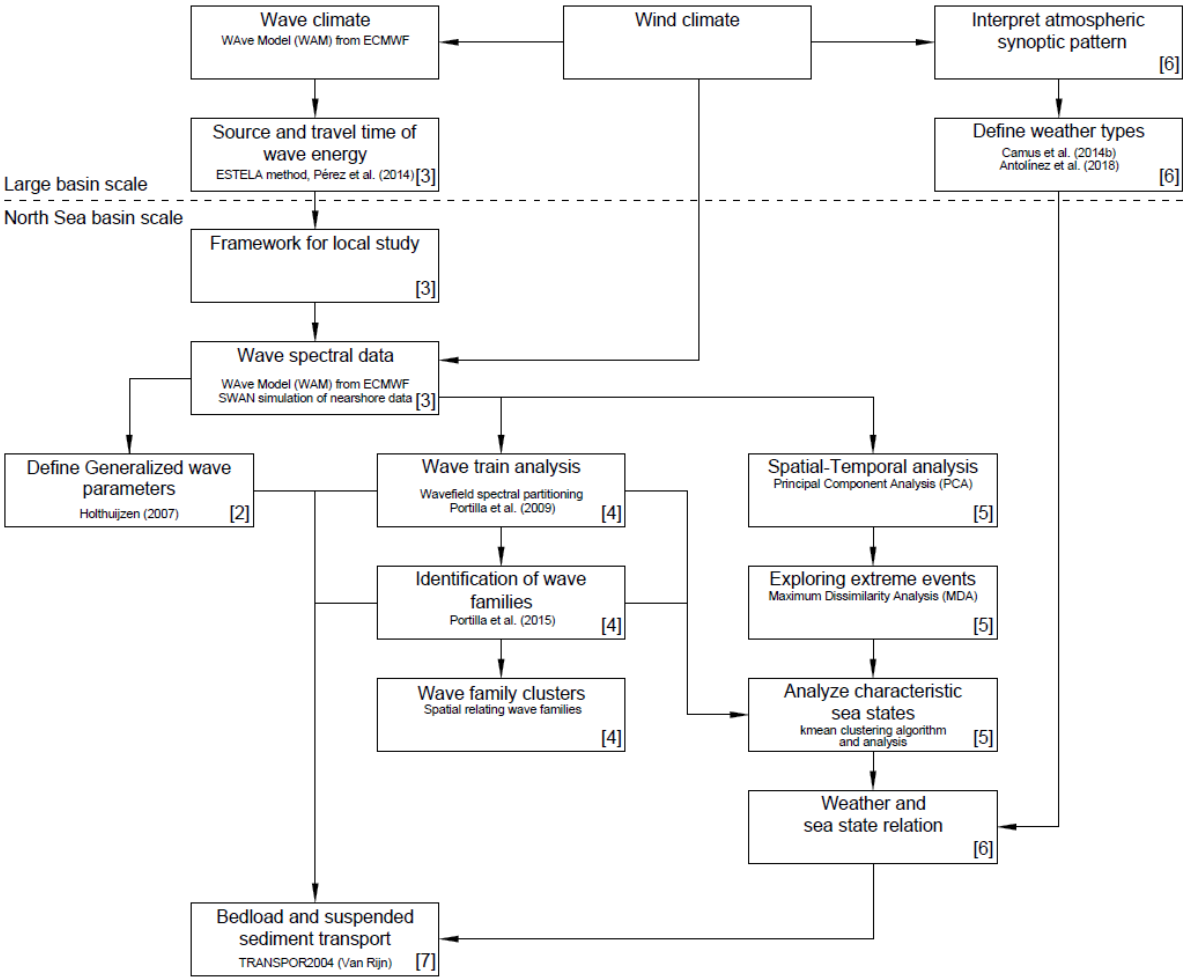

Figure 2: A schematic overview of the steps in the research, where a distinction is made between the large basin scale and the North Sea basin scale. The numbers in brackets indicate the chapter that elaborates on the corresponding part of the research.

1.5 Report outline

In this study are complex techniques used. The essence of chapters three and beyond are in plain language captured in an orientating introduction and concluding subchapter. These introductions elaborate on the content of that chapter compared to the whole study, the goal, approach, and activities in the upcoming chapter, and the new relevant terminology. The concluding subchapters elaborate on the research question-related discussions, conclusions, and sometimes recommendations.

The content of each chapter is depicted in Figure 1 and Figure 2. Here is visible that the next chapter will elaborate on the state-of-the-art methods and knowledge that are used as a starting point in this research. The third chapter elaborates on the creation of a framework in which the spectral data will be used in this research. This framework is based on temporal and spatial wave energy fluxes, derived by the ESTELA method. The fourth chapter elaborates on the spatial and temporal wavefield statistics, like the wave train propagation directions, the number of coexisting wave trains, and wave generation areas. In the fifth chapter, the temporal and spatial variability of the wavefield are considered together in a spatial-temporal analysis, where characteristic wavefields are described in Sea States. Here various techniques are used to get insight into the main wave propagation direction, wave energy fluxes, and the other wave train statistics. The sixth chapter elaborates on the weather, where characteristic conditions are expressed as Weather Types. Here the correlation between Sea States and Weather Types is analyzed. The last chapter elaborates on estimating sediment transport by wave partition and wave families in relation to traditional methods that use one representative significant wave. Here the sediment transport by Sea States and Weather Types is analyzed for two locations, one near the coastal foundation and one closer to the shoreline.

2 Theoretical background

This chapter elaborates on the state-of-the-art knowledge, with its limitations, of wind-wave-related hydrodynamics and sediment transport, applied statistical and machine learning techniques, and essential facts about sediment transport along the Dutch shore.

2.1 Coastal hydrodynamics

Changes in the water motions may significantly impact the sediment transport directions and rates and thus on the coastal evolution. Understanding the mechanism that affects the water motions is essential for accurate sediment transport estimations since the relation between hydrodynamics and sediment transport is highly non-linear (Ostrowski, 2018).

According to the relevance of different physical processes, the coastal zone is often divided into three zones. The first zone is the dune and beach zone, dominated by wind and wave forces. The surf zone is dominated by breaking waves and wave-induced currents. The third zone is the middle and lower shoreface, dominated by non-breaking waves and currents due to the tide, density gradients, and momentum exchange with the wind (Van Rijn, 2013).

The water depth can be classified into deep, intermediate, and shallow water. In deep water, the propagation speed of individual waves, the phase velocity, is unaffected by the seabed. The deep water phase velocity depends only on the wavelength, which the wave frequency affects. As a result, longer waves propagate faster than shorter waves, resulting in the separation of the different harmonic components, known as frequency dispersion. In the intermediate water depth, the bottom friction causes a decrease in the phase velocity, which induces various processes, like shoaling, refraction, wave breaking, and various non-linear interactions, with an exchange of energy, between waves. In shallow water, the wave celerity is independent of the wave period, resulting in non-dispersive waves (Bosboom & Stive, 2015; Cavaleri et al., 2018; van Rijn, 2013).

The ratio of water depth (d) to wave length (L) is used to make a distinction in the classification. The wavelength can by means of the dispersion relation be determined by the wave period (T) and water depth. The ratio for the lower boundary of deep water is 0.5 and is based on the depth reach of orbital motions. The upper limit of the water depth to wave length ratio in shallow water is 0.05 (Holthuijsen, 2007).

An overview of the water depth classifications for a combination of various water depths and wave periods is depicted in Figure 3. This figure shows that the depth classification barely changes for depths smaller than 20 meters and that the water depth can be considered deep when the wave period is smaller than approximately 7 seconds.
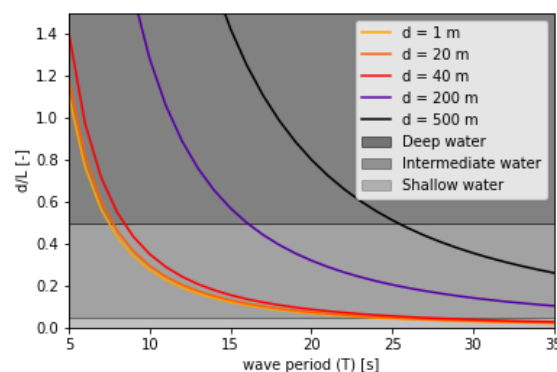

Figure 3: Classification of deep, intermediate, and shallow water for a range of water depths (d) and wave periods (T) according to the linear wave theory, described in Holthuizen (2007).

2.2 Parameterization of the wavefield

There are different parameters to describe the wavefield, the important parameters for this research are described below.

2.2.1 Commonly used generalized wave parameters

In commonly used methods, the sea surface elevation is approximated with a normal (or gaussian) distribution, with a mean level elevation of zero. Here the variance density spectrum can be used to estimate the wave height and representative wave period. For these estimations, the characteristics of the spectrum are expressed in terms of moments of the spectrum, which are defined as: (Holthuijsen, 2007).

$$m_n = \int_0^\infty f^n E(f) df \qquad (1)$$

The significant wave height is one of the most commonly used wave parameters, which describes the wave height wherein one-third of the wave is higher than this wave height. The probability that a wave height in deep water is larger than a particular value can be related to a Rayleigh distribution and is only dependent on the variance of the water surface elevation (m_0), leading formula 2 (Holthuijsen, 2007).

$$H_{m0} = H_s \approx 4\sqrt{m_0} = 4 \iint (df\, d\phi)^{0.5} \qquad (2)$$

The peak period (T_P) is the period where the energy in the spectrum is the largest and therefore related to the largest waves.

The assumption of normal distribution of water surface elavation is invalid for multimodal wave conditions and in shallow water, where the waves are non-linear. Therefore, the deep water estimation of the significant wave height and the wave periods are not accurate in these conditions (Holthuijsen, 2007).

2.2.2 Wave frequency-directional spectrum

The wavefield in open water consists of waves with different frequencies that can propagate in any direction. The energy of these waves can be described in a frequency-directional spectrum $E(f, \phi)$, which is also known as a "two-dimensional spectrum" and can be expressed through a "wave-number frequency space" $E(k_x, k_y, f)$, wherein the length and angle of the waves are expressed in two orthogonal wave numbers (Leckler et al., 2015). Compared to the significant wave height, the biggest advantage of the frequency directional spectrum is that it allows analyzing the various wave components and their characteristics (Wendell, 1969).

One exemplary frequency-directional spectrum is shown in Figure 4. In this discretized spectrum, the colors indicate the energy in each frequency-directional bin, as explained in the color bar. No wave energy is indicated with white. The propagation direction of the waves is described with the labels on the outer circle and is equal to the orientation of its bin to the center of the graph. The radial axis of the plot indicates the wave period, with short-perioded waves in the center and long-period waves in the outer edges. The periods vary from 0 to 25 seconds in this case. The radial axis is sometimes capped at 15 seconds in this report.

The wavefield shown in Figure 4 shows a unimodal wave spectrum in which most waves propagate in a direction between 90° and 225° and have a period of up to 20 seconds. The red spot on the graph shows the energy peak in the wave spectrum, indicating that the most energetic waves are within the boundaries of these frequency-directional bins. Theses bins have a similar wave period and direction and can therefore be interpreted as a wave train.
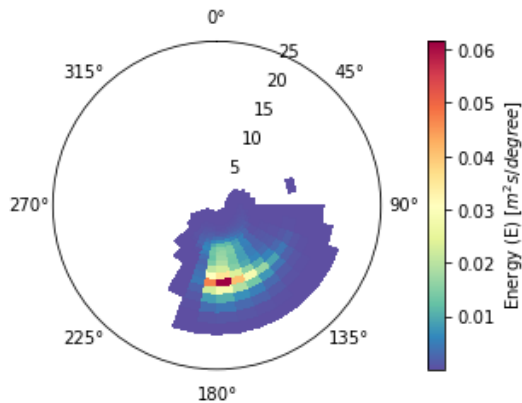

Figure 4: Frequency-directional spectrum wave spectrum, showing waves propagating easterly to south-westerly. The energy peak indicates that the largest waves are propagating south (175°) and have a period of around 12 seconds.
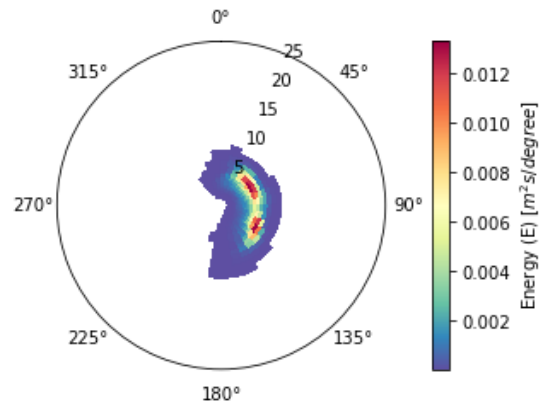
Figure 5: Frequency-directional spectrum wave spectrum showing a bimodal wave spectrum in which two wave trains are recognizable in red.

This wavefield would traditionally have been characterized by a significant wave height of 1.4 m. Based on the location of the energy peak, this significant wave has a peak period (T_P) of 12 seconds and a wave propagation direction of 175°. This means that the energy of all the other frequency-directional bins is attributed to the bin with the most energy.

Figure 5 shows a wave spectrum with two energy peaks and thus two wave trains. The spectrum can be described as a multimodal or bimodal wave spectrum. Although the wave period for both wave trains is approximately 5 seconds, the propagation direction for both wave trains is different. One of the waves propagates in the direction of 55° while the other propagates in the direction of 125°. If the wave spectrum is described with a significant wave height, it would have a significant wave height of 1.3 m with a peak period of 5 seconds and a propagation direction of 55°. All the energy is thus contributed to the wave train with the largest energy peak when there are two or more wave trains. The effect of the other wave train is thereby not accounted for in the correct direction. In this case, all the energy of the south-easterly propagating waves is contributed to the north-easterly propagating waves.

Ideally, every occurring wave frequency and direction is used to describe the wave field and assess their impacts. Unfortunately, this is not possible with state-of-the-art models. One possible way to analyze the wave trains separately is by partitioning the wave spectrum, as described in the following section.

2.2.3 Partitioning of the wave frequency-directional spectrum

The wavefield can consist of multiple wave trains with different propagation directions, wave periods, or both. These wave trains can be recognized by their energy peaks in the wave frequency-directional spectrum.

The different wave trains can be characterized by partitioning the frequency-directional spectrum based on the energy peaks in this spectrum, as described in Portilla-Yandún et al. (2015). After partitioning the spectrum, each partition consists of several frequency-directional bins, described by a wave partition matrix. The energy of each wave train, or partition, is the amount of energy within the wave partition's boundaries. The partitions are ordered by their energy, in which the first partition contains the most energy (Portilla-Yandún et al., 2015).

Each (wave) partition can be represented by a significant wave height and corresponding propagation direction. The significant wave height can be determined by applying the traditional formulation to the energy of the wave partitions. The corresponding peak direction and wave period are related to the bin that contains the most energy within the edges of the partition (Portilla-Yandún et al.., 2015).

The energy of an arbitrary discretized frequency-directional spectrum is shown in Figure 6 as a matrix and visualized in Figure 7. Here, four distinct areas with more energy can be recognized, which implies four partitions. However, the largest area will be split in two since the field describing the 23rd direction (225°) and the 23rd frequency (0.25 Hz) contains more energy than the surrounding fields. Therefore, five partitions can describe the spectrum, resulting in a partition matrix shown in Figure 8 and Figure 9.
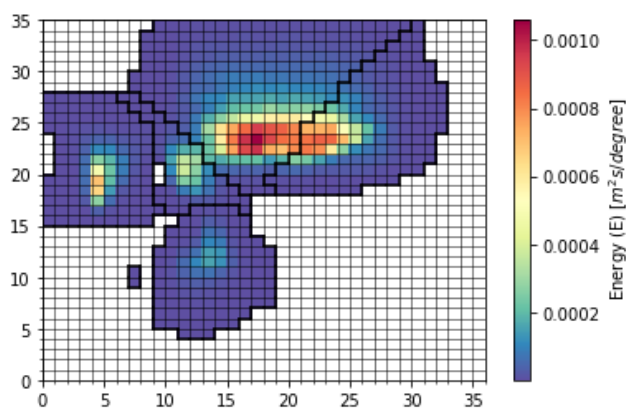
Figure 6: Matrix of discretized wave frequency-directional spectrum, with 36 directions (horizontal) and 35 periods (vertical), showing energy inside each bin, where white bins do not contain any energy. Boundaries of the wave partitions are indicated with black lines.

Figure 7: Visualization of the frequency directional spectrum of Figure 6, capped at 15 seconds, with wave partitions boundaries and energy peaks. The colors of the peaks refer to partition numbers visualized in Figure 9.

Figure 8: Wave partition matrix, showing the wave partition number for each bin.

Figure 9: Visualization of the partition matrix, capped at 15 seconds. Bins that contain no energy are white.

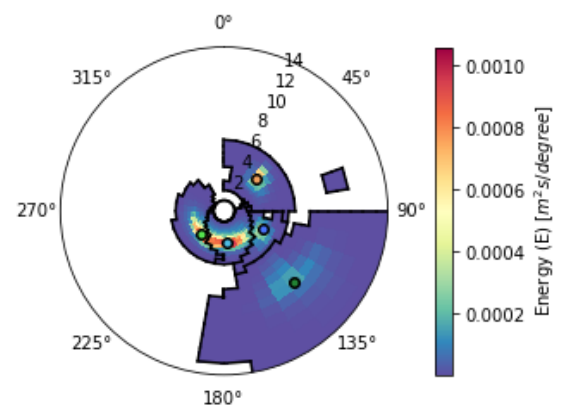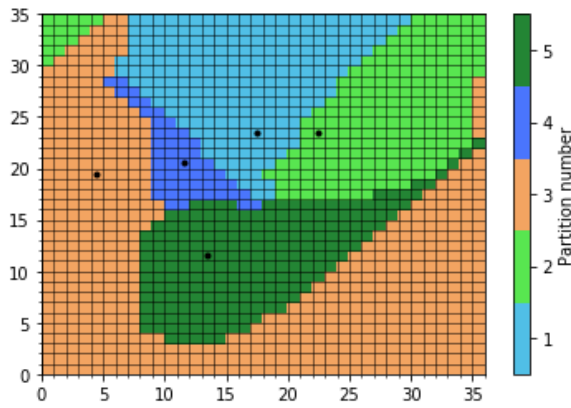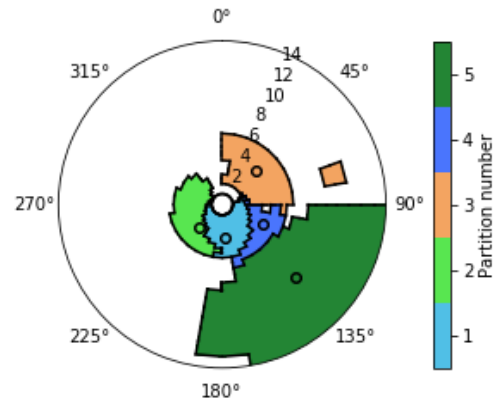Temporal analysis of the energy peaks in the wavefield can be used to identify long-term individual wave systems, described by wave families, which can be related to a specific generating mechanism. The temporal analysis of a time series of wave spectra counts how many times an energy peak is located at a particular bin inside the discretized frequency-directional spectrum (Portilla-Yandún et al., 2015). One exemplary matrix is shown in Figure 10. Here, frequently occurring combinations of frequency and direction of the peaks result in relatively large values.

The extremes in the counting are used to split the frequency-directional spectrum into wave families (Portilla-Yandún et al., 2015). Figure 11 supports the division of the wave families since it is visible that the peaks of the counting are centered in the wave families. The created matrix describing the wave families is shown in Figure 12 and visualized in Figure 13.

The wave generation area for each wave family can be determined by calculating the traveled path of the waves, called wave ray. This area is for each wave family different and limited since the waves inside a wave family are propagating in, more or less, a constant direction, as shown in Figure 11. The waves within wave family 2, the green arched area in Figure 13, generally propagate towards the south, the direction of 180°, so they approach from the north.
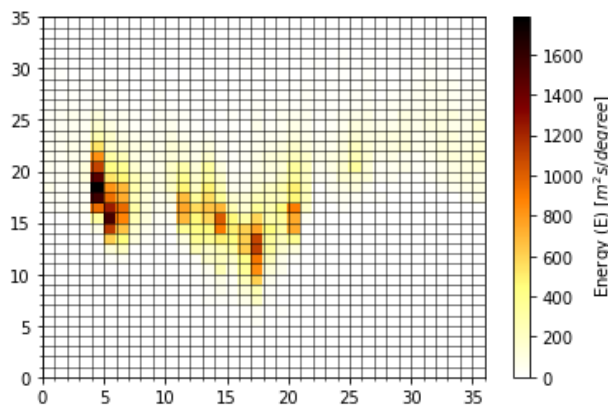

Figure 10: Counting how many times the energy peaks of the partitions have fallen at a particular bin.
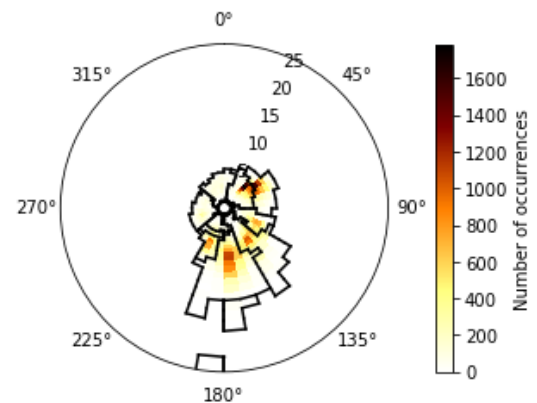

Figure 11: Visualization of the counting of the energy peaks and the boundaries it creates for the wave families, shown in Figure 13.
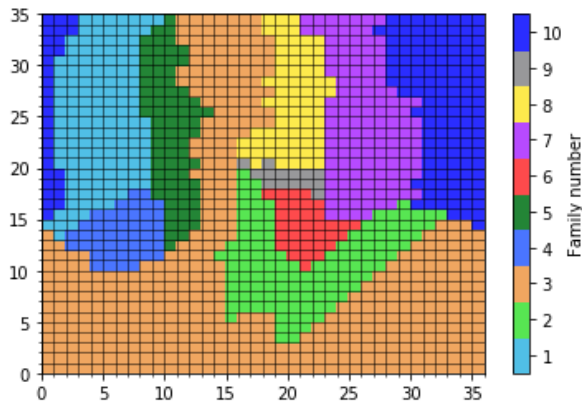
Figure 12: Wave family matrix, showing the wave family number for each bin.
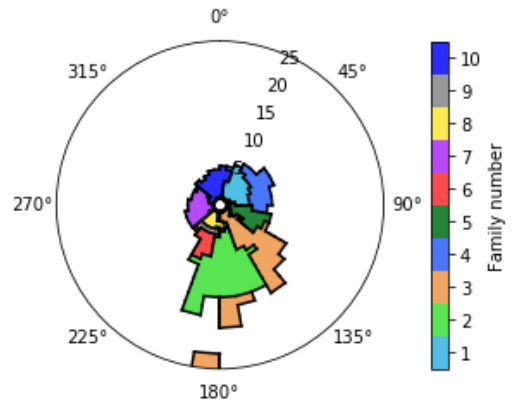

Figure 13: Visualization of the wave family matrix. Bins that never had an energy peak of a partition are colored white.

Wave families make it possible to do extreme value analysis, in which it is crucial to have the same forcing. This cannot be guaranteed if integrated parameters over the whole frequency-directional spectrum are used. The time series of the analysis should cover at least four years to be representative of multiple decennia (Portilla-Yandún et al. , 2015).

The temporal properties of the wave families can be determined by the locations of the energy peaks of the partitions. For each wave spectrum, the wave partition contributes all its energy to the wave family that is identified at its energy peak location. This energy can be used to estimate the significant wave height, following the traditional method by formula 2. When multiple families are determined, it is likely that some of the wave families have energy, even from two or more wave partitions, while other wave families do not contain any energy. When two or more partitions contribute energy to the same family, the peak direction of the significant wave of the wave family is located at the energy peak of the partition that contains the most energy (Portilla-Yandún et al. , 2015).

Several aspects concerning the realization of the wave partitions and families should be considered during the analysis of the wave partitions and wave families. So can multiple wave families be related to the same wave generation process, for example, if the wave characteristics are related to the wind conditions at a specific location sea, and some conditions occur more than others. These wave families may be merged manually for further analysis. Another aspect is the assumption that no more than ten wave partitions or families occur at any time step. If this occurs, processes will redistribute the partitions or families to reduce the number to 10. For extreme value analysis, the energy of a partition can be divided into two families, for example, when there are no distinct energy peaks in the wave spectrum. This situation may occur when two or more different forcing mechanisms have their energy peak on the same frequency-directional bin or when one energy peak is significantly smaller, resulting in a monotonical decrease of energy from the energy peak.

2.3 Wind-wave climate modeling

The wind-generated waves can be locally generated or arrive from adjacent waters. The locally wind-generated waves usually have a relatively high frequency and wave periods under 10 seconds. These short waves generate and interact with gravity waves arriving from adjacent seas (Jiang, 2022) or reflected from shores (A. J. Reniers et al., 2021). This section elaborates on wind-wave generation and propagation.

2.3.1 Climate modeling

Uncertainties in (wind) climate change are described in various Global Climate Models, where each model considers a different future scenario. Coastal strategies worldwide are focused on protecting or adapting coastal areas for hydrodynamic changes due to climate change and consider the uncertainties that the various Global Climate Models induce (Ranasinghe, 2016).

Changes in (wind) climate can affect both the direction and height of waves of the general wave climate, the storm wave characteristics, and the storm surges. These changes can induce significant changes in coastal wave-driven processes and their associated hazards. However, it is difficult to accurately describe the wave characteristics for each future (wind) climate due to large variations in the outcomes of different methodologies. The wave climate is often described with parameters like the significant wave height, mean wave period, and (mean) wave direction. At least two of these variables will change for approximately 40% of the world's coast for high emission scenarios (Morim et al., 2019). Even if the generalized parameters are kept constant, the distribution of wave energy of the frequencies and directions impacts sediment transport and thus coastal evolution (Divinsky & Kosyan, 2019).

The coastal impact due to (wind) climate change should be modeled for each climate model. However, the climate models have a spatial resolution of about 200 km, while national assessments of a changing climate are usually made on resolutions smaller than 10 kilometers. Therefore dynamically or statically downscaling the various climate models is required (Ranasinghe, 2016).

The difference between dynamical approaches and statistical approaches lies in the input of the models. Dynamical approaches are based on models that use the outcome of other models as boundary conditions, such as surface winds. Statistical approaches are based on measurements to obtain empirical/quantitative relationships between the input variables, known as predictor(s), and the output variable, known as the predictand. Biases due to measurement errors can significantly be reduced by standardizing the predictor quantities (Wang et al., 2009).

2.3.2 Wave generation by wind shear

Wind-generated waves are formed when air flows over a water surface. The surface stresses lead to a transfer of energy toward the water. Although different methods explain this energy transfer, the main result is that a steady wind leads to an exponential growth of waves over time until a fully developed sea condition is reached. Here the more efficient energy transfer from the wind to the larger waves balances the breaking of waves, called white capping (Miles, 1957, 1962).

The wind-induced wave height, period, and propagation direction depend on the characteristics of the wind field, the length of water over which the wind blows, called fetch, and the local water depth (Bosboom & Stive, 2015). The direction of the wind can be related to the isobars of air pressure, and the wind speeds are proportional to the pressure gradient (Camus et al., 2014a). Therefore, the sea-level pressure fields and their gradients can be used as predictands for estimating the (significant) wave height (Wang et al., 2009). These sea-level pressure gradients are depended on the positioning of the high- and low-pressure systems with their magnitude, also known as an atmospheric synoptic pattern.

Waves that are generated from different areas can reach a specific location at the same time. The ESTELA method can quickly provide insight into the area that can influence the wave spectrum at an particular location. For this, the assumptión is made that the wave's travel path is unaffected by the sea bottom so that the wave travels in a straight line from the source, along great circle paths around the globe. The area of influence is further limited by landmasses that block the traveling waves. Here the effect of waves reaching the sheltered area by dispersion, refraction, or deflection due to Coriolis is neglected. The ESTELA method uses the source location and the wave energy travel time, which propagates with the wave group velocity, to estimate the reachable area given a defined time frame. The energy losses due to viscous dissipation and radiation are considered in this process and can be used to obtain insight into the spatial development of the wave height (Pérez et al., 2014).

Weather types

The positioning of the high- and low-pressure systems leads to waves generated at specific locations. Due to the wave (group) travel speed, a spatial and temporal correlation exists between the local wave climate and the atmospheric circulation, both locally and on a basin-scale (Espejo et al., 2014).

Camus et al. (2014b) use this correlation in a statistical downscaling framework, with sea level pressure fields and the squared gradients of this field as predictors for the wave climate. For the classification of the weather types, three different machine learnings techniques are applied, namely Principal Component Analysis (PCA), a clustering technique k-means, and post organization in which a self-organizing map is formed by characterizing the clusters. The post organization eases the visualization and classification for further analysis. Chapter 2.6.2 elaborates on the Principal Component Analysis and the clustering technique kmean, which are used in this study.

2.3.3 From offshore wind-wave generation to a nearshore wave state.

As described in the previous sections, wind can generate waves that travel from their generation area toward the shore. These traveling waves are affected by depth-induced processes and interactions with coexisting waves that can be wind-generated or reflected from shorelines as long waves. Several studies have been conducted to investigate and quantify this process.

Portilla-Yandún et al. (2015) describe how storms at discrete regions can generate waves with a defined range in wave frequency and propagation direction. The temporal variability of these specific long-term wave systems can be derived by using energy peaks in the wave spectrum and described through so-called wave families by a significant wave height or spectral energy distribution, as explained in chapter 2.2.3. Portilla-Yandún (2018) applies this method to identify wave families globally from the ERA-Interim database so that spectral characteristics of the wave data can be derived for each location. GLOSWAC (n.d.) publishes the outcomes through an online database.

Hegermiller (2016) defines a method to use an atmospheric predictor to obtain a local wave climate and then define the wave families by following Portilla-Yandún et al. (2015). These wave families are then related to temporal atmospheric conditions in distant regions by analyzing the wave travel time. Therefore, this method is applicable not only for analyzing long-term wave systems but also for determining the wave climates in daily situations for multimodal wave spectrums.

The wave spectrum can be related to the energy spectrum, and the movement of waves can be related to energy fluxes. As a result, the change in wave state due to energy dissipation and radiation of energy can be taken into account when the wave travels from its source point (Pérez et al., 2014). So the wave energy at each location can be determined if the wave frequencies and propagation directions are known, for example, by measurements from buoys. (Cavaleri et al., 2018).

The relation between a local wave climate and the atmospheric conditions at relevant wave generation areas has been used to make predictions of nearshore wave spectrums based on the atmospheric conditions at adjacent waters in Hegermiller et al. (2017). The relation of the deep water wave field to the nearshore wave field has been achieved by creating a look-up table. The data inside this table has been generated by making a numerical simulation in SWASH for each offshore spectrum. So, if the offshore atmospheric conditions are known, an estimate can be made of the offshore spectrum, which then will be used to predict the nearshore wave field. The effect of bathymetric features on wave propagation and height can be considered in the generation of this nearshore wave field. However, since the offshore spectrum is based on offshore atmospheric conditions, the locally generated waves and their effect are not considered in this framework.

2.4 Sediment transport mechanism

This chapter elaborates on possible sediment transport mechanisms and strategies to determine sediment transport. In general, more sophisticated approaches are required if the spatial or temporal scale of interest decreases. So can large-scale processes be described with relatively simple formulations and generalized parameters, while smaller-scale processes need to be described in more detail. The values of (generalized) parameters may vary over time and space.

The sediment transport can be divided into suspended sediment transport, where hydrodynamics mainly suspend the sediment transport, and bed load, where interactions between soil particles and the bed are important. The bedload is related to the average flow velocity near the bed. However, the distinction between bedload and suspended load may vary for different studies since they use different approaches. The suspended load can be subdivided into current-related and wave-related components, with their corresponding direction (van Rijn, 2007a, 2007b, 2007c, n.d.).

2.4.1 Cross-shore varying processes

The different hydrodynamic processes that occur in the beach profile can be used to make a distinction between the various zones in which different sediment transport mechanisms play a role. At the lower shoreface, the sediment transport is driven by wave orbital motion, tide-induced currents, and residual currents induced by wind, density gradients, and waves (Deltares, 2019a; van Rijn, n.d.; van Rijn, 2013). In the upper shoreface, the wave skewness and breaking induced turbulence and currents should also be considered (Renier et al., 2013). Stratification and Eckman currents may affect the currents by upwelling and downwelling (Bosboom & Stive, 2015). Also, the tides and the freshwater output of rivers affect the velocity field, shear stresses, and sediment transport, both cross-shore and alongshore (Hop, 2017).

The sediment transport can be divided into suspended sediment transport, where hydrodynamics mainly suspend the sediment transport, and bed load, where interactions between soil particles and the bed are important. The bedload is related to the average flow velocity near the bed and is called a "sheet flow" when an entire layer of sediment moves on a plane bed. However, the distinction between bedload and suspended load may vary for different studies since they use different approaches. The suspended load can be subdivided into current-related and wave-related components, with their corresponding direction. Since this direction varies over the depth, the sediment transport directions may vary over the depth as well (van Rijn, 2007a, 2007b, 2007c, n.d.).

For non-breaking waves, the flow velocity due to the orbital motion of the wavefield can be an adequate starting point for estimating sediment transport. The series of successive waves can keep particles suspended. The bathymetric features, like ripples, affect the suspension of sediment and the waves itself impact the bathymetry itself (Atkins, 2005; Xu, 1998). The sediment transport under non-breaking waves is highly affected by the wave shape. An increase in skewness or asymmetry will lead to higher sediment concentrations (Bosboom & Stive, 2015). For broad (or multimodal) wave

spectra, all the wave frequencies in the spectrum should be considered to estimate sediment transport since the energy at the peak frequency is insufficient to estimate sediment transport. In this estimation, the interaction between sediment transport and all the wave frequencies should be considered (Podymov et al., 2011; Shringarpure et al., 2014).

Sediment transport over the bed occurs when the bed shear stress exceeds a critical value related to the grain's stability. The bedload is mainly related to bed shear stress caused by flow over the bed and barely due to turbulent motions, which are limited due to the presence of the bed. Both waves and currents cause the flow over the bed (Bosboom & Stive, 2015; Grüne et al., 2007). The bedload is affected by the flow over the bed, the grain sizes, the bottom slope, and the wave propagation direction. The flow under asymmetric and skewed waves is different in the onshore and offshore directions. Nearshore waves have a positive skewness, so a narrow crest and wide through, and asymmetry, resulting in a forward-leaning shape with a steep frontal face. The skewness causes a faster development of the onshore velocities, a thinner boundary layer, and a larger bed shear stress that causes sediment to move into the wave propagation direction (Gonzalez-Rodriguez & Madsen, 2007).

Wave refraction in an undulating coast causes wave stretching and a reduction of wave height, especially for waves that approach from deep water with an angle larger than circa 45 degrees. Due to this process, there is no relation between wave breaking height and wave breaking angle and, consequently, no constant wave breaking height along the coast (Ashton & Murray, 2006, Lim et al., 2020). Here turbulent kinetic energy can improve the sediment concentrations estimations when both the sources due to the wave orbital motion, the bed shear, and the surface-generated breaking are included. One new option is the Froud-scaled turbulent kinetic energy (Lim et al., 2020). Further research in sediment transport induced by breaking waves is required. Here improved insight into the hydrodynamics and measurement data could improve and validate various studies that have tried to link suspended sediment transport to turbulent kinetic energy, breaking wave shapes, and turbulent motions themselves (van der Zanden et al., 2017a, 2017b).

The temporal and spatial variance in grain size distribution affects the morphology and the shore dynamics. Here the wave breaking induced turbulence may result in a courser bed at the location of the wave breaking since the finer material is brought more onshore and offshore. So the wave height, for example, affects the local distribution of grain sizes (Reniers et al., 2013; Richmond & Sallenger, 1984), and this distribution affects the coastal evolution and, thereby, the required nourishments to prevent coastal erosion if it occurs (de Schipper et al., 2021).

2.4.2 Alongshore sediment transport
The shoreline evolution can be predicted due to the relation between climate and wave characteristics. Various mechanisms can be taken into account that affects, whether or not periodically, the sediment transport.

The coastline evolution is highly dependent on the incident wave angle. If the angle of waves is smaller than 45°, it causes an erosion of a perturbation since the relative angle increases at the undulation, which is in contrast to waves that have an angle larger than 45°. Here, the increase in relative wave angle decreases the sediment transport capacity and, consequently, sediment deposition (Ashton & Murray, 2006).

Anderson et al. (2018) use a relatively simple one-dimensional model to predict coastal changes based on gradients in longshore sediment transport by the height and angle of breaking waves. These parameters are determined for each wave generation area and are based on the offshore direction of the significant wave height. From this study could be concluded which wave-generation areas are the main contributor to the coastal development that was measured, taking into account

the effect of El Nino. For this study, climate indices are used to capture specific atmospheric conditions related to individual meteorologic events or large-scale climate variability.

Coastal development can also be predicted by different downscaling techniques, as described by Antolínez et al. (2018). These techniques determine the contribution to alongshore sediment transport for different sea states. The wave field, described by a significant wave height, is based on the temporal evolution of low and high-pressure systems at the generation area and the changes of this field during wave propagation, which include external forcing and the travel time.

2.5 Numerical modeling
This section elaborates on the numerical modeling of wave fields and sediment transport.

2.5.1 Phase-averaged and phase-resolving numerical models of wave fields
Phase-averaged and phase-resolving numerical models can simulate wave fields based on physical processes. The phase-averaged model uses the wave energy density, which is feasible for wind-wave prediction in the open sea. The phase resolving model considers the wave phase and amplitude, which is computationally demanding and, thereby, limits the computational domain (Eldeberky & Battjes, 1996). The phase-decoupled models can be combined with processes describing refraction, shoaling, wave generation and dissipation, and wave-wave interactions (L. Holthuijsen et al., 2003).

2.5.2 Sediment transport formulation TRANSPOR2004 (Van Rijn)
The transport model TRANSPOR2004 is used for sediment transport estimations in this research. This morphodynamic model is made in collaboration with RIKZ of Rijkswaterstaat and Delft Hydraulics, currently named Deltares. This model considers sediment transport mechanisms from waves and currents to determine the combined effect on suspended sediment transport and bed load. More specific information about the various complex formulas can be found in van Rijn et al. (2004).

Current related sediment transport mechanisms

The mobility parameter (ψ) is a measure of the fluid forces that causes the sediment particles to move, which is counteracted by stabilizing forces due to gravity. The mobility parameter is used to express certain hydrodynamic states in which specific bedforms occur, for example. This parameter is affected by the representative peak orbital velocity near the bed ($U_{\delta,r}$), the time- and depth-averaged return velocity below wave trough (u_r), the depth average current velocity (V_r), and the angle between wave and current motion (ϕ) (van Rijn et al., 2004).

$$\psi = \frac{U_{wc}^2}{(s-1)gd_{50}} = \frac{\left(U_{\delta,r} + |u_R|\right)^2 + V_r^2 + 2\sqrt{(U_{\delta,r} + |u_R|) * V_r * cos\,(\phi)}}{(s-1)gd_{50}} \tag{3}$$

The current-related friction coefficient (f_c) is based on the Darcy-Weisbach approach and shown in formula 4. Here the friction is affected by the water depth (d) and the current-related bed roughness (($k_{s,c}$). The bed roughness is related to the characteristics of the bed, like the presence of dunes and ripples (van Rijn et al., 2004).

$$f_c = \frac{8g}{\left(18\,log\left(\frac{12d}{k_{s,c}}\right)\right)^2} = \frac{0.24}{log\left(\frac{12d}{k_{s,c}}\right)^2} \tag{4}$$

The suspended sediment size (D_s) is estimated by the median grain size (D_{50}), the grain size wherein 10% of the grains are smaller (D_{10}), and the mobility parameter (ψ), is computed as (van Rijn et al., 2004):

$$D_s = \begin{cases} max\left(d_{10}, 1 - 0.0006\left(\dfrac{D_{50}}{D_{10}} - 1\right)(\psi - 550)d_{50}, & \psi < 550 \\ d_s = d_{50} & , \quad \psi \geq 550 \end{cases}$$

(5)

The sediment concentration over the depth is a balance of fluxes from the upstirring and settling of sediment. A rouse profile of sediment concentration is established due to the application of the k-ε turbulence closure model. Here the sediment mass concentration at any depth $c(z)$ can be determined by the representative concentration (c_a) at a specified reference height (a) (van Rijn et al., 2004).

$$c(z) = c_a\left(\frac{a(d - z)}{z(d - a)}\right)^A$$

(6)

Wave related sediment transport mechanisms

The wave-related friction coefficient (f_w) is affected by the bed forms with the peak length scale in the order of the wave orbital diameter at the edge of the wave boundary layer (A_δ). Here the empirical coefficient ($k_{s,c,r}$) is affected by the occurrence of ripples or sheet flow, resulting in (van Rijn et al., 2004):

$$f_w = exp\left(5.2\left(\frac{A_\delta}{k_{s,c,r}}\right)^{-0.19} - 6\right)$$

(7)

The representative bedload grain size (D_*) is used for the dimensionless shields criterion for the initiation of motion of fine sediments (θ_{cr}). The median grain size, the density of the sediment (ρ_s) and water (ρ_w), and the kinematic viscosity coefficient(v) can be used to estimate the bedload grain size and the criterion for initiation of motion, following formulas 8 and 9 (van Rijn et al., 2004).

$$D_* = \frac{D_{50}\left(\frac{\rho_s}{\rho_w} - 1\right)g}{v^2}$$

(8)

$$\theta_{cr} = \frac{0.24}{D_*}$$

(9)

The time-averaged bed-shear stress ($\tau_{b,w}$) is related to the water density (ρ_w), the friction, and the peak orbital velocity, which is represented by the peak orbital velocity forward ($U_{\delta,for}$) and backward ($U_{\delta,back}$) direction, resulting in (van Rijn et al., 2004):

$$\tau_{b,w} = \frac{1}{4}\rho_w f_w U_{\delta,r}^2 = \frac{1}{4}\rho_w f_w\left(0.5U_{\delta,for}^3 + 0.5U_{\delta,back}^3\right)^{2/3}$$

(10)

Wave and current-induced sediment transport

The bedload sediment transport at each arbitrary time ($q_{b,t}$) is affected by the instantaneous wave-current-induced grain-related bed-shear stress ($\tau_{b,cw,t}$) from the water motion by wave and current ($U_{\delta,cw,t}$) is given by (van Rijn et al., 2004):

$$\tau_{b,cw,t} = 0.5\rho_w f_{cw} U_{\delta,cw,t} \tag{11}$$

$$q_{b,t} = \frac{0.5\rho_s d_{50}}{D_*^{0.3}} \left(\frac{\tau_{b,cw,t}}{\rho_w}\right)^{0.5} \frac{max\left(0, \tau_{b,cw.t} - \tau_{b,cr}\right)}{\tau_{b,cr}} \tag{12}$$

The suspended sediment transport ($q_{s,w}$) is modeled by the peak orbital velocities in forward ($U_{\delta,for}$) and backward ($U_{\delta,back}$) direction, the wave-induced streaming velocity near the bed (u_δ) and a phase lag function (γ) (van Rijn et al., 2004).

$$q_{s,w} = \gamma \left(\frac{U_{\delta,for}^4 - U_{\delta,back}^4}{U_{\delta,for}^3 + U_{\delta,back}^3} + u_\delta\right) \int c \, dz \tag{13}$$

2.6 Statistical and machine learning techniques

Multiple unsupervised machine learning techniques will be applied in this research to analyze and structure the wave climate data and the weather types. This chapter will elaborate on how these methods are applied in this research.

2.6.1 Clustering technique kmeans

Kmeans is a data analysis technique in which the data is split into distinct subgroups with similar data. The parameters that describe the values can be used to assess the similarity of the samples, for example, over time. The values of the parameters can be used to describe the data in a mathematical space, wherein the parameters define the axis, called features, of the space. Points that are relatively close to each other in this space have similar data. The kmeans algorithm makes use of this reasoning to group the data (Dabbura, 2018).

The data is standardized so that each parameter has the same scale and thus weight in the kmean algorithm. The standardized parameters, or features, have a mean of zero and a standard deviation of one (Dabbura, 2018). Since the standardized data has the same format as the original data, the clustering results can be related to the original data.

The algorithm of kmean has a few steps. When starting the algorithm, the number of clusters (k) is defined. Then, to initialize the algorithm, a centroid is placed at the location of a random data point for each cluster. After that, all the data points are assigned to the closest centroid and form thereby a cluster. This distance is defined as the Euclidian distance, which is a summation of the squared distances over all the dimensions. Then an iterative process starts, which is practically the training part of the machine learning technique. In this iterative process, first, the averages of each parameter are determined for each cluster, then the centroids are repositioned to this new averaged location. The last step within the iteration is reassigning the data points to centroids and thus the clusters. Since the centroids have moved, some data points will be assigned to another cluster. This changes the averaged values of the parameters and will lead to a new location of the centroid, which will lead to a reassignment of the data points to clusters in the next iteration. This process continues until the assignment of data points to clusters no longer changes, or a stable situation occurs in which the assignment of data points changes between the same clusters. The sum of the squared distances between the data points and the corresponding centroid can define whether sufficient iterations have been applied (Dabbura, 2018).

Choosing the number of clusters that will be generated significantly impacts the outcome. Especially if the number of clusters is picked very low, then some data points that would have formed a distinct cluster will then be divided among other clusters. If more than the minimum number of clusters is defined, then some clusters will separate. The new clusters would be very similar and give more detailed information about the data. Therefore applying few, but not too few, clusters can give more insight into the general structure, with the cost that some information, called variance. Applying more clusters will give more detailed information but requires more extensive post-analysis.

Multiple techniques exist to determine the minimum amount of clusters, like the Elbow Method or the Silhouette Coefficient. In the Elbow Method, the sum of squared distance (SSE) between the data points and their centroids is calculated for a range of clusters after a given amount of iterations. The suggested amount of clusters is when the amount of SSE is not significantly reduced when adding more clusters. The optimal amount of clusters is recognizable as a relatively sharp angle, or elbow, on a graph where the number of clusters is plotted against the SSE. The Silhouette Coefficient calculates the degree of separation between clusters and has a value between -1 and 1. It calculates the difference in the average distance between all data points in the same cluster, called cohesion or intra-class distance, and the average distance to all the data points in the other clusters, known as the separation. The result is then normalized by dividing it by the largest average distance. If the silhouette coefficient is near one, then clusters are far away. If the value is zero, the clusters are very close to each other, and if the value is smaller than zero, the data points are assigned to the wrong clusters, which means that more iterations are required (Dabbura, 2018).

The clustering technique kmeans is an unsupervised learning method, which means that there is no manual control of the outcomes, and it is impossible to verify the outcome's quality by the algorithm. The random initialization of the centroids could affect the outcome. Therefore it is recommended to run multiple different initializations and then use the outcome with the lowest sum of squared distances between the data points and their centroids (Dabbura, 2018).

Due to the properties of the kmeans process, it is only recommended to do this clustering technique if the data can be described by spherically shaped clusters that do not overlap (Dabbura, 2018). However, studies are done to increase the capabilities and reduce the downsides of the kmeans clustering techniques (Jain, 2010).

Another point of attention is that rare situations, or outliers, do not have much influence during the clustering since they are averaged out. The consequence is that the centroid is more located in the space with a high density of points and therefore barely represents the characteristics of the few outliers. Here Maximum Dissimilarity Analysis (MDA) might reduce this effect since it will flatten the density, as described in chapter 2.6.3.

2.6.2 Principal Component Analysis (PCA)
Principal Component Analysis is a method to uncover the dominant combination of parameters in a dataset, called features, that describe as much of the data as possible. It can be used as a dimensionality reduction technique that reconstructs/describes the data so that it can be described with less uncorrelated parameters, called Principal Component. This reorganization will make it easier to analyze the structure of the data (Abdi & Williams, 2010). It will also increase the efficiency of the data analyzing techniques like the kmeans algorithm.

The philosophy behind the Principal Component Analysis is to rotate and translate the axis of the mathematical space so that it describes most of the information, or variance, of the data. This principle is visualized in Figure 14, where the axis of the two-dimensional space is rotated and translated so that the new x-axis is fitted through the data points and placed in the center of the

data. The data inside the rotated space does not necessarily have any physical meaning. However, the temporal variability is still present since the data is only projected on a new axis. Therefore, the physical processes that affect the Principal Components can be recognized, like continuous, periodic, or rare events. The visual reconstruction of the temporal variability of the data in Figure 14 is depicted in Figure 15.
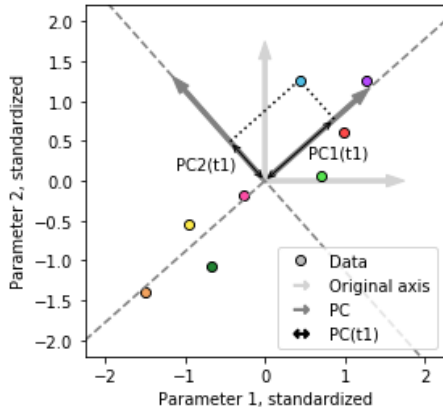

Figure 14: Visualization of the Principal Component Analysis. The colors indicate various times, as visible in Figure 15.
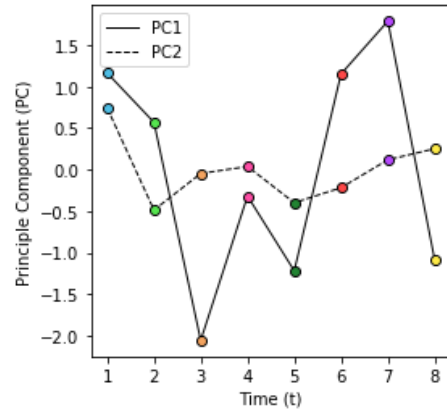
Figure 15: The Principal Components at various times, for the data of Figure 14.

The procedure of Principe Component Analysis starts with storing the data in a matrix. Here all (n) parameters of data at each time (x_t) are positioned next to each other, like formula 14, and vertically stacked over time to form a matrix shown in formula 15. Then each feature, or column (j), of matrix X is standardized so that the mean is zero with a standard deviation (s) of one, so that the influence of the parameters is equal, following formula 16. The next step is to calculate the covariance matrix (C), formula 17, which defines both the spread (variance) of the data and the orientation (covariance) of the data. The standardization does not affect the position that the data points have relative to each other. Based on the direction of the most variance, the eigenvectors (V) with their corresponding eigenvalues (λ) can be determined by the so-called characteristic equation, equation 18, and by formula 19 vectorized. The eigenvector, or Empirical Orthogonal Function, can be used directly to rotate the standardized mathematical space and obtain the Principal Component (PC) which is then scaled by the eigenvalue, following formula 20. By sorting the eigenvalues from large to small the most important eigenvectors and thus Principal Components can be determined.

$$x_t = \begin{bmatrix} x_{t,1} & x_{t,2} & \dots & x_{t,n} \end{bmatrix} \tag{14}$$

$$X = \begin{bmatrix} x_1 \\ x_2 \\ \dots \\ x_m \end{bmatrix} = \begin{bmatrix} x_{1,1} & x_{1,2} & \dots & x_{1,n} \\ x_{2,1} & x_{2,2} & \dots & x_{2,n} \\ \dots & \dots & \dots & \dots \\ x_{m,1} & x_{m,2} & \dots & x_{m,n} \end{bmatrix} \tag{15}$$

$$X_{std} = \frac{x_{t,j} - \bar{x}_j}{s_j} \tag{16}$$

$$C = cov(X_{std}) = X_{std}^T X_{std} \tag{17}$$

$$|C - \lambda I| = 0 \tag{18}$$

$$V = \begin{bmatrix} v_1 \\ v_2 \\ \dots \\ v_m \end{bmatrix}, \lambda = \begin{bmatrix} \lambda_1 \\ \lambda_2 \\ \dots \\ \lambda_m \end{bmatrix} \tag{19}$$

$$PC = V X_{std}^T \tag{20}$$

The minimum amount of Principal Components that are required to preserve a certain amount of the original data can be related to the variance that each Principal Component captures. Here the normal, or gaussian, distribution of independent datasets gives a relation between the amount of variance (σ^2) and the eigenvalue (λ) of the Principal Component. Therefore, this relation, described in formula 21, can indicate the amount of variance the Principal Component contributes to the total variance. This relation can be used to check if the applied (N) most important Principal Components cover the preferred minimum amount of variance by looking at the ratio of the summation of the variance of the applied Principal Components to the total amount of variance, shown in formula 22.

$$\lambda_i = \sigma_i^2 \qquad\qquad (21)$$

$$\sigma_{applied}^2 = \frac{\sum_{i=1}^{N} \lambda_i}{\sum_{i=1}^{m} \lambda_i} \qquad\qquad (22)$$

The realization of the eigenvectors can be interpreted as a linear fit through time. The positive and negative values of the elements in the PCA eigenvectors can be used to understand the positive or negative correlation between the variable and the Principal Component. If the parameters are spatial dependent, then spatial patterns can be analyzed by comparing the elements of the eigenvalues to each other. The eigenvalues between different Principal Components can be compared to each other after the elements have been scaled with the root square of the variance, the standard deviation, of its Principal Component. The scaled elements are called loads.

2.6.3 Maximum Dissimilarity Analysis (MDA)

When a time series of data with a consistent time interval is described in a mathematical space, then the data points, or observations, are not equally distributed throughout the space. The space that describes common situations will have a large density of points, while the space that describes rare events has a low density. This difference in density is because the common situation is described by many data points that, due to their similarity, are relatively close to each other, while the opposite holds for rare events, the outliers, which are described with fewer points that are relatively far from each other.

Maximum Dissimulariy Analysis (MDA) is a way to flatten the distribution of data points in the mathematical space by discarding some points in the space with a high density. This flattening is done by maximizing the sum of distances between a predefined number of points. In the newly formed data, the relative contribution/part of the rare events is larger and will, therefore, have more impact in post-analysis or algorithms such as kmean.

2.7 Sediment transport related conditions near the Dutch coast

The sea-bed characteristics, the disturbance induced by the waves, and general characteristics required for estimating potential sediment transport along the Dutch coast are described in this chapter.

The sediment in the North Sea basin entirely consists of sand and has a neglectable amount of mud and gravel. The median grain size (D_{50}) along the Dutch coast is smaller than 0.4 mm, and probably about 0.25 mm, as depicted in Figure 16. The suspended sediment grain size (D_s) is, after applying formula 5, estimated at 0.2 mm and the 90% cumulative mass passing diameter (D_{90}) is estimated at 0.3 mm. The density of the sediment is estimated at 2650 kg/m^3, whereas water has a density of 1030 kg/m^3.
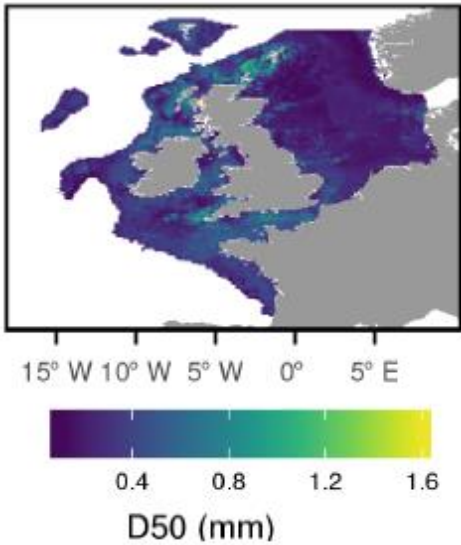
Figure 16: Median diameter at the north-west European Shelf (Wilson et al., 2018, p.120)
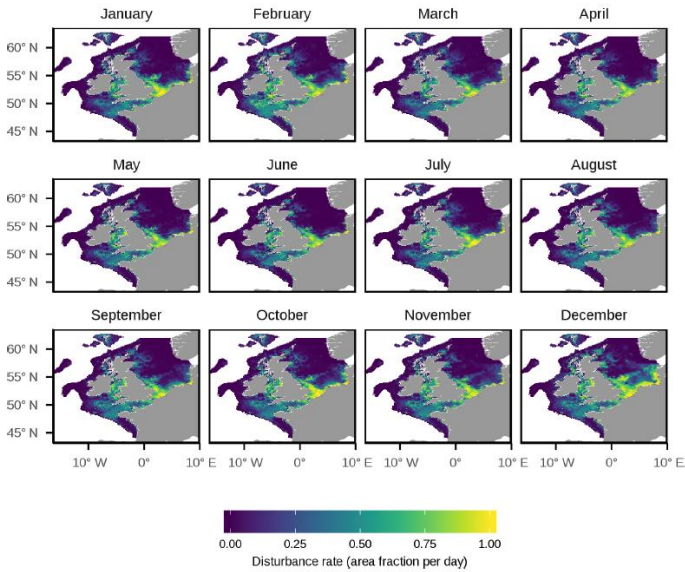
Figure 17: Monthly average sediment disturbance rate (Wilson et al., 2018, p.122).

3 Frame of reference

This chapter creates a framework to analyze the wavefield in front of the Dutch Shore and will be used to obtain a first impression of the wavefield, which will be used as a reference in the following chapters.

3.1 The approach

A case study at the southern part of the North Sea basin and along the Dutch shore is used to get insight into the wavefield and answer the research questions. The locations that will be analyzed thoroughly will be described in a framework. This chapter elaborates on the creation of this framework and a first impression of the wave frequency-directional spectrum at the described locations.

The framework is based on a first impression of the relevant wave generation areas and their wave energy fluxes, which are spatially dependent and show seasonal variability. The ESTELA method achieves insight into the wave energy fluxes, as described in chapter 2.3.2.

The framework will be used to obtain a first impression of the wavefield, which will be used as a reference in the following chapters. This impression consists of temporal and spatial analysis of the wave energy flux and the wave frequency-directional spectrum. The spatial analysis is based on the time-averaged wave frequency-directional spectrum. The temporal analysis consists of a seasonal and decadal average where anomalies are used to identify changes.

The ESTELA method and analysis of the wave frequency-directional spectra at the North Sea are based on the Wave Model (WAM) spectral data from the European Centre for Medium-Range Weather Forecasts (ECMWF). It has a spatial resolution of 1 latitude and longitude and a temporal resolution of 6 hours.

The wave spectral data along the Dutch coast from 2012 to 2016 is simulated with a Simulating WAves Nearshore (SWAN) model made by Lavidas & Polinder (2019), that uses the ERA-Interim wind dataset from by Dee et al. (2011) of the ECMWF and the WAM dataset from ECMWF. More information about the modeling of the nearshore data is described in chapter 3.3.

3.2 Wave generation area

The ESTELA method is used to determine which locations the wind-generated waves can potentially reach the shoreline at a specific location. Here the assumption is made that the wave propagates in a straight line, following circular paths across the globe, and that landmasses block the wave propagation.

The assumption that the bathymetry does not affect the wave propagation does not hold in an intermediate water depth, in which the nearshore processes affect the wave propagation. The expectation is that the impact of a changing water depth on wave propagation is minor and neglectable for analyzing trends in large-scale processes in the southern part of the North Sea basin.

Wave energy flux towards the location of interest

The area of influence for two locations at the nearshore near the land borders, Schouwenbank and Schiermonnikoog, are depicted in Figure 18 and Figure 19, respectively. The shaded areas show the locally, from 1797 to 2018, cumulative wave energy flux of the waves that propagate towards the location of interest, as described in Camus et al. (2014a). The results show that the cumulative wave energy flux is between 64 to 128 (times 360) kW/m/°. An increase in wave energy flux indicates that the wave energy flux towards the locations of interest increases. Furthermore, wave energy dissipation can be recognized by a local decrease in the wave energy flux.
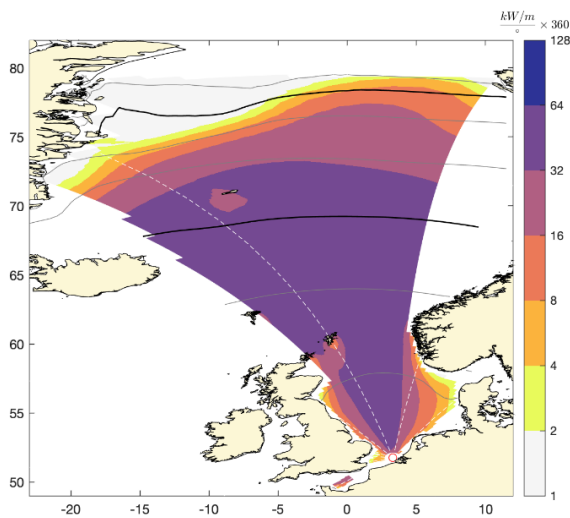
Figure 18: Wave energy flux reaching Schouwenbank with white striped travel paths and days of travel time indicated by grey and black lines.
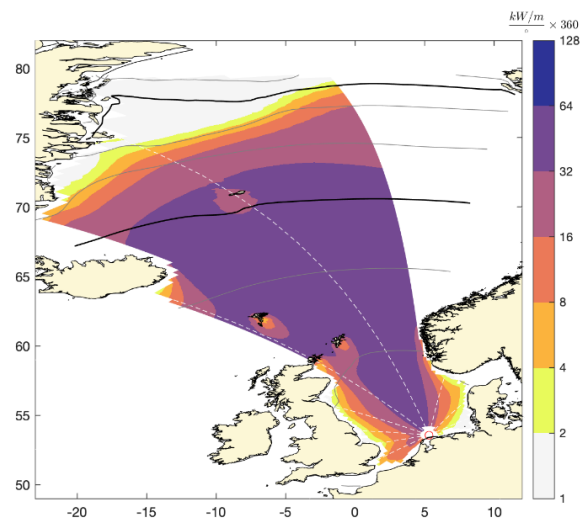
Figure 19: Wave energy flux reaching Schiermonnikoog, also known as Steunpunt Waddenzee, with white striped travel paths and days of travel time indicated by grey and black lines.

An important interpretation of the results is that wind-generated waves in the white areas do not impact the nearshore wave spectrum and thus sediment transport. Therefore only the shaded areas in Figure 18 and Figure 19 are relevant during this research.

Furthermore, the bands around the 75th latitude indicate the growth of waves while they are propagating in a southward direction. These waves become steady when they are between 64 and 128 (times 360) kW/m/°. Only some islands and their surrounding shallows, like Greenland, the Faeröer, and near the northern side of the United Kingdom, have an effect since they block and dissipate some energy locally.

The figures also show that waves are generated in the North Sea since the wave energy flux increases when the distance from the shorelines, the fetch, increases. So the wave height grows when the waves propagate from Great Britain, with a South Western to North Western wind, and from around Denmark if the wind is blowing from the East.

This leads to a general conclusion that wind can practically generate waves that propagate in any direction and that swell waves, due to the position of Great Britain and Norway, only come from the north-northwest towards the Netherlands.

<u>Coexistence of waves</u>

The grey and black lines on the ESTELA maps indicate the wave group travel time. Every third line, from the target location, is a black line that indicates steps of 3 days of travel time. These lines show that wave energy that is generated in the North Sea reaches the shore within approximately 1,5 days. However, the wave energy propagation time is about 4 to 7 days for the waves that are generated at Greenland, the latitudes of 70 to 80.

Due to this difference in propagation time (swell) waves generated at Greenland can coexist with new and locally generated waves at the North Sea that propagate in another direction.

<u>*Spatially and seasonally depended gain and loss of wave energy*</u>

The seasonally averaged gradients of the energy flux in the North Sea give additional insight into the local effect on wave energy and the seasonal variability. The averaged energy flux gradients over the North Sea for waves propagating towards Schiermonnikoog during winter (DJF) and summer (JJA) are shown in Figure 20 and Figure 21. These maps show during these two seasons where the wave energy flux increases and where wave energy is dissipated.

The energy flux gradients in Figure 20 indicate energy gain in the blue areas towards the coast of Greenland, at the 67th to 78th latitude. Waves also gain energy at the coast of Great Britain and the area west of Denmark and south of Norway. The red areas show energy dissipation due to the islands at the North-East tip of Great Britain

This figure also shows the energy dissipation of southerly propagating waves along the west coast of Norway and more to the south. The same spatial patterns can be recognized when comparing the energy flux gradients during winter to the summer. The main difference is that the magnitude of the gradients is larger during winter than during summer.

The spatial gradients agree with the conclusions that are made with the cumulative wave energy flux and show more detailed information about the specific wave generation areas and when these are relevant.
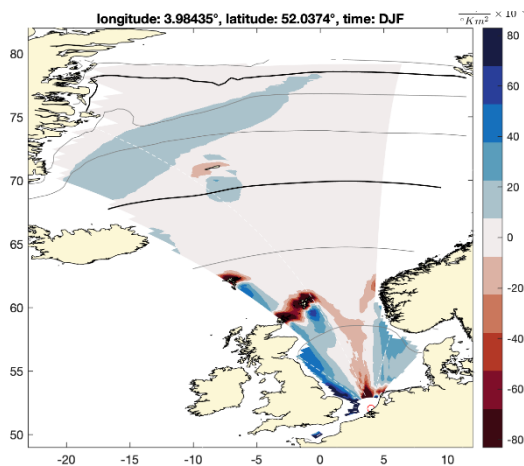

Figure 20: Detailed ESTELA map showing the energy flux gradients of waves propagating towards Hoek van Holland in winter (DJF). Blue indicates wave-flux increase and red wave energy (flux) dissipation.
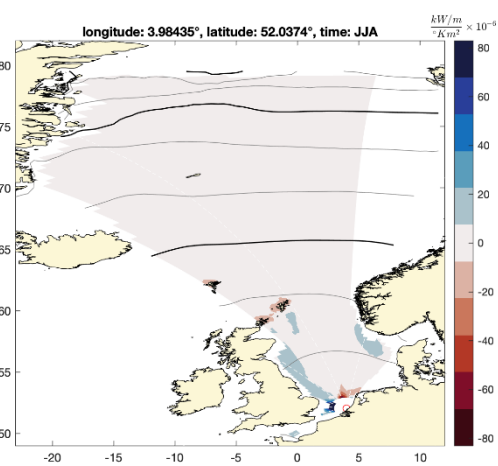

Figure 21: Detailed ESTELA map showing the energy flux gradients of waves propagating towards Hoek van Holland in summer (JJA). Blue indicates wave-flux increase and red wave energy (flux) dissipation.

3.3 Framework for analyzing spectral data

More insight into the waves in the wave field can be achieved by analyzing wave spectral data, rather than only their wave energy flux. For this analysis, a gridwork of points is set up to analyze waves propagating in various directions.

A distinction is made between offshore and nearshore points in this gridwork. The Coastal Foundation has been used as a boundary, where the water depth is 20 to 30 meters. For the offshore points are, various datasets available, like ERA-Interim, ERA-5, and HIRLAM. However, the spatial resolution is very coarse, and a higher resolution is required to analyze the data at the nearshore, where various processes affect the wave field. For this study, G. Lavidas conducted an extensive simulation of the wavefield along the Dutch coast. The model has been calibrated to measurements along the Dutch coast, whereby it uses ERA-Interim wind data as input. For consistency in this research is ERA-Interim data used for both the offshore and nearshore data. Here the period from 1 January 1979 to 31 August 2019 is used, except in chapter 5, where only the data from 2012 to 2016 is used to match the period of the nearshore data, and a six-hourly resolution of nearshore data is used to match the temporal resolution of the offshore data.
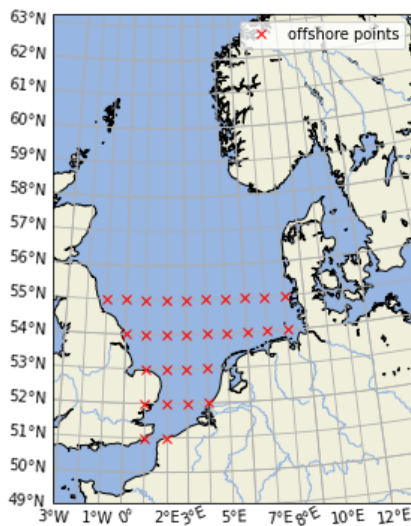

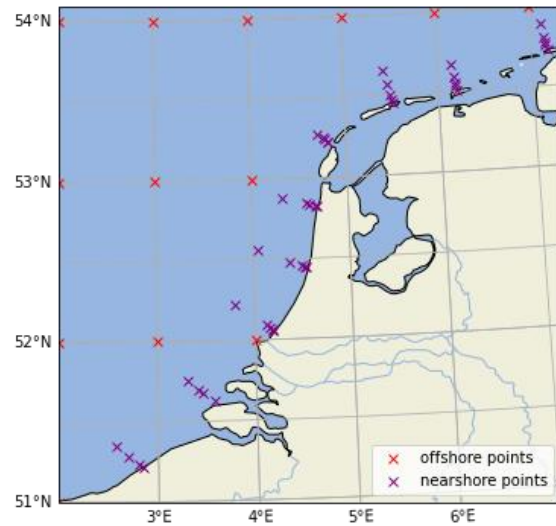Figure 22: Offshore gridpoints to analyze the wavefield.   Figure 23: Nearshore (grid) points to analyze the wavefield.

3.3.1 Offshore area

Wave frequency-directional data should be known over the entire North Sea to get a complete overview of the spatial development of the offshore wavefield, in which the effects of the island group in the northwest of Great Britain can be analyzed. When the ERA-Interim data is applied to the North Sea, 85 locations of spectral data are available. The steps of one latitude and longitude result in approximately 110 and 70 km spatial steps, respectively.

Only the points below the 56th latitude will be used in this study to find a relation between the synoptic situation and the wave field around the Dutch coast. In this way, the (swell) waves entering the North Sea and the wind-generated waves in the northern part of the North Sea can be identified at the 56th latitude. The area covered with spectral data captures the locally generated waves and the most significant energy gain and dissipation in front of the Dutch Coast, as visible in Figure 20. This reduction results in 29 offshore locations that are used to analyze the wave spectrum at the North Sea.

The water depth inside the offshore area ranges mostly from 20 to 40 meters, as depicted in Figure 24, and can be classified as intermediate, as shown in Figure 3. Only the short perioded waves with a period smaller than approximately 7 seconds can be considered in deep water. The other waves are considered in intermediate water, where their wave propagation is affected by nearshore processes.
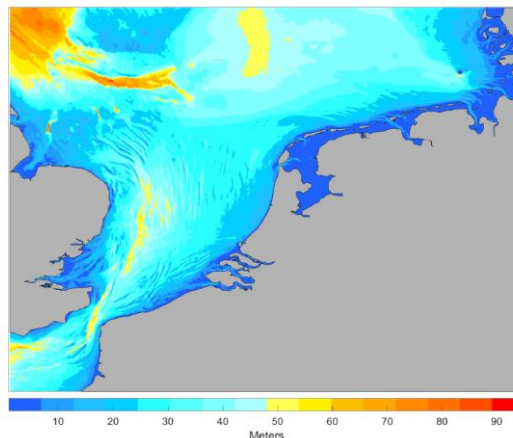

Figure 24:The water depth at the southern part of the North Sea, within the simulation domain of the SWAN model (Lavidas & Polinder, 2019, p. 4).

For this research is assumed that the changes in water depth in the offshore area are neglectable and do, therefore, not impact the wave propagation direction. As a result, the waves propagate in straight lines, and the ESTELA method can be applied to estimate the trajectories of the waves in the offshore area.

3.3.2 Nearshore area

The assumption of waves propagating in a straight line is not valid in the nearshore area, which is in contrast to deep water. The waves in this area could practically come from any direction, as shown in the ESTELA maps in Figure 18 to Figure 21. This results in a large variety of possible wave trajectories that should be considered. In the ideal case, the wave development along these trajectories can be analyzed by comparing wave spectral data. However, the generation and export of the wave frequency-directional spectral data is very computationally demanding and, therefore, a limiting factor in obtaining a fine resolution of nearshore spectral data in this research.

The nearshore data of waves that propagate shore-normal and oblique towards the shore is simulated by a phase-averaged model, which has been made for the study done by Lavidas & Polinder (2019). This model in Simulating WAves Nearshore (SWAN), developed and maintained by TU Delft (2014) has been set up with spherical coordinates that account for the Earth's curvature, with a resolution of 0.025°. Therefore, the grid sizes have a length of approximately 2.5 km in the longitudinal direction and 2 km in the lateral direction. This model is driven by the ERA-Interim wind dataset made by Dee et al. (2011) of the European Centre for Medium-Range Weather Forecasts (ECMWF) and has as boundary conditions spectral data reconstructed by the WAve Model (WAM) from ECMWF. More information about the applied formulas and calibration can be found at Lavidas & Polinder (2019).

Some considerations have been made for determining the locations and the periodic extent of the analysis. The output locations are described in a regular grid, which has a constant amount of normal and parallel lines with 43 nodes, which can be used as output locations for the SWAN model and are depicted in Figure 23. The considered period in the simulation is from 2012 to 2016 with an hourly resolution, which makes it possible to do the nearshore analysis described in this report.

The lines of the nearshore grid in the cross-shore direction are based on the paths of oblique incident waves, defined in Deltares (2020). The number of cross-shore lines, and thus the distance between these lines, is determined in such a way that the grid covers the whole length of the Dutch coast while the number does not exceed the computational possibilities when running the model.

Determining the location of the output locations in the cross-shore direction is more complex since the evolution of the wavefield is depth-dependent, and the depth does not decrease monotonically and equally along the coast. Therefore a regular grid is not suitable, and a depth-based approach is applied, in which the location of every point is related to a specific pre-defined water depth, namely the 5, 10, 15, 20, and 25-meter contour lines.

Three methods with a depth-based approach have been compared to each other. The results of each method to determine the 15-meter depth location for an arbitrary cross-section are visualized in Figure 25. The first method determines the point from which the depth is closest to the pre-defined water depth. However, this method does not take shallowness into account and could be randomly positioned before or after a possible shoal in the cross-section. This makes this method unsuitable since breaking large waves on the shoal results in a different wavefield. The second method finds all the intersections with the given water depth and then averages the coordinates and depths of the data points before this intersection. The downside is that when these points are relatively far apart, the newly defined location could be positioned at a location that is not representative of the given water depth. This second method is therefore rejected as well. The third and last method is applied for generating the nearshore grid. The offshore point just before approaching waves reach the predefined depth is chosen. In this way, the waves are not affected by shallows, and the locations are representative of the chosen depth.
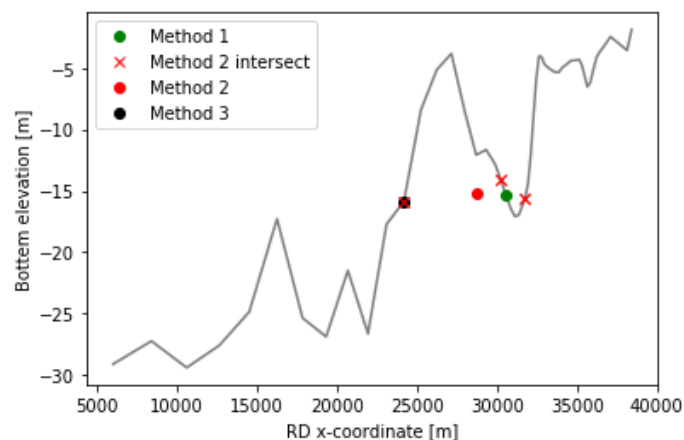

Figure 25: Visualization of depth-based methods to get the location of 15 meters of depth. Method 1 is the closest point, method 2 averages offshore positioned data points at intersections, and method 3 is the most offshore point before the depth condition is met.

3.4 Spatial wave analysis

The fetch length of locally wind-generated waves and the bathymetry affect the wavefield and create a spatial dependency of the wavefield, as described in chapter 2.1. The spatial dependency of the wave frequency-directional spectrum can be analyzed by comparing the time-averaged spectrums at the locations shown in Figure 22 and Figure 23.

For this analysis, the frequency-directional spectrum is averaged over the period from 1979 to 2018 for all the offshore and nearshore locations. The averaged energy is then used to describe the dominant and most wave energetic propagation directions and frequencies.

<u>Analysis in one location</u>

The time-averaged wave frequency-directional spectrums give an impression of the waves that contain the most energy. The energy of the time-averaged spectrum at the 55th latitude and 3rd longitude is shown in Figure 26. This graph shows the wave frequencies expressed in wave periods from 0 to 25 seconds on the radial axis. The propagation direction of the waves is related to their position compared to the center of the graph and expressed along the outer circle. On this graph are two energy peaks visible, indicated with red and black encircled.
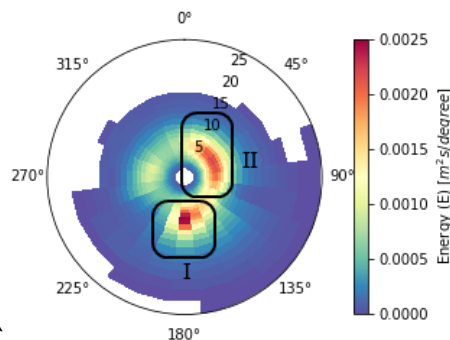

Figure 26: Averaged wave frequency-directional spectrum at latitude 55 and longitude 3, showing two energy peaks.

These energy peaks probably indicate the energy of two consistent wave trains, which are groups of waves with a similar wave period and propagation direction. Both the wave trains have a wave period of approximately 5 seconds. The wave train indicated with an "I" propagates in a southerly direction while the other one propagates in the direction of 60°. The southerly propagating wave train follows the third longitudinal line and has traveled along the Norway coast, as visible in Figure 18. The waves could be locally generated, but that is not likely since energy dissipation occurs along this trajectory, rather than an increase in wave energy flux, as visible in Figure 20. This energy dissipation is probably from the largest waves since energy dissipation is much smaller during summer, as visible in Figure 21, since the weather is relatively calm and the wind-generated waves are not as energetic and large.

<u>Comparing locations</u>

Spatial influences can be recognized by comparing two or more adjacent time-averaged wave spectrums. The time-averaged spectrums for the offshore locations are depicted in Figure 27. On the locations are the wave trains that are depicted in Figure 26 recognizable, together with waves that have a period of approximately 5 seconds, are propagating in all directions, and low wave energy on average.

At each longitude along the 55th latitude are the southerly propagating waves recognizable. The intensity of wave energy decreases in these waves when they travel along their path in a southward direction, which is probably caused by friction.

Another observation is that the propagation direction of these southerly propagating waves varies over the longitudes, as visible at the 55th latitude. The propagation direction at the longitudes at four and lower is mainly in a southerly direction, and the propagation direction changes towards the east for higher longitudes. So, the waves at the lower longitudes originate from one other location than the wave trains indicated at the higher longitudes and are therefore influenced by stormy conditions in different regions, which is also visible when comparing Figure 18 to Figure 19. Here the wave influencing area of Schiermonnikoog is related to the southerly propagating waves at the higher longitudes.

The prevailing western wind results in a local peak in this band indicated with a "II" in Figure 26. The energy of this peak increases when the distance from Great Britain's shore increases, and thus the fetch increases. The narrowing of the North Sea on the southern side results in a smaller fetch and less energetic waves. So the Northern part of the Dutch shore is more exposed to the western wind than the southern part.

The short perioded waves are most likely related to locally generated waves, where the frequently changing direction results in alternatingly much or little wave energy.
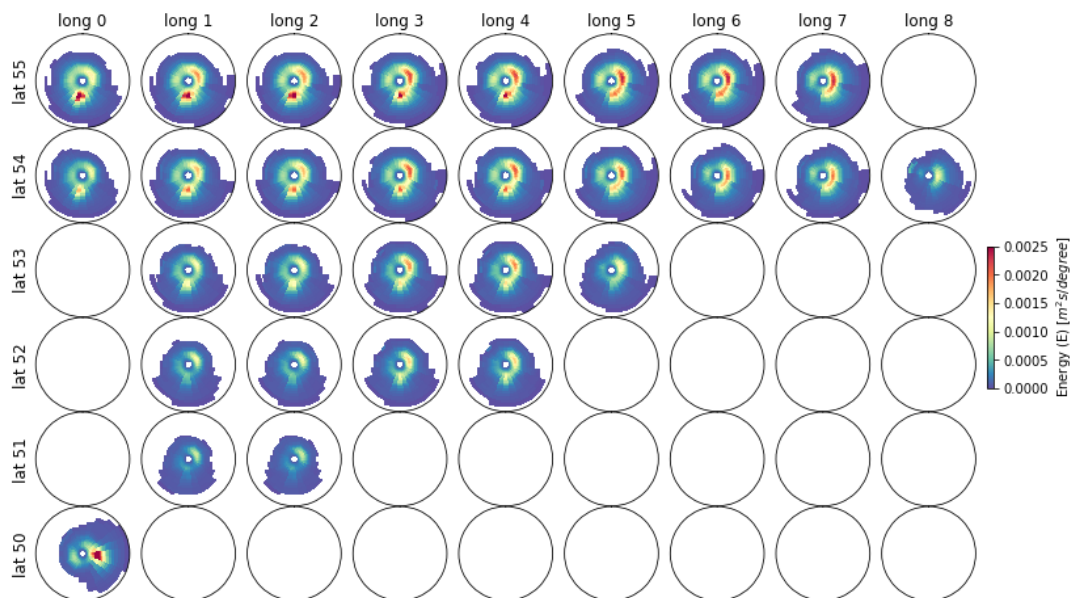

Figure 27: Time-averaged frequency-directional spectrum for all offshore locations at the North Sea, data from 1979 to 2018. The blank spectra are land, namely Great Britain on the west side, on the south-east side, Belgium, The Netherlands, and Germany and Denmark on the northeast side.

The wave energy of waves that propagate in the nearshore area is depicted in Figure 28. The nearshore locations are shown in a map in Figure 29.

The results show the transformation of the waves as they propagate towards the shoreline. The effect of refraction at each location is clearly visible. At the locations G, H, and I is the energy deflected towards a more perpendicular direction of the coast, resulting in the focusing of the energy into a smaller frequency-directional domain. At the other locations is the deflection of two distinct peaks distinctive. This deflection causes the waves to propagate almost perpendicular to the shoreline at the most nearshore point. As a result, the distinct wave peaks almost merge into one group of waves.
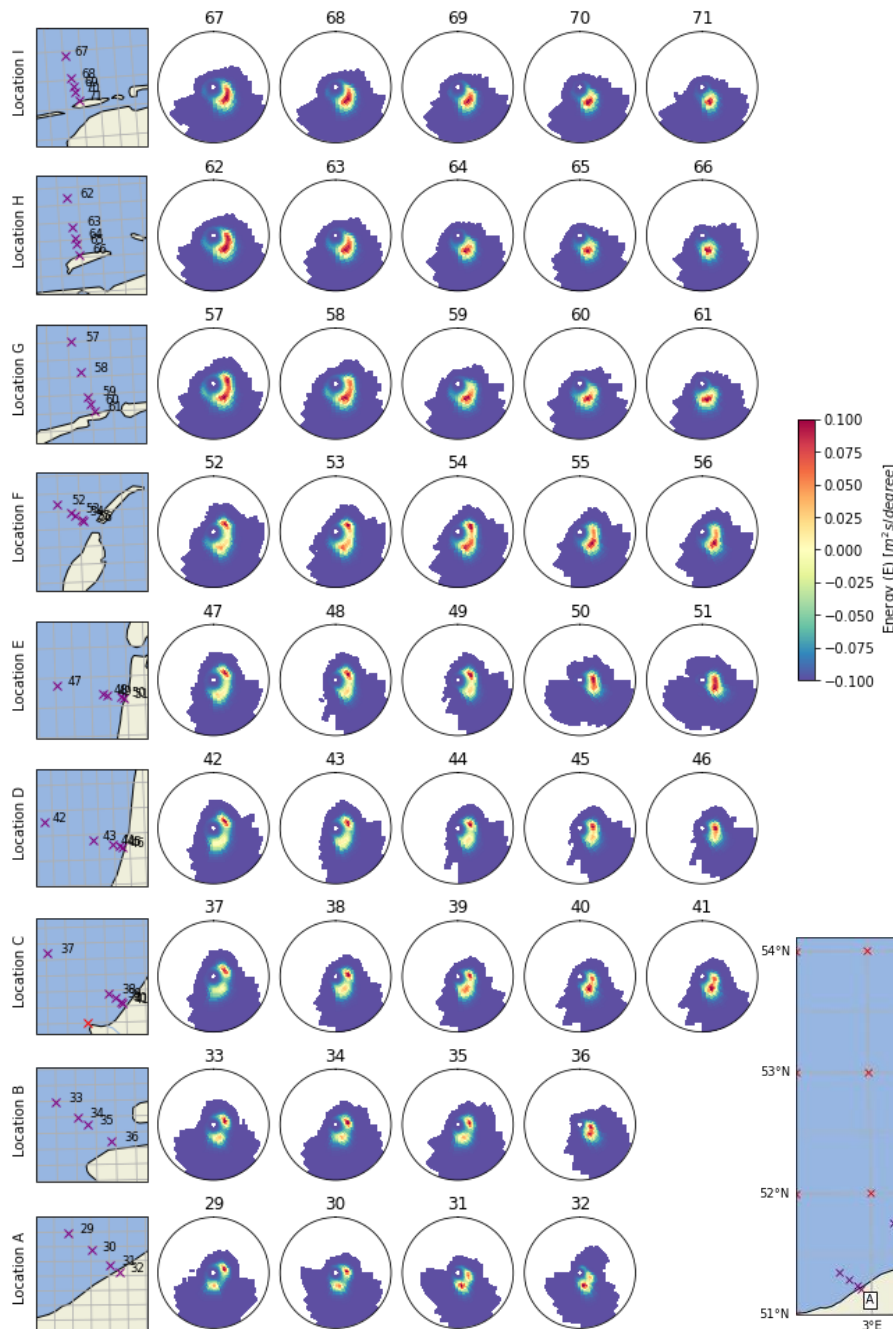
Figure 28: Averaged nearshore wave spectrums from 1797 to 2018, with label positioning visualized in Figure 29. The lowest number at each ribbon is the most offshore located.
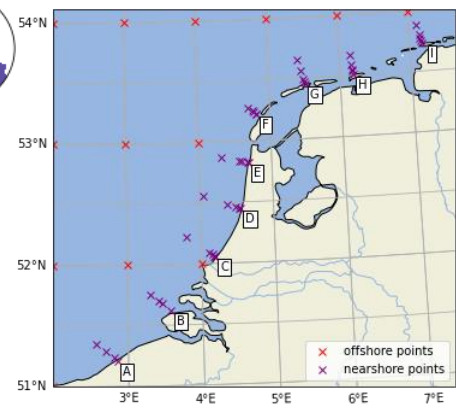
Figure 29: Nearshore cross-shore oriented locations with their names "A" through "I"

3.5 Temporal wave analysis

The temporal variability of the wavefield can be analyzed through the (periodic) anomaly, which is the difference between the periodic mean and the overall mean. The anomaly of the wavefield over the seasons for both the North Sea and the nearshore area is depicted in appendix I.

3.5.1 Seasonal variability

The seasonally averaged spectrums at the 55th latitude and 3rd longitude are depicted in Figure 30, and its anomaly is in Figure 31.

The spectrum and its anomaly show that the wavefield is most energetic during the winter period, which is from December to February. Especially the short waves have much energy, probably driven by the stormy conditions that can create waves propagating in all directions. The frequently occurring westerly wind significantly affects the easterly propagating waves. Only some short waves that propagate from the north are less energetic, as visible on the anomaly. However, the situation is the opposite during spring, from March to May, when the wavefield is relatively calm, and only a few southerly propagating waves are slightly more energetic than average The months June, July and August, the summer period, are relevantly mild. Then two peaks of south-westerly propagating short perioded waves can be recognized together with an increase of waves with a period of 15 seconds. During the autumn, a distinction can be made between a decrease of waves with a period of about 10 seconds while two wave trains with a period of 5 seconds and some northwesterly propagating waves are more energetic. Furthermore, some southerly propagating waves are less energetic, which will last through the winter period.
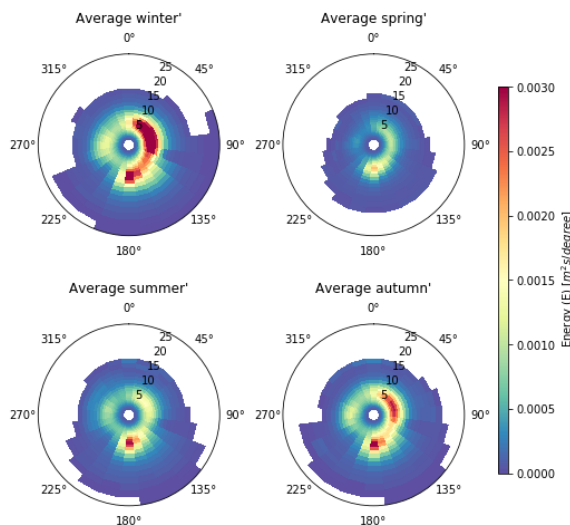

Figure 30: Seasonal averaged frequency-directional spectrum, at the 55th latitude and 3rd longitude.
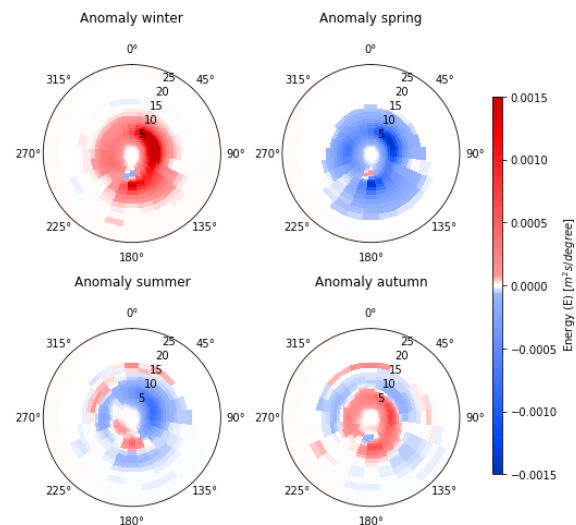
Figure 31: Seasonal anomalies in the frequency-directional spectrum at the 55th latitude and 3rd longitude.

3.5.2 Multidecadal trends

The decadal averaged spectrum and its anomaly, Figure 32 and Figure 33, can be used to identify trends that occur over multiple decennia. These trends can be found when comparing parts of the averaged wave spectrum from one decade to another. One of these trends could, for example, be an increase in wave energy propagating in one direction. However, no such trends can be distinguished.

The decadal anomalies show that the wave climate during the eighties had a higher energy flux towards the east and from some waves with a period of 15 seconds to the northeast. During the nineties, the wave energy is above average in almost all directions. While the southerly propagating waves are mainly more energetic during the first decade of 2022. The waves were mainly offshore directed during the second decade, from 2010.
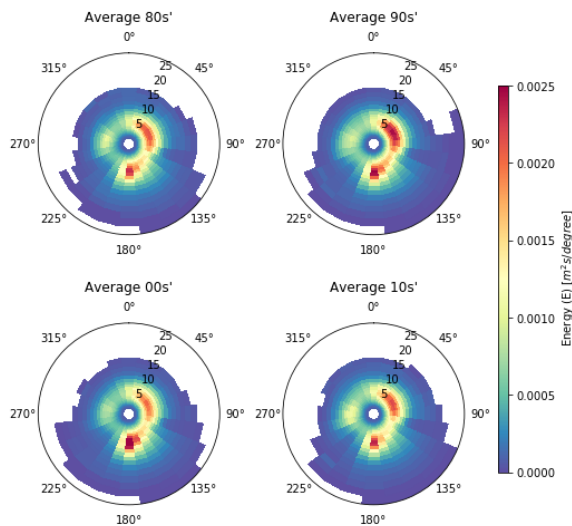
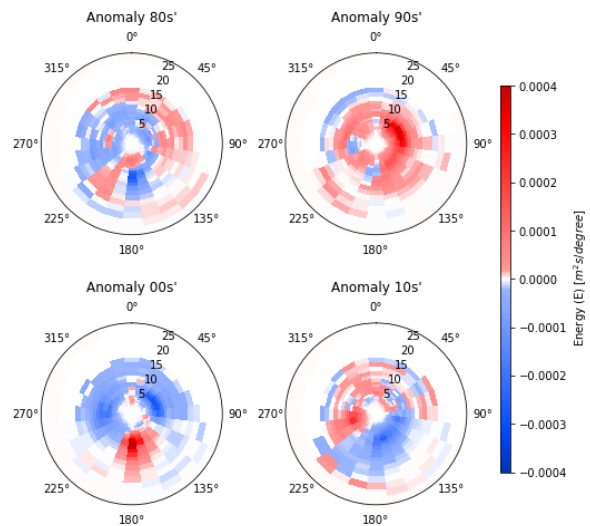Figure 32: Decadal averaged wave spectrums at the 55th latitude and 3rd longitude

Figure 33: Decadal anomalies in the wave spectrum at the 55th latitude and 3rd longitude

Although increased and decreased energy can be recognized for certain waves, the decadal anomalies do not show a consistent change of energy in parts of the spectrum or on its whole. Therefore, no multidecadal processes are identified.

3.6 General Discussion and Conclusion

This subchapter elaborates on the main discussion and conclusions of subchapters 3.2 to 3.6, which can be used to answer the two main research questions. In these subchapters are the wave energy-flux and time-averaged wave frequency-directional spectrums used to analyze the wave field.

3.6.1 Discussion

The available data has some limitations, so is the nearshore data only available for five years and has the offshore data a resolution of six hours. ERA-Interim offers data that can reduce the resolution to 3 hours, but this data is modeled and not from direct measurements. This additional data might be useful to track specific wave conditions over time and space if this is preferred.

The biggest drawback of the performed time-averaged wave frequency-directional spectrums is that it is difficult to distinguish groups of waves based on the energy. One energy peak does not necessarily belong to one group of waves, so caution is advisable. Chapter 4 uses a more advanced method to analyze the group of waves. Another drawback is that there is no insight into highly energetic (stormy) wave conditions, which contribute a lot to sediment transport, as concluded in chapter 7.

3.6.2 Conclusions

The waves are generated in areas near Greenland, Great Britain, and east of Denmark. At other locations, the wave energy dissipation is larger than the energy gained from the wind, which results in a decrease in wave energy and smaller wave heights.

The time-averaged wave spectrums are used to make several conclusions. So do the energy peaks indicate consistently occurring energetic wave trains that are propagating towards the east and south. Energetic short-perioded waves occur in all directions and are probably related to locally-generated waves that are probably formed during stormy conditions.

The travel times of southerly propagating (swell) waves, which propagate along the shore of Norway, might coexist with locally generated waves. This makes it possible that, for example, the earlier recognized high energetic eastern and southern propagating waves might coexist.

The maximum wave-energy fluxes and the periodic averaged wave spectrum give insight into the wave energy. However, they do not give insight into the wave characteristics, such as the wave height and the coexistence of waves, which is a limitation in the applicability of using time-averaged wave frequency-directional data.

Seasonal fluctuations can be found. So is the wave energy the largest during the winter months, and do short waves propagate in almost all directions during autumn. Trends in changes in wave energy over multiple decades, for example related to climate change, are not found.

4 In-depth analysis of the wave spectrum

This chapter uses three techniques to get more insight into the coexistence of wave trains and their statistical characteristics in the southern part of the North Sea and in more detail along the Dutch coast. These conclusions can not be made by periodic wave energy fluxes or averaged wave frequency-directional spectrums, which are performed in chapter 3. This chapter focuses on the importance of accounting for coexisting groups of waves and their generation and also the applicability of wave partitions and wave families in describing the wavefield so that it can be used to estimate potential sediment transport.

4.1 The approach

Traditional methods that predict (potential) sediment transport assume that there is only one dominant wave propagation direction. However, multimodal wave spectrums may occur, which have at least two groups of waves with similar wave periods and directions, called wave trains.

Waves that reach the Dutch shore are generated at various locations, like west of Great Britain, East of Denmark, and near Greenland, as visible in The ESTELA map in Figure 20. These waves reach the Dutch shore in different directions and might coexist due to the different travel times. The energy of these wave trains causes an energy peak in the wave frequency-directional spectrum. This energy peak is used to split the wave frequency-directional spectrum in parts, called wave partitions, where each wave partition captures the energy that is related to one wave train, as described in chapter 2.2.3.

The wave trains that are generated in the various locations might show unique characteristics due to their relation with local wind conditions and the effect of nearshore processes on their wave propagation. Wave systems can describe consistently occurring wave trains. In this study, these wave systems are analyzed by wave families, which are determined by temporal statistics of wave partitions, as described in chapter 2.2.3.

There are no spatial relations between the wave families since they are determined independently at each location. The clustering algorithm kmean spatially groups the wave families in chapter 4.6, as explained in chapter 2.6.1. The formed groups can be used to analyze the wave systems spatially and show, for example, the effect of nearshore processes on waves within this wave system.

Chapter 4.7 focuses on the applicability of wave partitions and wave families in estimating potential sediment transport by waves and focuses on the second main research question.

In this chapter is the hourly resolution of the nearshore data used. The period from 2012 to 2016 resulted in 43.849 wave frequency-directional spectrums, which statistics are analyzed with wave partitions and wave families. Statistics of the wave families across the North Sea are analyzed with data from GLOSWAC (n.d.).

4.2 Considering coexisting wave trains

The occurrence of coexisting waves and their relative angle will be analyzed in this subchapter. The analysis starts with analyzing what kind of multimodal wave spectrums are occurring. Then statistics about the number, direction, and relative angle between coexisting wave trains are analyzed. The importance of considering coexisting wave trains will be discussed for each of these results. A more in-depth analysis of the wave train propagation will show the main wave train propagation direction and the applicability of wave partitions and answers partly the second main research question. The results are based on the statistics of wave partitions, which describe the wave energy, propagation direction, and peak period of their corresponding wave train.

Multimodal wave spectrum types

Many kinds of spectrums can be identified when analyzing the wave frequency-directional spectrums. So does the number of coexisting wave trains and the angle between the wave's propagation directions highly vary. The angle difference, or relative propagation direction, can be classified by following waves that propagate more or less in the same direction, crossing waves, and waves propagating in the opposite direction, the opposing waves.

The energy of three wave frequency-directional spectrums are depicted in Figure 34. Here are the energy peaks indicated with dots. Each dot is the basis of one wave partition, from which the boundaries are indicated with black lines. The left wave spectrum shows two prominent energy peaks related to two wave trains that propagate in a direction between 180° and 135°. These two wave trains can be considered as following wave trains with different peak periods, 6 and 9 seconds. Towards the east can also two wave trains be identified that contain significantly less energy. These two wave trains together can also be considered as following wave trains. The relatively large angle between the south easterly and easterly propagating waves can be described as crossing waves, where the southerly propagating waves contain significantly more energy. The middle spectrum shows crossing waves that both contain a considerable amount of energy. The wave trains propagate towards 160 and 45° and have a peak period of 4 and 10 seconds. Also, two low-energetic wave trains can be identified that propagate towards the north and thus in the opposite direction of the southerly propagating waves. The third wave spectrum, on the left, shows a large band of waves. Here 4 energy peaks can be found in the high energetic part, which leads to 4 wave partitions. The adjacent wave trains can be described as following waves. However, the large angle between the two outermost wave trains is orthogonal and can be considered as crossing waves.

Traditional methods that use only representative (total) wave height with its corresponding period and propagation direction can not account for coexisting wave trains. The first impression is that there are situations that are hard to describe with one representative wave, due to varying wave propagation directions and peak periods. The upcoming subchapters will elaborate on this.
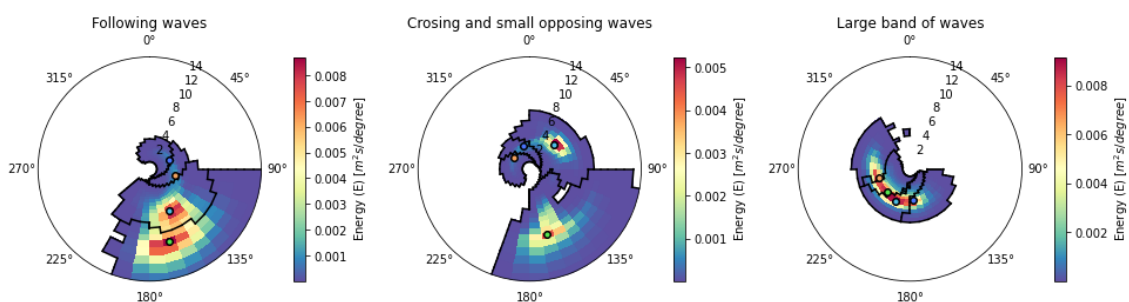

Figure 34: The wave energy of various kinds of multimodal wave spectrums containing following, crossing, and opposing waves. The dots are related to the energy peaks in the spectrum that are used to make the black-bordered wave partitions. The wave period is capped at 15 seconds, and the propagation direction is described in the outer circle.

The probability of how many wave trains are occurring is depicted in Figure 35. A unimodal wave spectrum occurs only 35% of the time, so in 35% of the 43.849 wave spectrums. The other times a multimodal wave spectrum occurs. Two coexistent wave trains occur 39% of the time. The maximum number of coexisting wave trains is 9, but it has a very minor probability of occurrence.

The traditional methods assume a unimodal wave spectrum. However, an error is introduced 65% of the time since more than wave trains are occurring. The error will be small if the waves are propagating in the same direction and have a similar wave period, but this is not always the case as shown in Figure 34. The upcoming subchapter will elaborate on the angles between the propagation direction of the waves and in which direction the waves are propagating.
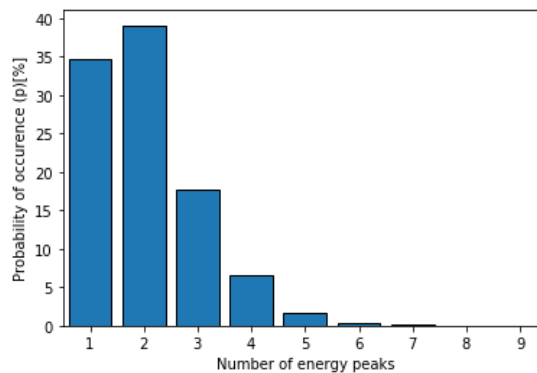

Figure 35: Probability of number of wave trains in the spectrum at location 42, in Figure 28, near the coast of North Holland.

The relative angle between coexisting wave trains

Coexisting wave trains can propagate in different directions. The (relative) angle between these wave trains can be divided into three classes. Following waves are wave trains in which the angle between the propagation direction, or bearing, is smaller than 60°. The angle of crossing waves is between 60° and 120°, and for opposing between 120° and 180°.
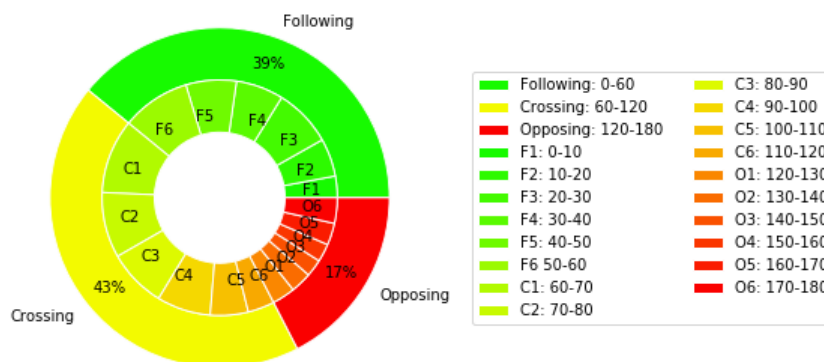

Figure 36: Probability of direction of wave trains compared to the most energetic wave train for multimodal wave spectrums. The outer circle describes the probability of occurrence of following, crossing, and opposing waves, where a complete circle is 100%. The inner circle describes the distribution in more detail, where numbered bands of 10° are used rather than 60° , as shown in the legend. The statistics are for location 42, shown in Figure 28.

Statistics about the relative angle between wave trains and the most energetic wave train during multimodal wave conditions at one nearshore location on the coast of North Holland are depicted in Figure 36. The outer circle describes the probability of occurring of following, crossing, and opposing waves. The inner circle gives more detailed information about the distribution of waves, for the following (F_i), opposing (O_i) and crossing (C_i) wave trains, as shown in the legend. The results show that only 39% of the wave trains have an angle smaller than 60° compared to the most energetic

wave trains. The probability that the wave trains are crossing each other is even more prominent, namely 43%. For the remaining 17%, the wave trains are propagating in the opposite direction. The inner circle indicates with F_1 that only a minor fraction of the relative wave angles is smaller than 10°, and that the probability C_1 to C_5 is larger than that of F_1, for example.

The results show that only a minor fraction of the times the relative angle is smaller than 10°, as shown with F_1. In all the other cases, where the relative angle increases, the assumption of a narrow banded spectrum to describe the wave spectrum with a generalized wave parameter becomes less valid, and the error increases. The relatively large occurrence of crossing and opposing waves indicate that it is essential to account for the coexistent wave trains since they may cause sediment transport in various directions.

The propagation direction of following, crossing, and opposing waves

This chapter analyzes if the wave partitions can be used for a more in-depth analysis of the propagation direction of waves when following, crossing, and opposing waves are occurring and can therefore be used to answer the second sub research question that focuses on the applicability of the parameters. The outcomes themself will give additional insight into the importance of coexisting wave trains.

Results

The probability that the most energetic wave propagates in a specific direction is shown in Figure 37, which has bandwidths of 10 degrees. Here is visible that the most energetic wave train mostly propagates in the direction of 65° or 175°. Another result is that the most energetic wave train is seldom towards the north, under an angle of 5 °. A similar graph is visible in Figure 38, where all the wave trains are considered. The numbering of the wave partition is related to the amount of energy each wave partition captures, where wave partition 1 captures the most energy and wave partition 10 the least. Figure 39 shows the relation between the most energetic wave trains and the wave propagation directions of the simultaneously occurring less energetic wave trains. So is there, for example, a 50% chance that a wave train is traveling in the direction of 45° (vertical axis) when the most prominent wave train propagates in the direction of 5° (horizontal axis). The distribution of probabilities also shows that the chance of occurrence is not equally divided for all the relations. The lines show the angle between the most energetic wave train and the less energetic wave train and can be used to identify following, crossing, and opposing waves and their probability of occurrence. Along the line indicating following waves are only probabilities larger than zero when the direction of the most energetic wave is between 135 and 225 °. The less energetic wave trains have a bearing of 135° to 225° when following waves occur.
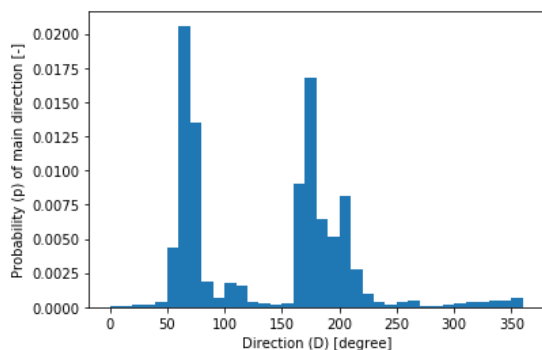

Figure 37: Probability per degree of main wave direction, at location 42, which is shown in Figure 28.
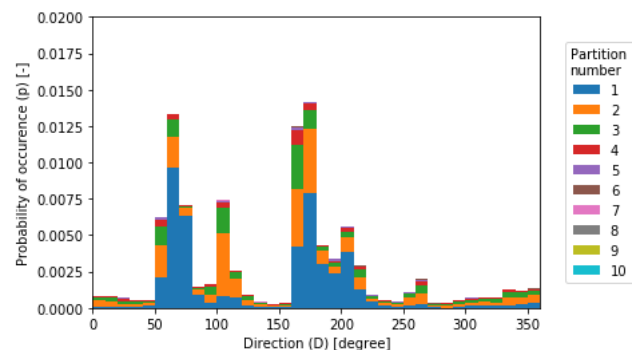

Figure 38: Probability per degree of the direction of all the wave trains, at location 42, which is shown in Figure 28
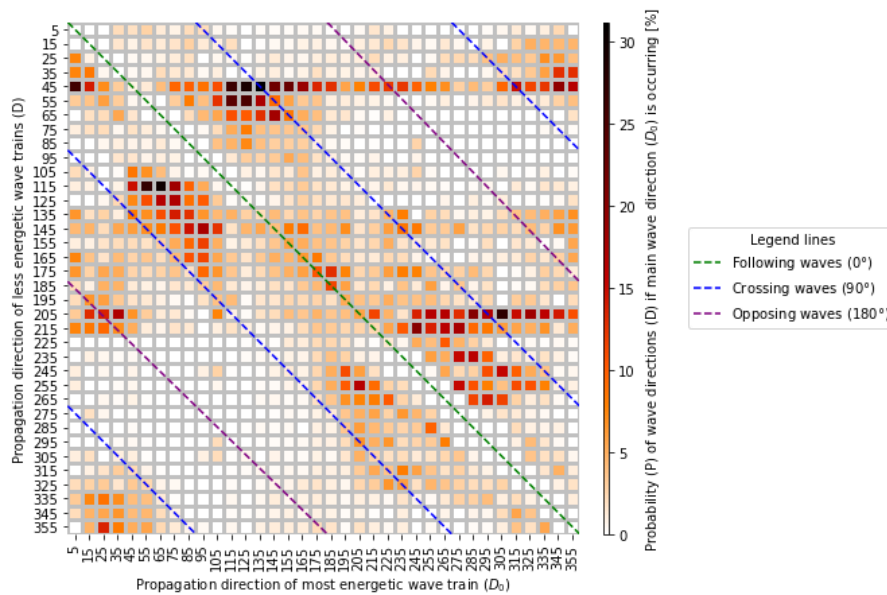
Figure 39: Probability (P) of coexisting wave trains, the probability of wave train directions (D) compared to the propagation direction of the most energetic wave train (D_0). The lines show the angle between the most energetic wave train and the less energetic wave train. The wave data is from location 42, which is shown in Figure 28.

Discussion and conclusion

The interpretation of Figure 37 is the probability distribution of the wave direction when the traditional methods are applied when these are based on the (energy) peak direction and peak period. So traditional methods will relatively frequently describes waves towards 65° and 175°.

When looking at the relatively blue part of the bars in Figure 38, some of the directions are mainly blue, as it is for the directions 65° and especially 75°, and for other directions is the blue part very minor, such as in the direction of 115°. Energy is mainly received from other directions when the most energetic wave train is relatively frequent in that specific direction compared to the other wave trains, so when the bar in the graph is mainly blue. The blue part is relatively small when waves in a specific direction are not the largest in the wave spectrum. Therefore, their energy will be relatively often contributed to another direction when the traditional methods are used. Consequently, the impact of these waves on sediment transport is accounted for in another direction.

Figure 39 gives additional insight into the direction from which energy is attributed and to which direction it is. Ideally, when the directional error when applying traditional methods is minimal, the most energetic wave train should propagate in the same direction as the other wave trains. In this ideal case, the cells in Figure 38 along the green line should have values of 100%. However, the opposite situation occurs since almost all the cells near this line have very low values. The probability around this diagonal is only slightly larger for the wave propagating in a southerly direction, around 180°. So the following waves, shown in Figure 36, mainly occur between southerly propagating waves. Furthermore, the opposing waves occur when the largest wave trains are propagating towards the north-northeast (25°), the south-west (215°), or north-west (325°), where the probabilities are high along the line indicating opposite waves.

Another conclusion of Figure 39 is that some combinations of wave train propagation directions are relatively frequent. The probability of occurrence will be more or less equally distributed over all the combinations when there is no correlation between the propagation direction of the wave trains. So when there is no correlation, the probability of each combination will be about 2.8% since 36 bands in a column cover the total 100%. However, in Figure 39 are groups of similar combinations of wave train propagation directions with a higher probability of 20%, creating groups of adjacent cells with a

reddish to black color. These combinations might indicate a relation between the coexistence of the wave trains. In cases where the most energetic wave occurs only a few times, this high probability might be due to a coincidence of circumstances. So are some of the directions only occurring 50 to 150 times. This coexistence seems not to be a coincidence when the most energetic wave train propagates to about 65° and 125° since these occur more than 4000 and 3000 times, respectively. Chapter 5.5 will go deeper into this coexistence.

<u>Relative wave angles for more energetic wave conditions</u>

No threshold for wave height is used in the above analysis. This threshold can be based on the energy of the whole spectrum expressed in the significant wave height or by a threshold to the significant wave height of wave trains. Since many smaller wave trains can contain the same amount of energy as one larger wave train, they might induce a similar impact on, for example, sediment transport.

The relative probability of following, crossing, and opposing waves when the threshold of motion is based on the significant wave height representing the energy of the whole wave spectrum is depicted in Figure 40.

When comparing the probabilities within Figure 40 and Figure 36, than can be concluded that the maximum angles between wave trains decrease when the threshold decreases. However, the angle between wave trains remains considerable since the angle is still larger than 50° for half of the time in both cases in Figure 40.

Figure 40: Probability of direction of wave trains compared to the most energetic wave train for multimodal wave spectrums, with a threshold of 0.5 m left and 1 m right, containing 75% and 37% of the data, the layout of the graph and considered location is similar to that of Figure 36.

4.3 Wave trains across the North Sea and nearshore cross-sections

The propagation directions of wave trains can be analyzed by counting how many times the wave train induced energy peak in the wave spectrum is at a specific frequency and direction, as mentioned in chapter 2.2.3. This section elaborates on the wave propagation directions at various locations across the North Sea, depicted in Figure 41, and the wave heights and direction of the wave trains along two cross-sections in the nearshore area.

The waves that reach the Dutch shoreline come from the north, through the English channel, or are locally generated, as concluded after applying the ESTELA method in chapter 3.1 and depicted in Figure 18. A more in-depth analysis of the wave train propagation direction across the North Sea is analyzed in this subchapter. The considered locations are shown in Figure 41, and the counting of the location of the energy peaks inside the frequency-directional spectrum is depicted in Figure 42.
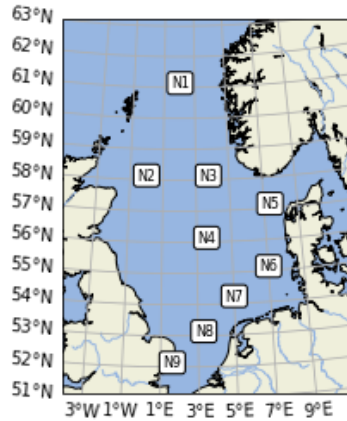

Figure 41: The locations of which the spectrum wave families are shown in Figure 42, and some nearshore locations.
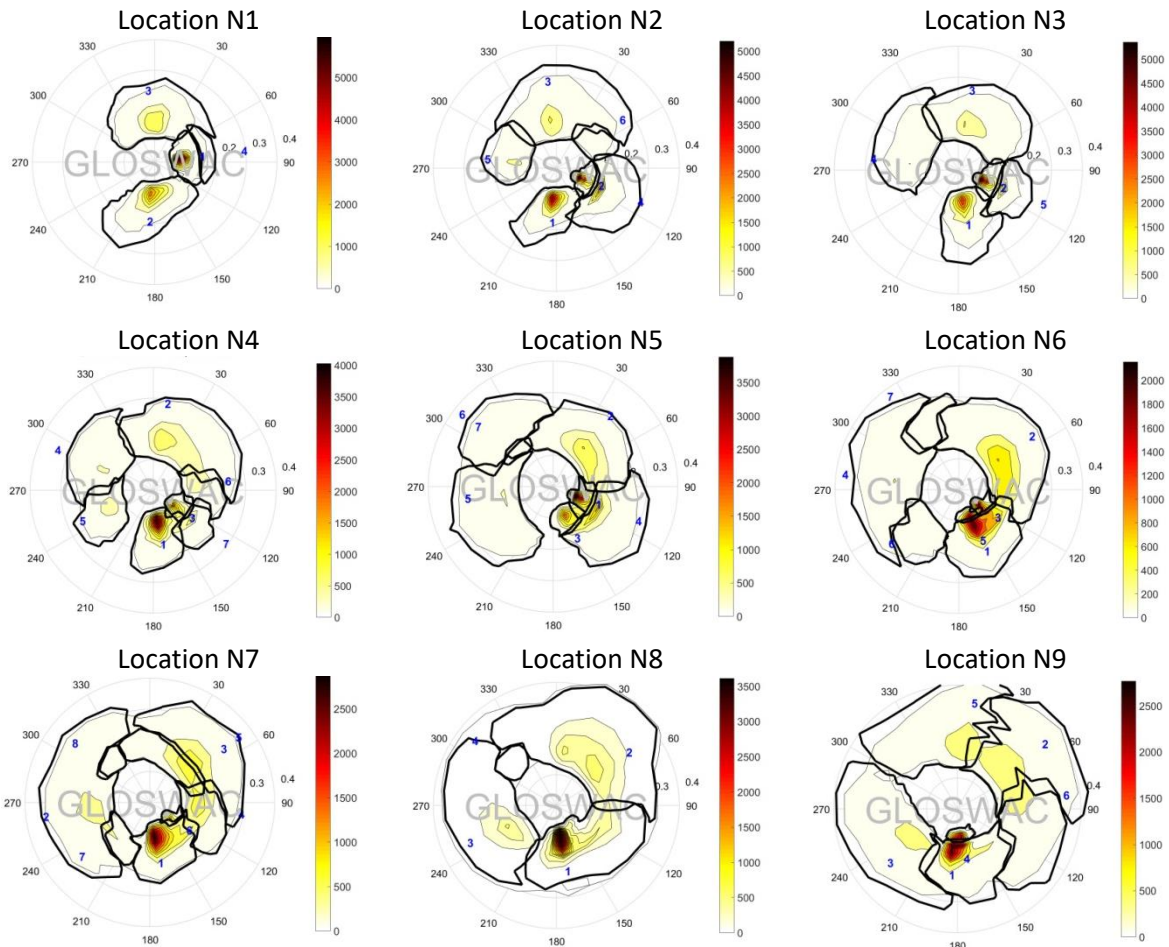
Figure 42: Wave families at offshore locations are shown in Figure 41. The images showing the peak location counting for each frequency-directional combination at locations N1 to N9 were requested at GLOSWAC (n.d). As described in chapter 2.2.3, each peak can be described with a wave family. The black lines indicate wave family boundaries, and the blue numbers refer to the wave family number. The locations are depicted in Figure 41.

Location N1 has three major peaks in the counting. The first peak, indicated with a blue 1, shows locally waves propagating to the east, thus the coast of Norway. The peak of the southerly propagating waves, related to family 2, enters the North Sea. These southerly propagating waves are also recognizable at location N2, as family 1. Some waves pass the islands in the northeast while propagating towards the southwest and form families 2 and 4. These two families are also at location N3, where also the southerly propagating waves arrive from location N1. Location N4 has a similar wavefield as location N3. The main difference is that locally generated waves arrive from Skagerrak, the waterbody between Norway and Denmark, near location N5. These wind-generated waves are recognizable by their broad range of wave frequencies and propagation direction and the lack of a distinct peak in the counting, as shown by family 5 at location N5. More to the south at location N6 is a similar pattern. The main difference is that the (swell) waves from outside the North Sea do reach this area, creating families 1, 3, and 5. The offshore-directed wind creates waves propagating in all westerly directions. The south-westerly propagating waves reach the Dutch Shore and are recognizable on locations N7, N8, and N9 by respectively wave families 7, 3, and 3. At these locations are also northeasterly and southerly propagating waves distinctive.

The results show that the statistics about wave partitions are useful in describing the frequently occurring wave trains in the wave field.

Wave trains across cross-sections in the nearshore

The energy and the propagation direction of the wave trains can be analyzed by a wave rose. Figure 43 shows the wave roses for the locations along two cross-sections. Each wave rose shows bars indicating the number of occurrences of significant wave heights within certain limitations, as shown in the legend. The counting is based on 43.849 spectrums, which means that the length of the bars can also be interpreted as a probability or frequency of occurrence. So, the probability or frequency is related to the length of the bar. The titles above the wave roses refer to the considered location, shown in the map on the right.
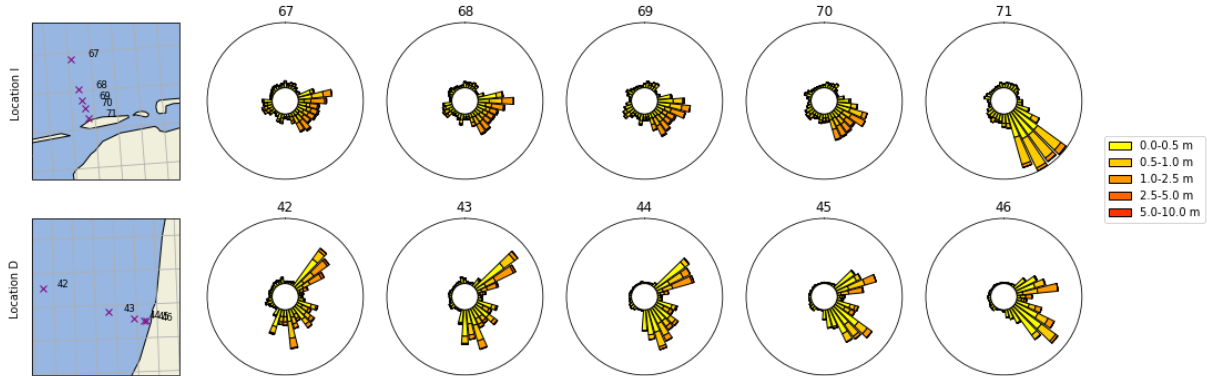

Figure 43: Wave rose for various locations along the Dutch coast. The bars describe the number of occurrences of wave heights in the direction of the bar within the 43.849 considered spectrums. The bars are also relatable to the frequency and probability of occurrence. The significant wave height in each bar is based on the energy of the wave partitions within the directional boundaries of the bar. The titles refer to the locations shown in the maps on the right side, at cross-sections D and I.

The wave trains at location 67 have a wave height between 1.0 and 2.5 and are mainly propagating towards the east, slightly northwards, and to the southwest. These waves can be described with different wave families, as shown in Figure 45. The wavefield at location 68 is similar but shows a deflection of the eastwards propagating waves towards the shoreline. The same trends can be found at locations 69 and 70. The significant wave height decreases to about 1 meter for many wave trains when they propagate towards location 71, which follows from the reduced occurrences of wave heights larger than 1 meter and the longer bars related to wave heights smaller than 0.5 meters and

between 0.5 and 1 meter. The reduced wave height might be related to depth-induced breaking from intermediate shallower water, but this requires further analysis of the bathymetry. The easterly propagating waves are also further deflected towards the shoreline, which reduces the distinction of the wave families. At location 42 are wave trains mainly propagating in a northeasterly direction, but waves to the south-east, south, and south-west can be recognized. The wave trains are deflected towards the shoreline, just as the waves at location/cross-section "I". The contribution of locally wind-generated waves at various locations is distinctive by their widespread propagation direction and height, which is usually smaller than 0.5m.

The interpretation of the results shows that wave partitions make it possible to analyze (significant) wave height statistics in the nearshore region, which has never been performed earlier. Compared to periodic averages, as performed in chapter 3, this analysis makes it possible to do a statistical analysis of the wave heights distribution of waves that have a propagation direction within certain limits. Smaller steps in significant wave height make it possible to do a more accurate statistical and extreme value analysis of wave heights.

4.4 Wave generation areas

Insight into the temporal variability of the wave trains and the wave generation area is obtained through temporal analysis of the wave partitions wherein wave families are formed, as explained in chapter 2.2.3. This section will elaborate on nearshore locations 33, 42, 57, and 69, shown in Figure 44, and the wave families at these locations, shown in Figure 45. An overview of the wave families at all the nearshore locations is added as appendix II.

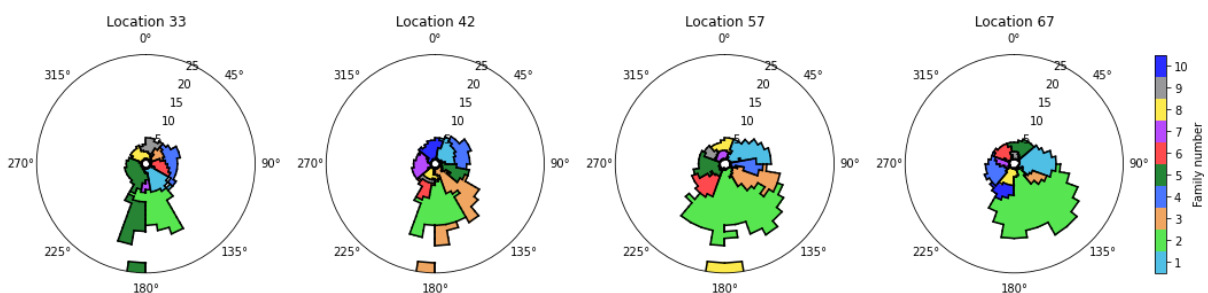Figure 44: Position of locations 33, 42, 57, and 67.

Figure 45: Wave families at locations 33, 42, 57, and 67, shown in Figure 44,with a depth of approximately 25 meters.

The wave families limit the propagation direction of the waves it describes. The traveled path of these waves can be traced back by considering the influences that the water depth gradients have on its path, called wave ray. For the most offshore located nearshore points, at a depth of more than 25 meters, it is assumed that the effect of the bathymetry on wave propagation is neglectable. Therefore, the propagation of all the waves is along great-circular paths around the globe. The waves captured by the wave family can be generated along the wave ray up to the point that this wave ray intersects a shoreline since landmasses block the wave propagation.

The wave rays for all the families at locations 33, 42, 57, and 67 are shown in Figure 46. Here is visible that wave family 2 at location 42 describes southerly propagating waves. The direction is between 200° and 150° and most of the time towards 180°, as shown in Figure 45 and Figure 11. The corresponding wave ray in Figure 46 shows that the waves traveled along the coast of Norway. Most wave families describe locally generated waves since most of the wave rays cross shorelines around the North Sea basin. So are waves of wave family 3 at location 42 generated at the northern part of Great Britain, those of wave family 4 at the southern part, and the waves corresponding to wave families 6, 8, and 9 are generated around the northern tip of Denmark. Furthermore, waves through the English Channel can be recognized by wave families 3 and 1 at locations 33 and 42.

Similar agreements at other locations can be found along the North Sea, where wave families of the four nearshore locations seem to have their origin in more or less the same area. This similarity gives the impression that there might be a relation between the wave families at the various locations. Chapters 4.5 and 4.6 elaborate on this relation between wave families.
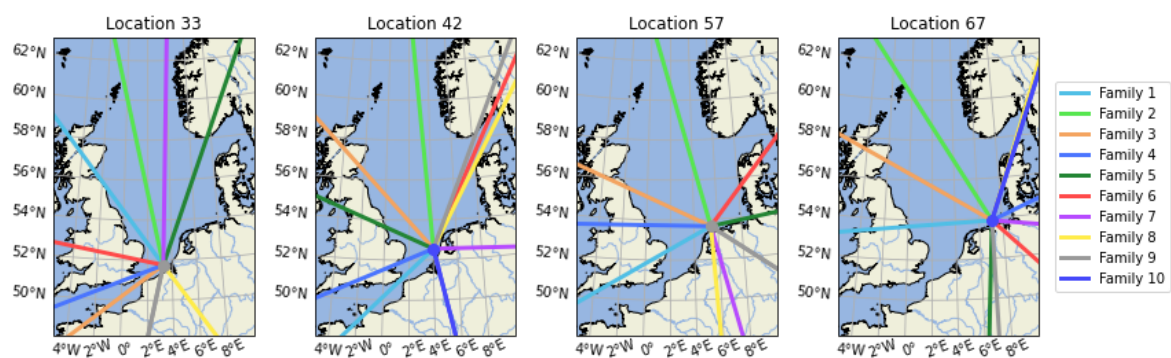

Figure 46: Wave rays of families at locations 33, 42, 57, and 67.

4.5 Temporal variability of wave systems described by wave families

The temporal variability of wave families gives insight into the temporal variability of the wave trains, or rather wave systems. Wave families do not consider the energy of an individual wave train but all the wave energy related to the wave trains inside its domain, as explained in chapter 2.2.3.

The energy of the wave systems is related to the characteristics of the wind-generating wave field and the fetch length. Waves that are generated in the same region might show similar trends in the wave energy. This wave area has been related to the statistical distribution of offshore wave height, but this analysis has never been performed on nearshore data.

This section will perform a short temporal and spatial analysis of the wave energy captured by wave families at location 42, shown in Figure 44. The temporal analysis consists of an investigation of seasonal trends in periodic averages, which have been found in the results of chapter 3.5, and statistical analysis of the wave energy described through a significant wave height. The monthly averages are depicted in Figure 47 and Figure 48, and the statistical analysis of wave heights of wave family 3 is in Figure 49 and Figure 50.
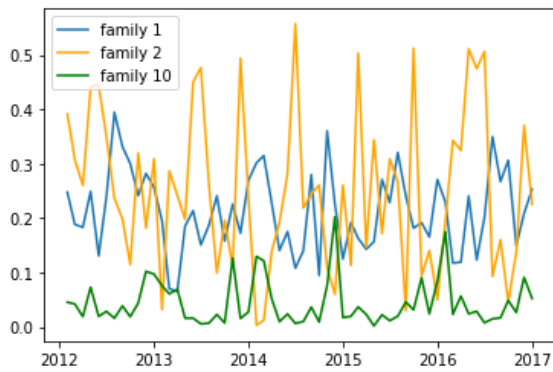
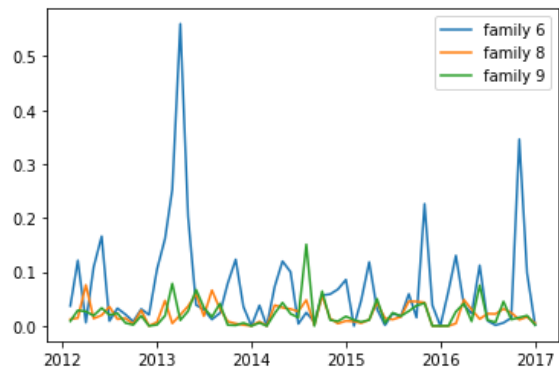Figure 47: Monthly mean of energy of three families at location 42 with different characteristics

Figure 48: Monthly mean of energy of three families at location 42 with a similar wave propagation direction

Trends by periodic averages

The results in Figure 47 show that the wave system described by wave family 1 has more energy than wave family 10. The lower wave energy could be due to the short fetch (length) at which the waves can obtain wind energy and grow. The waves related to family 1 could get the energy of wind blowing through the English Channel and the southern part of the North Sea, while family 10 has a limited fetch and can only get energy from offshore wind, as shown in Figure 46.

Figure 47 shows that the wave heights of wave systems are independent when the waves are propagating from different angles. The peaks in wave height of wave families 1 and 2 alternate over time, so is the wave height of wave family 2 relatively large and family 1 near average during the summer of 2013, 2014, and 2016. Furthermore, sharp peaks in the energy of family 2 can be found, which might be related to windy conditions in the north. The energy is low during the year transition, which might indicate some relation to the seasons. However, the weather conditions might vary over the months, and no hard conclusions can be drawn. Chapter 6 will elaborate on the weather conditions and the corresponding waves.

Some wave families are related to the same forcing conditions, like families 6, 8, and 9. The area that influences the wave spectrum is the same for these families. This similarity allows merging these families into one "large" wave family to analyze wave generation on the east side of the North Sea. The main difference between these families is the wave period, so the wave families might give insight into the impact of varying forcing conditions on wave periods. However, in this case, no hard conclusions can be drawn from the wave energy captured by the wave families.

Statistical analysis of the wave height in family 3

The wave families can be used for the temporal analysis of wave height, from which the results are depicted in Figure 49 and Figure 50. The wave family has relatively a lot of times no energy and thus a wave height of zero since wave families only have energy when at least one partition has its energy peak within the boundaries of the family. The distribution of wave heights with and without a threshold of 0 energy is depicted in Figure 49 and Figure 50.

The difference in the left bar of the two graphs shows that the wave family does not contain any energy about 68% of the time. The other bars give insight into the wave height variability, as long as the energy peak is within the boundaries of the wave families. Here is visible that the wave height is most of the time 0.2 to 0.3 meters. The probability decreases when the wave height increases, which can go up to 2.0 m. Merging wave families will reduce the number of occasions where waves from one area are outside the boundaries of the wave family and might thereby help analyze the distribution of wave heights of waves related to one wave system's energy. Possibilities in this grouping will be analyzed in the upcoming subchapter.
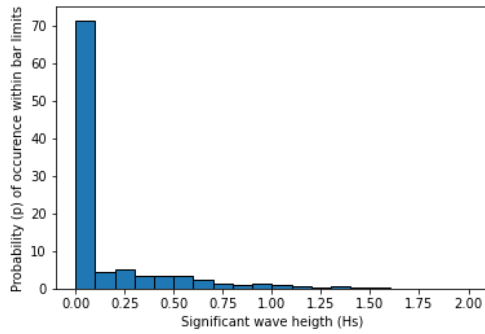
Figure 49: Probability of significant wave height of wave family 3. The wave height is based on the energy captured with this family and includes cases with no energy.
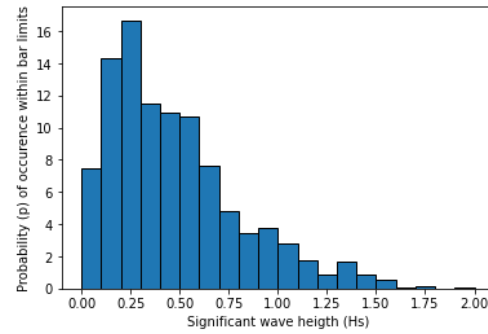

Figure 50: Probability of significant wave height in wave family 3. The wave height is based on the energy captured with this family and only considers conditions with wave energy, so a threshold of $0 \ m^2/s$.

4.6 Spatial relation of wave families

Wave families are determined at each location separately by counting the locations of the energy peaks in the spectrum. So there is no relation between wave family numbers at adjacent locations. It would be beneficial to have some insight into the spatial variability and relations of the wave families since it will give insight into the spatial extent and influence of waves related to one wave system. It is time-consuming to manually analyze the relations between the wave families at all the locations, so the preference goes to an automated process to match similar wave families.

The kmean algorithm, explained in chapter 2.6.1, has been applied to check if it can merge wave families in the nearshore region into a specific number of so-called (wave) family clusters. The expectation is that more detailed information will be obtained when more different groups are formed. Here is probably an upper limit, where too many groups will lead to unnecessary separation of wave families and will diminish the goal of combining the wave families. The expectation is that the considered area impacts the results. When only a small area is considered, only waves from a specific direction can influence the wave spectrum. The number of relevant wave systems is less than for cases where a larger domain is considered. Therefore, the grouping has been done for all the nearshore locations at once and for individual cross-sections only.

The result gives insight into the wavefield transformation when the waves are affected by nearshore processes, like refraction. Although the waves do not reach the other locations in the cross-section, the expectation is that the wavefield at adjacent shorelines is similar, with only a minor change in shoreline orientation and the corresponding change in wave propagation. So the wave family clusters can give an overview of the surrounding wavefield and help analyze the depth-induced changes on the wavefield.

The outcome of the kmean algorithm cluster depends on the definition of the mathematical space and the data itself. When similar situations are grouped over time, the mathematical space is described with the parameters, called features, of the data, as explained in chapter 2.6.2 and applied in chapter 5. Another definition of the mathematical space is used for clustering wherein the similarity in time is also crucial. Here the axis, or features, of the space are defined for each parameter at each time interval. This means that for clustering the wave families, axis 1 is the energy at time 1, axis 2 is the energy at time 2, etcetera. The data points in this mathematical space are the 10 wave families at each location, which are 50 points when 5 locations are considered. When a particular event occurs, all the wave families related to this forcing gain energy and will be closer to each other in the mathematical space than families that are not related since they gain no energy from this event. The data in the mathematical space that is closer to each other will be grouped together, and thus the wave families that are impacted by the same events.

4.6.1 Grouping wave families in one cross-section

The original wave families and the result after grouping for location D are depicted in Figure 51 and Figure 52. The family cluster describes waves propagating from the same direction at various locations. So do the wave family clusters distinguish the southerly propagating swell waves from the coast of Norway and the northeast of Great Britain, easterly propagating wind-generated waves, and low energy wind-generated waves that propagate in all directions in family cluster 1.

At location 42 is a distinction made between the swell waves from Norway, cluster 3, and from Great Britain, cluster 5. The propagation direction changes due to refraction towards are more shore normal direction. The nearshore processes reduce the distinction of the southerly propagating waves and will form one group of waves. The wind-generated waves from southern Great Britain, family clusters 2 and 4, initially have a slightly northward direction and are deflected towards the south when they propagate towards the shoreline. The focusing of wave energy of the southerly propagating swell waves and the refraction of the wind-generated waves was already recognizable in Figure 28.
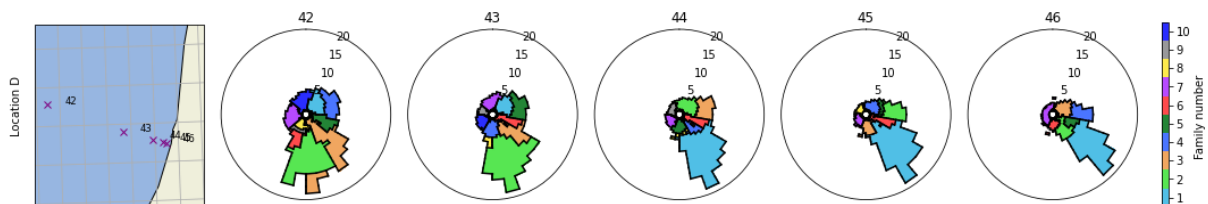

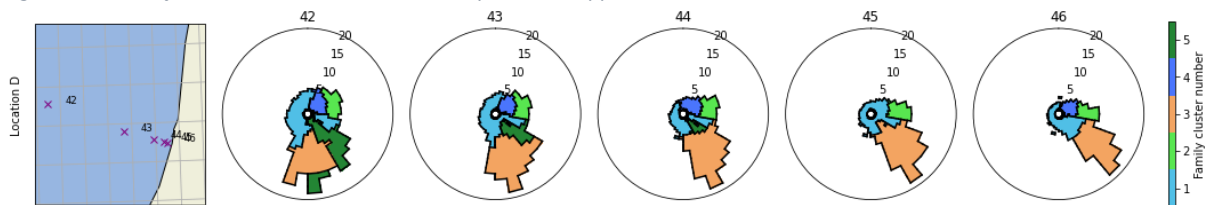Figure 51: Wave families at location D, the wave period is capped at 22 seconds

Figure 52: Wave family clusters, the result of kmean clustering of wave families at location D, the wave period is capped at 22 seconds.

4.6.2 Grouping wave families in all the locations

The results of doing all the nearshore locations in the grouping operation are depicted in appendix III. The results related to cross-section D are depicted in Figure 53.

This figure shows that when only 3 family clusters are formed, family cluster 3 at location 42 describes southerly propagating waves, with periods longer than 10 seconds. Family cluster 2 describes short perioded waves in all directions and south-westerly propagating waves. Family cluster 1 describes north easterly propagating waves. The family clusters at locations 43 and 44 describe almost the same distinction. The main difference is that family cluster 2 only describes short-perioded waves and not long-perioded ones to the southeast. These are captured by family cluster 3. So at location 43 a distinction is made between short perioded waves in all directions, south easterly propagating waves, and easterly propagating waves. These wave systems are also described at location 45. At location 46 are family clusters 2 and 3 combined into one family cluster. When comparing the wave system described with family cluster 3 at the various locations than is visible that shows the impact of nearshore processes, like refraction, on the wave propagation direction.

A similar distinction in family clusters can be recognized when comparing the outcomes of forming 3 family clusters to 4 family clusters. The main difference at location 42 is that family cluster 2 with 3 family clusters is divided into family clusters 1 and 2 when 4 clusters are applied. Family cluster 1 and 2 do at locations 43, 44, and 45 describes the same families similarly as family cluster 2 has done when 3 family clusters are formed. The results for 3 and 4 family clusters are the same at location 46. The only difference is its label, thus the family cluster number.

Applying 5 wave family clusters result in more distinction of short waves, although the division between family cluster 2 and 5 is quite complex at location 42. The division of the easterly propagating waves, with family clusters 3 and 5 can indicate that wave trains with different periods are occurring at different times. The fact that family cluster 3 describes south westerly and short perioded easterly waves at locations 42 to 44 might indicate a relation between waves, but this might also be a coincidence that the corresponding families have energy at the same time.

The independence of these wave families is shown by applying 10 family clusters at locations 42 and 43. The energy described by the wave families at these locations shows similar patterns and results in a similar description of wave clusters at these locations. However, there seem to be some inconsistencies along this cross-section when 10 family clusters are formed. So does family cluster 3 mainly describe short period waves in changing directions, and does family cluster 7 describe easterly propagating waves at location 44, while this is described with family cluster 8 at the other locations in this cross-section. These inconsistencies, where different family cluster numbers describe the same families, can also be found in the various locations along the coast.
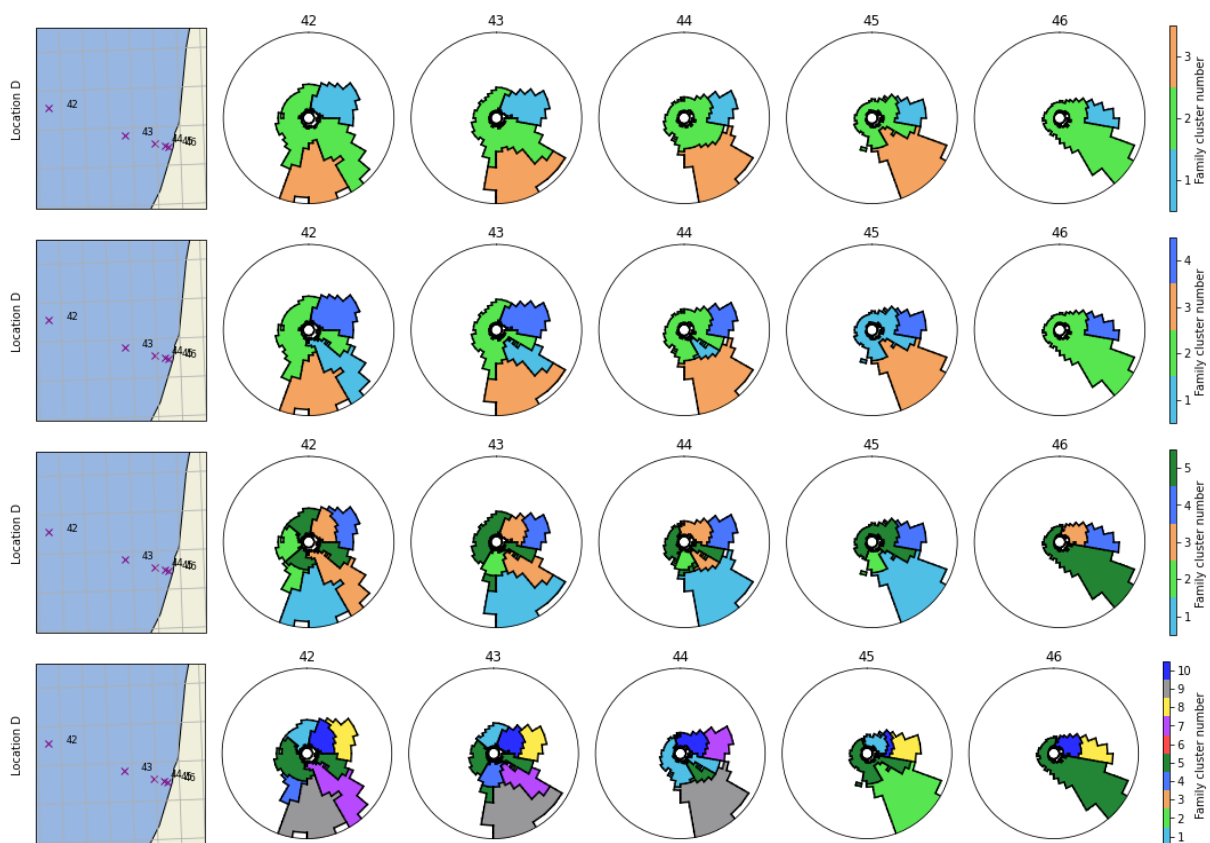

Figure 53: Wave family clusters at cross-section D for various grouping operations where all the nearshore locations are considered. This is a part of the total result, which is depicted in appendix III. Each row is related to another clustering operation, where 3, 4, 5, or 10 family clusters are formed. The number of family clusters that are formed is depicted in the legend. The titles on the figures relate to the locations depicted on the maps on the right. The radius is the wave period, which is capped at 15 seconds.

4.6.3 Applicability of family clusters

In the end, it can be concluded that family clusters give insight into the relations between wave families at various locations and might give insight into the temporal and spatial variability of the energy of the wave systems.

When too many family clusters are applied, the cluster number may switch at various locations. The varying definition of the family clusters and their direction reduce the insight gained from the clustering. Correcting the outcome by hand is work-intensive, especially if many locations are considered. So having too many family clusters reduce the insights y the clustering operation.

When fewer family clusters are made, the outcomes are consistent amongst the locations and may give insight into the energy of waves that are propagating in specific directions amongst the coast. However, the expectation is that, for example, 3 or 4 family clusters cannot distinguish the various wave systems that are occurring.

In chapter 5, various machine learning techniques are applied. Here is analyzed if these could give insight into the wavefield, with its temporal and spatial variability, and which conclusion can be made from their outcomes. Chapter 6 analyzes the relation between wave and weather conditions.

4.7 Wave energy by partitions and families

The wave families, or clusters, give insight into specific wave conditions but could have an error in the wave period and propagation direction, just as by implementing the significant wave height on the complete wave spectrum. Wave families and their clusters gain energy through the partitions that have their energy within their boundaries. The representative frequency and direction are related to the largest energy peak in the spectrum. So, once two or more partitions contribute energy to the same family, an error could be induced in the propagation direction, the representative period, or both. This subchapter elaborates on these situations and the impact of applying the wave partitions and wave families on the description of the wave field compared to traditional methods.

4.7.1 Error in the representative wave propagation direction, period, or both

An example of the error in the wave propagation direction, and its energy, is depicted in Figure 54. Here both partitions 1 and 3 contribute energy to wave family 4. The wave direction and period of partition 1 are normative since the energy of partition 1 is larger than that of partition 3. An error in the wave period is depicted in Figure 55, where partitions 2 and 3 contribute energy to family number 3. Here the energy peak characteristics of partition 2 are normative.

The expectation is that this error increases when the wave family or cluster in size increases since it gives more opportunity for two energy peaks to fall within the boundaries of the wave family or the cluster, and the magnitude of the error could also increase.
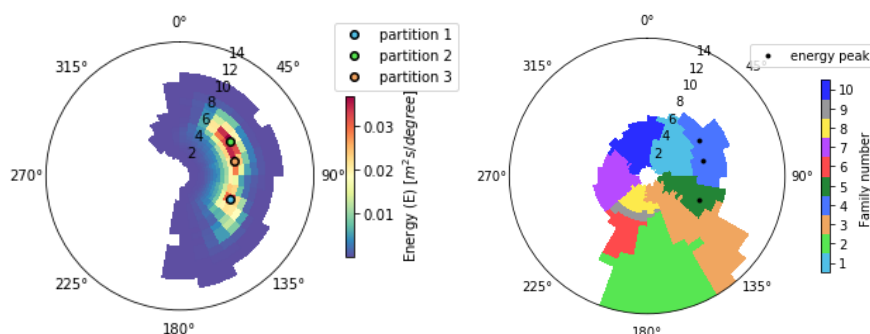

Figure 54: Change of energy/wave propagation direction when partitions contribute their energy to a wave family
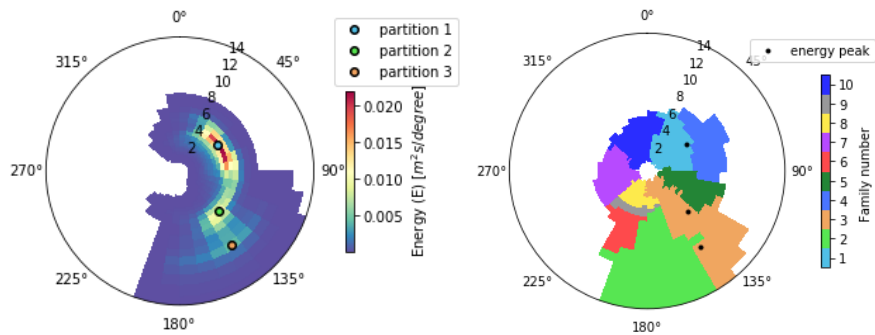
Figure 55: Change of wave period when partitions contribute their energy to a wave family

4.7.2 Wave rose according to different methods

The wave partitions and wave families are alternative solutions to traditional methods that use the significant wave height to describe the wavefield. The effect of parameterizing the wavefield with wave partitions and wave families, compared to the traditional methods, is depicted in Figure 56.

The largest difference between the traditional methods and the wave partitions and families is the occurrences of events and the wave height. The traditional method does not capture the various wave trains and combines the coexisting wave trains, resulting in larger waves and smaller bar lengths. The wave partitions and families show a similar wavefield. The wave families describe more waves between 1 and 2.5 meters and less between 0.5 and 1.0 meters, especially at location 71. The impact of the error on sediment transport is unknown but could be non-neglectable. The application of wave partitions and families in estimating sediment transport is explored in chapter 7.3.
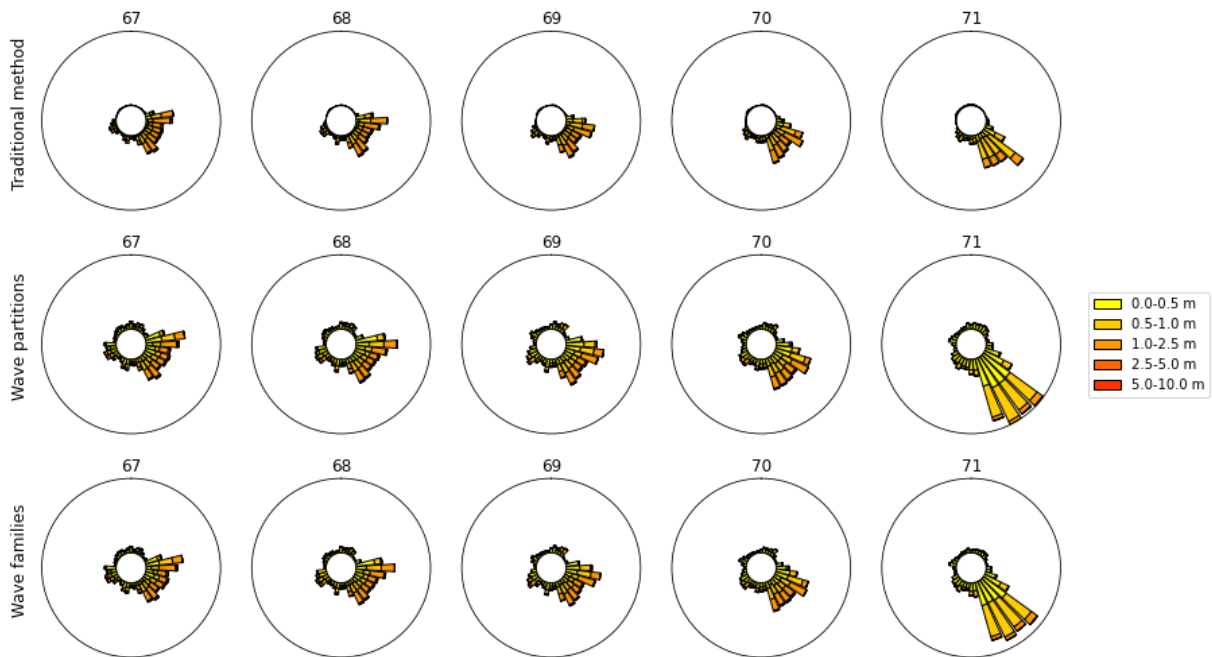

Figure 56: Wave rose along the cross-section described by the traditional method, wave partitions, and wave families. The bars describe the number of occurrences of wave heights in the direction of the bar within the 43.849 considered spectrums. The bars are also relatable to the frequency and probability of occurrence. The significant wave height in each bar is based on the energy of the wave partitions within the directional boundaries of the bar. The titles refer to the locations near Schiermonnikoog and are depicted in Figure 43.

4.8 General Discussion and Conclusion

This subchapter elaborates on the main discussion and conclusions of subchapters 4.2 to 4.7 to answer the two main research questions. In these subchapters are wave partitions and wave families used to analyze the wave field and sometimes compared to the traditional methods.

4.8.1 Discussion

The wave height distribution for each direction is different when one representative wave height by traditional methods, wave partitions, and wave families are used to describe the waves. The wave families and the traditional method are probably less suitable to describe wave height statistics of wave trains due to the combination of wave energy. The impact on sediment transport is unknown but might be considerable.

The kmeans clustering has been used to relate wave families at the same and other locations to so-called wave family clusters. Less wave family clusters gives more consistent result but might not be able to make sufficient distinction between the various occurring wave systems.

4.8.2 Conclusion

The wind-generated waves frequently coexist and can travel in various directions simultaneously. The wave trains can travel in the same direction, but crossing and opposing waves also occur frequently.

The wave families are used to track wave trains across the North Sea and in nearshore regions. They show that waves are generated at various locations in the North Sea, such as Great Britain and east of Denmark, which corresponds with the conclusions that are made in chapter 3.

Wave partitions are capable of describing the wave trains that are simultaneously occurring. The distribution of the wave heights and their propagation direction, shown with a wave rose, varies with that of wave families and wave partitions. The main reason for this is that wave families, and the traditional method combines the energy of coexisting wave trains, and this combined energy is used to describe the (significant) wave height statistics.

Wave families are used to describing the wave height of the wave trains related to one wave system. It gives thereby insight into the statistical distribution of wave trains that are more or less propagating in the same direction and prevents the division of wave trains amongst two bars in the wave rose, which uses strict and not physically related divisions in the wave propagation direction.

The wave families have been used to find seasonal trends in the wave energy flux by averaging their energy monthly. However, no seasonal trends could be recognized, and consequently, no insights into the forcing weather condition could be retrieved.

Wave families at various have been grouped together to see if this gives the possibility to analyze spatial relations between the wave families. The conclusion is that grouping allows analyzing the wave transformation in small spatial domains, such as cross-sections at the coast. Spatial influences affect the grouping of the wave families when the spatial domain of interest increases. This complicates the result and reduces the simplification, which is the goal. Another conclusion is that the outcomes are mostly consistent when few groups are made.

5 Spatial-temporal wave analysis

An analysis covering both the spatial and temporal aspects of the data can be used to analyze complex structures and trends in multidimensional data. This usually computational analysis can link events, or forcing conditions, with their consequences in spatial extent and variation over time.

5.1 The approach

This chapter applies a more complex approach to analyzing the offshore and nearshore spectral data than Chapter 4. The main goal of this chapter is to group similar wavefields that are occurring over time. Statistics of each group are used to get additional insight into the complex wavefield and its statistics. For this analysis is the offshore and nearshore spectral data used from 2012 to 2017 with a 6-hour resolution. The 5 years of data resulted in 7308 wave spectrums at each location.

The first technique that is used in this chapter is Principal Component Analysis (PCA), where the data is described in fewer independent wave parameters called Principal Components, as explained in chapter 2.6.2. How much information each parameter captures of the data is analyzed in chapter 5.2.1. The newly formed parameters might have a physical meaning. If and what this meaning is will also be analyzed in chapter 5.2.2 and 5.2.3. The meaning of these parameters will be verified in Chapter 5.5.2 and substantiated in 6.5, where it is related to weather data.

The second technique that is used is Maximum Dissimilarity Analysis (MDA), as explained in chapter 2.6.3. By applying this technique, the relative part of frequently occurring situations is reduced. The expectation is that rare events have a larger impact on grouping similar wavefields when more frequently occurring situations are not considered during the formation of the groups. After the groups are formed, neglected data will be assigned to their most relevant group. Chapter 5.3 will elaborate on the subsets formed by Maximum Dissimilarity Analysis.

Chapter 5.4 elaborates on the grouping procedure with the kmean algorithm, as explained in chapter 2.6.1. The optimal number of groups to classify the data are determined through the Elbow method and the Silhouette Coefficient. After that, similar wave spectrums are grouped over time, so each group consists of spectral data that is occurring at one or more specific times. The results are analyzed for the original dataset and four subsets created by Maximum Dissimilarity Analysis. The impact of reducing the number of frequently occurring events is analyzed in chapter 5.4.4. Based on this analysis, a decision is made on the optimal number of points that is used in the grouping operation for this study.

The physical interpretation of each group formed with the kmean algorithm is a Sea State. The Sea States can be visualized through a representative wave frequency-directional spectrum at each location. The statistics of the wave spectral data that is attributed to each Sea State can be used for further analysis, which includes statistics about Principal Components, wave partitions, and wave families, as described in chapter 5.5.

5.2 Defining new parameters to describe the data (PCA)

This section elaborates on the outcome of applying Principal Component Analysis on the standardized offshore and nearshore spectral data, with a resolution of 6 hours. The first subchapter will focus on the general properties of the Principal Components and the possibility of reducing the number of Principal Components for further analysis. The subsequent subchapters will elaborate on the temporal and then spatial characteristics of the Principal Components. Each subchapter ends with an intermediate discussion and conclusion.

5.2.1 Data captured with Principal Components

The wave spectrum at each offshore location is described by 30 frequencies and 24 directions. The 27 locations result in 19.440 parameters that describe the wavefield in the north sea at any time. The nearshore data, generated by SWAN, contains 42 locations in which the wave spectrum has been discretized into 36 frequencies and 36 directions and can therefore be described with 54.432 parameters, resulting in 73.872 parameters, that have 539.856.576 values for 7308 samples over time.

The Principal Component Analysis is used to describe the data with new uncorrelated parameters, called Principal Components, as described in chapter 2.6.2. The amount of information each Principal Component describes is expressed by the variance and thus spreading or standard deviation of its data. This knowledge can be used to reduce the number of parameters for further analysis. Reducing the number of parameters can considerably reduce the computational demands and time of the machine learning techniques.

The amount of variance that the Principal components capture is depicted in Figure 57 and Figure 58. Here is visible that the majority of the information can be described with relatively a few Principal Components. So do the two largest Principal Components together capture 30% of the variance, and can 95% of the variance be described with 263 Principal Components. The low values and the flat 'tail' around the 263rd Principal Components indicate that the variance captured by Principal Component 264 and higher is very minor.
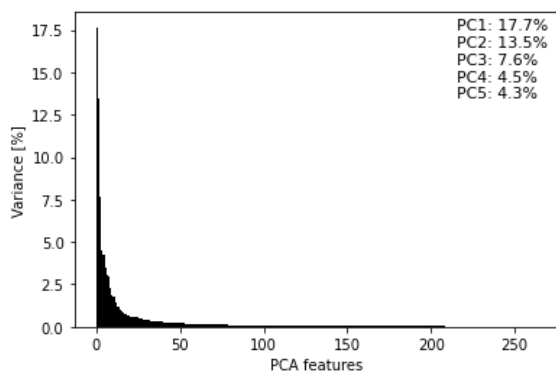

Figure 57: Variance captured by each Principal Component, representing both the offshore and nearshore data
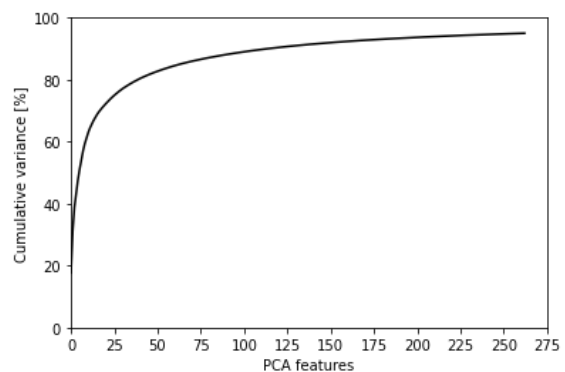
Figure 58: The considered cumulative amount of variance when a specific number of the most important Principal Components are used

For further study is chosen to use the 263 largest Principal Components, which capture 95% of the variance. Increasing the number of Principal Components will barely result in an increase in variance. However, it will significantly increase the number of parameters and, consequently, increase the computationally demands and time of machine learning techniques Maximum Dissimilarity Analysis and the kmean algorithm applied in chapters 5.3 and 5.4.

5.2.2 Temporal statistics of Principal Components

The Principal Components describe both the temporal the spatial patterns of the data. This section elaborates on the temporal analysis of the data, which are the values of the data projected on the new axis described by Principal Components, as described and visualized in chapter 2.6.2.

The time series of four Principal Components and running averages are depicted in Figure 59. Here is visible that Principal Component 1 varies a lot over time and that there are no significant peaks, which is in contrast to Principal Components 3 and 4. The influence described with the Principal Components varies over seasons, as depicted in Figure 60 and Figure 61. Here should be taken into account that the error could be relatively large since only five years of data is considered. This error holds for Principal Component 1, where a yearly pattern could be recognized with lower values around march. However, the periodic averaged patterns in Figure 59 are very irregular for Principal Component 1, especially compared to Principal Component 3. So has Principal Component had a relatively low average value in early 2013 while these were high at the beginning of 2014.

The values along the Principal Components are based on standardized data, where positive values indicate that the parameters are above average and negative values indicate below average. A similar conclusion can be made for the values of the Principal Components, where its average is near zero, and the standard deviation is a few orders larger.

When the same temporal patterns arise for more years of data, it can be concluded that Principal Component 1 is related to a yearly process that has the most impact during March and then slowly changes until December, where it has another limit. Principal Component 2 has its peak during the summer, and Principal Component 3 in August. Principal Component 4 follows a similar trend as Principal Component 2 but has less impact on average, which is recognizable by its milder averages.
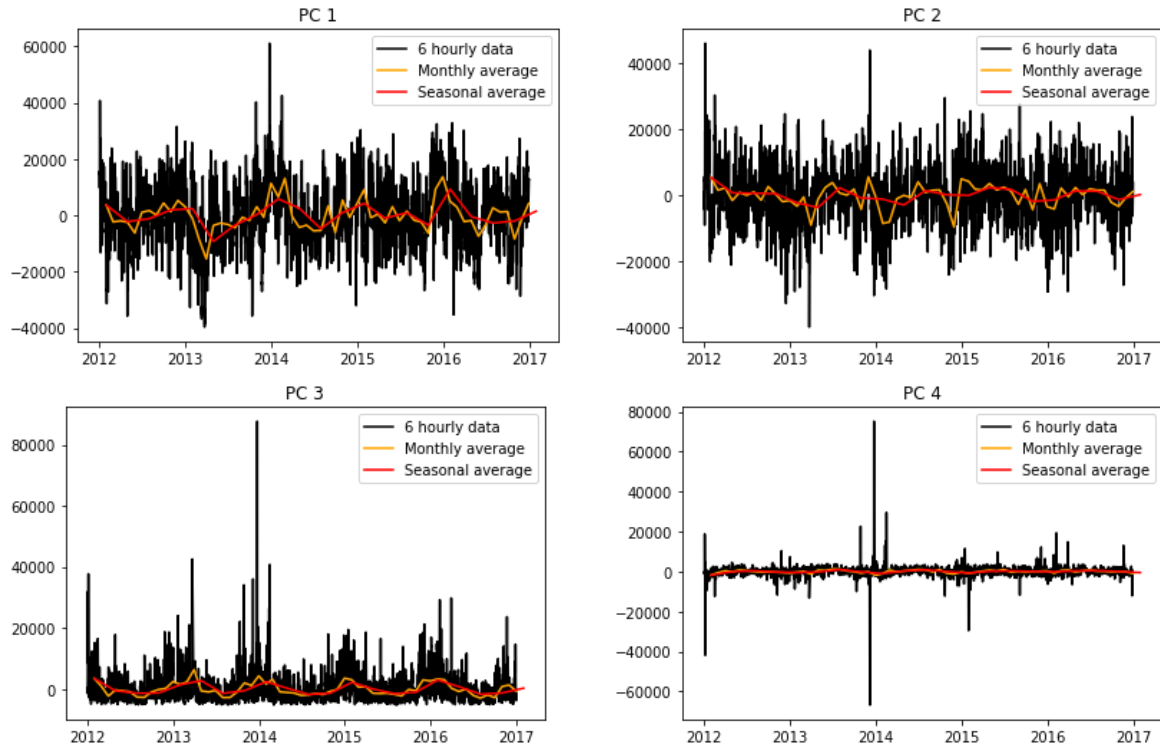

Figure 59:Time series of loads of Principal Components (PC) 1 to 4, indicated by the number in the title. The horizontal axis is the time in years. The yellow and redline are running averages of the raw data, both considering time data in the past as the future.
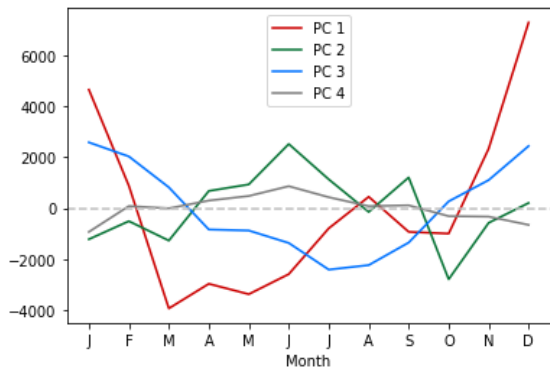
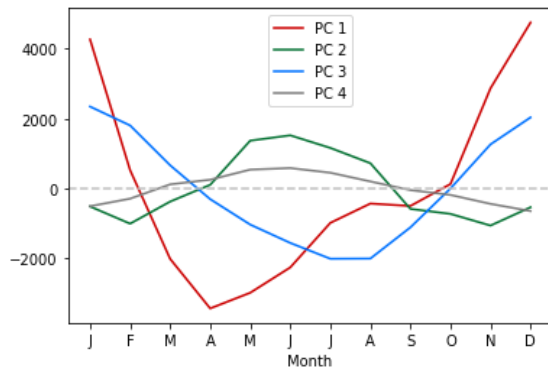Figure 60: Monthly mean of the loads of Principal Components (PC) 1 to 4.

Figure 61: Running average over three months of the loads of Principal Components 1 to 4. The mean is the average over the previous, current, and coming months.

The results indicate that each Principal Component is probably related to different forcing conditions or physical processes. The expectation is that Principal Component 1 is related to large-scale processes that are relatively slow evolving, while higher numbers of Principal Components become more related to smaller processes or rare conditions that are recognizable by the temporal peaks in Figure 59.

Insight into the temporal characteristics of the Principal Components might be helpful for further analysis where relations between weather, waves, and sediment transport are established.

5.2.3 Spatial statistics related to Principal Component Analysis

The spatial description of the Principal Components can be analyzed by the relation with the elements of the eigenvector. Here each frequency-directional bin of the wave spectrum at each specific location is described with one or probably multiple Principal Components. So, the values of the elements in the eigenvalue can be given a physical meaning. Here positive values indicate that the elements are in the same direction as the eigenvector, and negative values will have the opposite impact. The impact of the eigenvectors can be compared to each other by scaling it with its standard deviation, thereby forming a so-called load.

When all the 73.872 parameters are projected on the Principal Component, a new map can be generated, which does not show the original frequency-directional spectrum at each location but the impact of a Principal Component on the energy on each wave frequency and direction. Since all the Principal Components are based on wave energy, the expectation is that the Principal Components describe the impact on wave energy. Where high values of wave energy would lead to high values of Principal Components, following Figure 14, this means that high values of Principal Components might indicate more wave energy. One small remark is that when the eigenvector is rotated 180 degrees, the meaning of the eigenvector will be opposite, so caution is advised when conclusions are made.

In Figure 62 and Figure 63 are the scaled eigenvectors for the most contributing Principal Components for one offshore and one nearshore location depicted. When the philosophy mentioned above is applied, then positive values of Principal Component 1 describe waves that are more energetic while they propagate towards the North East and less energetic to the southwest. The opposite holds for situations where Principal Component 1 is negative. Then the energy flux is towards the higher to the southwest and lower to the northeast. A similar effect is described with Principal Component 2, which describes the energy of waves propagating towards the southwest if the value is positive. The higher Principal Components show smaller scale patterns. So does Principal Component 4 show positive and negative values at the low and high frequencies, which might be related to the transition of wave energy between long and short perioded waves.
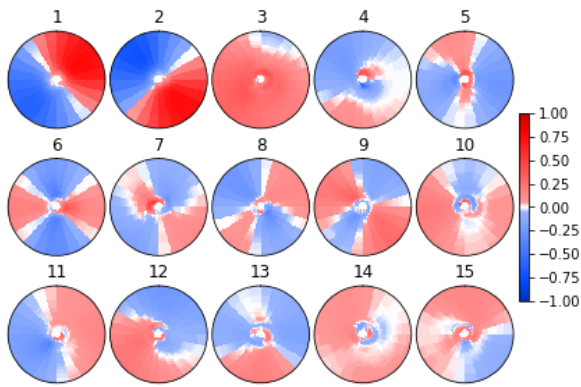
Figure 62: Overview of the loads of the most important Principal Components at one offshore location, at the 55th latitude and 3rd longitude.
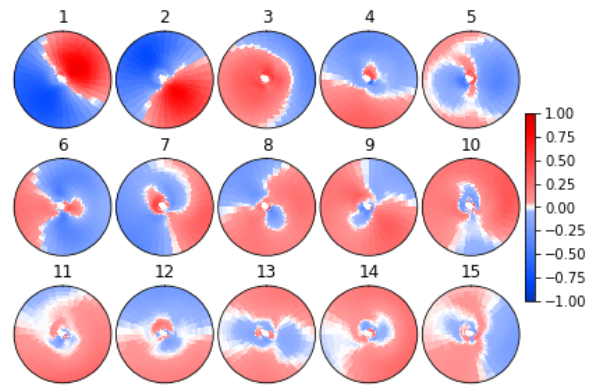
Figure 63: Overview of loads of the most important Principal Components at nearshore location 52.

The results for Principal Component 1 and the offshore locations are depicted in Figure 64. In appendix II are the four most contributing Principal Components depicted at all the offshore and nearshore locations. When comparing the locations, it is visible that the Principal Components describe similar information at all the locations. The values are positive in the northeast wards direction and negative in the southwest direction. Small scale changes can be found between the locations. The orientation of the positive and negative values changes when the data along longitude 1 are compared. At latitude 55 are the positive values orientated towards the east, which changes towards the north for the lower latitudes. Furthermore, no large differences in the loads can be distinct. The magnitude of the loads is at most locations between approximately -1 to 1. The magnitude of the load is slightly smaller at longitude 0 at latitude 55.

Based on these spatial trends, it is very likely that there are indeed spatial relations between the various locations. When the Principal Component describes wave energy, Principal Component 1 describes north easterly propagating waves that are more northward orientated at the southern part of the North Sea and eastwards north of the Netherlands. The lower loads at longitude 0 and latitude 55 would mean that the wave energy, en thus wave height, near the coast of Great Britain is smaller at other locations if the wave spectrum is mainly described with Principal Component 1.
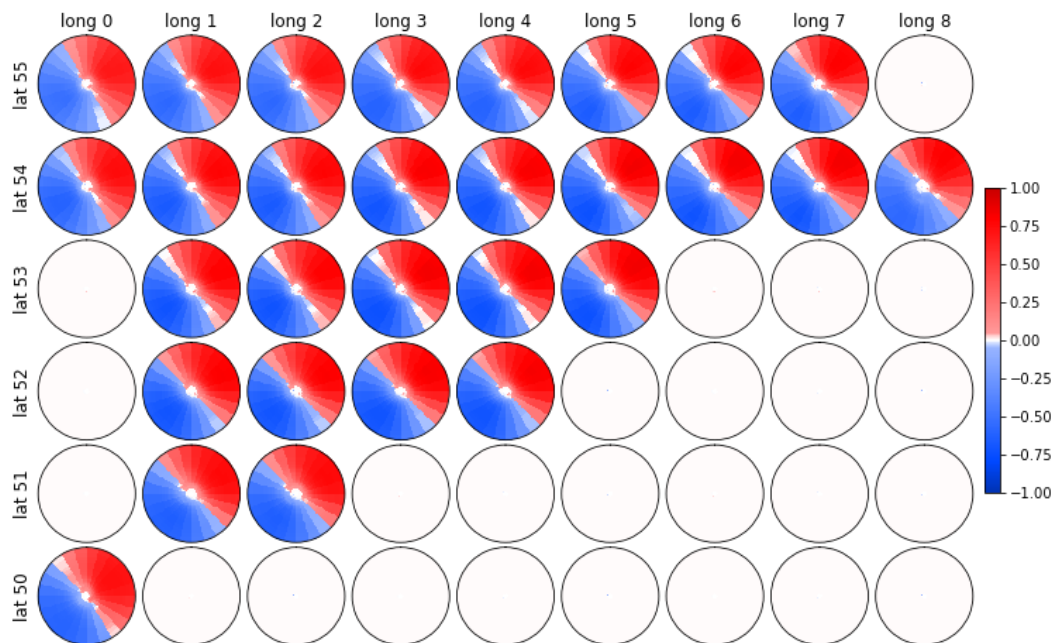

Figure 64: Principal Component 1 at offshore locations for various latitudinal (lat) and longitudinal (long) coordinates.

The conclusions that can be made by the spatial analysis show that, probably, Principal Components describe wave energy at the considered locations. Positive values might indicate more wave energy within certain frequency-directional bins. All the Principal Components together describe the original wave frequency-directional spectrum. Here, the Principal Components that capture the most variance describe more large-scale impacts on the wave spectrum, like north easterly or south easterly propagating waves. The higher Principal Components capture less variance and describe the impact on a more detailed level on the wave spectrum.

Chapter 5.4.2 will validate the physical meaning of the Principal Components and the contribution of each Principal Component to the description of each wave spectrum. The similarity of the wave propagation direction and height of spectral data within each Sea State should result in similar values of the Principal Components, which will ease the analysis and its interpretation.

5.3 Feature rare events (MDA)

Maximum Dissimilarity Analysis is performed to flatten the density distribution of the data points inside the mathematical space that the Principal Components describe. This flattening is done by selecting a predefined number of points in which the sum of distances is maximized. The new and smaller dataset contains fewer points in the area that initially had a higher density, so the relative part of the rare events in the area with a low density is more represented in the reduced dataset.

Figure 65 shows the distribution of data points on the first two Principal Components for the original and by MDA reduced datasets, which are named to the size of the remaining points. The original dataset had 7308 wave spectrums and is represented by 7308 points. The gaps in the red dotted area and the change in histograms indicate that the points are initially removed in the center of the data, where the density of points is the highest. The reduction of the point in the center increases the probability that the remaining points lie in the lower and upper tail of the histogram. The peaks of the distribution in Principal Components 1 and 2 are flattened out when the reduced dataset has a size of 2000 points. Moreover, when the dataset becomes smaller than 500 points, the tails of the graph become prominent in the distribution.

The whole dataset will be used in the clustering process, not only the reduced dataset. The reduced dataset will be used in the iterative process that assigns data to the closest centroids and relocates these centroids to a representative location of the cluster. When the groups are formed, the not considered data points, or time samples, are attributed to the group that fits best to their properties, which is the cluster related to the nearest centroid, as described in chapter 2.6.1.

So, with the application of Maximum Dissimilarity, five different clustering results will be made from the same original dataset. The main difference in the process is the number of data points considered in defining the groups. Chapter 5.4 elaborates on the clustering and the impact of applying Maximum Dissimilarity Analysis.
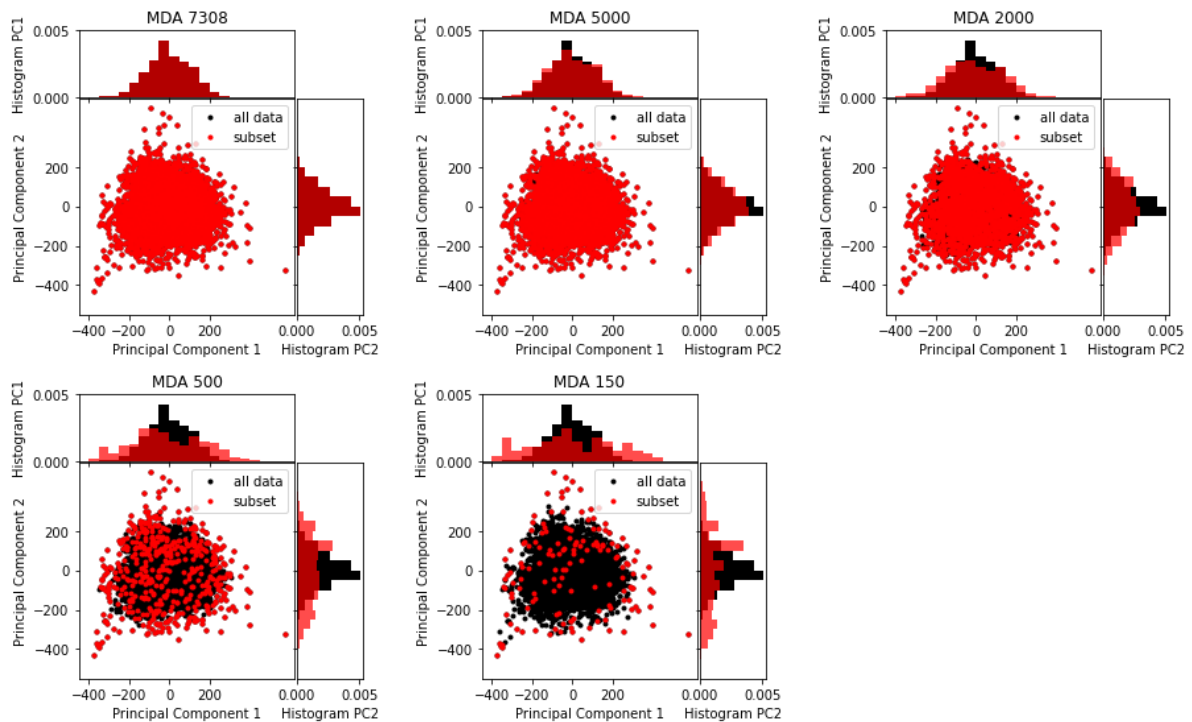
Figure 65: Applying Maximum Dissimilarity (MDA) to create datasets with sizes of 7308, 5000, 2000, 500, and 150 points, which are used in the titles. The data points over Principal Components 1 and 2 for each MDA are red-colored and visualized against the original dataset shown in black.

5.4 Formation of Sea States (kmean)

The kmean algorithm is used to group similar wavefields over time, wherein the wavefield is defined by a wave frequency-directional spectrum at all the nearshore and offshore locations. Each group that is formed describes one Sea State, which has a characteristic wave frequency-directional spectrum at each location.

This section elaborates on determining the most important input parameter in the kmean algorithm, which is the number of groups that are formed. After that, five different clustering operations are performed, each with a different subset generated by Maximum Dissimilarity Analysis. By comparing the results, the impact of Maximum Dissimiliartiy Analysis on outcomes of the kmean algorithm is analyzed. Chapter 5.4.4 concludes which clustering result gives the most useful results and will be used for further analysis. Chapter 5.5 will elaborate on the physical meaning and the application of this clustering outcome.

5.4.1 Choosing the ideal number of groups

The most important choice when applying the kmean clustering algorithm is the number of groups that are formed, which are usually called clusters. Here a trade-off has to be made between the accuracy of the classification and the workability of the outcomes. Increasing the number of clusters that are formed will increase the accuracy but requires more extensive post-analysis. The Elbow method and the Silhouette Coefficient are used to get insight into the required and optimal number of clusters to classify the data, as explained in chapter 2.6.1. The number of clusters depends on the characteristics of the dataset and might thus be affected by the subset that MDA forms.

The Elbow method calculates the sum of squared distance (SSE) between the data points and their centroids for all the groups. The optimal number of clusters is where the curvature of the line is the largest. The Silhouette coefficient is another tool to get insight into the optimal number of clusters. Positive values indicate spaces between clusters and negative values overlapping clusters. The ideal number of clusters is where the silhouette coefficient becomes zero.

The SSE for the datasets made by MDA is depicted in Figure 66. Here is visible that approximately 150 clusters are optimal to classify the data when both offshore and nearshore data are considered, independently of the results of various subsets by MDA. Increasing the number of clusters further does relatively a lot less efficiently decrease the SSE, while fewer clusters will increase SSE and thereby reduce the accuracy of the outcome.

The silhouette coefficient for applying a range of clusters in the kmean algorithm is depicted in Figure 67. It shows that the number of required clusters increases when the subset used in the kmean algorithm increases. When the entire dataset is used in the kmean algorithm, so MDA 7308, then more than 360 clusters are required to get a Silhouette coefficient near zero. A Silhouette Coefficient of zero can be achieved for MDA 5000 and MDA 2000 when applying 315 and 233 clusters.

The preferred number of clusters lies around 100, which gives a workable outcome. According to the Silhouette coefficient, the ideal number of clusters is higher than that estimated by the Elbow method.

The choice is made to reduce the number of clusters with the cost of some accuracy. The criteria for the preferred number of clusters are that number of the clusters should be around 100, that applying more clusters will lead to a deviation from zero, and no substantial gain in accuracy is obtained when relatively few more clusters are made. The results are depicted in Figure 67. Here is visible that the preference number of clusters lies between 125 and 180 clusters for clustering based on MDA 2000, 5000, and 7308.
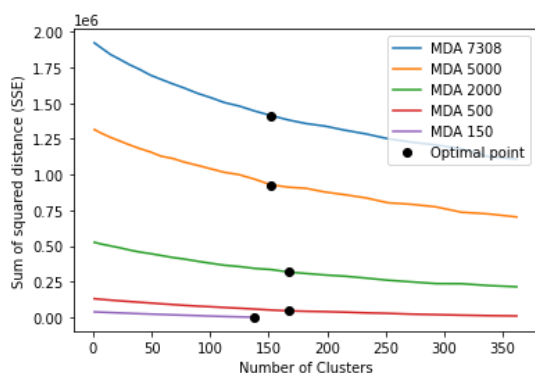

Figure 66: The Elbow Method applied to various datasets and a range of clusters.
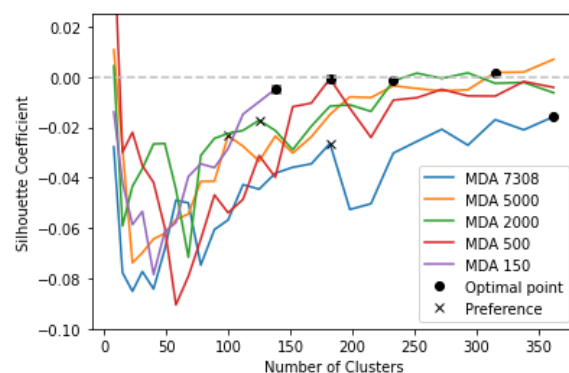
Figure 67: Silhouette coefficient determined for various datasets and a range of clusters.

5.4.2 The positioning and interpretation of clusters in the mathematical space

The distribution and positioning of the clusters in the mathematical space are used to get insight into the clustering results. The results for various subsets formed by MDA considered in the positioning of the centroids are depicted in Figure 68, where each cluster is projected on the first two Principal Components and depicted in a unique color. Although the same number of clusters are applied, the results are very different for each dataset.

Three main differences are found by comparing the outcomes of the clustering operation. Firstly, the results from MDA7308 give the impression that more clusters are formed than when a small subset is used in positioning the centroids. Another result is that the clusters based on MDA 7308 are positioned in a narrow space and that the size of the space increases when smaller subsets are used. This is related to a third observation, the position of the centroids is more located in low values of Principal Component 1 and 2 for clusters based on MDA 7308 than for clusters based on a smaller subset, where the centroids are more located on the outer edge of the cloud of data points. The coming paragraphs elaborate on the interpretation of these findings.

Many small clusters based on MDA 7308 can be recognized in the plane formed by Principal Components 1 and 2. The number of distinctive clusters seems to decrease in Figure 68 when smaller subsets are considered in the positioning of the centroids, which is not the case since this number is an input parameter. The main reason for this change is the change in the distribution of the cluster sizes. MDA 7308 will lead to many large clusters, while MDA 150 results in only a few clusters containing many data points and clusters with only a few data points. The distribution of cluster sizes is depicted in Figure 69.
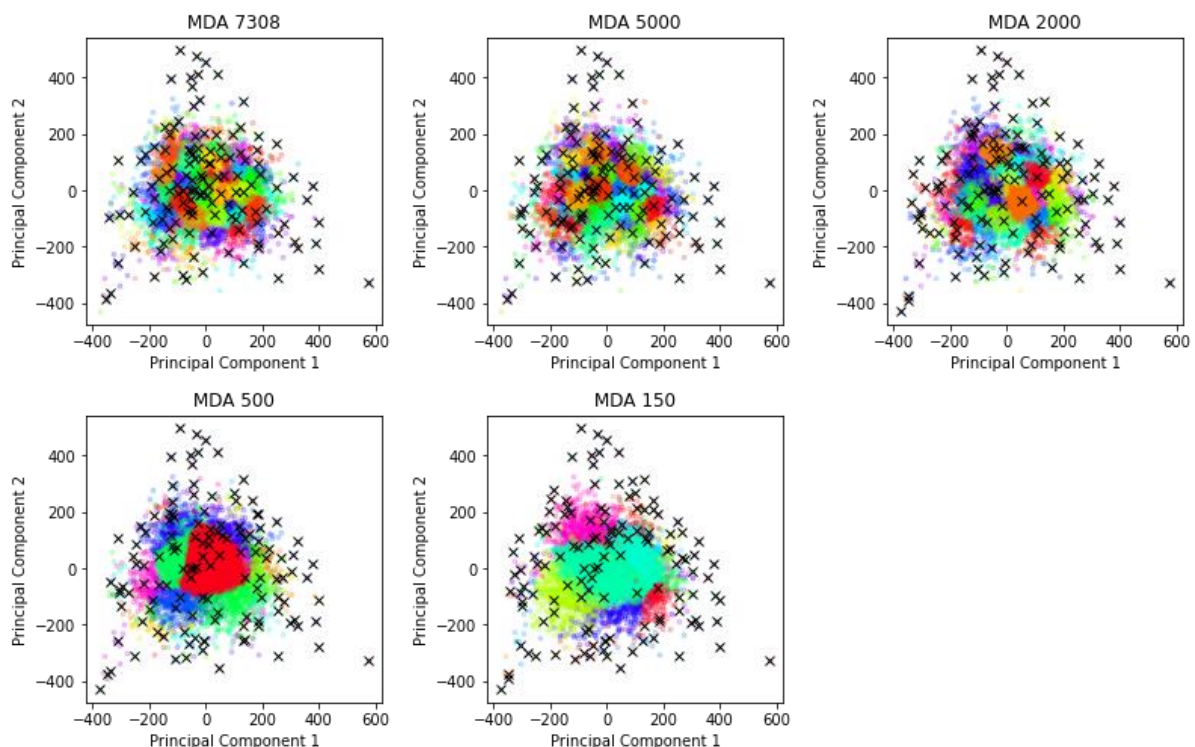

Figure 68: Applying the kmean algorithm to datasets of different sizes, which MDA creates. The centroids of the clusters are indicated with a black 'X'.

The formation of small clusters in the plane formed by Principal Components 1 and 2 for MDA 7308 indicates that these two parameters are dominant in the description of the clusters since each cluster describes a narrow banded combination of Principal Components 1 and 2. The structured division over Principal Component 1 and Principal Component becomes less apparent when the number of points used for positioning the centroids decreases. So the possible range of Principal Components 1 and 2 within a cluster increases for the largest clusters. In other words, the higher Principal Components have more effect on the clustering outcome when smaller subsets are used for positioning the centroids than when the whole dataset is used. Since the higher Principal Components are related to more detailed changes in the wave spectrum, the clusters made by smaller subsets focus more on smaller-scale processes than large-scale processes. This agrees with the predictions and arguments described in chapter 5.2.

The positioning of the centroids supports the conclusion that clusters describe more extreme events when the subset made by MDA decreases. The centroids are, just like the clusters, more or less equally divided over the plane formed by Principal Components 1 and 2 when all the data is used in the clustering. So many of these clusters have a relatively low value of Principal Components 1 and 2 and do therefore describe circumstances that with a low energy flux towards the north-east, south-west, south-east, or north-west, and thus describe relatively calm weather, which is less interesting for predicting sediment transport. Here the interest lies in events with energetic waves.

When the subset formed by MDA decreases, the clusters describe more frequently data points that lie on the extremes of Principal Components 1 and 2. In these subsets, groups of centroids can also be recognized that are not on the extremes of Principal Components 1 and 2. Here the influence of higher Principal Components can be recognized, which are all orthogonal to each other. The large variability of other Principal Components within that particular combination of Principal Components 1 and 2 causes the creation of clusters in a narrow region of the plane formed by Principal Components 1 and 2.

So, the distribution of the clusters and the positioning of the centroids indicate that clustering results based on MDA 7308 capture more nuance in mild energetic wave conditions, and the results with lower subsets capture more nuance in more energetic wave conditions.

5.4.3 General properties of the clusters based on various MDA

The subset used in the positioning of the centroids in the kmean clustering process affects the sizes of the formed clusters and the distribution of parameters within each cluster, as concluded in chapter 5.4.2. This section elaborates on the cluster sizes and the distribution of the representative significant wave height of each cluster.

Distribution of cluster sizes and total significant wave height

The number of clusters with a specific size is depicted in Figure 69. Here is visible that the number of clusters that have one event increases when the subset made by MDA decreases. The opposite holds for large clusters that contain more than 50 events. When MDA 7308 is used, then 47 clusters are made that capture at least 50 events. The number of occurrences drops when a smaller subset is used, with only five large clusters that are formed by MDA 150.

Figure 70 shows the distribution of wave height for each clustering result. From this picture can be concluded that MDA 7308 will lead to relatively many clusters that describe wave heights smaller than 1 meter and that this number decreases if the size of the subset by MDA decreases. The number of clusters that describe wave heights larger than 3 meters is substantially more when the subset decreases, especially for cases with a significant wave height larger than 2 meters, according to traditional methods.
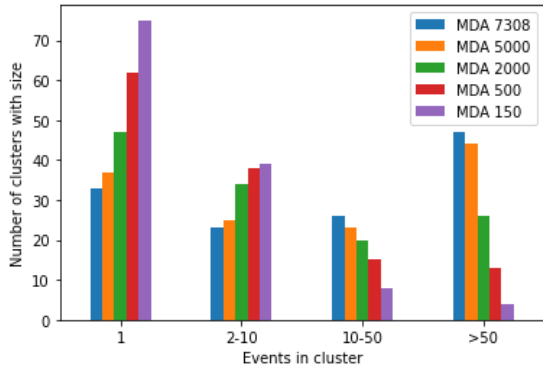
Figure 69: Cluster size distribution after applying MDA 7308, 5000, 2000, 500, and 150 in the clustering operation.
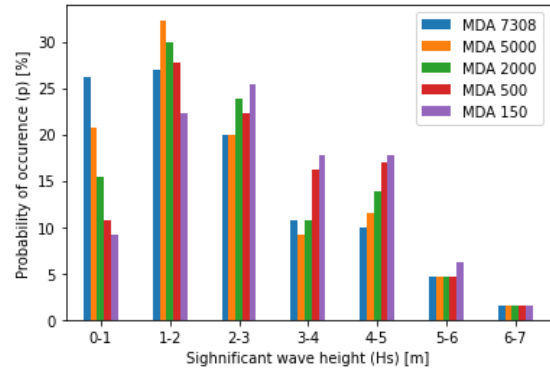

Figure 70: Distribution of wave heights for clusters based on MDA 7308, 5000, 2000, 500, and 150 in the clustering..

The results substantiate the earlier made conclusions that the subset made by MDA affects the focus of the clustering operation. The cluster size distribution development supports the conclusion that the clusters focus more on rare events when the subset decreases. The distribution of wave heights indicates that the outcomes of MDA 500 and MDA 150 are more sensitive to extreme situations. In contrast to the outcomes of MDA 7308 and MDA 5000 that describe the commonly occurring low energetic wave conditions more accurately. The clustering results based on MDA 2000 show a balance of the results from MDA 7308 and MDA 150.

Detailed analysis of cluster sizes

A more detailed analysis of the cluster sizes is depicted in Figure 71, where the probability of occurrence for each cluster is depicted. Clusters that contain wave spectral data from many time intervals contain many data points and thus have a relatively large probability of occurrence. The cluster that only occurs once in the 7308 samples can be identified by its probability of occurrence, which is 0.014%.

These singular events describe rare events, both in energetic and low energetic wave spectrums, which can be concluded by comparing the probabilities of occurrences with the representative spectrums shown in appendix VI. Chapter 5.5 will elaborate on this relation.

Many clusters of MDA 7308 have a probability of around 1 or 2%, and the largest clusters have a probability of 7%, as shown in Figure 71. While the clusters of MDA 150 mainly have a probability around 0.014% and thus mainly consist of singular events. The result from MDA 150 shows a very large cluster. This is cluster 62, which contains 47% of the 7308 samples. Also, cluster 59 is larger than 20% of the data.
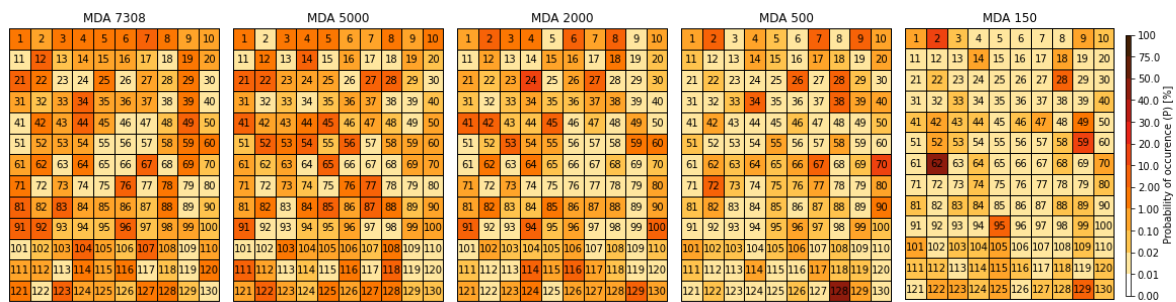

Figure 71: Probability of occurrence of 130 clusters that are based on various subsets generated by MDA.

When comparing the distribution of probabilities of all the clusters from MDA 5000, MDA 2000, and MDA 500 then can be concluded that there is a relatively smooth transition in cluster distribution from applying MDA 7308 to MDA 150. The number of singular events increases, and the largest probability increases when going from MDA 7308 to MDA 150, which corresponds to Figure 69.

So concluding, the results of Figure 71 substantiate the smooth transition of many clusters with the same size in the results by MDA 7308 and the description of more singular events and larger clusters when a smaller subset is used.

5.4.4 Further analysis of the clustering result

Based on the conclusions in chapters 5.4.1 to 5.4.3 is chosen to investigate the results of MDA 2000 further in this study. Here the balance between large-scale processes and the relatively large number of clusters with high wave heights gives an optimal insight into the forcing mechanisms and the most critical events that drive sediment transport.

The subset MDA 5000 also provides good insight into the relationship with the weather but has fewer clusters that describe wave heights between 3 to 5 meters, which contribute a lot to sediment transport, as concluded in chapter 7. Clustering based on MDA 5000 is therefore considered less suitable for further analysis.

The clusters based on MDA 500 might be a good alternative when the focus lies on important sediment transport events themselves since they capture many different wave spectrums with a wave height larger than 3 meters. Since small changes in the hydrodynamics greatly impact sediment transport, the expectation is that the nuances captured with these clusters will describe the event important for sediment transport more accurately.

The clusters made by MDA 150 describe mainly extreme events since most of the clusters contain at most ten events and have the most clusters that describe waves larger than 2 meters and might describe the variety of sediment transport events the most accurately. The centroids of the clusters are due to MDA positioned at the edges of the multidimensional cloud of data points and therefore describe the most extreme conditions.

However, the concern is that the structure of the data is poorly represented with these points. If this is the case, the expectation is that the Sea State that describes extremes in MDA 150 can be related to Sea State formed by MDA 7308, 5000, or 2000 and give thereby additional information. This study will not analyze this hypothesis.

5.5 Analysis of the Sea States

This section elaborates on the physical meaning and interpretation of the Sea State formed by MDA 2000 and the information that can be obtained from the Principal Components, wave partitions, and wave families. This analysis shows that each Sea State captures specific wave conditions, as expected, and will substantiate the importance of considering coexisting wave trains in a wavefield analysis, as concluded in chapter 4.

The agreement between the values of the Principal Components and the wave frequency-directional spectrum is also used to verify the physical meaning of the Principal Components, for which it was in advance not possible to say with certainty whether these Principal Components have a meaning.

5.5.1 Clustering results that are based on MDA 2000

The kmean clustering algorithm is used to group similar occurring wave fields over time. The 130 groups that are formed are called Sea States since they describe the wave condition at all the locations.

The results of the Principal Component Analysis, the formation of wave partitions and wave families, the occurring Weather analyzed in chapter 6, and the potential wave-driven sediment transport estimation in chapter 7, give additional information to each Sea State. This ultimately results in one large package of data that describes the Sea States and provides more insights than when all the applied techniques are considered individually. Chapters 5.5.1 to 5.5.4 use this data to make conclusions that are mainly related to answering the research questions and explain and substantiate the applicability of the used techniques. Many more conclusions can be drawn from this data.

Grouping of wave spectral data

The kmean algorithm gives each time index a specific group number, so is 1 January 2012 at 0.00 hr attributed to cluster 7, just as the wave spectrums occurring on 1 January 2012 at 6.00 hr. The wave spectral data within each group can be represented with one of the spectrums. This exemplary spectrum lies the closest to the centroid in the mathematical space and is only used for visualizing the Sea State. Conclusions of Sea States will be based on the characteristics of all the spectrums within the Sea State.

The spectrums at location 42 attributed to Sea State 1, 10, 12, and 22 are depicted in Figure 72. Here is visible that Sea State 1 is occurring 12 times. These spectra describe waves propagating toward the northeast to the east, with some less energetic short waves propagating in the opposite direction. The (total) significant wave height, following traditional methods, is between 1.8 and 3.3 meters.
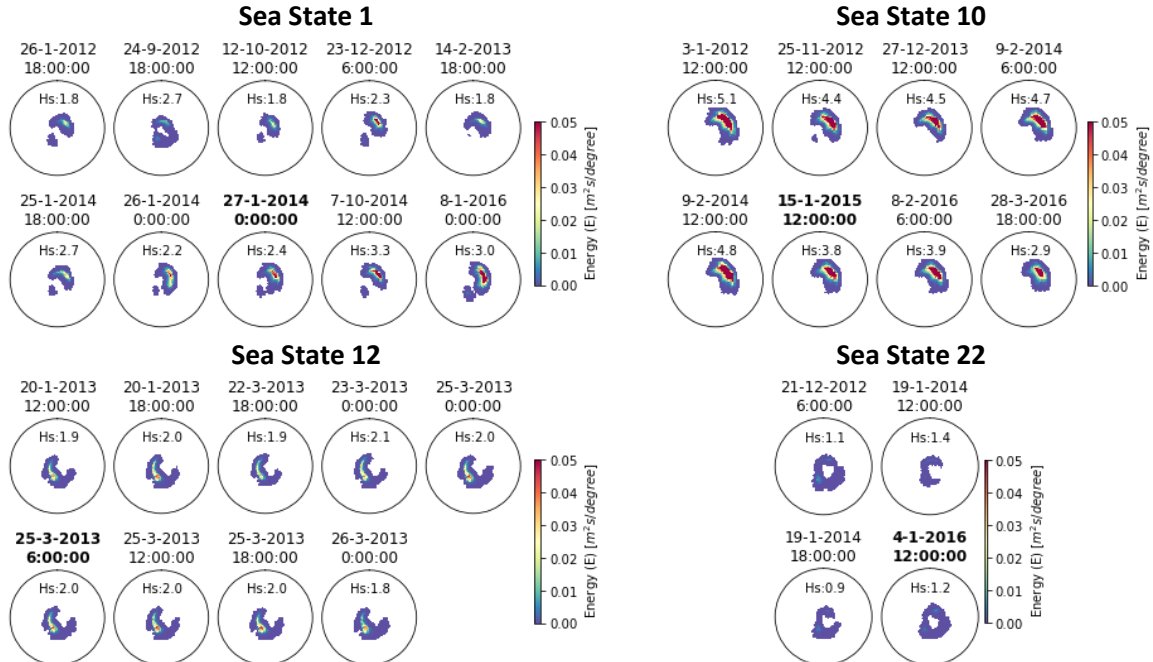

Figure 72: The wave spectrums at location 42 corresponding to Sea States 1, 10, 12, and 22. The times in the title describe when the wave spectrum is occurring. The spectrum with the bold title is the representative spectrum. The significant wave height is based on the energy within the total wave spectrum, the (total) significant wave height from traditional methods.

Sea State 10 captures 8 conditions where waves also are mainly propagating towards the northeast. The significant wave height is larger than described by Sea State 1. The (total) significant wave height is from 2.9 to 5.1 meters. The spectrum occurring on 15 January 2015 represents the spectra within South easterly propagating waves with a significant wave height of about 2 meters are described with Sea State 12. Sea State 22 describes waves propagating to the north, southwest, and southeast.

The representative wave spectrum for one nearshore location for the Sea States is shown in appendix VI. The representative spectrums show the large variety of wave conditions that are occurring. The expectation is that each of these conditions are affected by one or more forcing conditions. Chapters 6 and 7 will elaborate on this.

Spatial trends

Spatial trends can be investigated when comparing representative spectrums at all the locations, as described below for Sea State 59 in Figure 73 and shown for Sea States 65 and 121 appendix V. Since 130 Sea States are formed, 130 of these maps can be made by MDA 2000.

The representative spectrums of Sea State 59 at the offshore locations are depicted in Figure 73. This Sea State describes easterly propagating waves. Here is visible that along the 55th latitude the energy of the waves can be described, according to traditional methods, with a total significant wave height of 2.6 to 3.2 meters. The wave height increases as they travel to the east, probably since the energy gained from the wind is larger than the bottom friction. On this latitude is also visible that the direction of the propagating waves changes. At longitude 0 is the propagation main towards the southwest, which changes towards the east when the longitudinal coordinate increases. When comparing these representative wave spectrums to the ones at the lower latitudes than can be concluded that the significant wave height decreases in the southward direction. Only at the 50th latitude are higher waves, which can come directly from the Atlantic Ocean.
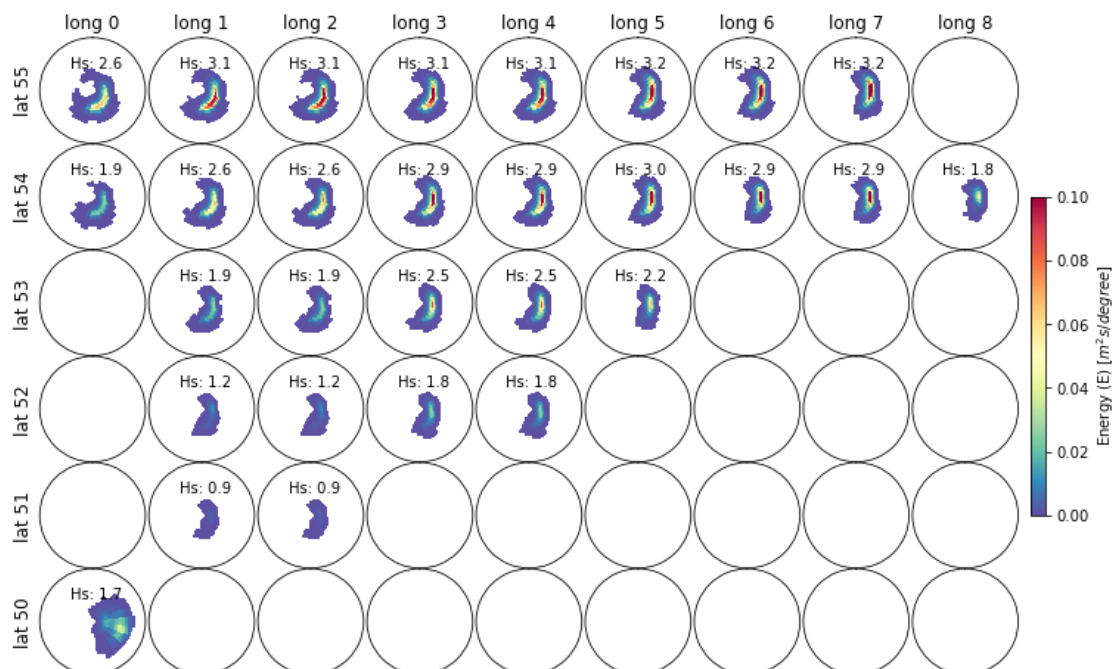

Figure 73: The representative wave spectrum for the offshore locations of Sea State 59.

5.5.2 Physical meaning and importance of Principal Components

The Principal Components describe energy over the wave frequencies and directions, as described in chapters 2.6.2 and 5.2. The characteristics of the Sea States are used to validate this meaning. After that is the relative importance of the Principal Components for various Sea States analyzed. This subchapter ends with a concluding section.

<u>The relation between loads and wave energy described by Principal Components</u>

The physical meaning of the Principal Components can be validated by comparing the value of the Principal Component related element of the eigenvectors with the spectrums attributed to each Sea State. The elements should have approximately the same value since all the wave spectrums describe waves propagating in approximately the same magnitude and direction. Here positive values of the elements would indicate larger waves in the direction described by the Principal Component, and negative values would indicate waves propagating in the opposite direction if the theory described in chapter 5.2 is valid.

The results of the Principal Component Analysis and the results of grouping similar wave spectrums, the Sea States, are compared to each other in the discussion below. The loads of the four most important Principal Components at one offshore are depicted in Figure 74, as a recap. The representative wave spectrums of the Sea State mentioned in this section are depicted in Figure 75. The probability that a Sea State has a load within certain bands is depicted in Figure 76 for Principal Component 1 and in Figure 77 for Principal Component 2.
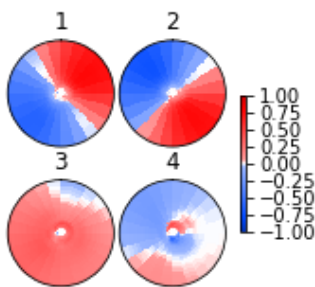
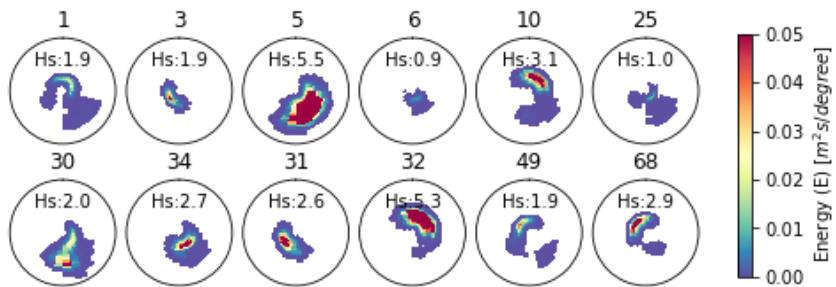*Figure 74: Recap of loads of Principal Components 1, 2, 3, and 4 at one offshore location.*

Figure 75: The representative wave spectrums for Sea States that are based on the subset made by MDA 2000, the titles refer to the Sea State number.
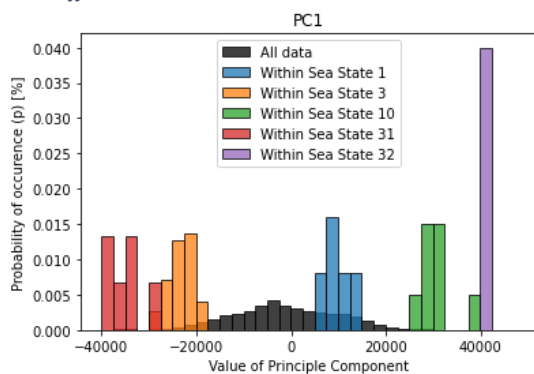

Figure 76: Distribution of the values of the loads related to Principal Component 1 (PC 1) for various Sea States.
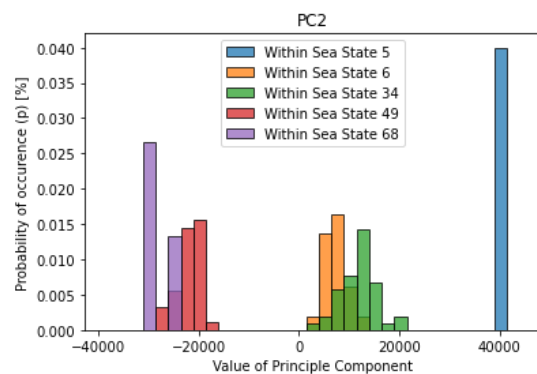
Figure 77: : Distribution of the values of the loads related to Principal Component 1 (PC 1) for various Sea States.

The distributions of loads for some of the Sea State strongly related to Principal Components 1 and 2 are depicted in Figure 76 and Figure 77. On the upper limit of Principal Component 1 is Sea State 32, which is a singular event of northeasterly propagating waves with a (total) significant wave height of 5.4 meters. Sea State 10 captures north easterly waves with a significant wave height of 3.2 meters. The loads and wave height of Sea State 10 are both smaller than that Sea State 32 and larger than Sea State 1, which has a (total) wave height of 1.9 meters. The results for negative values show indeed waves propagating in opposite directions. Here the larger negative value of loads of Sea State 31 to Sea State 3 corresponds with a larger significant wave height of waves propagating towards the southwest.

Similar results are found when the relationship between the loads of Principal Component 2 and the significant wave height of south-easterly propagating waves are compared. Here Sea State 5 has the highest value of the examples and captures waves of 4.9 meters propagating to the southwest. Sea States 6 and 34 have lower positive values and describe smaller south-easterly propagating waves. Negative values of Principal Component 2 indicate north-easterly propagating waves, where Sea State 68 has larger waves than Sea State 49, which corresponds with more negative values of the loads related to Sea State 68 than Sea State 49.

Principal Component 3 can roughly be interpreted as an overall increase in wave energy. Both Principal Component 1 and 2 cause negative wave energy, which is physically impossible. So Principal Component 3 can practically be seen as an overall increase of wave energy to prevent negative wave energy and will have relatively high values in relatively energetic wavefields.

The relative importance of Principal Components
The waves in the Sea State depicted in Figure 76 and Figure 77 are mainly propagating in the direction described by the Principal Component. The correlation between the load of the Sea State and its significant wave height is therefore very strong. The correlation is less strong when the waves are propagating in another direction since the contribution of other Principal Components increases. So are waves that are propagating towards the east described with both Principal Component 1 and 2. The higher Principal Components describe the wavefield more accurately by adding or decreasing the wave energy within a smaller domain in the frequency-directional spectrum.

The ratio of the loads by the Principal Components can be used to get insight into the importance of the Principal Components and their forcing mechanisms. The proportion of the averaged absolute values of the loads related to the 50 largest Principal Components is depicted for 50 Sea States in Figure 78. The directional component of the Principal Component has become irrelevant by taking the absolute values of the elements before averaging.

The results show that Sea State 1 is for 40% described by Principal Components 1 and 2. Principal Components 1, 2, and 3 do at many times capture half the loads of the Sea States. However, Sea State 13 has very low loads for Principal Components 1 to 3 and is largely influenced by Principal Components 4, 5, and 8. Also, Sea State 25 is mainly described with Principal Components 10 to 50.
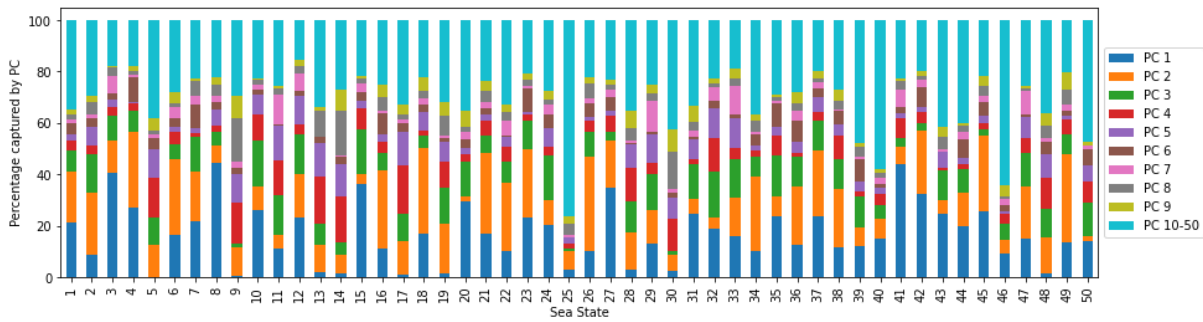
Figure 78: Contribution of the Principal Components for each Sea State when the absolute values of the components are averaged.

The expectation was that Principal Components 1, 2, and 3 mainly describe the wave spectrum since they capture the most the variance, as shown in Figure 57. However, also cases can be found where higher Principal Components play an important role, like Sea State 13. Sea State 25 is mainly described with Principal Components 10 to 50. Which might have been seemed irrelevant due to their low variance. This Sea State has wave trains propagating in many southerly directions but lacks a pronounced energy peak, while there is a considerable significant wave height of 1 meter, as shown in Figure 75.

As concluded in chapters 5.3 and 5.4, some of the clusters (now called Sea States) focus on rare events, which are described with the higher number of Principal Components, as stated in chapter 5.1. These two statements will indeed lead to Sea States that are mainly described with high numbered Principal Components.

Conclusion

The results show that the Principal Components describe wave energy in specific wave-frequency directional bins. Positive large values of the loads indicate waves propagating in the direction described by the Principal Component. Large negative values indicate a large wave energy flux in the opposite direction. So the values of the loads can be used to find - and get insight into specific wave propagation directions.

The three largest Principal Components capture most of the variance of the data. These three Principal Components do usually describe 40 to 60% of the load. However, in some rare cases, these Principal Components are not important at all. Since Principal Components are related to specific forcing conditions, it can be concluded that not all the wave spectrums can be related to large-scale events, but some of them are related to small-scale or rarely occurring large-scale events.

5.5.3 Coexistence of wave trains and their propagation direction

The wave families and the wave direction described by the wave partitions can give insight into the sea states that can have following, crossing, and opposing waves, as described in chapter 4.2. The characteristics of a Sea State can be determined by analyzing the wave spectrums that are attributed to a specific Sea State. Six Sea States will be analyzed in this section, which are depicted in Figure 79.
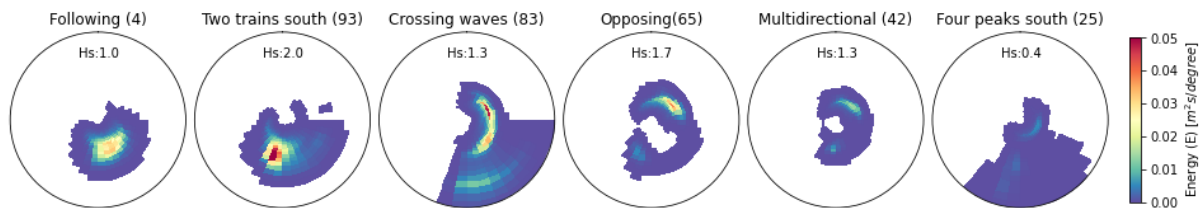

Figure 79: Representative spectrums of Sea States of interest at nearshore location 42. The title describes the kind of waves that are occurring, the number refers to the index of the Sea State.

Wave families have energy when a wave train has its energy peak within the boundaries of the wave family. The probability that a wave family has energy can give insight into the propagation direction of the waves captured with each Sea State. When the probability is 100%, it means that all the spectrums related to that Sea State have at least one wave train with a peak period and direction within the boundaries of the wave family. This means that when two wave families have a probability of 100%, both wave families capture a different coexisting wave train, and at least a bimodal wave spectrum occurs. In this case, it might be possible that two wave trains have their peak within the boundaries of the same wave family, and that there are more than two coexisting wave trains. So for analyzing the number of wave trains, the statistics about wave partitions are required.

(Relative) Wave propagation direction

The probability that a wave family has energy is depicted in Figure 80. These probabilities show that Sea State 4 has waves propagating southwards. The cumulative probability is about 100%, which indicates a high probability that Sea State 4 describes a unimodal wave spectrum. If there is more than one wave train, they are likely propagating in the same direction, so Sea State 4 has probably following waves. Southerly propagating waves are also described with Sea State 93, which is at least a bimodal wave spectrum since two wave families always contain energy from at least two different wave trains, which can be considered as following waves. It might be possible that this multimodal wave spectrum has three or more wave trains since they attribute their energy to the same family. Sea State 83 describes crossing waves, which go to the southwest and northeast. Here one or two energy peaks are going to the northeast. The second north easterly propagating wave train contributes half of the time energy to the short perioded wave family. The other times, the wave train does not occur or contributes energy to the wave with the longer wave period. Statistics about wave partitions are required to make this conclusion. Sea State 65 shows opposing waves that are propagating towards the northeast and southwest, and Sea State 42 captures waves that could propagate in multiple directions since many wave families gain energy. Sea State 25 has at least 3 wave trains that contribute energy to 3 wave families. The following section shows that this Sea State captures 4 wave trains.
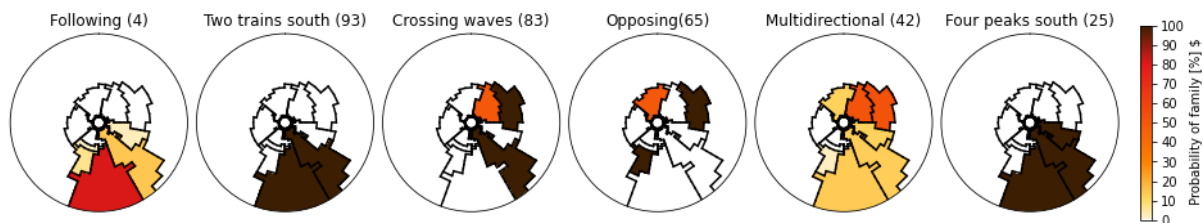

Figure 80: The probability of occurrence of wave families indicates wave trains and their propagation directions. The title describes the kind of waves that are occurring, the number refers to the index of the Sea State.

Coexisting wave trains in Sea States

The number of wave trains in the Sea State can be analyzed by counting the number of partitions each wave spectrum has since the energy peaks of wave trains are used to partition the wave spectrum. The distribution of wave trains is mostly consistent with the conclusion drawn by the probability that a wave family has energy. So describes Sea State 4 mainly a unimodal wave spectrum, and Sea State 93 has two wave trains. However, Sea State 83 has half of the time 4 wave trains, which means that two wave trains are in the same wave family since maximal three wave families have energy simultaneously. Further, the results show that Sea State 65 has 2 or 3 coexisting wave trains and that Sea State 42 describes half of the time a unimodal wave spectrum. It has a large variability in the number of partitions and can describe up to 6 coexisting wave trains. Sea State 25 has 4 coexisting wave trains, although 3 wave families have energy, which means that two wave trains contribute energy to the same wave family.
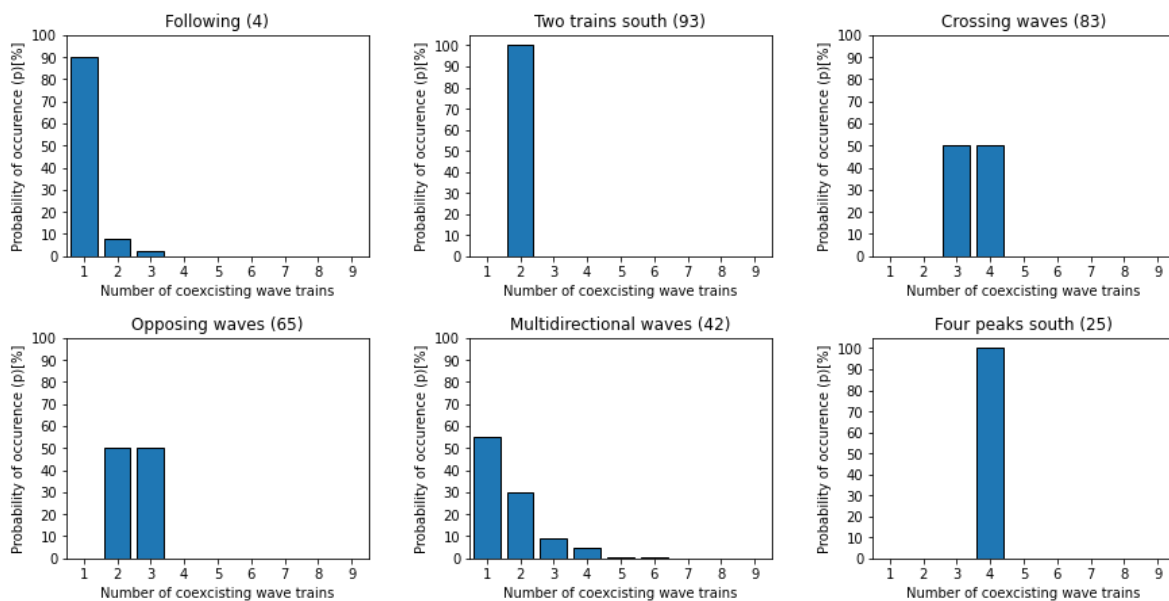
Figure 81: Distribution of the number of coexisting wave trains for six Sea States of interest, depicted in Figure 79.

The relative angle between wave trains within a Sea State

Sea States not only make a distinction in the number of wave trains but also the angle between these wave trains, as shown in Figure 82. The angles between waves in multimodal conditions are between the bearing of the most energetic wave train to the other wave trains in the spectrum. The results show that Sea State 4 has mainly following waves. Sea State 93 barely occurs but describes waves with an angle between 70 and 80 degrees. Sea State 83 describes following waves for the easterly propagating wave trains and crossing waves that are probably related to the southerly propagating waves. Sea State 65 describes opposing waves and some crossing waves that are related to the northerly propagating wave trains, as mentioned above. The various wave families that gain energy in Sea State 43 propagate in various directions resulting in following, crossing, and opposing waves, which are likely to occur simultaneously. The last example shows that when four wave trains coexist, the angle of one wave train to the most energetic wave of the wave trains goes up to about 95 degrees.
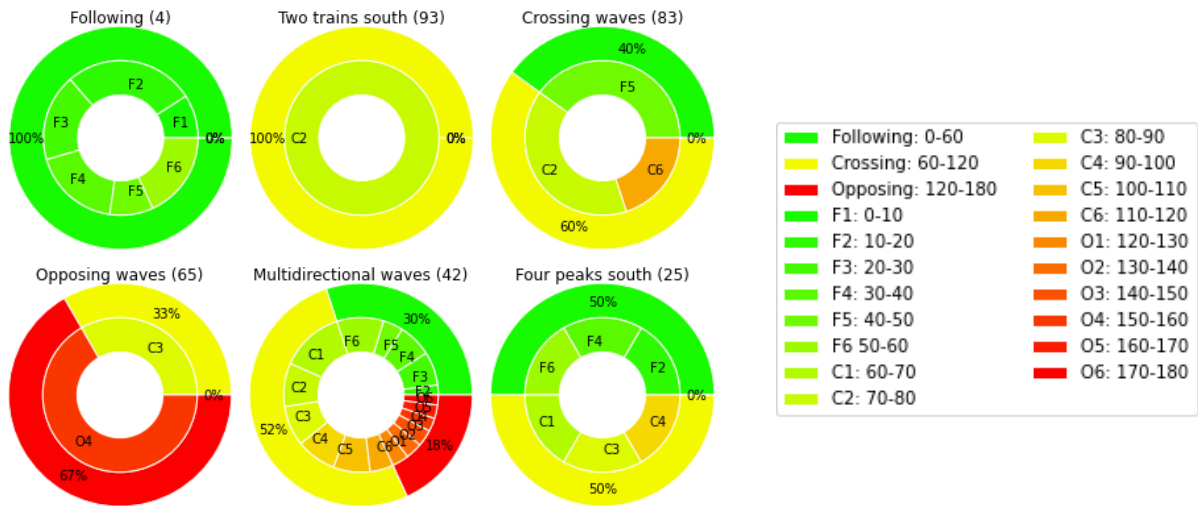
Figure 82: Distribution of angels compared to the most energetic wave train, for multimodal wave spectrums.The two rings describe the probability of occurrence of relative wave angels. The outer ring, in total 100%, makes a distinction of 60 degrees, related to the distinction of following, crossing, and opposing waves. The inner ring gives more detailed information about the distribution of relative wave angles, as described in the legend.

The directions of the waves can be analyzed by comparing the bearing of the most energetic wave trains to other wave trains, similarly to the whole wavefield depicted in Figure 39. The results for Sea State 42 in Figure 83 show that the most energetic waves propagate south when opposing waves occur, among other things. Detailed analysis might relate coexistence of wave families as well.
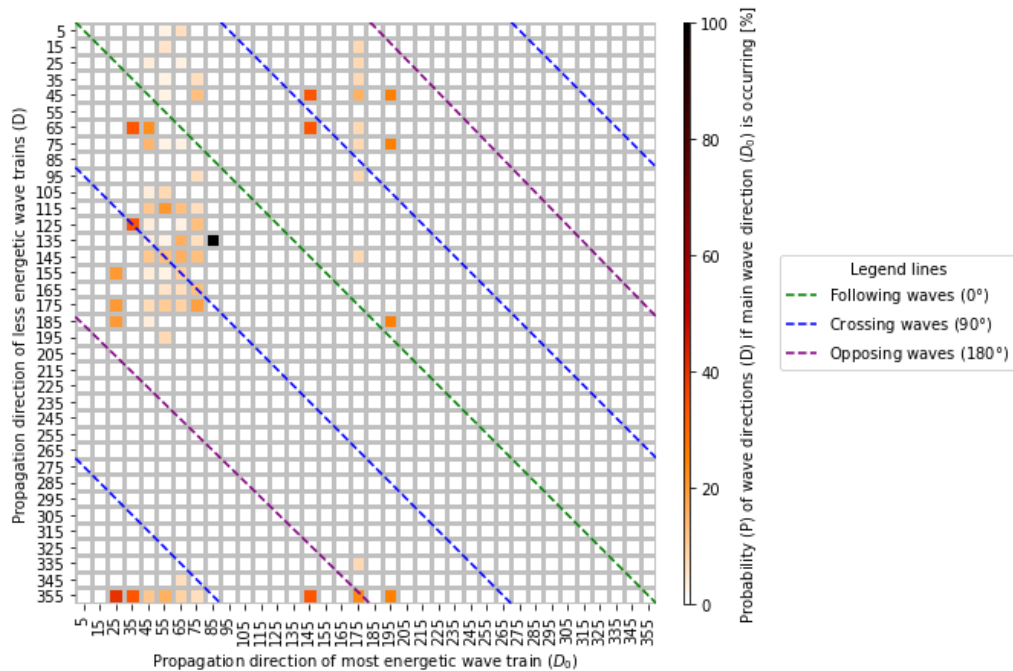
Figure 83: Probability (P) of coëxcisting wave trains for Sea State 42, the probability of wave train directions (D) compared to the propagation direction of the most energetic wave train (D_0). The lines indicate following, crossing, and opposing waves for the most energetic wave train compared to the less energetic wave train.

5.5.4 Probability of Sea States and seasonality

The Sea State consists of one or spectrums occurring at a specific time. The timestamp of these spectrums can give insight into the probability of occurrence, both yearly and seasonal. The yearly probability is discussed in chapter 5.4.3. The seasonal probability gives more detailed insight into the period at which certain wave spectrums are dominant and when certain rare events are occurring.

Sea States that only occur once in a quarter of the 7308 samples can be recognized by their probability of 0.055%, the only possibility for a value between the boundaries of 0.02% and 0.1%.

The probability of occurrence of Sea State shows that some of the Sea State occur throughout the year and that some wave climates are more seasonal related. So has summer a relatively stable climate, with a third of the time small south-easterly propagating waves, described with Sea State 24. The winter months have the most dynamic weather, resulting in a very dynamic wave climate and a large variety of occurring Sea States. Especially Sea States that describe easterly propagating waves have a larger probability of occurrence, like Sea State 7. These waves sometimes occur during the autumn and not during the spring and the summer. Sea State 22 is only occurring during the winter. It has short waves propagating in all directions and shows the dynamic weather during this season, where wind can blow from various directions in a relatively short period. Furthermore, can the strong northeasterly wind in the autumn and winter create waves with a significant wave height of 4.6 meters, as described in Sea State 36. Chapter 6 elaborates on the relation of waves with the weather.
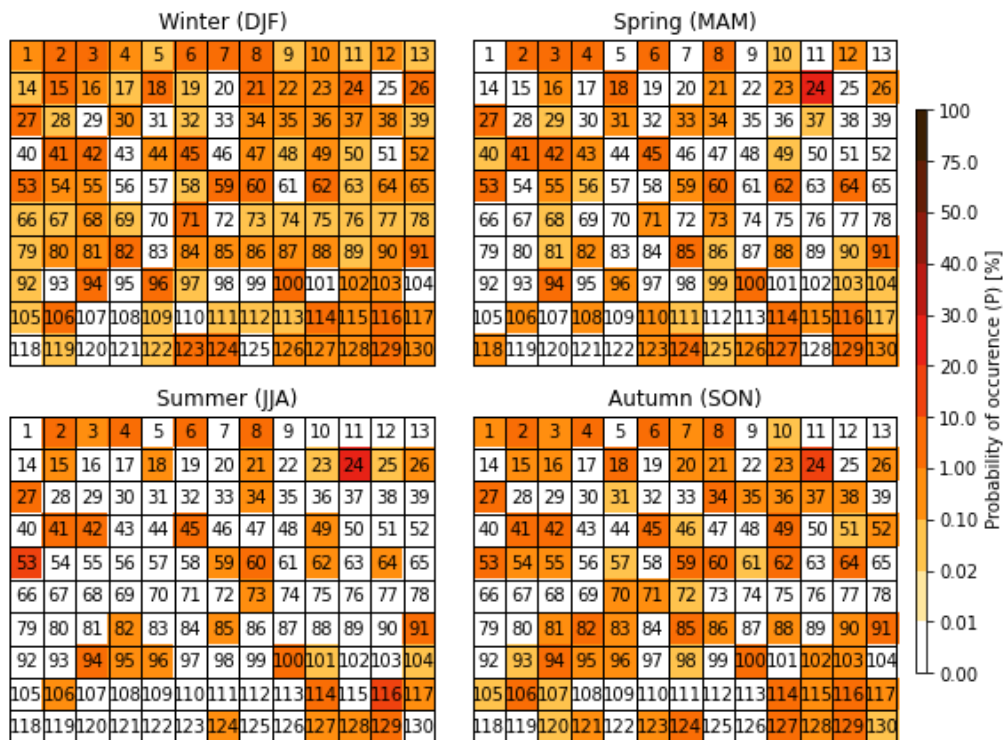

Figure 84: Seasonal probability of occurrence of Sea State formed by MDA 2000.

5.6 General Discussion and Conclusion

This section elaborates on the main discussions and conclusions in chapters 5.2 to 5.5. Here various machine learning techniques are used to get insight into the wavefield.

5.6.1 Discussion

The wave data is standardized before it is analyzed with Principal Component Analysis, Maximum Dissimilarity Analysis and processed with the kmean algorithm. Due to this parameterization is the standard deviation of all the parameters the same. The spreading affects the description of the data and thus orientation, density, and Eucladian distances between the data points, which affects the outcome of the used machine learning techniques. So, the parameters that describe only minor wave energy have the same importance as those that capture more wave energy and thus have a larger variability. The expectation is that if the data is not standardized, the bins that describe higher wave energy densities and thus have a larger variability will have more impact and therefore results in more nuance of high energetic wave conditions. This is possible since the units of all the parameters are the same. This study does not investigate the impact of standardizing the data on the outcomes or delibaratly changing the scale and thus importance of the data.

The Principal Components that are generated with Principal Component Analysis are probably related to specific (weather) conditions, which follow from the conclusions described below, and will be studied in chapter 6.5.

The specific wave conditions in each Sea State might be relatable to specific weather conditions and a narrow-banded distribution of (potential) wave-driven sediment transport, which will be analyzed in chapters 6 and 7.

5.6.2 Conclusion

Many conclusions can be made from the results. This chapter elaborates on the conclusion that can be used to answer the two main research questions. More detailed analysis is possible, such as the sea states that are related to the 5% largest wave heights and the return periods of specific wave conditions, for example.

The Principal Components that describe most of the variance are related to spatially large-scale processes and sometimes seasonality. The other Principal Components are more related to rare events, like stormy conditions.

Similar occurring wavefields are grouped and used to form the so-called Sea States. Each Sea State has a representative wave frequency-directional spectrum at all the locations. The Sea States show the spatial development and the temporal variability of various wave conditions and describe one or multiple wave trains with a small range in height, propagation direction, and period.

The Principal Component Analysis is used to describe the data with newly defined and independent parameters, called Principal Components. The results show that parameters are able to describe both spatially and temporally the wave energy of specific wave frequency-directional bins. The load of the temporal values shows that some Principal Components can be very important in describing high energetic are rare occurring wave spectrums and can be used to analyze wave energy (fluxes) in specific directions. The parameters can also be used to reduce the number of parameters considered in Maximum Dissimilarity Analysis and the kmean algorithm, reducing the computationally demands and increasing their efficiency.

Maximum Dissimilarity Analysis is used to select a part of the original data set, where especially the frequently occurring situations are left out. The subset is used in defining Sea States. The results show that Sea States focus on large-scale (natural) processes and frequently occurring situations when all the data is used to define them. The Sea States capture more nuance in rare and more energetic events when the size of the subset decreases.

The Elbow method and the Silhouette Coefficient can give insight into the optimal number of Sea States. Here a trade-off has to be made between the accuracy and the workability of the outcome. More groups will increase the accuracy but require more extensive post-analysis.

The wave partitions and wave families can be used to analyze the number of coexisting wave trains and the direction of following, crossing, and opposing waves within each Sea State.

6 Wind-waves originated from synoptic conditions

This chapter elaborates on the characteristic wind climates, called Weather Type, and its relation with Sea States, which are derived in chapter 5. The applicability of Weather Types and Sea States, including Principal Components and wave family related statistics, are analyzed.

6.1 The approach

The sea level pressure and its gradient can be used to identify characteristic weather conditions, called Weather Types, in a similar way the Sea States are derived in chapter 5. Principal Component Analysis and the kmean clustering algorithm are used for the formation of the Weather Types, which are explained in chapter 2.6 and also used for the formation of the Sea States. Chapter 6.2 will elaborate on the formation of the Weather Types and the corresponding Principal Components.

Each Weather Type has a unique positioning and magnitude of high and low-pressure systems. This creates a specific sea-level pressure gradient that can be used to estimate wind-wave generation, as explained in chapter 2.3. Each Weather Type is expected to create more or less the same wave field. The travel time of waves might reduce the direct relationship between Weather Types and Sea States, and will be analyzed in chapters 6.3 to 6.5.

The sea level pressure data from ERA-Interim for 1979 to September 2018 with a daily resolution is used to analyze the sea level pressure and its gradients and to generate the Weather Types. The Sea States are based on the subset of 2000 points generated with Maximum Dissimilarity Analysis, as explained in chapters 5.3 and 5.4, and cover the period from 2012 to 2016 with a six-hourly resolution.

6.2 Analyzing atmospheric synoptic patterns

The Principal Components that are based on the sea level pressure data give insight into the temporal variability of the weather or the atmospheric synoptic conditions. Principal Component 1, depicted in Figure 85, shows the positioning of a high or low-pressure system at this location. The negative value of the time series, corresponding to the green dot, indicates that a high-pressure system is almost periodic at this location. The magnitude difference between the maxima and minima indicates that the high-pressure system deviates more from the mean sea level pressure than the low-pressure systems. Principal Component 2, in Figure 86, shows a situation where a high-pressure system is below the Netherlands and reaches into the North Sea when the temporal value is positive. Principal Component 1 captures 50% of the variance, and Principal Component 2 does 19%.
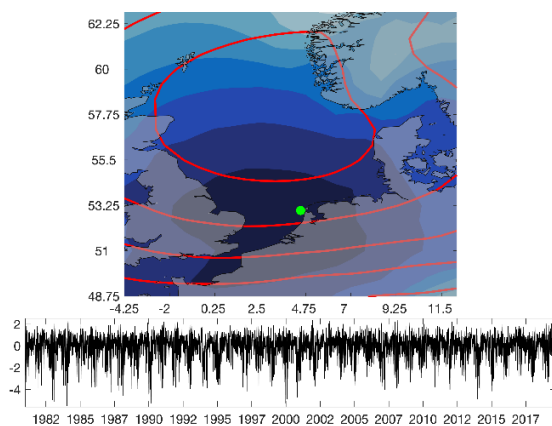

Figure 85: Principal Component 1, based on the sea level pressure and sea level pressure gradient.
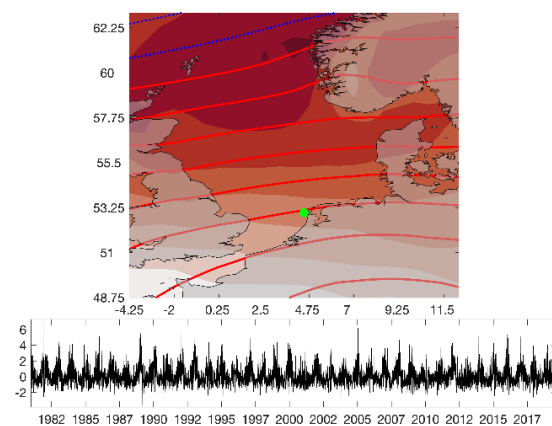

Figure 86: Principal Component 2, based on the sea level pressure and sea level pressure gradient.

These and more principal components are used to group the characteristic weather conditions into so-called Weather Types. The results for 25 and 81 Weather Types (WT) are depicted in appendix VII. The main difference between the outcomes is that 81 conditions capture more nuance in weather variability. This nuance is visible when two very similar Weather Types are compared, like Weather Type 7 and 9, shown in Figure 87. Both Weather Types capture a low-pressure system with a position north of the Netherlands with a similar magnitude. Their difference is mainly visible when comparing the sea level pressure gradients, which are more prominent for Weather Type 9, and will thus create larger waves.
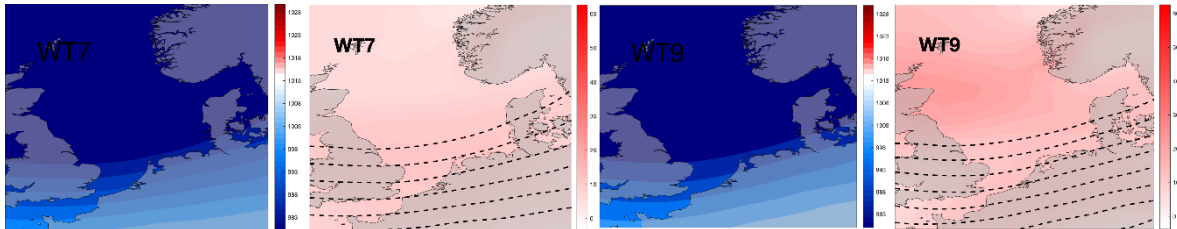
Figure 87: Weather Type (WT) 7 and 9, the sea level air pressure left and its gradients on the right side. The dotted lines in the sea level pressure correspond with the sea level pressure. For the sea level pressure, white indicates the global average sea level pressure of 1013 millibars, red indicates a high-pressure system, and blue a low-pressure system.

6.3 The relation between Weather Types and Sea States

The atmospheric condition is the driver of the wind-generated waves in the North Sea. Patterns in the sea level pressure gradient are used to describe the atmosphere by Weather Types, which has a unique wind field. A correlation between the Weather Types and the Sea States is therefore expected. This correlation is likely to be high for locally generated waves and less for swell waves due to their relatively long wave travel time, which is up to 6 days, as concluded in chapter 3.2.

The coexistence of Weather Types and Sea states is used to get insight into the relation between weather and waves. This relation is analyzed in two ways, namely through the probability that a Weather Type occurs when a Sea State occurs and, the opposite, the probability that a Sea State occurs when a Weather Type is occurring. The correlation between the sea state and the weather type is stronger when the probability increases.

Analyzing this correlation has some challenges. So is the resolution of the Weather Types 24 hour and 6 hours for the Sea States, and many clusters do not occur when the resolution of the Weather Types is used. Having one Weather Type representative for the whole day reduces the accuracy of analysis since the Weather Types do not account for the temporal variability as the Sea States do.

The expectation is that increasing the number of Weather Types and Sea States with post organization and a higher temporal resolution will give more insight into the relation between weather and waves. The post organization can, for example, be by ordering the clusters by their characteristics.

The upcoming subchapters will analyze the relationship between the 130 Sea States with 25 and 81 Weather Types. The benefit of applying 25 Weather Types is that it gives a broader overview and makes it easier to analyze results since no necessary distinction in weather conditions is made by irrelevant details, if these 25 Weather Types can accurately describe the data. When details about the weather conditions are relevant, then 81 Weather Types are more suitable.

6.3.1 The relation between 130 Sea States and 25 Weather Types

This chapter analyzes if Sea States and the Weather types are happening at the same time. This concurrence is used to analyze the relation between Sea States and the 25 considered Weather Types.

The probability of one of 25 Weather Types when a Sea State occurs

The probability of occurrence of a weather type when a sea state is occurring is depicted in Figure 88. Here are the 7308 samples of spectral data considered. The weather condition defined at the start of the day is assumed to be representative of the whole day, which can introduce some noise since the weather also represents a wave spectrum that occurs 6, 12, and 18 hours later.

Of the 130 Sea States 47 Sea States occur only once, as shown in Figure 69. These Sea States have a unique relationship with a Weather Type, which is visible by a 100% probability. The results in Figure 88 show that a unique weather type occurs for 57 of the 130 sea states. Therefore, this unique relationship is not only for these 47 Sea States.

A high percentage can also be found for Sea States that describe rare conditions with locally generated waves and unimodal wave spectrums. Frequently occurring sea states have a wider spread over the weather types, resulting in lower probabilities. The expectation is that the spreading is mainly over similar weather types, which can create similar wave fields.
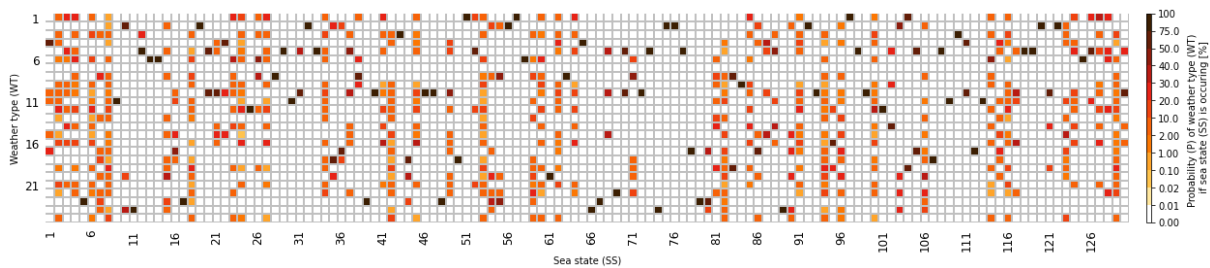
Figure 88: Probability (P) of weather type (WT) when sea state (SS) occurs when 25 weather types are considered in a framework with a temporal resolution of 6 hours.

The probability of a Sea State when one of 25 Weather Types occurs

The probability that a sea state occurs when a weather type occurs is depicted in Figure 89. The main difference between Figure 88 is that the summation of each row is now 100% rather than each column.

Both figures show the same connectivity between the Sea States and the Weather Types. However, Figure 89 does not show a distinct consequence of the Weather Type on the sea state since the probabilities are relatively low and distributed to the same sea states. The 25 weather types may thus be insufficient to capture forces that induce the various sea states but accurate enough to gain a general understanding of the weather types that occur when a sea state occurs.
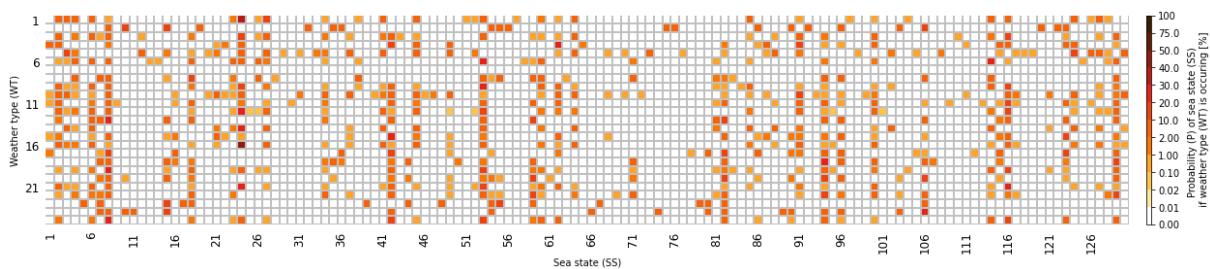

Figure 89: Probability of sea state (SS) when weather type (WT) occurs when 25 weather types are considered in a framework with a temporal resolution of 6 hours. Appendix VIII shows the results of applying 81 weather types, which is more accurate.

6.3.2 The relation between 130 Sea States and 81 Weather Types

The relation between 81 Weather Types and 130 Sea States is analyzed in the same manner as done in chapter 6.3.1. The results are depicted in appendix VIII. The graphs are similar to those shown in Figure 88 and Figure 89.

The probability of one of 81 Weather Types when a Sea State occurs

The probability that a Weather Type occurs when a Sea State occurs gives similar results to the case where 25 Weather Types are analyzed, shown in Figure 88. Now 56 unique relations between Weather Types and Sea States are defined, which is slightly less than the case with 25 Weather Types, which has 57 unique relations.

This result shows that the application of 81 Weather Types, in contrast to 25 Weather Types, gives more detailed insight into the Weather Types that occur when a Sea State occurs. More nuance is captured in the Sea Level Pressure and the corresponding wave field when more Weather Types are applied, as shown in Figure 87. So with approximately the same number of unique relations can be concluded that, for those cases, the Weather Types accurately describe the occurring weather condition.

So, 25 Weather Types are able to give an impression of the occurring weather conditions when the wave conditions are analyzed. More detailed insight into the weather conditions can be achieved by applying 81 Weather Types.

The probability of a Sea State when one of 81 Weather Types occurs

The Probability that a Sea State occurs when a Weather Type occurs is increased compared to the case with 25 Weather Types. Now 8 relations with a probability of 100% can be identified, and many high probabilities between Weather Types and Sea States can be recognized.

The different results of 25 and 81 Weather Types show that high correlations between Weather Types and Sea States can be established when 81 Weather Types are considered, which is not the case when 25 Weather Types are used.

So, 25 Weather Types are not able to predict the wave conditions. This means that the 81 Sea States should be used as a starting point to predict wave conditions in this study.

6.4 Wave families and Weather Types

Wave families show the wave propagation direction of wave trains in a spectrum and might give insight into the wave direction when a Weather Type, with a unique wind field, occurs.

The sea level pressure can roughly estimate the wind field that drives the waves. The high-pressure systems rotate clockwise, and the low-pressure systems counterclockwise in the northern hemisphere. Practically, the wind that would have blown from the high pressure to the low pressure is deflected towards the right by Coriolis.

A temporal resolution of 24 hours is used for analyzing wave propagation directions, described by wave families, when Weather Types are occurring. The benefit of this resolution is that the weather data represents the occurring wave field. The 24-hour resolution for data from 2012 to 2016 results in 1827 samples that are considered.

This analysis results in the probability that a wave family has energy when a specific Weather Type is occurring. The upcoming chapter will elaborate on three examples. All the results are depicted in appendix IX.

Three Weather Types with their corresponding sea level pressure gradient and the probability that a wave family has energy are depicted in Figure 90. The sea level pressure field of Weather Type (WT) 9 indicates a low-pressure system north of the Netherlands. This means that the local wind is blowing towards the east and slightly to the north. The wave families describe waves propagating in the same direction. The wave families also describe south-easterly propagating waves. The wave ray of this family, shown in Figure 46, indicates that these waves might originate from the northern tip of Great Britain. The sea level pressure gradient of weather type 9 shows increased values at this location, the wind here can probably generate the southeasterly propagating waves. The two wave systems created with this Weather Type will result in crossing waves. Crossing waves can also be identified by the wave families during Weather Type 29, which are related to north westerly and north easterly propagating waves. The high-pressure system on the east will create northerly offshore wind and, consequently, northerly propagating waves. The northeasterly propagating waves that might come through the English Channel, where the curvature from the low-pressure system gives the impression that here northeasterly propagating waves are generated that arrive at the Dutch shore. The probability that wave families have energy for weather type 4 is more challenging to explain. The circular wind pattern of the high-pressure system will create a southerly wind near Norway, which explains the high probability of southerly propagating waves. However, it is tough to explain the very consistent opposite propagating waves by Weather Type 4, especially since the local eastern wind will not directly create north-easterly propagating waves.
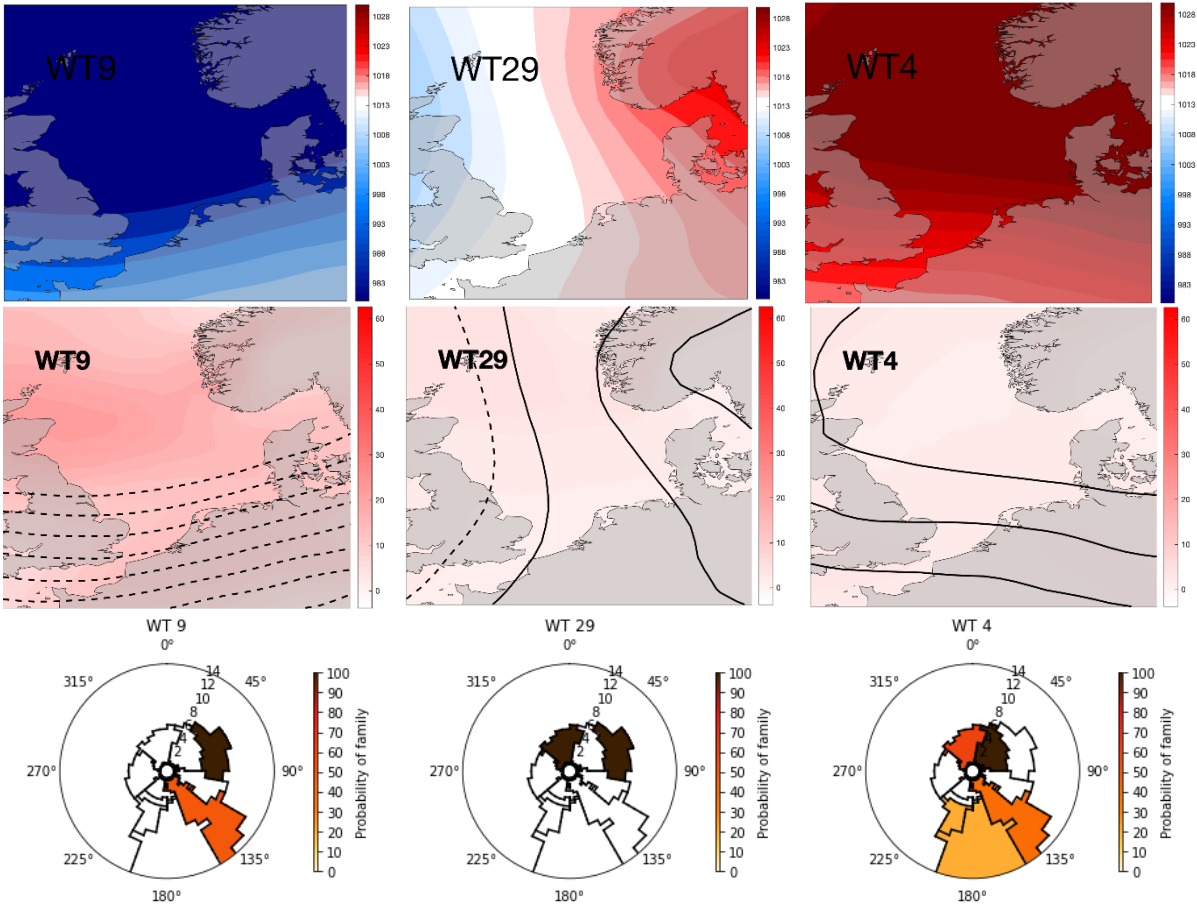
Figure 90: Weather types (WT) in the top row, with below the corresponding sea-level pressure gradient and lines indicating sea level pressure. The probability that a wave family captures wave propagation is depicted at the bottom. All the Weather Types are related to the set of 81 Weather Types. On the top row, white indicates the global average sea level pressure of 1013 millibars. Red indicates a high-pressure system, and blue a low-pressure system.

The results show that estimations on the wavefield by the sea level pressure field give some insight into the wave propagation direction captured by the wave families. However, the pressure field can not explain the whole wave field since it does not consider the wave travel time, nearshore processes that affect the wave propagation, and details about the wind field, that can be related to both spatially and temporal variability.

6.5 Correlation between wave Principal Components and Weather Type

The principal components that are based on the wave spectral data describe the wave energy of wave propagating in a specific direction and are thus related to de wave energy flux, as described in chapter 5.5.2. The Principal Components can give insight into wave propagation directions for each Weather Type. This chapter elaborates on this relation of the temporal values, the elements in eigenvector, related to Principal Component 1 and 2 and 8 Weather Types, depicted in Figure 91. The Weather Types are from a set of 25 Weather Types.

The element of the eigenvector related to Principal Component (PC) 1 describes wave energy flux towards the northeast when it is positive and towards the southeast when it is negative. The element related to Principal Component 2 is positive for southeasterly propagating waves and negative for northwesterly propagating waves.
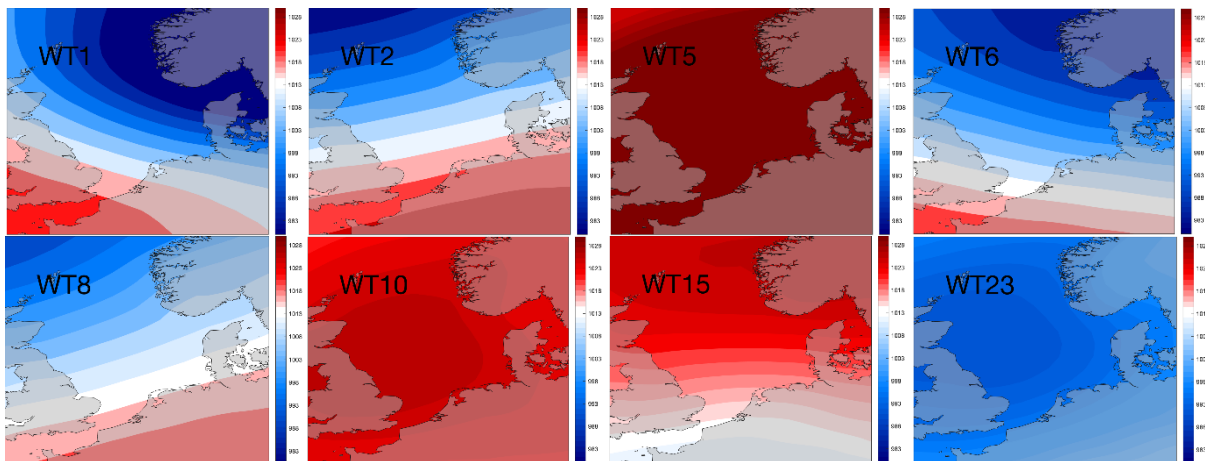
Figure 91: Some Weather Types (WT) when 25 Weather Types describe the weather conditions. High-pressure systems are indicated in red, low-pressure systems are indicated in blue, and white indicates sea level pressures equal to the global average sea level pressure of 1013 millibars.
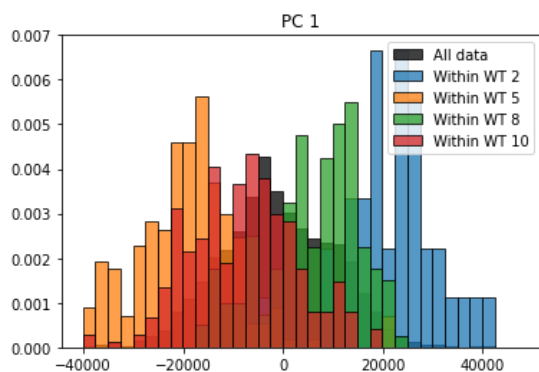
Figure 92: Probability of temporal values of Principal Component (PC) 1 when a particular weather type (WT) occurs.
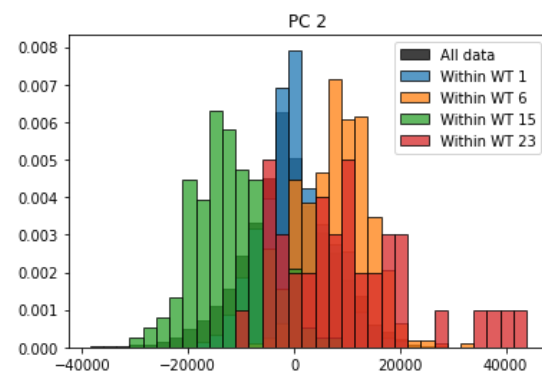
Figure 93: Probability of temporal values of Principal Component (PC) 2 when a particular weather type (WT) occurs.

The probability that a specific value of PC 1 occurs is depicted in Figure 92. The large values related to Weather Type 2 indicate a large positive energy flux towards the northeast, which is related to the southwestern wind that generates north easterly propagating waves. Weather Type 8 has a similar wind field. The isobars of this Weather Type are more widely spread, which indicates a lower wind speed that will generate a less energetic wave field, which is also reflected in the values of the Principal Components. Weather Type 10 shows a high-pressure system that rotates clockwise. It will generate a southwestern blowing wind and thus southwestern propagating waves. These waves propagate in the opposite direction described by Principal Component 1, and the Principal Component values are thus negative, at least for most of the captured conditions. A vast high-pressure system is described with Weather Type 5. This high-pressure system has its center north of the Netherlands, creating similar conditions as Weather Type 10. The main difference is the scale of the process, which leads to larger waves and thus a higher energy flux towards the southeast, thus a more negative temporal value for Principal Component 1.

The eigenvector values related to Principal Component give insight into the wave propagating into the northeast and southwest. The distribution of the temporal values is depicted in Figure 93. For Weather types 1 and 6, a northwestern wind generates a wave energy flux towards the southeast. The larger values of the Principal Components 6 indicate that the waves in the direction of Principal Component 2 are slightly larger during Weather type 6. A low-pressure system in the North Sea can create very large waves propagating towards the southwest, as shown by Weather Type 23. A counter-clockwise rotating low-pressure system south of the Netherlands described by Weather Type 15 has a large chance of creating offshore wind and consequential waves towards the northeast, which are recognizable by their negative values of the eigenvector.

The consistent agreement in sign and magnitude of the temporal values of the Principal Components related to wave spectral data and the estimated wind strength and direction substantiate the meaning and applicability of the Principal Components in analyzing the data. This information can therefore be useful in further analysis of the relation between wind and wave conditions.

6.6 General Discussion and Conclusion

This section elaborates on the main discussions and conclusions in chapters 6.2 to 6.5 to answer the two main research questions. In these subchapters are characteristic weather conditions formed into so-called Weather Types. The probability that Sea States and the Weather types are happening at the same time, the energy in wave families, and wave spectral data related principal components are used to analyze the relation between weather and waves and to substantiate the applicability of the used techniques.

6.6.1 Discussion

The expectation is that increasing the number of Weather Types and Sea States with post organization and a higher temporal resolution will give more insight into the relation between weather and waves. More Weather Types and Sea States will probably give more detailed insights but require more extensive post-analysis.

6.6.2 Conclusion

Strong relations between the weather and wave conditions can be found when Weather Types and Sea States are used to describe them. Estimations of the wind field by the position of the high and low-pressure systems correspond with simultaneously occurring wave fields.

Insight into the wave propagation direction is gained by analyzing the wave families. The wave families show that the wave propagation direction is related to the wind direction. The wave families show that waves can propagate from the pivot point of a high or low-pressure system and cross with waves generated at the same system's outer boundaries. Also, the curvature of the pressure systems plays an essential role in the wind direction and the direction of waves it generates.

The outcomes of clustering based on sea level pressure and its gradients are used to form and analyze 25 and 81 Weather Types. The 25 Weather types are useful for understanding the weather conditions when specific wave conditions are occurring. Applying more Weather Types will give more detailed insight into the relationship. Moreover, when Weather types are used as a starting point, at least 81 Weather types are required to analyze their impact in this study. More Weather Types will give more detailed insights but requires a more extensive post-analysis.

The wave families are able to describe the wave propagation directions. This information is useful for analyzing the wave propagation direction under certain conditions, such as the occurrence of the Sea States and Weather Types.

The Principal Components that are based on the wave spectral data give insight into the energy of waves, and are thus related to the wave energy flux. This meaning is substantiated during the analysis, where estimated wind directions and speeds are used to estimate wave propagation directions and heights. The Principal Components, including their temporal variability, can give insight into the wave field under specific (weather) conditions.

7 Spatio-temporal wind-wave driven potential sediment transport analysis

This chapter elaborates on the importance of the wave height and period, the water depth, and considering coexisting wave trains in estimating potential wave-driven sediment. Furthermore, the application of wave partitions, wave families, and potential impact of Sea States and Weather Types on wave-driven sediment transport is analyzed.

7.1 The approach

This chapter estimates the potential wave-driven sediment transport for the nearshore spectral data from 2012 to 2016 with an hourly resolution for each wave partition, wave family, and the whole spectrum, resulting in the 43.849 spectrums.

The sediment transport estimations are used to analyze the impact of using wave partitions and wave families on potential wave-driven sediment transport. An uncertainty factor is introduced that focuses on the interaction between coexisting waves when sediment transport is calculated for each wave partition or family separately. It gives insight into the importance and difficulties in the application of considering coexisting waves

Sediment transport estimations following traditional methods are used to get insight into the impact of Sea States and Weather Types and to get insight into the applicability of sediment transport estimations based on one representative wave. The similarities between Sea States and Weather Types are used to substantiate the relationship between Sea States and Weather Types.

7.2 Wave-induced (potential) sediment transport

The sediment transport formulation TRANSPOR2004 of Van Rijn, with 20 vertical grid points, is used to study potential sediment transport. Some simplifications in the boundary conditions are assumed to analyze the impact of various wave climates on bedload and suspended sediment transport. Such as flat bottom with median grain size (D_{50}) and 90% cumulative mass passing diameter (D_{90}) of respectively 0.25 and 0.3 mm and suspended sediment grain size (d_s) of 0.2 mm, at all the locations. Here is also the current (R_C) and wave (R_W) related roughness heights estimated at 5 cm.

The impact of sediment transport by various wave heights and periods is depicted in Figure 94. Here is visible that the sediment transport increases when the wave height increases and is strongly affected by the wave period, especially around a wave period of 5 seconds. Here a transition occurs between no sediment transport and a significant sediment transport flux increase with a minor increase in the wave period. More details about this transition are depicted in Figure 95. Here is visible that for waves with a significant wave height between 1 and 2 meters, the sediment transport is initiated at a wave period of 4 seconds. The sediment transport increases to a wave period of 18 seconds. The sediment transport increases relatively the most at the low wave periods, so does a wave period increase from 5 to 7 seconds increases the sediment flux by waves of 1.5 m from 0.021 kg/s/m to 0.087 kg/s/m, which is a factor 4.1 difference.
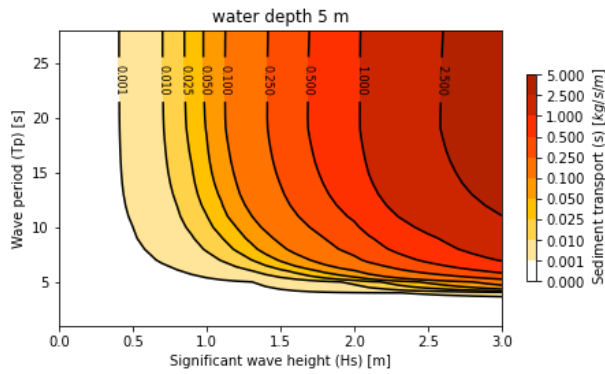
Figure 94: Wave induced: Sediment transport flux per meter of wave crest for various wave heights and periods for a water depth of 5 m, both bedload and suspended sediment transport are considered, following TRANSPOR2004 of Van Rijn. The sediment flux is expressed per meter of a wave crest, wherein 1 kg/s ≈ 31.500 tons/year.
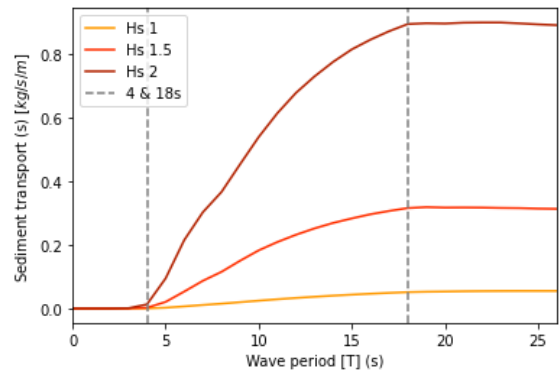
Figure 95: The wave-induced bedload and suspended sediment transport for a range of wave periods and wave heights, with a water depth of 5m, following TRANSPOR2004 of Van Rijn. The sediment flux is expressed per meter of a wave crest, wherein 1 kg/s ≈ 31.500 tons/year.

The water depth affects the sediment transport, just as the wave height and period. The wave orbital motion is more affected by the sea bed when the water depth decreases. The larger orbital velocities increase the stresses that induce bedload and turbulent motions that suspend sediment. This effect is visible in Figure 96, where the bedload and suspended sediment transport is depicted. The suspended sediment has a larger contribution than the bed, as shown in appendix X.
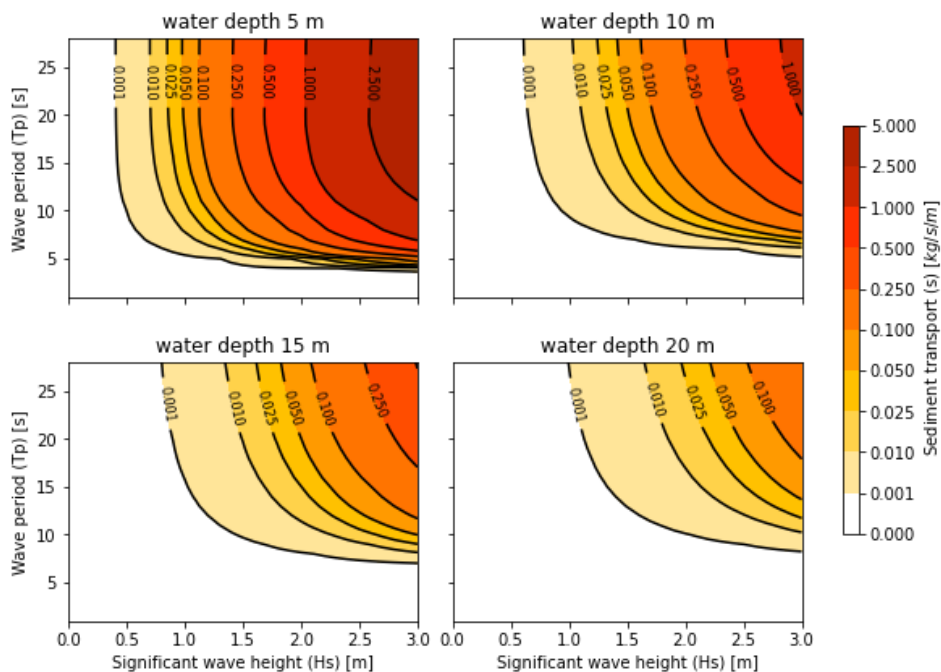
Figure 96: The effect of water depth on sediment transport for a range of wave heights and periods, following TRANSPOR2004 of van Rijn. The sediment flux is expressed per meter of a wave crest, wherein 1 kg/s ≈ 31.500 tons/year.

The relative contribution is probably related to grain size distribution and wave height, which this study will not investigate.

7.3 Sediment transport by traditional methods, wave partitions, and families

The wavefield shows different distributions of wave heights, period, and propagation direction when parameterized by one significant wave height, as done in many traditional methods, wave partitions, or families, as shown in chapter 4.7. This chapter maps the consequences of these parameterizations on sediment transport. It will then elaborate on the causes of the differences and potential solutions.

7.3.1 Sediment transport estimation approach

In the ideal case, the sediment transport can be calculated based on the water motion in multimodal wave spectral conditions, which is impossible with state-of-the-art methods. The challenges for estimating potential wave-driven sediment transport are investigated in this chapter.

<u>The philosophy and initial assumptions</u>

The sediment transport estimations when different wave trains are considered are very complex. The starting point of this approach is to assume that the sediment transport of traditional methods gives accurate results. Another assumption is that the coexisting wave partitions or wave families should transport the same amount of sediment as the traditional methods, with as main difference a difference in the direction of the sediment transport, which is related to the wave propagation direction.

For analyzing the impact of coexisting wave trains in this study, the assumption is made that the various wave partitions and families do not interact with each other, which is not valid. The mathematical interpretation is that the sediment transport of each wave partition or family can be considered as a vector. The length of the vector is the potential sediment transport. The length is based on the TRANSPOR2004 formulations where the significant wave height, period, direction, and water depth are considered together with constant boundary conditions described in chapter 7.2. The combined effect of the wave partitions or families is the superimposition of the vectors and is represented by a resultant vector.

This concept is depicted in Figure 97, where the sediment transport by the traditional method is contributed to two wave trains. The schematization corresponds with a wave train propagating towards the east and one to the north-northeast. The wave train towards the east transports about twice as much (potential) sediment as the other wave train. In traditional methods, the more energetic wave peak would lead to only sediment transport towards the east. Using the wave partitions or families results in sediment transport towards the east-northeast.
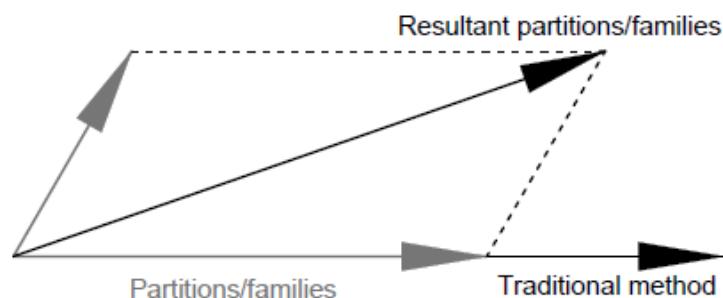

Figure 97: Sediment transport by vectorizing the potential wave-driven sediment transport for multiple wave partitions or families. The length of the vector is the amount of potential wave-driven sediment transport. The analogy corresponds with waves propagation towards the east and north-northeast. The traditional method accounts for all the sediment transport in the direction of the most energetic wave. Wave partitions or wave families account for sediment transport by the waves in both directions. The superimposition leads to the resultant vector.

Wave interaction

The amount of wave energy that causes sediment transport is equal when traditional methods, wave partitions, and wave families describe the wave field. If only the wave energy would be relevant, then is the expectation that wave partitions or families would cause the same sediment transport as the traditional method. So, the combined length (modulus) of the partitions or families would have the same length as the vector of the traditional method.

However, the sediment transport is not linear. This non-linearity can be related to the non-linear relation between shear stresses and flow velocities, the implementation of the threshold of motion to bedload, and the reference concentration that affects sediment suspension. Even when the wave period is considered constant, this non-linearity results in larger sediment transport predictions by traditional methods than by wave partitions or wave families, when the energy in the spectrum is used to estimate the significant wave height and their sediment transport.

This difference can be related to the fact that no interaction between wave partitions and wave families is considered when the sediment transport is estimated for each of them separately. So the threshold of motion and reference concentration is considered multiple times in multimodal wave conditions when wave partitions or wave families are used.

The physical interpretation is that energy within each wave partitions or family is used to induce the motion of grains and suspend sediment, which has to be done only once for each grain. So the energy of other waves can relatively more efficiently transport sediment transport. Here should also complex processes be considered. So does the increase of suspended sediment requires more energy to keep the sediment suspended. This energy will be used to counteract the gravity to force and thus the settling of sediment. So when more sediment is suspended, more sediment has to be stirred up, and thus more energy is converted to potential energy.

Cooping with non-linearity

This study aims to analyze the importance and application of coexisting waves and not to make an accurate estimation of potential wave-driven sediment transport. A so-called uncertainty factor is introduced to analyze the importance of considering coexisting waves and the impact of the wave period, which has been assumed constant before.

The impact of not-considering wave interaction and the uncertainty factor application is depicted in Figure 98, which corresponds to the situation described in Figure 97. When the wave period is assumed to be constant for all the waves, the impact of not considering wave interaction results in less potential wave-driven sediment transport by wave partitions or wave families and smaller sediment transport vectors (v_i). The sediment transport vectors are scaled by the uncertainty factor (f) to match the total length of the vectors with the length of the vector of the traditional method (T).
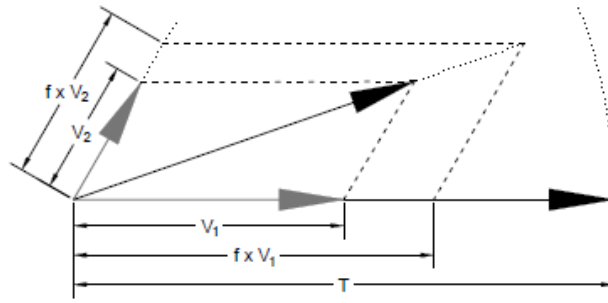
Figure 98: Sediment transport by vectorizing the potential wave-driven sediment transport for multiple wave partitions or families. The length of the vector is the amount of potential wave-driven sediment transport. Wave interaction is considered by scaling the sediment transport vectors(V_1 and v_2) from wave partitions and families with a factor (f). The combined length (modulus) of the scaled vectors matches that of the traditional method (T). The analogy of with wave propagation is explained in Figure 97.

Discussion of the applied approach

There are some downsides to scaling the sediment transport in this manner, which lead to inaccuracies. The linear scaling of sediment transport does not follow the non-linear relation between flow velocities and sediment transport. Furthermore, the sediment transport is scaled after considering the threshold of motion related to the Shield's critical shield stress. So waves that independently barely or not can move or suspend sediment are neglected. However, they might impact sediment transport, especially in multimodal wave conditions where many coexisting wave trains occur. Here the wave energy is divided among many waves, resulting in a relatively low amount of energy and wave height for many of the wave partitions and families.

Another aspect that should be considered is that the resultant vector will always be shorter than the traditional method when there is an angle between the waves described by the wave partitions or families. This means that the resultant potential sediment transport estimations from the wave partitions and families will always be smaller, although the vectors lengths and corresponding sediment transport match that of the traditional method. This does not match the philosophy for following waves, where the expectation is that the quantity of sediment transport is not affected. For crossing and opposing waves is the expectation that they could counteract each other, resulting in smaller resultant sediment transport. This reduction implies that scaling the resultant vector length to the vector of the traditional method is no option since elongating the resultant vector will neutralize the consequences of crossing and opposing waves. Due to the complexity of sediment transport, no straightforward implementable solution is found to analyze this issue.

Limitations of the applied approach

A general division in following, crossing, and following waves might be possible. For each of these classes, different mechanisms in the hydrodynamics could affect the sediment transport by waves. This study will not elaborate on this wave interaction, but it shows the importance of understanding the relation between hydrodynamics and sediment transport, which is part of the second sub-research question of the first main research question.

For following waves is the expectation that the waves cause sediment transport in a similar direction. The magnitude of the sediment transport caused by these waves might be larger than when these waves are considered independently. The peaks in intra-wave flow velocities for both wave harmonics could keep more sediment suspended and higher up in the water column. The combined shear stresses might increase the bedload. So the expectation is that the wave period of coexistence of the following waves might be very relevant.

Crossing waves will probably also cause additional sediment transport. The waves under an angle create in the horizontal plane an elliptical movement, wherein the flow velocities along the diagonal are probably larger than when the flow velocities in the direction of the waves are considered independently. The wave period could have a similar impact as in the case of following waves.

Opposing waves might cause less sediment transport. The bedload will consist of sediment that is moved back and forth, and the wave orbital motions in opposite directions might reduce the flow velocities at the bed. However, further analysis of the hydrodynamic motions and their impact on sediment transport is required.

7.3.2 The impact of wave period on potential sediment transport

One of the strong points of considering wave partitions and families is that it takes into account the wave period of the wave trains. The period significantly impacts sediment transport, as shown in chapters 7.2 and 7.3.3.

Wave partitions describe the wave period and direction for each wave train in the wave spectrum, while wave families and the traditional method describe the location of the largest energy peak in the frequency-directional spectrum and can therefore attribute the energy of two coexisting wave trains to one wave train. The energy of less energetic long perioded waves can be attributed to more energetic short waves, as explained in chapter 4.7. The change of wave period could impact the sediment transport since less energetic, and thus lower, waves can transport more efficiently transport sediment when their wave period is longer, as shown in Figure 94 to Figure 96.

The cumulative length of the vectors by wave partitions and wave families is compared to the length of the traditional method by the uncertain factor (f), described in chapter 7.2. The sediment transport by wave partitions and families is smaller than that of the traditional method when the uncertainty factor is larger than 1. The wave partitions and families estimate more sediment transport even without wave interaction if the uncertainty factor is smaller than 1.

A histogram of the scaling factor for wave partitions and families is shown in Figure 99 and Figure 100. It shows that the uncertainty factor for wave partitions (f_p) is 58% of the time smaller than 1. The factor is 37% of the time between 0.9 and 1, and 8% of the time smaller than 0.1. The uncertainty factor for wave families (f_f) is smaller than 1 for 17.4% of the time, 82.6% of the time larger than 1, for 48% of the time between 1 and 1.1, smaller than 0.1 for 3.7% of the time, and at least 2.0 for 12.8% of the time. Furthermore, when comparing the upper tails of the scaling factor for wave partitions and wave families than is visible that the upper tail related to wave families has a larger probability of occurrences, especially above a factor of 3.
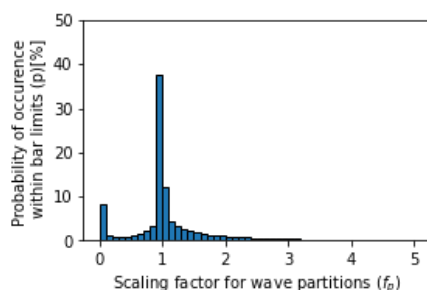

Figure 99: Histogram of the uncertainty factor for wave partitions (f_p). It is based on the 43.849 spectrums at location 42, depicted in Figure 45. The bin width is 0.1.
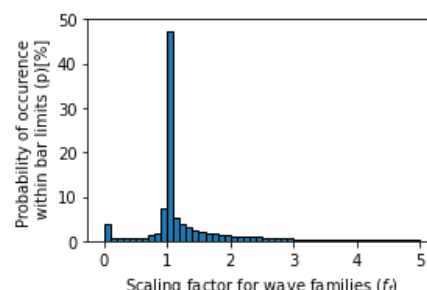
Figure 100: Histogram of the uncertainty factor for wave families (f_f). It is based on the 43.849 spectrums at location 42, depicted in Figure 45. The bin width is 0.1.

The frequent occurrence of an uncertainty factor smaller than 1 for wave partitions indicates that most sediment transport estimations are larger than that of the traditional methods most of the time, even without considering wave interaction. The uncertainty factor is smaller than 0.1 for 8% of the time, meaning that the sediment transport by wave partitions is at least ten times as large as the one by the traditional method for 8% of the time. The expectation is that sediment transport for each wave partition further increases when wave interaction is considered.

The uncertainty factor for wave families indicates that the sediment transport is under-predicted for 48% of the time when wave families are used. The sediment transport by wave families is less than half of that by traditional methods for 12.8% of the time. Sediment transport is at least a factor 10 larger for wave families for 3.7% of the time. This could be related to multimodal conditions where each wave family only gets energy attributed from one wave partition, and the energy from long perioded waves is not attributed to the short perioded waves in the same wave family.

When comparing the uncertainty factor from wave partitions and wave families, the impression is that sediment transport by wave partitions is frequently larger than that of the traditional methods since it distinguishes the long and short perioded waves. Wave families will attribute the energy from long perioded waves to short perioded waves when these are in the same wave family. The slight increase in wave height of the short waves results in a small increase in potential wave-driven sediment transport and a decrease in sediment transport by longer perioded waves. Considering the threshold of motion and reference concentration multiple times in multimodal wave conditions, together with the non-linear relation of flow velocity and sediment transport, results in a general underestimation of sediment transport described by wave families.

7.3.3 Sediment transport by one significant wave height, wave partitions, and wave families
This section elaborates on the importance of wave height and period in translating a wavefield to sediment transport. Here both the frequency of occurrence of sediment transport fluxes and their contribution to yearly sediment transport at location "I" near Schiermonnikoog will be analyzed. The wave distribution of the wave height is depicted in Figure 56. The analysis has been performed for multiple cross-sections, and the results show similar things.

<u>Results</u>
The number of occurrences that sediment transport fluxes are occurring towards a specific direction in the locations along the cross-section near Schiermonnikoog according to the traditional method, wave partitions, and wave families is depicted in Figure 101. The bars describe the number of occurrences that sediment transport fluxes are occurring within specific ranges and in the direction of the bar. The sediment transport flux, indicated with a specific color, occurs more often when the bar length increases.

The most nearshore location, location 71, of the traditional method shows that the waves are causing sediment transport fluxes towards the southeast. The sediment transport fluxes varies between 0 and 0.1 kg/m/s. Each bar captures waves within 10 degrees, so the waves that cause sediment transport are mainly within an angle of 40 degrees. At location 70 are smaller bars visible in a different direction, in general slightly more towards the east. Here two separate long bars with a smaller bar in between can be found. The difference that has been identified between locations 71 and 70 can be found when comparing locations 69 to 70, 68 to 69, and 67 to 68. The wave partitions at location 71 show waves that cause sediment transport fluxes between 0.001 and 0.005 kg/s per meter of wave length. When comparing the lengths of the bars at location 71 and other locations for the traditional method and wave partitions, than is visible that the traditional method describes relatively more occasions with high sediment transport. The wave families at location 71 describe frequently occurring low sediment transport flux events, but these are less than at the wave partitions. Furthermore, when comparing the more energetic sediment transport flux conditions

between wave families and partition, the wave families describe slightly more high sediment transport flux events. At location 70, the wave families mainly describe sediment transport in the south-southeast direction and fewer conditions towards the southeast compared to the traditional method and wave partitions. These differences can also be found at locations 67 and 68.

The relative contribution of each band of sediment transport at these locations is depicted in Figure 102. This has been achieved by summating all the sediment transport within each band, so within waves that cause 0.001 to 0.005 kg/m/s, 0.005 to 0.01 kg/m/s, etcetera. The figure shows only the cumulative (potential) sediment transport of bands of which the fluxes are larger than 0.01 kg/m/s, so the other cases lead to bars that are not recognizable. The largest upper limit of the recognizable bars has an upper limit of 1.0 kg/m/s. The direction of the sediment transport shows a similar pattern as the counting of events. The main difference is that the length of the high sediment transport events is more prominent compared to the counting. For the traditional method, the prominent direction of the sediment transport at location 71 is more towards the south-eastern direction than towards the most eastern direction of the four elongated bins. This bin shows in the counting of events, Figure 101, a high number of sediment transport events that transport at most 0.0001 kg/s/m, which are not visible in Figure 102. The traditional method at location 70 shows a relatively large bar in the south-southeast direction representing the sediment transport caused by events wherein sediment transport is within 0.5 to 1.0 kg/m/s. The total length of this bar is more prolonged than all the bars at location 71. The sediment transport towards the other directions is also caused by events that cause sediment transport within 0.5 to 1.0 kg/m/s but mostly by events that transport up to 0.5 kg/m/s. The bar lengths at location 69 are shorter than at location 70. Moreover, the same holds for locations 68 and 67 when the traditional method describes sediment transport.
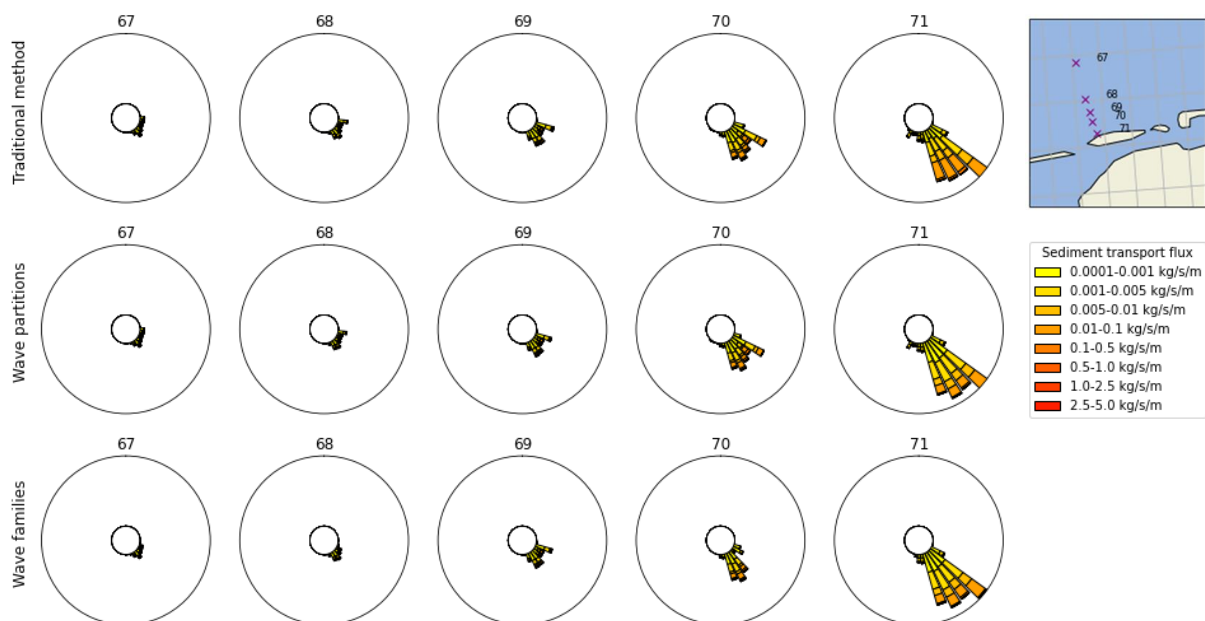
Figure 101: A sediment flux rose, the occurrence of sediment transport bands with their direction, for the traditional method, wave partitions and wave families, indicated on the left side of the figure. The bars describe the number of occurrences of sediment fluxes in the direction of the bar within the 43.849 considered spectrums. The bars are also relatable to the frequency and probability of occurrence. The significant wave height in each bar is based on the energy of the wave partitions within the directional boundaries of the bar. The sediment flux is expressed per meter of a wave crest without considering wave interaction, wherein 1 kg/s ≈ 31.500 tons/year. The titles refer to the locations near Schiermonnikoog at cross-section "I" and are depicted in the top right corner. From offshore to nearshore is the water depth approximately 25, 20, 15, 10, and 5 meters.
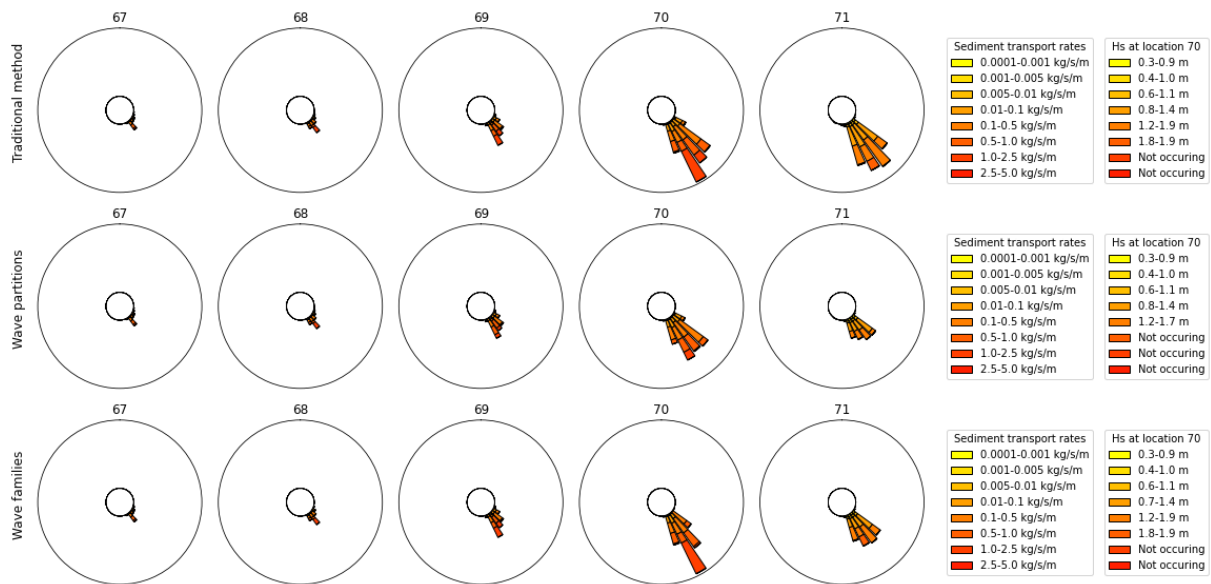
Figure 102: Cumulative sediment transport for each direction at the locations in cross-section "I", the locations 67 to 71, from 2012 to 2016. It shows similar information as Figure 101, with the main difference that the sediment transport is summated within each band of sediment transport flux. The bars show the summation in each direction rather than the counting. The legend shows the range in not only sediment transport flux but also the range of wave heights related to each sediment transport flux.

The traditional method, in Figure 102, shows different results when it is compared to the outcomes of the traditional method. So is, at location 71, the length of the bars shorter, and are the most eastern bars are the longest, while these are the middle two in the traditional method. At location 70 are the bars about the same length, except in the south-southeastern direction, which is significantly shorter than when it is described by the traditional method. The length of the bars degrees at location 69 compared to location 70. The length of the bars is slightly smaller than that of the traditional method. The cumulative sediment transport at locations 67 and 68 are relatively small and look similar to the outcomes of the traditional method.

The outcomes by the wave families at location 71 also describe less (potential) cumulative sediment transport than the traditional method but describe more sediment transport than the wave partitions. The relative length of the bars in the wave families is the same as that of the wave partitions, they are only slightly larger. When the bars are compared to the traditional method, the length of the most eastern bar is slightly larger. At location 70 is one large bar visible in the south-southeastern direction for both the traditional method and the wave families. This bar is shorter for the wave partition case. The other bars of the wave families are slightly shorter than that of the traditional method but larger than the wave partitions case. The outcomes of the wave families at locations 67 to 69 show similar results to the traditional method.

The maximum and minimum wave height for each sediment transport band is for each method depicted at location 70 in the most right legend. Here is visible that waves of 0.3 to 0.9 meters can cause sediment transport fluxes smaller than 0.001 kg/m/s. Sediment transport between 0.001 kg/m/s and 0.005 kg/m/s is caused by waves with a height between 0.4 and 1.0 meters. The other sediment transport bands also show an increase in wave height ranges. The ranges for each method are more or less the same and show wave heights overlap with adjacent sediment transport rate bands. The legend also shows that the maximum sediment transport rate is lower for the wave field described by wave partitions than when it is described by the traditional method or wave families. These two methods describe waves of 1.8 to 1.9 meter that causes sediment transport rates of 0.5 kg/m/s up to 1.0 kg/m/s. The maximum wave height in the traditional method is 1.7 meters for location 70.

<u>Discussion</u>

The description of the wavefield by traditional methods, wave partitions, and wave families affect the sediment transport events, as visible in Figure 101. The traditional method results in more events with larger sediment transport, while wave partitions and families describe the same waves more events with a low sediment flux, as visible at location 71. The wave partitions and families generally show the same results in counting the sediment transport rate events. However, a significant difference in the impact of south-easterly propagating waves can be distinct at location 70. In contrast to the wave families, the wave partitions show that the south-easterly propagating has many occurrences with sediment transport. This difference can be related to the description of the wave families, which describes the southerly and south-easterly propagating waves with one representative wave height, period, and direction. The results are similar to the case where the southerly propagating waves generally have more wave energy, and will be the representative wave direction within the wave family. So a large part of the sediment flux is attributed to another direction when wave families are applied. This case is similar to the example in Figure 54.

The importance of each sediment transport rate is shown by the cumulative sediment transport of each band. The waves at location "I" become essential for sediment transport when their flux is more than 0.01 kg/s/m, as visible in Figure 102. When comparing the sediment transport for the various methods, it is visible that the wave partitions make more distinction in sediment transport flux events than the traditional method and wave families, as explained above for location 70. The traditional method and the wave families probably contribute the energy of coexisting wave trains to the southerly propagating waves, thereby increasing the sediment flux in that direction and reducing the flux to the southeast.

When comparing the cumulative sediment transport for each method, it is visible that the traditional method estimates more sediment transport than the other methods, especially at location 71.

The importance of the wave period can be found when comparing the wave heights for each sediment transport rate band, which overlap considerably. When a wave height of 1.0 meters is considered in the traditional method, the wave can have a sediment flux between 0.001 kg/s/m up to 0.1 kg/s/m, which has a factor of 100 difference. This variation is smaller for many wave heights but often reaches a factor of 10. This large variation of sediment transport for one wave height shows the importance of considering the wave period in addition to the wave height.

Another aspect is that the impact of the nearshore processes on wave height and their sediment transport along the various locations can be recognized. This may imply that the nearshore conditions might be predictable when the offshore wave conditions are known.

<u>Conclusion</u>

The traditional method, wave partitions, and wave families describe the wave field differently. A different description of the wave height, propagation direction, and period impacts the sediment transport amount and direction when the TRANSPOR2004 formulations of van Rijn are used for each wave partition and family separately.

The wave period could be a very important parameter, the wide spread of potential potential sediment transport rates for a specific wave height could be up to a factor of 100. This range shows the possible consequences of combining two wave trains in the wave description.

Another conclusion is that estimating sediment transport for each wave partition or wave family independently, so without considering wave interaction, can greatly impact the sediment transport estimations. It can reduce the sediment transport estimated by wave partitions and wave families in multimodal wave conditions.

7.3.4 Sediment transport directions

This section elaborates on the resultant direction of the sediment transport estimations by wave partitions and wave families. The resultant sediment transport direction for each wave frequency-direction spectrum is affected by their description, as explained in 7.3.1 to 7.3.3. This chapter analyses if this impacts the resultant/net sediment transport direction over five years, from 2012 to 2016.

The sediment transport is less for multimodal wave conditions. The sediment transport is fully accounted for in unimodal wave spectrums, but when two or more wave partitions or families describe the wave field, the resultant sediment transport could reduce unintended, as explained in chapter 7.2.1.

This chapter analyzes the resultant sediment transport direction for two cases, the direct outcome of the sediment transport formulations and a case where the length of the vectors is scaled to the length of the traditional method.

This scaling aims to avoid cases where separation of the energy in multimodal spectrums would lead to minor sediment transport and, consequently, an underestimation of the impact of waves that propagate in different directions on the resultant sediment transport direction. The scaling is not intended to increase the accuracy of estimations, only as a straightforward way to include the impact of multimodal wave spectrums.

The unscaled approach

This section elaborates on the direct results and interpretation of the potential wave-driven sediment transport estimations.

Results

Various spatial patterns in the sediment transport captured by the wave partitions, families, and one significant wave height are recognizable in Figure 103. The outer rings are wave roses that show the distribution of wave heights according to wave partitions, as depicted in Figure 56. The arrows represent the resultant/net vectors for each considered method. The length is related to the amount of potential wave-driven sediment transport over five years, and the direction of the arrow shows the resultant sediment transport direction.

The arrows for the different methods have different lengths at various locations and show different results in sediment transport quantities. So is the arrow of wave partitions at location 71 about half the length of the arrow representing the traditional method. The arrow related to wave families is not much longer. A similar thing occurs at location 61, where the resultant sediment transport of partitions is longer than that of the wave families, and both are relatively short compared to the traditional method.

Also, minor changes can be found in the sediment transport angle. These deviations are the largest at location 70, where the sediment transport quantities of the different methods are also about the same.

A third observation is that, based on the arrow length, the sediment transport mainly occurs at the two most offshore locations and is very minor at the most offshore locations.

Many more results are observable in this figure like the relations between the wave propagation direction described in the wave rose on the outer circle and the net sediment transport direction, but that is not the scope of this section.
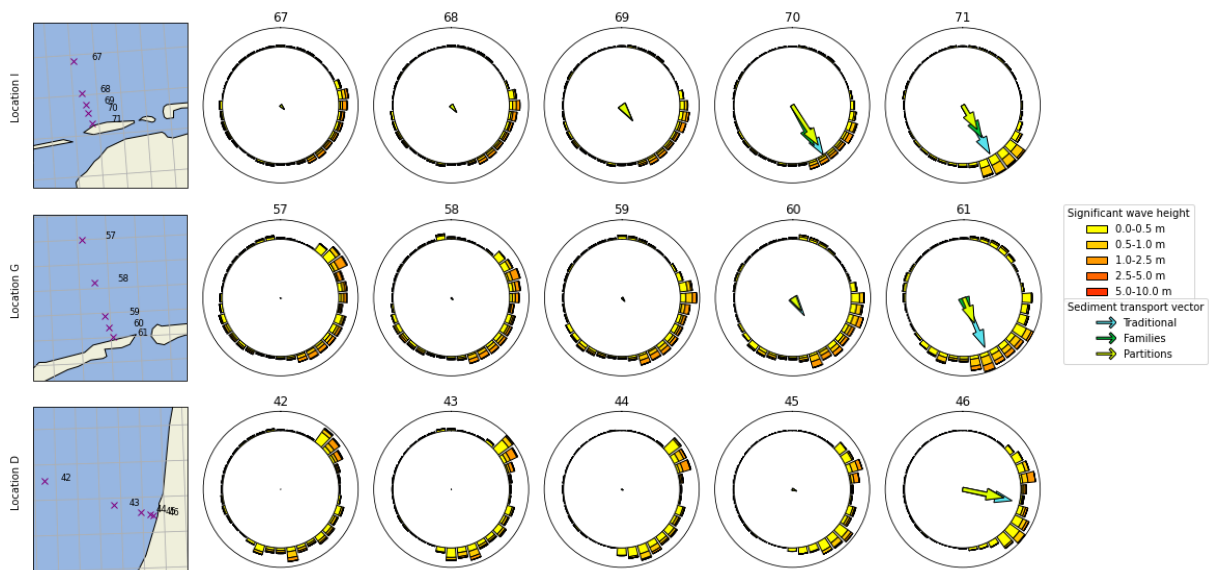
Figure 103: Unscaled sediment transport at various locations by traditional methods, wave partitions, and wave families. The sediment transport vectors are scaled to the maximal sediment transport within each cross-section. The outer ring shows the distribution of wave trains described by the wave partitions. The titles above each graph refer to the location depicted on the right. The depths from offshore to nearshore are approximately 25, 20, 15, 10, and 5 meters.

Discussion

The smaller arrows representing the sediment transport by wave partitions and wave families indicate that the sediment transport is affected when the sediment transport for each wave is calculated independently in multimodal wave conditions, as explained in chapter 7.2.1. The difference can lead to a factor of two or more differences in the final result, like locations 61 and 71.

Furthermore, minor deviations in the sediment transport directions are recognizable. These deviations are underestimated in the unscaled approach since the waves that are propagating in another direction have a reduced impact on sediment transport, especially if three or more wave trains are occurring. So with a reduced sediment transport capacity of following, crossing, and opposing waves propagating, their impact on the resultant direction is also reduced. The actual impact on the net sediment transport direction can hardly be analyzed due to the low sediment transport capacity of waves in multimodal conditions.

When comparing the sediment transport at the various locations can also be concluded that the sediment transport at the two most offshore locations at each cross-section, with a depth of 25 and 20 meters, has minor sediment transport compared to the nearshore locations. This corresponds with the statement that the coastal foundation is more or less the boundary of the sediment transport.

Conclusion

The resultant sediment transport direction and magnitude are affected by the method that is used, the traditional method, the wave partitions, or the wave families. The wave partitions and families estimate less sediment transport than the traditional method when no interaction between waves is considered.

<u>The energy-scaled approach</u>

This section elaborates on the scaled approach, where the sediment transport vectors of the multimodal wave conditions are scaled to the sediment transport by the traditional method.

Result

The result of the net sediment transport for the scaled approach is depicted in Figure 104. Here, scaling the sediment transport of wave partitions and families results in longer arrows of net sediment transport and a deviation in the net sediment transport direction for the different methods, compared to the results shown in Figure 103. Especially at location 70 are relatively large differences in sediment transport direction recognizable between the various methods.

Discussion

The results show that the sediment transport capacity and the impact of multimodal conditions on the net sediment transport direction at most locations are increased when scaled sediment transport by wave partitions and families are used. Here should be realized that there are cases where sediment transport is reduced in multimodal conditions. Hence, the expectation is that the deviations in sediment transport direction can be larger than what the results show.

The angle between the waves and the cross-shore impacts alongshore sediment transport. The sediment transport calculated in this study is only related to the wave orbital motion. The effect of wave-breaking induced currents and other mechanisms are not considered. The angle difference between the vectors at location 70 indicates that the wavefield parameterization affects the dominant/resultant wave direction. The wave-breaking induced currents and consequential sediment are thus also affected.

Conclusion

Scaling the wave-driven potential sediment transport of wave families and partitions to the outcome of the traditional method generally increases sediment transport for wave partitions and families. This increases the impact of multimodal conditions on the sediment transport estimation and leads to a larger deviation in the resultant sediment transport direction. However, for some spectrums, the sediment transport estimation will be reduced, which will affect the outcomes.
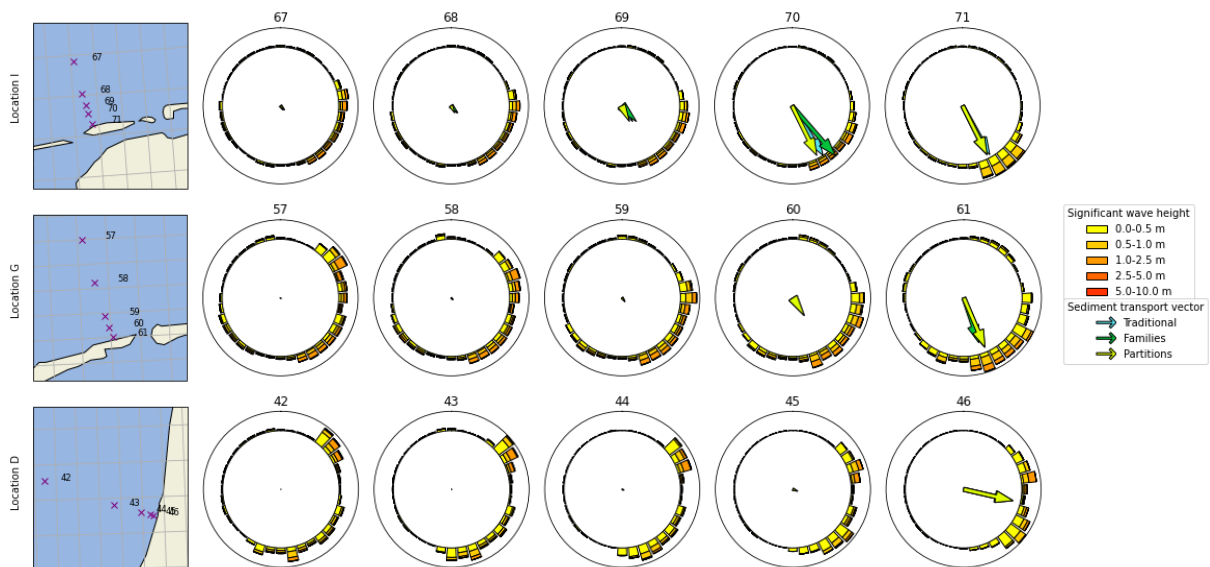
Figure 104: Scaled sediment transport by traditional methods, wave partitions, and wave families at various locations. The sediment transport vectors are scaled to the maximal sediment transport within each cross-section. The outer ring shows the distribution of wave trains described by the wave partitions. The depths from offshore to nearshore are approximately 25, 20, 15, 10, and 5 meters. Waves only potentially drive sediment transport, in this estimation.

7.4 Sediment transport by Sea States

The positioning of the low and high-pressure systems and their magnitude impact the wavefield, as concluded in chapters 6.3 and 6.4. This section elaborates on the contribution of each Sea State to sediment transport, estimated by the traditional method, for location 42 at the Coastal Foundation and location 46 near the shoreline. These locations are depicted at Location D in Figure 104. Chapter 7.5 elaborates on the relation of the Sea States with Weather Types.

7.4.1 The relevant Sea States at the Coastal Foundation

The yearly average impact of each sea state on sediment transport at location 42 is depicted in Figure 105. Here is visible that the impact difference for each sea state is very different. Four outliers cause more than 1 ton of sediment transport for each event, which has a duration of 6 hours. A remarkable observation is that these events only occurred in 2012 and 2013. In 2015 only a relatively minor event occurred, captured with sea state 54, from which the impact during 6 hours is about an order smaller than the four most prominent events.
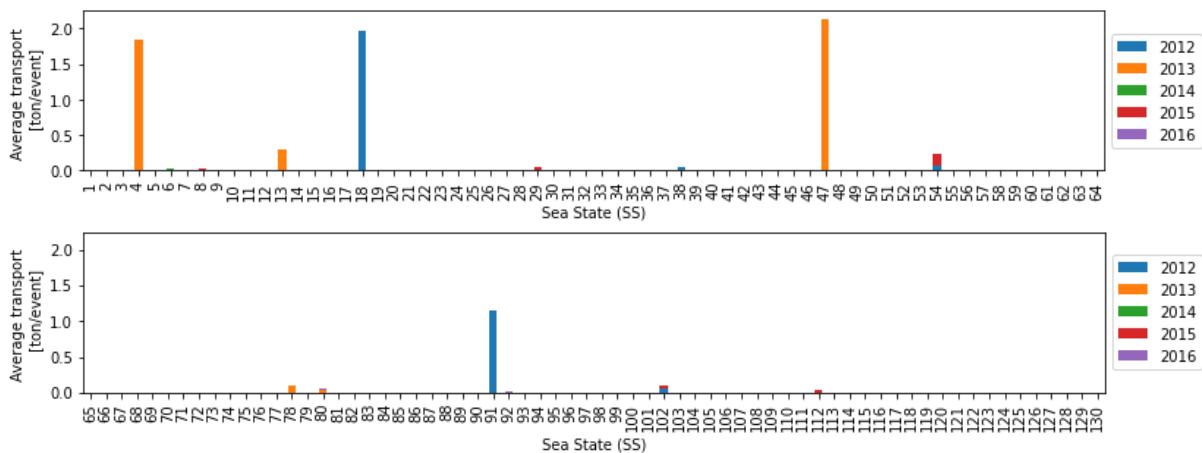
Figure 105: Average sediment transport for each Sea State (SS) at location 42.

The cumulative sediment transport by each sea state (SS) for each year is depicted in Figure 106. This figure shows that about 25 of the 130 sea states contribute to the yearly sediment transport. It also shows that the four events with a significant impact on sediment transport only occur once, and Sea State 54 has a large contribution to sediment transport due to its persistence, especially in 2015.
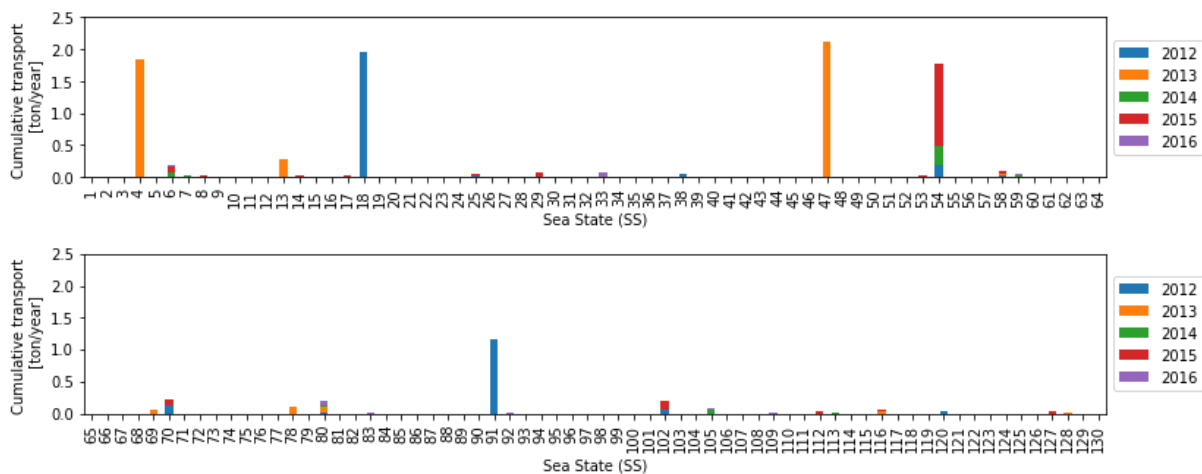
Figure 106: Cumulative sediment transport for each Sea State (SS) at location 42

The yearly sediment transport caused by Sea States that contribute at least 0.1 ton in five years is depicted in Figure 107. It shows the relative contribution of each of the 11 Sea States that impact sediment transport most. The ten largest are depicted in Figure 108. Here, the wave spectrums with the most considerable wave heights contribute most to the sediment transport. Cluster 6 shows that the very frequent occurrence of south-westerly propagating waves with a height of around 1.0 meters still contributes a noticeable amount of sediment transport. However, this is still minor compared to Sea States 4, 18, 47, 54, and 91.
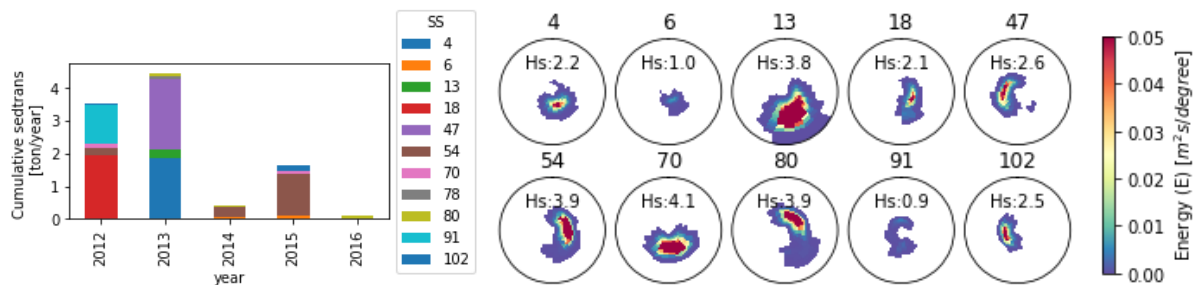
Figure 107: Yearly sediment transport at location 42 with the most contributing Sea States. A threshold of 0.1 ton over five years is set as a threshold.

Figure 108: The most contributing Sea States at location 42, according to the traditional method for estimating sediment transport.

The large contribution of sediment transport in 2012 by Sea State 91 is remarkable since this spectrum shows 3 energy peaks related to northerly, southerly, and westerly propagating waves. Traditional methods do not account for the different directions in sediment flux, and there is no method to consider the combined impact on sediment transport by these waves.

7.4.2 The relevant Sea States near the coastline

The average contribution of Sea States on sediment transport near the coastline, location 42, is depicted in Figure 109. Here is visible that more and different Sea States are important near the coastline than at the Coastal Foundation. The average amount of sediment transport is also more significant at the nearshore location than at the Coastal Foundation, which corresponds with the analysis of chapter 7.2 and the concept that the sediment transport is mainly between the Coastal Foundation and the shoreline.
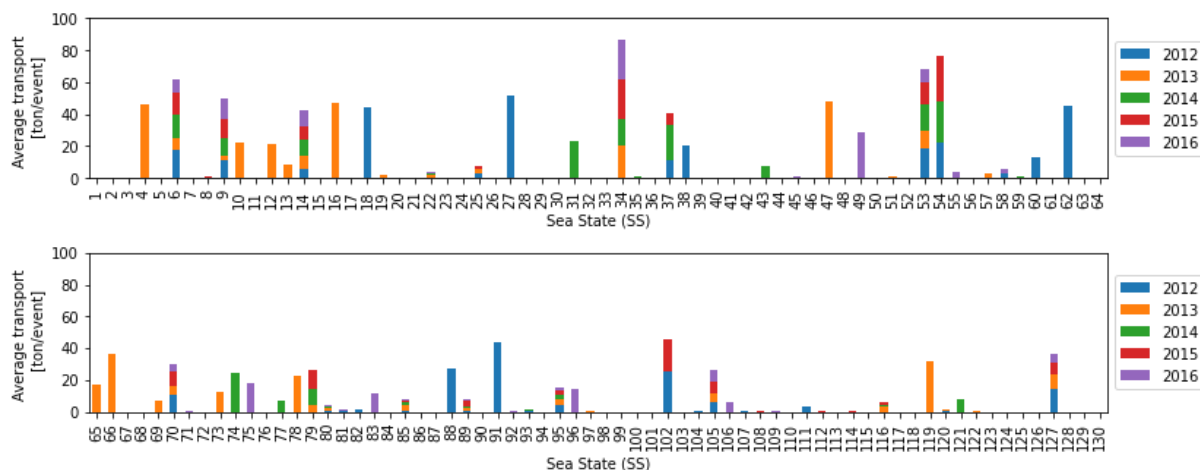
Figure 109: Average sediment transport by Sea States at location 46.

The yearly cumulative sediment transport for the Sea States is depicted in Figure 110. The contribution of each Sea State to sediment transport is up to two orders larger and is affected by more Sea States than at the offshore location 42, just as their impacts per event.
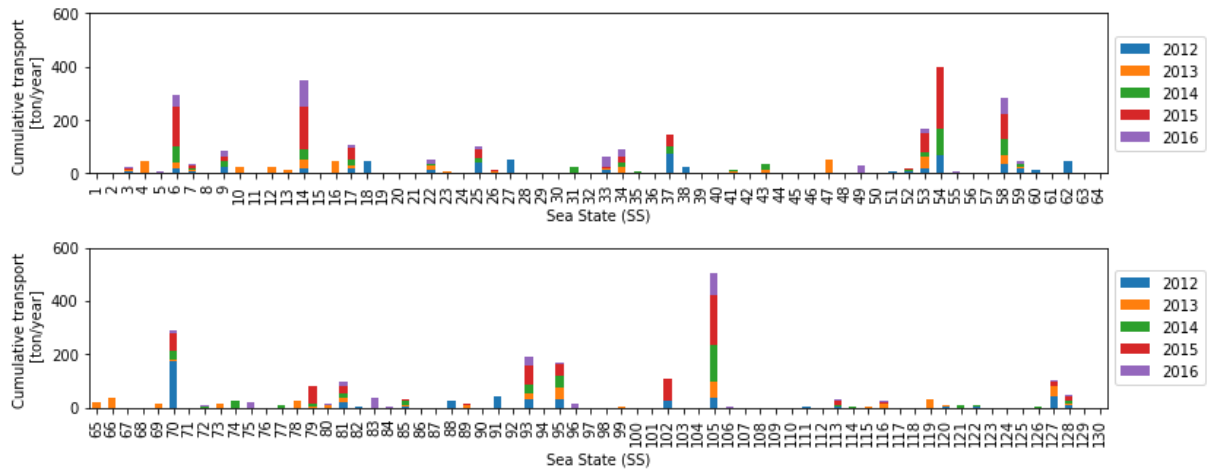
Figure 110: Cumulative sediment transport by Sea States at location 46.

The yearly sediment transport is more constant near the shoreline than offshore. Without considering wave breaking, wave-induced currents, and other influences, the wave motion transports potentially about 1000 tons/year of sediments each year, Figure 111. The six most contributing Sea States are depicted in Figure 112. Here is visible that long periaded southerly propagating waves and a wide range of short periaded easterly propagating waves cause a lot of sediment transport.
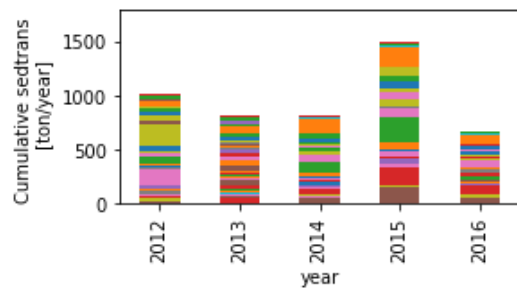
Figure 111: Yearly wave orbital-motion driven sediment transport at location 46.
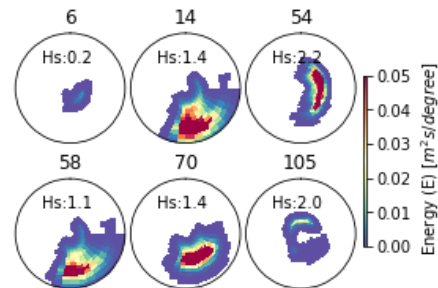
Figure 112: The six most contributing sediment Sea States to sediment transport by wave orbital motion at location 46, the wave period is capped at 20 seconds.

The large contribution of Sea State 6 to sediment transport is not expected since it describes relatively low short waves. Despite that, it caused more than 200 tons of sediment in 5 years and contributed mainly in 2015. Sea State 105 describes the most dominant wavefield regarding sediment transport, although the average sediment transport in 6 hours is not very much. The sediment transport of this predominant sea state shows waves propagating in many directions and a considerable amount of opposing waves.

7.4.3 Concluding remarks

The sediment transport at the coastal foundation is very minor and only affected by a few Sea States. More Sea States become relevant and induce more sediment transport when the water depth decreases. These Sea States become relevant due to their high sediment transport capacity or due to their consistent occurrence. These Sea States cover waves propagating in a wide range of directions.

7.5 Sediment transport by Weather Types

This section elaborates on the potential sediment transport when one of the 81 Weather Types occurs. The Weather types, derived in chapter 6, are considered to be representative of the whole day, wherein sediment transport is caused by four Sea States, each representative for 6 hours. This section elaborates on location 42 near the Coastal Foundation and location 46. The locations are depicted in Figure 104.

7.5.1 The relevant Weather Types at the Coastal Foundation

The average sediment transport at location 46 caused when a Weather Type is occurring is depicted in Figure 113. Here is visible that the sediment transport during Weather Type 47 and 75 is significant compared to the other weather types.
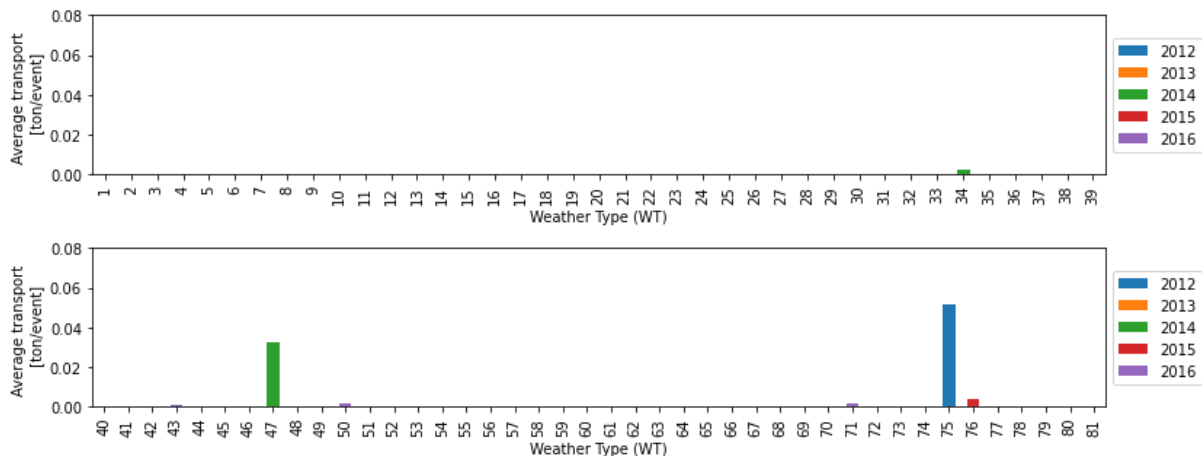
Figure 113: Average sediment transport caused by each Weather Type (WT) at location 46.

The cumulative yearly sediment during the Weather Types is depicted in Figure 114. This figure shows that Weather Type 20 impacts sediment transport most, regardless of its low sediment transport capabilities. Weather Type 34 shows similar patterns, with the main difference that it contributes sediment mostly in 2012 and 2015 rather than in 2013. The large sediment transport that occurred during Weather Type 75 does not occur very frequently and is therefore not dominant at this location. The Weather Types give a similar trend as the Sea States, which is a relatively low amount of sediment transport restricted to a limited number of conditions.
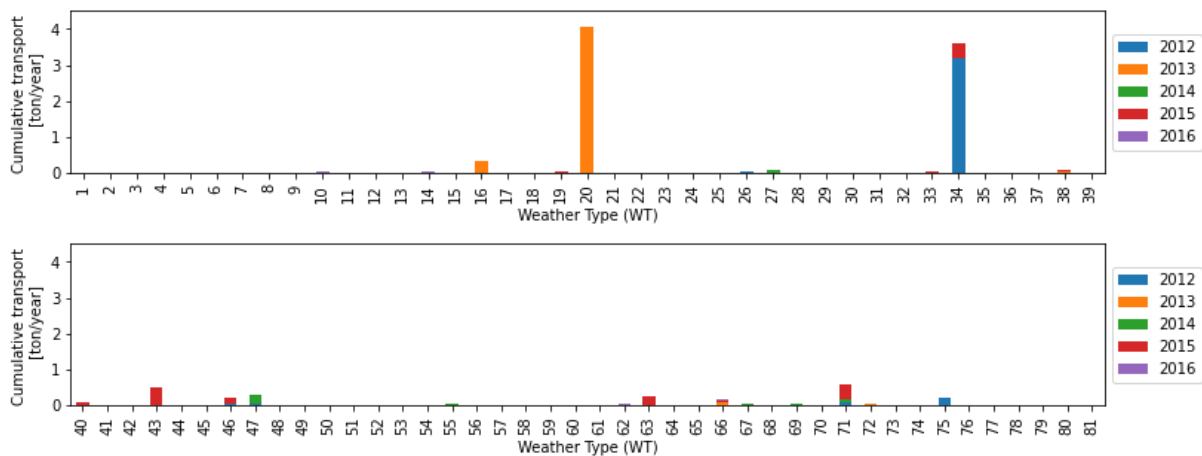
Figure 114: Cumulative sediment transport caused by Weather Types at location 46.

The yearly sediment transport corresponding to the most contributing Weather Types is depicted in Figure 115. The three largest Weather Types are depicted in Figure 116. This figure shows that the large sediment transport in 2012 is related to a low-pressure system that pivots around Denmark's east side. This counter-clockwise rotating system will generate waves that propagate towards the south to south-west if nearshore processes are not considered. The sediment transport by this Weather Type is probably related to Sea States 18 and 91 that caused the main sediment transport in 2012, as shown in Figure 107 and Figure 108. These wavefields describe westerly propagating waves and a multimodal wave spectrum. In 2013 the sediment transport was mainly caused by a high-pressure system positioned north of the North Sea. It will create an eastern wind and thus wave propagating towards the west. This corresponds with the predominant Sea States 47 and 102 that describe westerly propagating waves with a significant wave height of around 2.5 meters. The sediment transport in 2015 is mainly caused by Sea State 54, which describes easterly propagating waves, as shown in Figure 107. This wavefield corresponds with Weather Types 43, 54, 63, and 71 that cause a western wind.
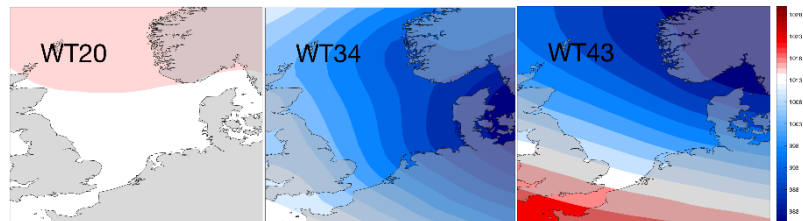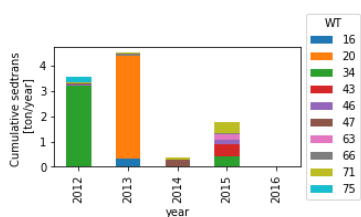
Figure 115: Yearly sediment transport at location 46 captured by Weather Types, with a threshold of 0.1 ton per 5 years

Figure 116: The Three most important Weather Types for sediment transport. White indicates the global average sea level of 1013 millibars, red indicates a high-pressure system, and blue is a low-pressure system.

7.5.2 The relevant Weather Types near the coastline

This section elaborates on the sediment transport at location 46 and its relation with the occurring Weather Types. The average sediment transport for each Weather Type and year is depicted in Figure 117.

This figure shows that more Weather Types cause considerable sediment transport compared to location 42. The average sediment transport is also higher.
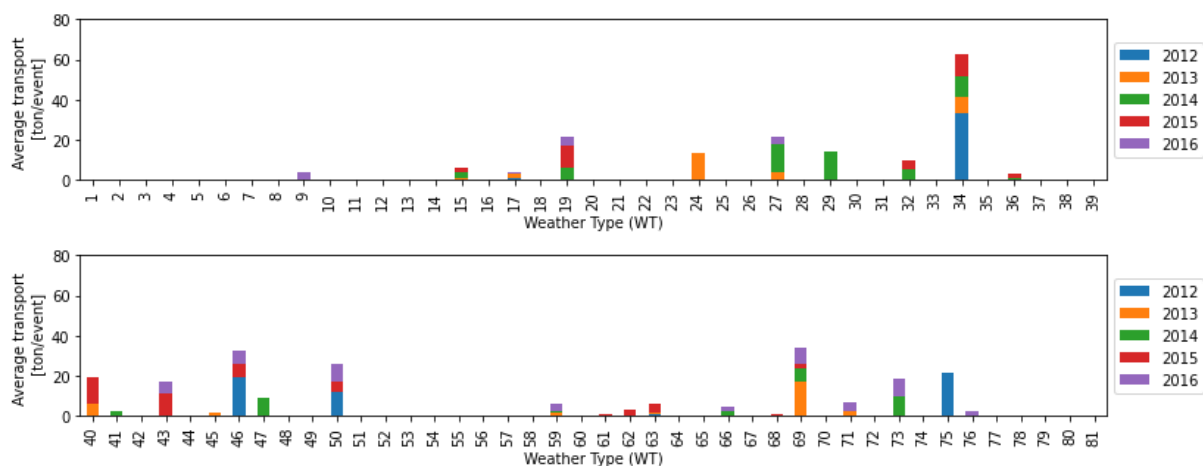
Figure 117: Average sediment transport caused by each Weather Type (WT) at location 46, for 81 Weather Types.

The cumulative sediment transport for 2012 to 2016 is depicted in Figure 118. This figure shows that Weather Types 16, 20, 27, 34, 43, 46, and 71 have the largest contribution to sediment transport. Each is responsible for at least 200 tons in five years.
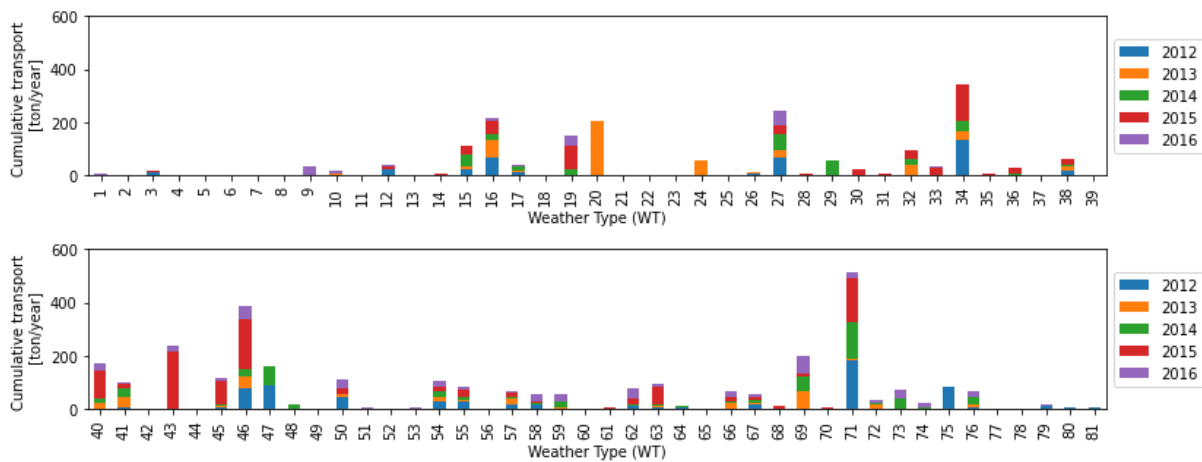
Figure 118: Cumulative sediment transport caused by Sea States at location 46, for 81 Weather Types.

The yearly potential contribution of each Weather Type on wave-driven sediment transport is depicted in Figure 119. Here is visible that many Weather Types cause a considerable amount of sediment transport, not only the Weather Types that cause high sediment transport on average but also other Weather Types.
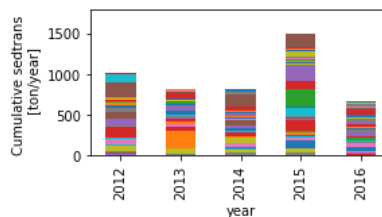
Figure 119: Yearly wave orbital-motion driven sediment transport at location 46 by 81 Weather Types.

The results show that there are more relevant Weather Types at the nearshore location than offshore and causes more sediment transport, which is similar to the Sea States.

7.5.3 Concluding remarks
The analysis and outcomes of the Weather Types have many similarities with the Sea States. The sediment transport at the coastal foundation is minor and only affected during a few Weather Types. More Weather Types become relevant and induce more sediment transport when the water depth decreases. This increases the complexity of the post-analysis.

7.6 General Discussion, Conclusion, and recommendation

This subchapter uses the main discussions and conclusions made in subchapters 7.2 to 7.5 to answer the two main research questions. The subchapters elaborate on the importance and complexity of analyzing the impact of coexisting waves on sediment transport. It also focuses on the relation between waves and sediment transport, weather and sediment transport, and their substantiation in the relationship between weather and waves.

7.6.1 Discussion

Sediment transport by multimodal wave spectrums is complex. Predicting the sediment transport relatively straightforwardly requires simplifications that reduce the outcome of the sediment transport models. The large variety in sediment transport estimations by the traditional method, wave partitions, and wave families show that the parameterization impacts the quantities and directions of sediment transport. The extent of these impacts could not be defined with certainty but might be considerable.

The relation between weather, waves, and sediment transport has been analyzed by comparing the outcomes of two different grouping operations and the statistics of wave spectral data that is attributed to each group. Although agreements could be found at the offshore location, it is very complex and time-consuming to do this for nearshore locations, where the nuances captured by the Weather Types and Sea States become important. Further analysis is required to verify the relation to nearshore locations, but the expectation is the relation between weather, waves, and sediment transport also holds on the nearshore. Here may insight into the nearshore processes help predict sediment transport between the Coastal Foundation and the shoreline by offshore conditions.

7.6.2 Conclusion

The analysis shows that the wave height, wave period, wave direction, and the coexistence of wave trains are important when considering potential wave-driven sediment transport.

The co-occurrence of matching wave fields and weather conditions that cause sediment transport in the years 2012 to 2016 substantiate the relation between waves and weather, where the wind data for each Weather Type is relatable to wave conditions and, consequently, sediment transport.

The analysis also shows that it is complex to analyze the influence of coexisting waves on sediment transport. This complexity is due to the non-linear relation between flow velocities and shear stress and other aspects like a threshold before sediment transport and sediment suspension by other wave trains, for example, through a reference concentration.

7.6.3 Recommendation

Analyzing the specific impact of Weather types on Sea States and their impact on sediment transport is complex nearshore when the results of two different clustering operations are compared.

Reducing the number of the Sea States and Weather types gives more insight into the prominent trends, but at the cost of information about the rare events that drive a lot of sediment transport. Increasing the number of Sea States and Weather Types gives a more distinct picture of the relation between Weather Types and Sea States but requires more extensive post-research. The minimal number of Sea States and Weather Types should also be analyzed and considered.

Another alternative to comparing the outcomes of two different grouping operations is to consider all the data in the grouping operation. This operation might combine the relevant Sea States and Weather Types, which eases the post-analysis and gives a more detailed insight into the relation between Sea States, Weather Types, and their impact on potential wave-driven sediment transport.

Discussion, limitations, and recommendations

When answering the two main research questions, certain considerations and choices have been made. This chapter elaborates on this and its impact on the research outcome.

The used data
The wave spectral data at the offshore and nearshore location and the wind data that has been used in this study induces some limitations.

The offshore data from ERA-interim has a six-hourly resolution from 1978 to 2018 at every longitudinal and latitudinal coordinate. The temporal resolution is relatively coarse when both the offshore and nearshore data are considered. It reduces the temporal resolution of which the nearshore data could have been analyzed. ERA-5 is an alternative solution, but this has not been used for consistency with the modeled nearshore spectral data.

The nearshore data is only considered for five years at 42 locations along the coast due to the computational and time limitations. The considered period does not capture all the situations occurring on the Dutch coast, which is visible because one of the 25 Weather Types, based on weather data from 1978 to 2018, did not occur between 2012 and 2016. Another drawback is that uncertainties are pretty high when only five years of data are considered, which reduces the accuracy of the outcomes. Furthermore, the 42 locations make it possible to analyze changes along the coast, but not in great detail locally.

The weather data that has been used has a resolution of 24 hours. The choice is made to have the weather condition representative for the whole day, thus also for wave condition 18 hours later. This induces some noise in the outcomes when the impact and relations to Weather Types are analyzed. This noise can be reduced by only taking representative wave spectral data, but this greatly reduces the number of wave conditions that are considered in the analysis.

Sediment transport estimation approach
The sediment transport in this study has been estimated straightforwardly, while it is a complex process. The approach, required assumption, and outcomes give a first impression of the importance and application of estimating sediment transport, as concluded in the next chapter.

It is recommended to further analyze the sediment transport by coexisting wave trains to make the estimations more accurate and physically substantiated. A thorough investigation would be to examine the hydrodynamics under multimodal wave conditions. If this is known, then the effects of tidal, wave breaking, and density-induced currents and their effect on turbulence can be taken into account, which highly impacts sediment transport. Another approach could be to describe the impact of these mechanisms and the coexistence of wave trains by additional terms or factors in currently existing sediment transport models, like the implementation of Turbulent Kinetic Energy in the sediment transport formulations of Van Rijn. The impact of coexisting wave trains might be relatable to the threshold of motion and the reference concentration in the formulation of Van Rijn.

Wave-driven sediment transport by Weather Types and Sea States

The Sea States and Weather Types give insight into the importance of each weather condition and sea state on the potential wave-driven sediment transport. Changing the probability and corresponding contribution of each condition on sediment transport can give insight into the impact of wind and wave climate changes on the magnitude and direction of the sediment transport.

However, the estimations do not consider the impact on the alongshore currents and their impact on sediment transport. It does also not consider the impact of temporary changes in the bathymetry and shoreline characteristics on sediment transport. Both aspects are critical to assess when performing a local analysis, which requires more detailed information.

The next step to study could be to include other sediment transport related processes as well in the description and analysis of Weather Types and Sea States. On the Dutch shore this could be processed related to tides, density-driven residual currents, and the influence of the freshwater from, for example, the Rhine.

Further analyzing the wind, weather, and wave relations

This study uses several distinct machine learning operations' outcomes to analyze the relation between weather and waves, requiring extensive post-analysis. A more accessible insight into this relation might be possible by performing one operation where all the wave and weather data are considered. Based on this research is the expectation that the computational demands are pretty extensive.

The relative importance of the wave and weather parameters is affected by the scales of the parameters since the parameters that have a larger spreading have more influence on the Euclidian distance and the point density, which are used in the machine learning techniques. When the data is standardized, each parameter has the same range and impact on the outcome. Not standardizing the data or using different scales can change the focus of the outcomes, which is not analyzed in this study. Different importance of the parameters might be useful if more value is attributed to the wave data than weather data, for example, due to the wave travel time that impacts the direct relation between wind and waves.

In this study is the wave data is standardized before it is analyzed with Principal Component Analysis, Maximum Dissimilarity Analysis and processed with the kmean algorithm. So, the parameters that describe only minor wave energy have the same importance as those that capture more wave energy and thus have a larger variability. The expectation is that if the data is not standardized, the bins that describe higher wave energy densities and thus have a larger variability will have more impact and therefore results in more nuance of high energetic wave conditions. This is possible since the units of all the parameters are the same. This study does not investigate the impact of standardizing the data on the outcomes.

Conclusion

This study analyzes the importance and application of accounting for coexisting wave trains in sediment transport estimations, wherein the wavefield's temporal and spatial relations and variability are important. The temporal and spatial relations are affected by (wind) climate and wave propagation, where nearshore processes play an essential role. Insight into these relations is achieved by analyzing trends in weather data, wave spectral data, and sediment transport predictions. Spectral data along the Dutch shore and the southern part of the North Sea basin, large-scale weather data, and sediment transport predictions are used, in combination with machine learning techniques, to get insight into these trends.

The outcomes of the study are used to answer the two main research questions, "**What is the relation between large-scale atmospheric patterns, the wind-wave frequency-directional spectrum, and potential sediment transport in the nearshore of the Netherlands?**" and "**Can wave partitions, wave families, groups of similar wave frequency-directional spectrums, and characteristic weather conditions be used to predict potential sediment transport by waves?**". Two sub questions are used to answer the first main question: "What is the relation between large-scale atmospheric patterns and the wind-wave frequency-directional spectrum" and "What is the relation between the wave frequency-directional spectrum and potential sediment transport?".

The relation between wind, wave, and potential sediment transport

The answer to the first research question is that the positioning and magnitude of high and low-pressure systems create a specific wind field and sea level pressure gradient, called a synoptic atmospheric pattern. More energy is transferred to the waves when the pressure gradient and thus the wind speed increases, resulting in larger waves. The wind generates waves with different periods and, consequently, travel speed. These waves travel to adjacent waters, potentially causing coexisting wave trains in the wavefield with a different period, direction, or both. Even one high- or low-pressure system can generate a multimodal wave spectrum locally, where waves generated at its pivot point cross waves that are generated more towards the edge of the weather system.

This study shows that multimodal wave spectrums occur 65% of the time, even though Great Brittain partially shelters the North Sea. A large part of these multimodal spectrums shows crossing and opposing waves. Following waves only occur for southerly propagating (swell) waves that have passed along the coast of Norway.

The outcomes of the potential wave-driven sediment transport estimations show that the wave height, the wave period, the wave direction, and the number and relative angles of all the wave trains should be considered when estimating sediment transport in a multimodal wave condition. The wave period significantly impacts sediment transport, up to a factor of 10 and sometimes a factor of 100, and the coexisting wave trains can impact the direction and magnitude of sediment transport considerably.

The dominant wave and weather conditions for sediment transport have shown that they predict sediment transport for similar environments. At the offshore locations are relatively few conditions important. The variety of conditions that are relevant for sediment transport increases when the distance to the shoreline decreases. This development, combined with the increase in sediment transport rates, makes the analysis more extensive for these locations.

The sediment transport estimations for each Weather Types and Sea State can quickly give insight into the impact of various wave and weather conditions on sediment transport. This study has shown that the conditions that impact the sediment transport the most vary over the years and capture rarely occurring stormy and highly energetic conditions but also consistently low energetic conditions. The most important wave conditions show coexisting wave trains that can be classified as crossing and opposing waves. The wave angles in these conditions show the importance of considering wave trains independently.

Insight into the impact of a changing (wind) climate can relatively easily be obtained by changing the probability that a certain weather or wave condition occurs and summing the sediment transport for each condition. So does, for example, the sediment transport increases when the consistently occurring situations become more energetic, or the frequency of high energetic conditions becomes more frequent than the situation between 2012 and 2016. Also, the sediment transport direction might be impacted if the wind and consequential wave direction change. This change does not only impact the sediment transport driven by the waves but also the consequential currents along the shoreline. Here, the positioning of the high and low-pressure systems and their consequential wind and waves impact the number of coexisting wave trains, their relative angle, and thus the sediment transport.

The applicability of wave partitions, wave families, Sea States, and Weather Types

The relation between weather to waves and sediment transport has been analyzed by spatial-temporal analysis. Here Principal Component Analysis, Maximum Dissimilarity Analysis, and a kmean clustering algorithm have been applied to analyze the wave spectral data and form representative characteristic wave conditions, called Sea States. A similar approach, without Maximum Dissimilarity Analysis, is used to describe the weather data by Weather Types, which can be described by the sea level pressure and its gradient, related to the positioning and magnitude of high- and low-pressure systems.

The wave partitions make it possible to analyze groups of waves with a similar propagation direction and periods, called wave trains. Temporal statistics of wave partitions are used to form wave families, and give insight into frequently occurring wave trains, called wave systems. The wave partitions and families give additional insight into the main propagation direction and relative angles for wave trains in spectral data that are described with a Sea State or occurring during a specific Weather Type. Both analyses show similar results and substantiate the relationship between - and the applicability of Sea States and Weather Types.

The distribution of the wave heights and their propagation varies by the description for the traditional method, wave partition, and wave families. The wave partitions use the energy peak related to a wave train, while wave families and the traditional method sometimes attribute the energy from one wave train to another more energetic wave train. As a result, energy is attributed to waves propagating in another direction or from long perirded waves to the more energetic short perired waves when traditional methods and wave families are applied. Due to this attribution is the wave field description by wave partitions the most physically substantiated.

The potential wave-driven sediment transport for coexisting waves, described by wave partitions or wave families, is analyzed by assuming the sediment transport for the various waves can be interpreted as vectors. Here, the length of the vector is related to the magnitude of the sediment transport and the direction of the vector in the wave propagation direction. The outcomes show that the direction and the magnitude of the sediment transport are affected by the parameterization. Also, the wave interaction and the non-linear relation between hydrodynamics and sediment transport are very important to consider

When two different operations are used, it is complex to analyze the impact of each Weather Type and Sea State on potential sediment in the nearshore region. Information is lost when too few Sea States or Weather Types are used, but the analysis becomes very complex when more of them are used.

Reference list

Abdi, H., & Williams, L. J. (2010). Principal component analysis. *Wiley Interdisciplinary Reviews: Computational Statistics*, *2*(4), 433–459. https://doi.org/10.1002/wics.101

Antolínez, J. A. A., Murray, A. B., Méndez, F. J., Moore, L. J., Farley, G., & Wood, J. (2018). Downscaling Changing Coastlines in a Changing Climate: The Hybrid Approach. *Journal of Geophysical Research: Earth Surface*, *123*(2), 229–251. https://doi.org/10.1002/2017jf004367

Ashton, A. D., & Murray, A. B. (2006). High-angle wave instability and emergent shoreline shapes: 1. Modeling of sand waves, flying spits, and capes. *Journal of Geophysical Research*, *111*(F4). https://doi.org/10.1029/2005jf000422

Baldock, T., Huntley, D., Bird, P., O'Hare, T., & Bullock, G. (2000). Breakpoint generated surf beat induced by bichromatic wave groups. *Coastal Engineering*, *39*(2–4), 213–242. https://doi.org/10.1016/s0378-3839(99)00061-7

Bosboom, J., & Stive, M. J. F. (2015). *Coastal dynamics 1* (5th ed.). Vssd.

Camus, P., Losada, I. J., Izaguirre, C., Espejo, A., Menéndez, M., & Pérez, J. (2017). Statistical wave climate projections for coastal impact assessments. *Earth's Future*, *5*(9), 918–933. https://doi.org/10.1002/2017ef000609

Camus, P., Méndez, F. J., Losada, I. J., Menéndez, M., Espejo, A., Pérez, J., Rueda, A., & Guanche, Y. (2014a). A method for finding the optimal predictor indices for local wave climate conditions. *Ocean Dynamics*, *64*(7), 1025–1038. https://doi.org/10.1007/s10236-014-0737-2

Camus, P., Menéndez, M., Méndez, F. J., Izaguirre, C., Espejo, A., Cánovas, V., Pérez, J., Rueda, A., Losada, I. J., & Medina, R. (2014b). A weather-type statistical downscaling framework for ocean wave climate. *Journal of Geophysical Research: Oceans*, *119*(11), 7389–7405. https://doi.org/10.1002/2014jc010141

Cavaleri, L., Abdalla, S., Benetazzo, A., Bertotti, L., Bidlot, J. R., Breivik, Ø., Carniel, S., Jensen, R., Portilla-Yandun, J., Rogers, W., Roland, A., Sanchez-Arcilla, A., Smith, J., Staneva, J., Toledo, Y., van Vledder, G., & van der Westhuysen, A. (2018). Wave modelling in coastal and inner seas. *Progress in Oceanography*, *167*, 164–233. https://doi.org/10.1016/j.pocean.2018.03.010

Dabbura, I. (2018, September 17). *K-means Clustering: Algorithm, Applications, Evaluation Methods, and Drawbacks*. Towards Data Science. Retrieved 15 December 2021, from https://towardsdatascience.com/k-means-clustering-algorithm-applications-evaluation-methods-and-drawbacks-aa03e644b48a

Dee, D. P., Uppala, S. M., Simmons, A. J., Berrisford, P., Poli, P., Kobayashi, S., Andrae, U., Balmaseda, M. A., Balsamo, G., Bauer, P., Bechtold, P., Beljaars, A. C. M., van de Berg, L., Bidlot, J., Bormann, N., Delsol, C., Dragani, R., Fuentes, M., Geer, A. J., . . . Vitart, F. (2011). The ERA-Interim reanalysis: configuration and performance of the data assimilation system. *Quarterly Journal of the Royal Meteorological Society*, *137*(656), 553–597. https://doi.org/10.1002/qj.828

de Hauwere, N. (2016, September 6). *Bathymetry of the North Sea and adjacent seas*. Marineregions. https://www.marineregions.org/maps.php?album=3747&pic=115811

Deltares. (2020, September). *Description and methodology of the process maps*. https://publicwiki.deltares.nl/download/attachments/131138867/11205236-005-ZKS-0004_v0.1-Description%20and%20methodology%20of%20the%20process%20maps.pdf?version=1&modificationDate=1640167594553&api=v2

de Vriend, H. J., van Koningsveld, M., Aarninkhof, S. G., de Vries, M. B., & Baptist, M. J. (2015). Sustainable hydraulic engineering through building with nature. *Journal of Hydro-environment Research*, *9*(2), 159–171. https://doi.org/10.1016/j.jher.2014.06.004

Eldeberky, Y., & Battjes, J. A. (1996). Spectral modeling of wave breaking: Application to Boussinesq equations. *Journal of Geophysical Research: Oceans*, *101*(C1), 1253–1264. https://doi.org/10.1029/95jc03219

Espejo, A., Camus, P., Losada, I. J., & Méndez, F. J. (2014). Spectral Ocean Wave Climate Variability Based on Atmospheric Circulation Patterns. *Journal of Physical Oceanography*, *44*(8), 2139–2152. https://doi.org/10.1175/jpo-d-13-0276.1

GLOSWAC. (n.d.). The Global Signature of Ocean Wave Spectra. Retrieved December 9, 2021, from https://modemat.epn.edu.ec/nereo/

Gonzalez-Rodriguez, D., & Madsen, O. S. (2007). Seabed shear stress and bedload transport due to asymmetric and skewed waves. *Coastal Engineering*, *54*(12), 914–929. https://doi.org/10.1016/j.coastaleng.2007.06.004

Grasmeijer, B., Huisman, B., Luijendijk, A., Schrijvershof, R., van der Werf, J., Zijl, F., de Looff, H., & de Vries, W. (2022). Modelling of annual sand transports at the Dutch lower shoreface. *Ocean & Coastal Management*, *217*, 105984. https://doi.org/10.1016/j.ocecoaman.2021.105984

Haasnoot, M.; Kwadijk, J.; van Alphen, J.; Bars, D.L.; van den Hurk, B.; Diermanse, F.; van der Spek, A.; Essink, G.O.; Delsman, J.; Mens, M.: Adaptation to uncertain sea-level rise; how uncertainty in antarctic mass-loss impacts the coastal adaptation strategy of the netherlands. Environmental Research Letters, 15(3), 034007, 2020.

Hegermiller, C. A., Antolinez, J. A. A., Rueda, A., Camus, P., Perez, J., Erikson, L. H., Barnard, P. L., & Mendez, F. J. (2016). A Multimodal Wave Spectrum–Based Approach for Statistical Downscaling of Local Wave Climate. *Journal of Physical Oceanography*, *47*(2), 375–386. https://doi.org/10.1175/jpo-d-16-0191.1

Hegermiller, C. A., Rueda, A., Erikson, L. H., Barnard, P. L., Antolinez, J. A. A., & Mendez, F. J. (2017). Controls of Multimodal Wave Conditions in a Complex Coastal Setting. *Geophysical Research Letters*, *44*(24). https://doi.org/10.1002/2017gl075272

Holthuijsen, L. H. (2007). *Waves in Oceanic and Coastal Waters*. Cambridge University Press.

Holthuijsen, L., Herman, A., & Booij, N. (2003). Phase-decoupled refraction–diffraction for spectral wave models. *Coastal Engineering*, *49*(4), 291–305. https://doi.org/10.1016/s0378-3839(03)00065-6

Hop, M. (2017). The impact of the Rhine ROFI on the alongshore variability in cross-shore sediment transport of the Holland coast. https://repository.tudelft.nl/islandora/object/uuid%3Acc6049ef-aefe-4e39-988a-06bb46a0f874

IPCC. (n.d.). *IPCC â Intergovernmental Panel on Climate Change*. Retrieved April 25, 2022, from https://www.ipcc.ch/

Jain, A. K. (2010). Data clustering: 50 years beyond K-means. *Pattern Recognition Letters*, *31*(8), 651–666. https://doi.org/10.1016/j.patrec.2009.09.011

Jiang, H. (2022). Wind speed and direction estimation from wave spectra using deep learning. *Atmospheric Measurement Techniques*, *15*(1), 1–9. https://doi.org/10.5194/amt-15-1-2022

Kroon, A., de Schipper, M. A., van Gelder, P. H., & Aarninkhof, S. G. (2020). Ranking uncertainty: Wave climate variability versus model uncertainty in probabilistic assessment of coastline change. Coastal Engineering, 158, 103673. https://doi.org/10.1016/j.coastaleng.2020.103673

Lavidas, G., & Polinder, H. (2019). North Sea Wave Database (NSWD) and the Need for Reliable Resource Data: A 38 Year Database for Metocean and Wave Energy Assessments. *Atmosphere*, *10*(9), 551. https://doi.org/10.3390/atmos10090551

Leckler, F., Ardhuin, F., Peureux, C., Benetazzo, A., Bergamasco, F., & Dulov, V. (2015). Analysis and Interpretation of Frequency–Wavenumber Spectra of Young Wind Waves. *Journal of Physical Oceanography*, *45*(10), 2484–2496. https://doi.org/10.1175/jpo-d-14-0237.1

Lim, G., Jayaratne, R., & Shibayama, T. (2020). Suspended sand concentration models under breaking waves: Evaluation of new and existing formulations. *Marine Geology*, *426*, 106197. https://doi.org/10.1016/j.margeo.2020.106197

Lobeto, H., Menendez, M., & Losada, I. J. (2021). Projections of Directional Spectra Help to Unravel the Future Behavior of Wind Waves. *Frontiers in Marine Science*, *8*. https://doi.org/10.3389/fmars.2021.655490

Jain, A. K. (2010). Data clustering: 50 years beyond K-means. *Pattern Recognition Letters*, *31*(8), 651–666. https://doi.org/10.1016/j.patrec.2009.09.011

Ministerie van Verkeer en Waterstaat. (2020). 3e Kustnota Traditie, Trends en Toekomst. https://puc.overheid.nl/rijkswaterstaat/doc/PUC_43195_31/

Kroon, A., de Schipper, M. A., van Gelder, P. H., & Aarninkhof, S. G. (2020). Ranking uncertainty: Wave climate variability versus model uncertainty in probabilistic assessment of coastline change. Coastal Engineering, 158, 103673. https://doi.org/10.1016/j.coastaleng.2020.103673

Miles, J. W. (1957). On the generation of surface waves by shear flows. *Journal of Fluid Mechanics*, *3*(02), 185. https://doi.org/10.1017/s0022112057000567

Miles, J. W. (1962). On the generation of surface waves by shear flows. Part 4. *Journal of Fluid Mechanics*, *13*(3), 433–448. https://doi.org/10.1017/s0022112062000828

Murray, A.B., Antolínez, J.A.A., 2019. Forecasting future coastline change: how to address limitations and opportunities?, in: Coastal Sediments 2019. World Scientific, pp. 1077–1085. https://doi.org/10.1142/9789811204487_0094

Ostrowski, R. (2018). Influence of Wave Shape on Sediment Transport in Coastal Regions. *Archives of Hydro-Engineering and Environmental Mechanics*, *65*(2), 73–90. https://doi.org/10.1515/heem-2018-0006

Pérez, J., Méndez, F. J., Menéndez, M., & Losada, I. J. (2014). ESTELA: a method for evaluating the source and travel time of the wave energy reaching a local area. *Ocean Dynamics*, *64*(8), 1181–1191. https://doi.org/10.1007/s10236-014-0740-7

Portilla-Yandún, J., Ocampo-Torres, F. J., & Monbaliu, J. (2009). Spectral Partitioning and Identification of Wind Sea and Swell. Journal of Atmospheric and Oceanic Technology, 26(1), 107–122. https://doi.org/10.1175/2008jtecho609.1

Portilla-Yandún, J. (2018). The Global Signature of Ocean Wave Spectra. *Geophysical Research Letters*, *45*(1), 267–276. https://doi.org/10.1002/2017gl076431

Portilla-Yandún, J., Cavaleri, L., & Van Vledder, G. P. (2015). Wave spectra partitioning and long term statistical distribution. *Ocean Modelling*, *96*, 148–160. https://doi.org/10.1016/j.ocemod.2015.06.008

Ranasinghe, R. (2016). Assessing climate change impacts on open sandy coasts: A review. *Earth-Science Reviews*, *160*, 320–332. https://doi.org/10.1016/j.earscirev.2016.07.011

Reniers, A. J., Naporowski, R., Tissier, M. F. S., de Schipper, M. A., Akrish, G., & Rijnsdorp, D. P. (2021). North Sea Infragravity Wave Observations. *Journal of Marine Science and Engineering*, *9*(2), 141. https://doi.org/10.3390/jmse9020141

Rijksoverheid. (2013). *National Coastal Strategy Compass for the Coast*. https://rijksoverheid.minienm.nl/nvk/NationalCoastalStrategy.pdf

Rijnsdorp, D. P., Reniers, A. J. H. M., & Zijlema, M. (2021). Free Infragravity Waves in the North Sea. *Journal of Geophysical Research: Oceans*, *126*(8). https://doi.org/10.1029/2021jc017368

Shringarpure, M. S., Cantero, M. I., & Balachandar, S. (2014). Mechanisms of Complete Turbulence Suppression in Turbidity Currents Driven by Mono-Disperse and Bi-Disperse Suspensions of Sediment. *The Journal of Computational Multiphase Flows*, *6*(3), 221–245. https://doi.org/10.1260/1757-482x.6.3.221

Stive, M. J., Aarninkhof, S. G., Hamm, L., Hanson, H., Larson, M., Wijnberg, K. M., Nicholls, R. J., & Capobianco, M. (2002). Variability of shore and shoreline evolution. *Coastal Engineering*, *47*(2), 211–235. https://doi.org/10.1016/s0378-3839(02)00126-6

Toimil, A., Camus, P., Losada, I., Le Cozannet, G., Nicholls, R., Idier, D., & Maspataud, A. (2020). Climate change-driven coastal erosion modelling in temperate sandy beaches: Methods and uncertainty treatment. *Earth-Science Reviews*, *202*, 103110. https://doi.org/10.1016/j.earscirev.2020.103110

TU Delft. (2014). SWAN Scientific and Technical Documentation Cycle III Version 41.01. Delft University of Technology. http://www.swan.tudelft.nl

van der Zanden, J., Fernandez Mora, M. D. L. A., van der A, D. A., Hurther, D., Caceres, I., O'Donoghue, T., & Ribberink, J. S. (2017a). Inclusion of wave breaking turbulence in reference concentration models. In T. Aagaard, R. Deigaard, & D. Fuhrman (Eds.), *Proceedings Coastal Dynamics 2017, Helsingør, Denmark* (pp. 629-641)

van der Zanden, J., van der A, D. A., O'Donoghue, T., Hurther, D., Caceres, I., Thorne, P. D., van der Werf, J. J., Hulscher, S. J., & Ribberink, J. S. (2017b). SUSPENDED AND BEDLOAD TRANSPORT IN THE SURF ZONE: IMPLICATIONS FOR SAND TRANSPORT MODELS. *Coastal Engineering Proceedings*, *35*, 30. https://doi.org/10.9753/icce.v35.sediment.30

van Rijn, L. C. (n.d.). *SIMPLE GENERAL FORMULAE FOR SAND TRANSPORT IN RIVERS, ESTUARIES AND COASTAL WATERS*. Leovanrijn-Sediment. http://www.leovanrijn-sediment.com/papers/Formulaesandtransport.pdf

van Rijn, L. C. (2007a). Unified View of Sediment Transport by Currents and Waves. I: Initiation of Motion, Bed Roughness, and Bed-Load Transport. *Journal of Hydraulic Engineering*, *133*(6), 649–667. https://doi.org/10.1061/(asce)0733-9429(2007)133:6(649)

van Rijn, L. C. (2007b). Unified View of Sediment Transport by Currents and Waves. II: Suspended Transport. *Journal of Hydraulic Engineering*, *133*(6), 668–689. https://doi.org/10.1061/(asce)0733-9429(2007)133:6(668)

van Rijn, L. C. (2007c). Unified View of Sediment Transport by Currents and Waves. III: Graded Beds. *Journal of Hydraulic Engineering*, *133*(7), 761–775. https://doi.org/10.1061/(asce)0733-9429(2007)133:7(761)

van Rijn, L. C. (2013). *BASIC HYDRODYNAMIC PROCESSES IN THE COASTAL ZONE*. Leovanrijn-Sediment. http://www.leovanrijn-sediment.com/papers/Coastalhydrodynamics2013.pdf

van Rijn, L. C., Walstra, D. J. R., & van Ormondt, M. (2004, November). *Description of TRANSPOR2004 and Implementation in Delft3D-ONLINE* (FINAL REPORT). Delft Hydraulics. https://puc.overheid.nl/rijkswaterstaat/doc/PUC_114092_31/

Wang, X. L., Swail, V. R., & Cox, A. (2009). Dynamical versus statistical downscaling methods for ocean wave heights. *International Journal of Climatology*, *30*(3), 317–332. https://doi.org/10.1002/joc.1899

Wendell, L. L. (1969). A study of large-scale atmospheric turbulent kinetic energy in wave-number frequency space. *Tellus*, *21*(6), 760–788. https://doi.org/10.3402/tellusa.v21i6.10144

Wilson, R. J., Speirs, D. C., Sabatino, A., & Heath, M. R. (2018). A synthetic map of the north-west European Shelf sedimentary environment for applications in marine science. *Earth System Science Data*, *10*(1), 109–130. https://doi.org/10.5194/essd-10-109-2018

XBeach. (2020). *XBeach manual - XBeach BOI-phase1-5867*. XBeach. https://xbeach.readthedocs.io/en/latest/xbeach_manual.html

Zarifsanayei, A. R., Antolínez, J. A., Etemad-Shahidi, A., Cartwright, N., & Strauss, D. (2022a). A multi-model ensemble to investigate uncertainty in the estimation of wave-driven longshore sediment transport patterns along a non-straight coastline. *Coastal Engineering*, *173*, 104080. https://doi.org/10.1016/j.coastaleng.2022.104080

Zarifsanayei, A. R., Antolínez, J. A. A., Etemad-Shahidi, A., Cartwright, N., Strauss, D., & Lemos, G. (2022b). Uncertainties in the Projected Patterns of Wave-Driven Longshore Sediment Transport Along a Non-straight Coastline. *Frontiers in Marine Science*, *9*. https://doi.org/10.3389/fmars.2022.832193

Appendix I: Seasonal anomalies in the wave spectrum

The deviation of the average seasonal spectrum to the mean spectrum from 1979 to 2018 for the offshore data retrieved by ERA-interim and the nearshore data modeled by SWAN is depicted in this appendix. The offshore and nearshore locations are also depicted in Figure 22 and Figure 23.

The winter period is from December to February, the spring last to may, the summer is from June to August, and the Autumn is from August to November.
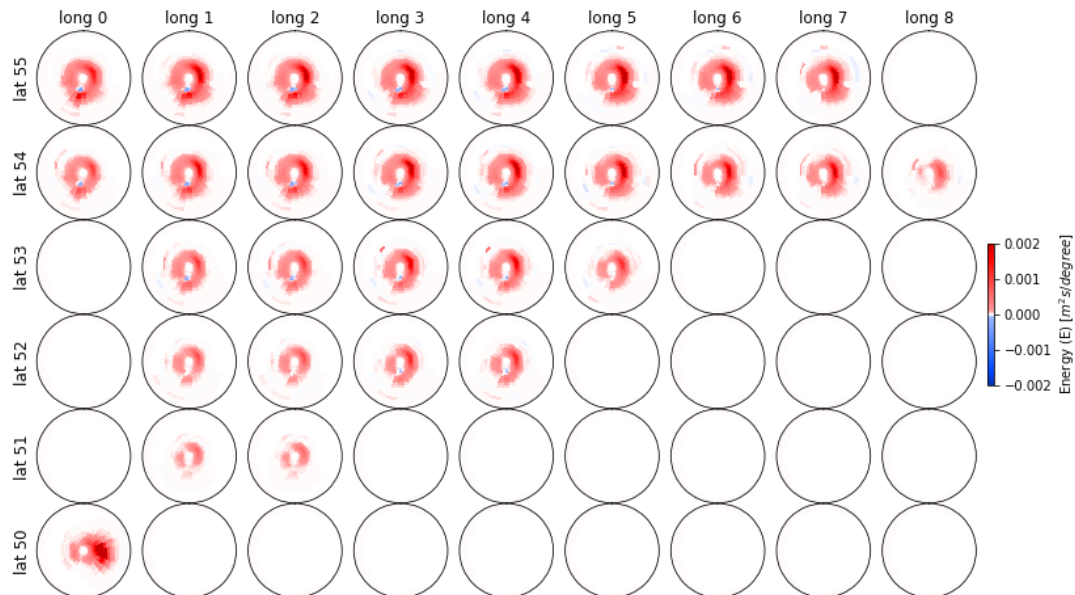
Figure 120:Winter (DJF) anomaly in the offshore region
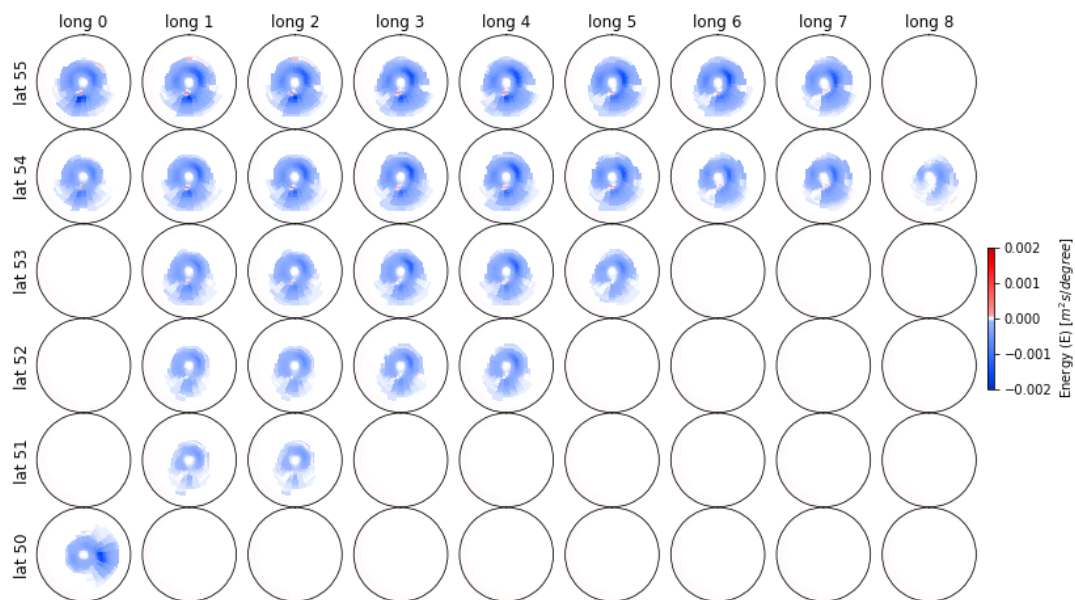
Figure 121: Spring (MAM) anomaly in the offshore region
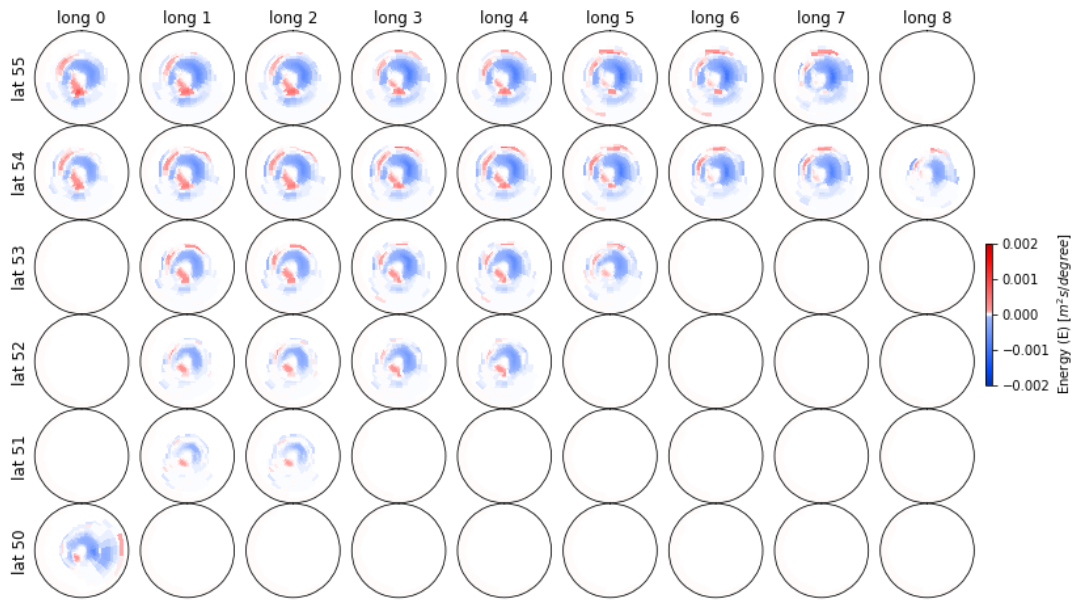
Figure 122:Summer (JJA) anomaly in the offshore region
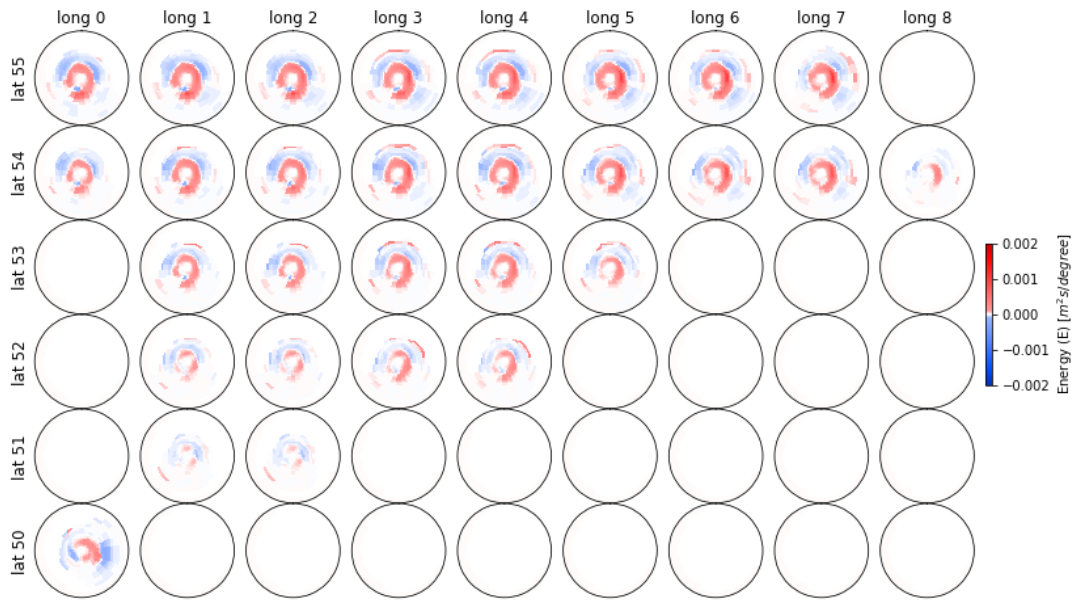
Figure 123: Autumn (SON) anomaly in the offshore region
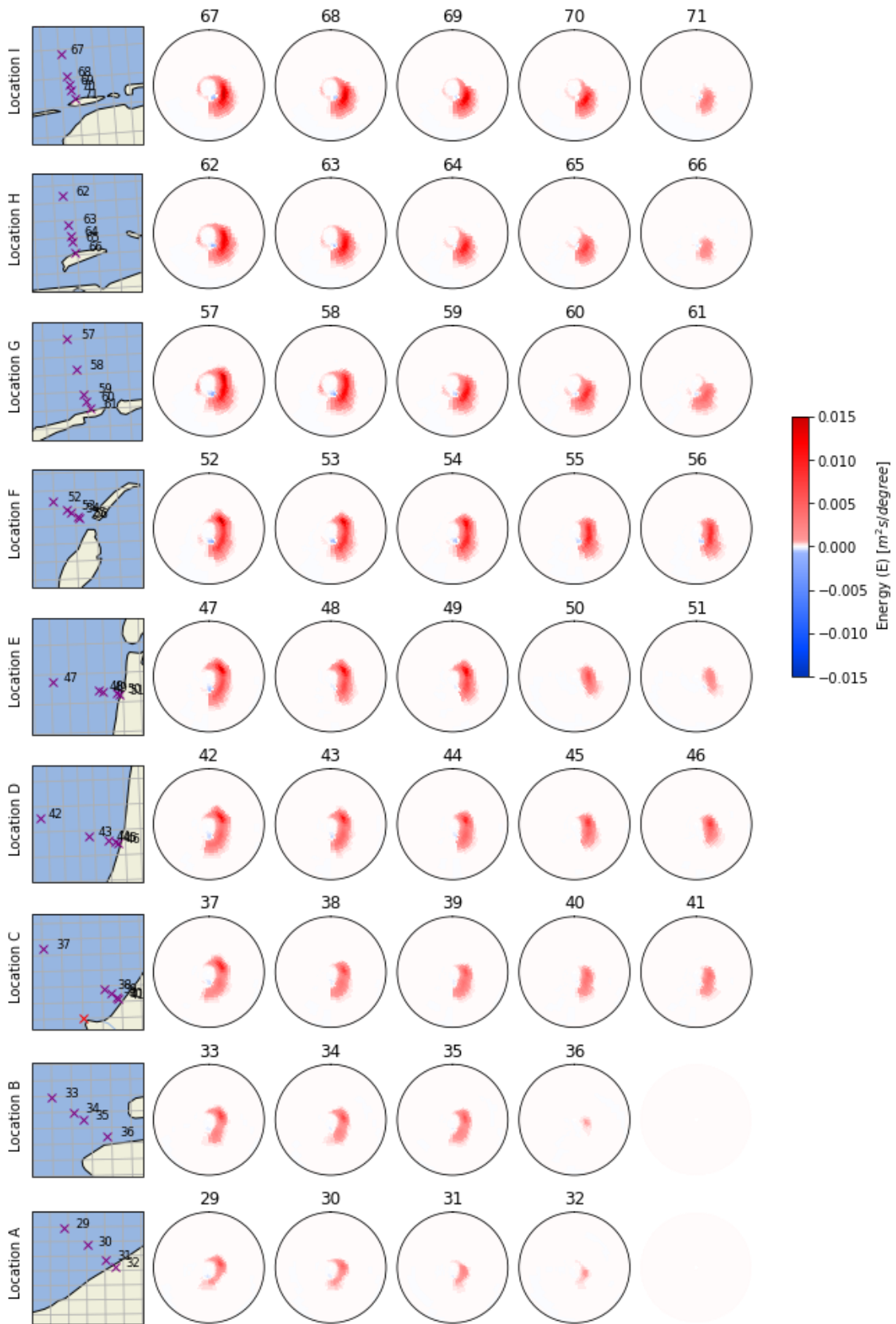
Figure 124: Winter (DJF) anomaly in the nearshore region
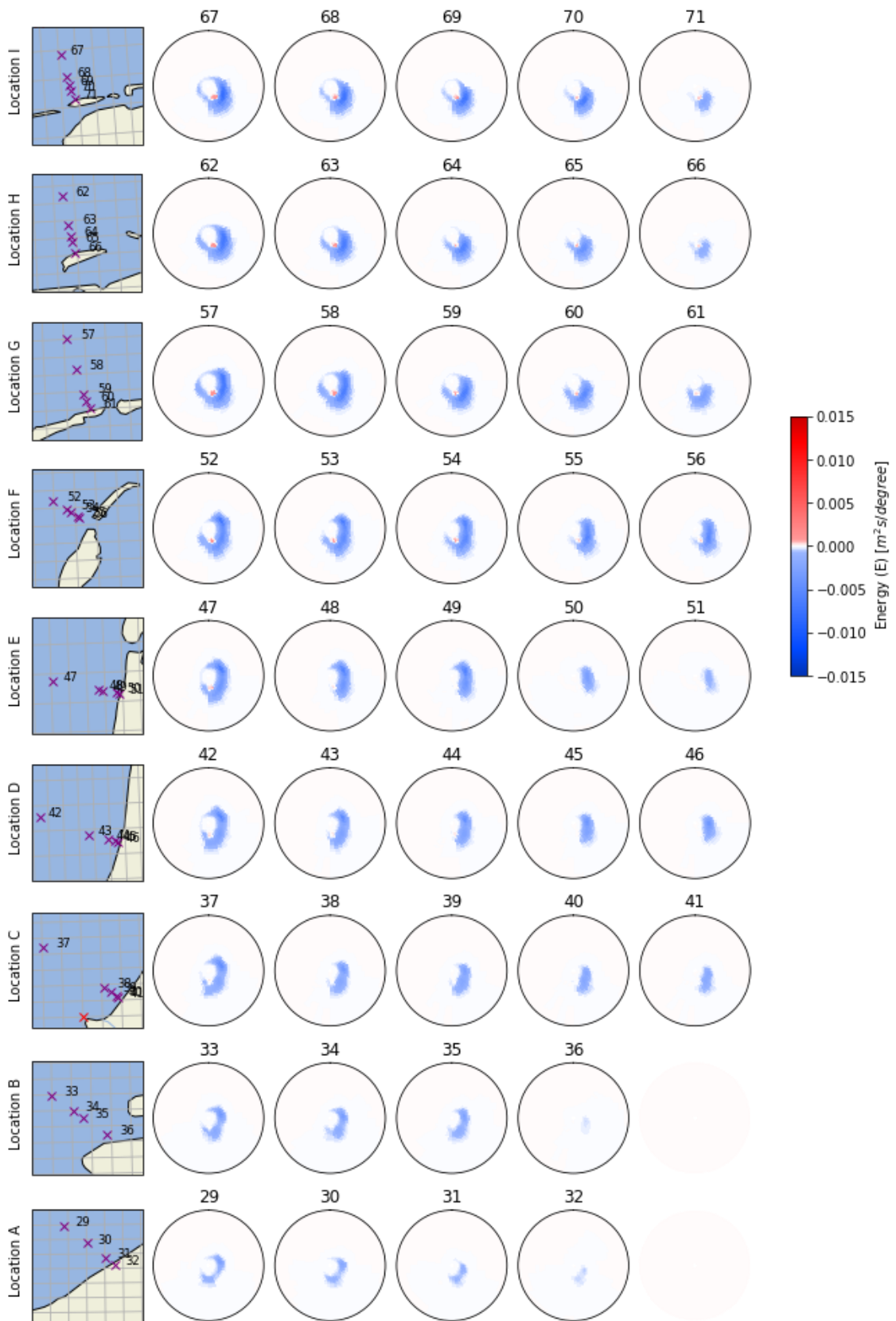
Figure 125: Spring (MAM) anomaly in the nearshore region
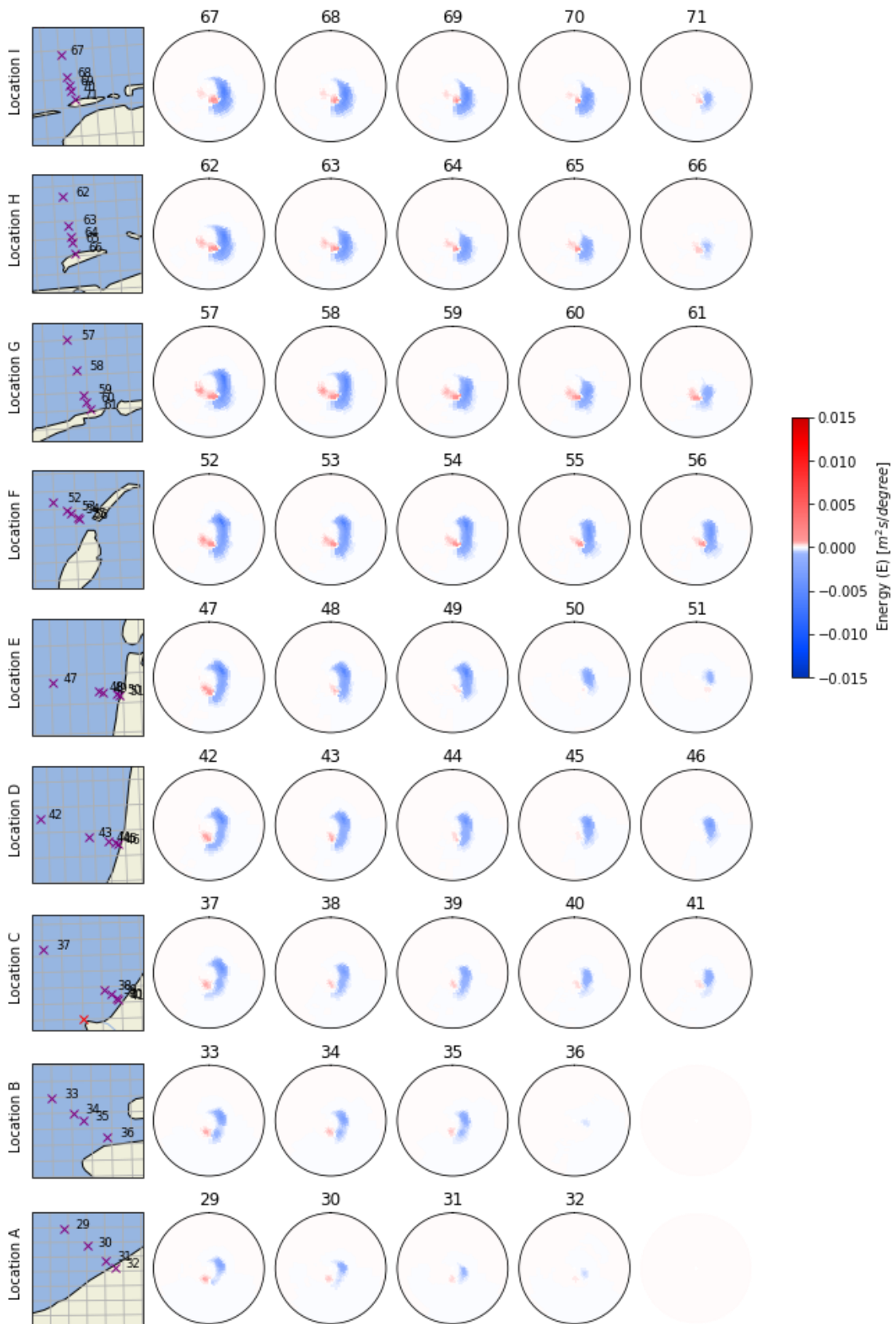
Figure 126: Summer (JJA) anomaly in the nearshore region
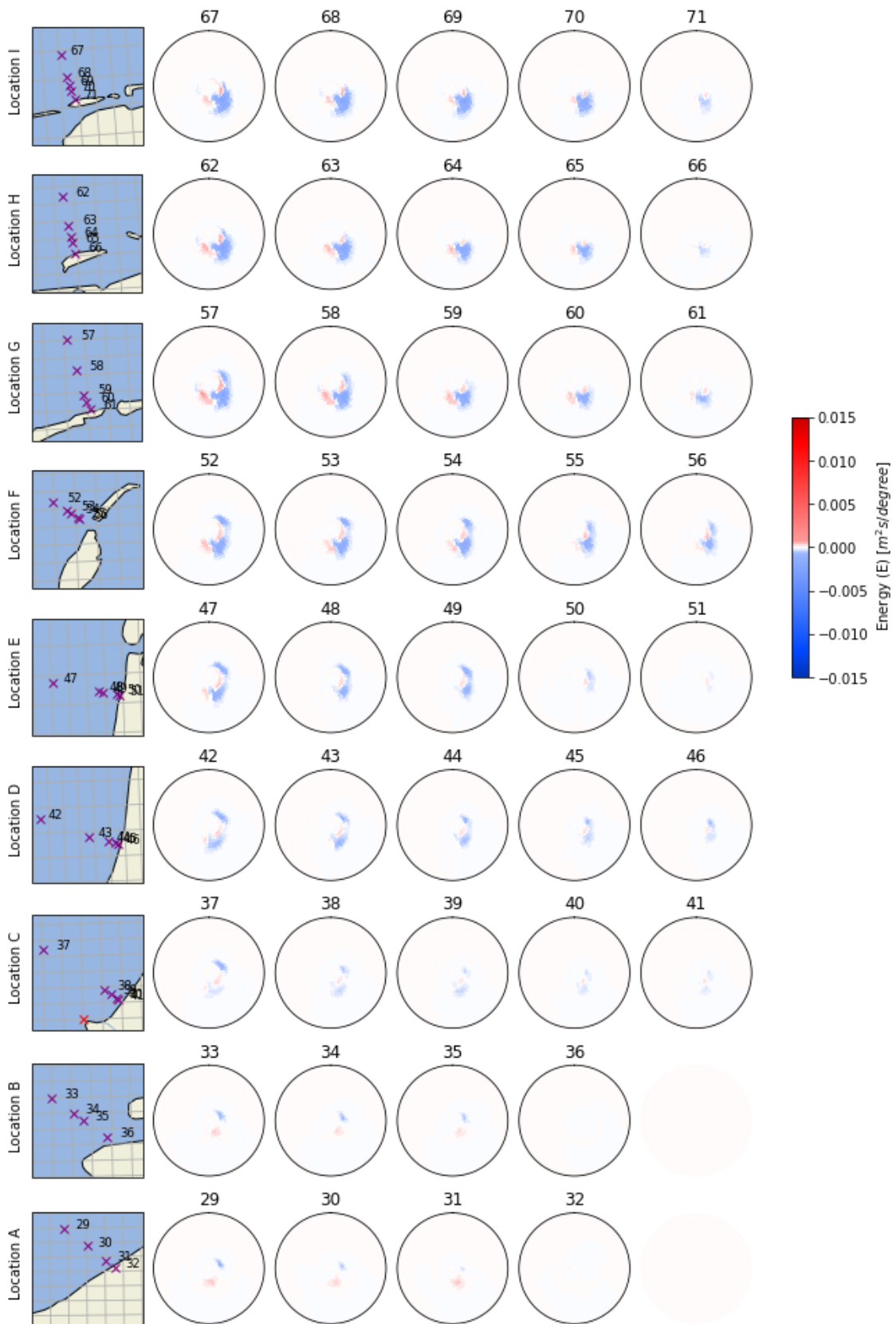
Figure 127: Autumn (SON) anomaly in the nearshore region

Appendix II: Wave families in the nearshore region

The wave families at all the locations are depicted in the figure below. Each wave family describes certain frequency-directional bins. The position of the bin indicates the wave propagation direction, and the radial axis indicates the wave period, where short perioded waves on the inside and periods of 15 seconds on the outer circle. Bins that never had an energy peak from a wave partition are colored white. The content is explained in chapter 2.2.3.
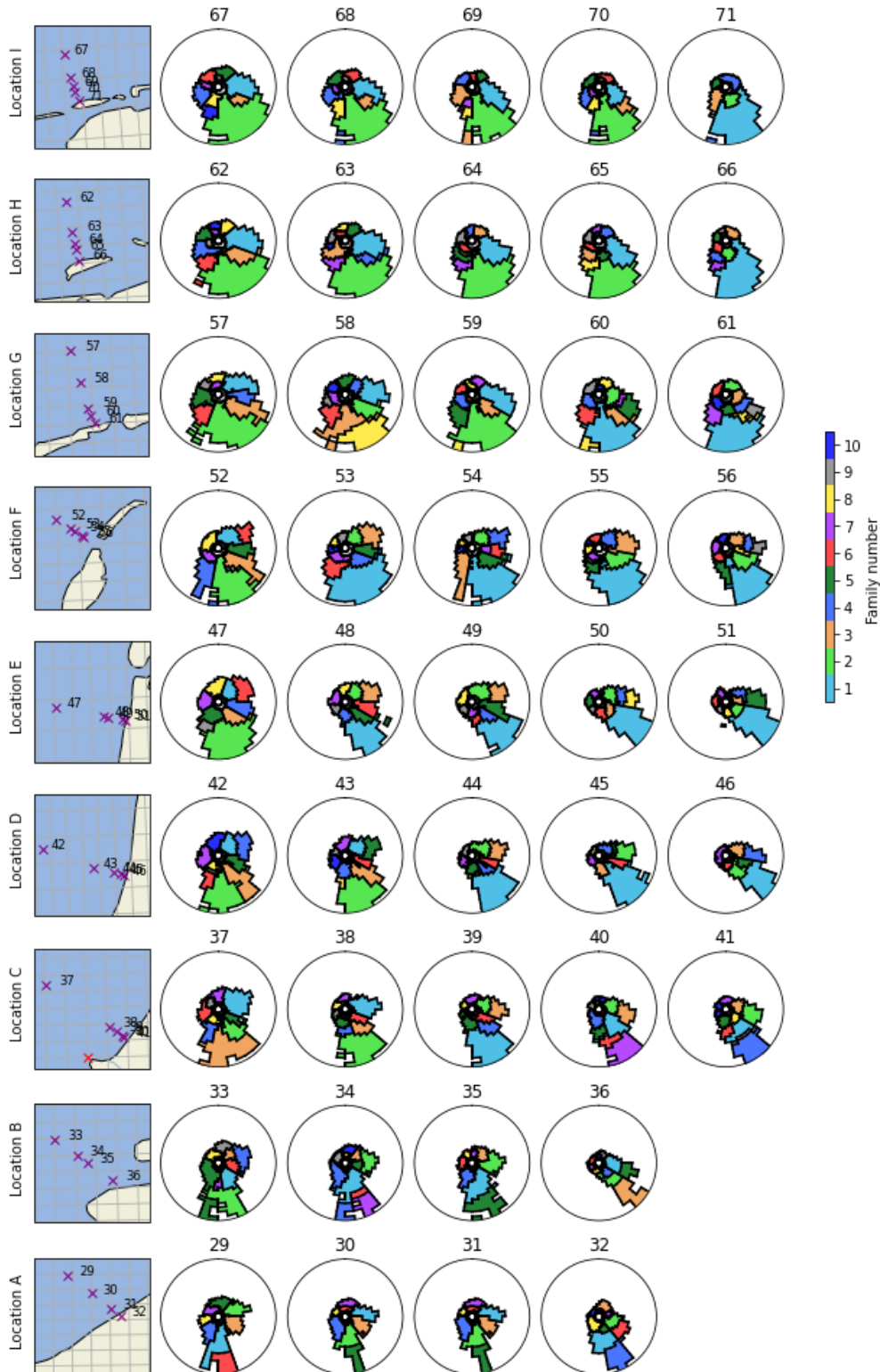
Figure 128: The wave families at all the nearshore locations

Appendix III: Wave family clusters at the nearshore

The wave families across the nearshore locations are grouped by the kmean algorithm so that they are spatially related, as discussed in chapter 4.6. This appendix shows the results of forming 3, 4, 5, and 10 groups. The figures represent the frequency-directional spectrum, where the period is on the radial axis and capped at 15 seconds.
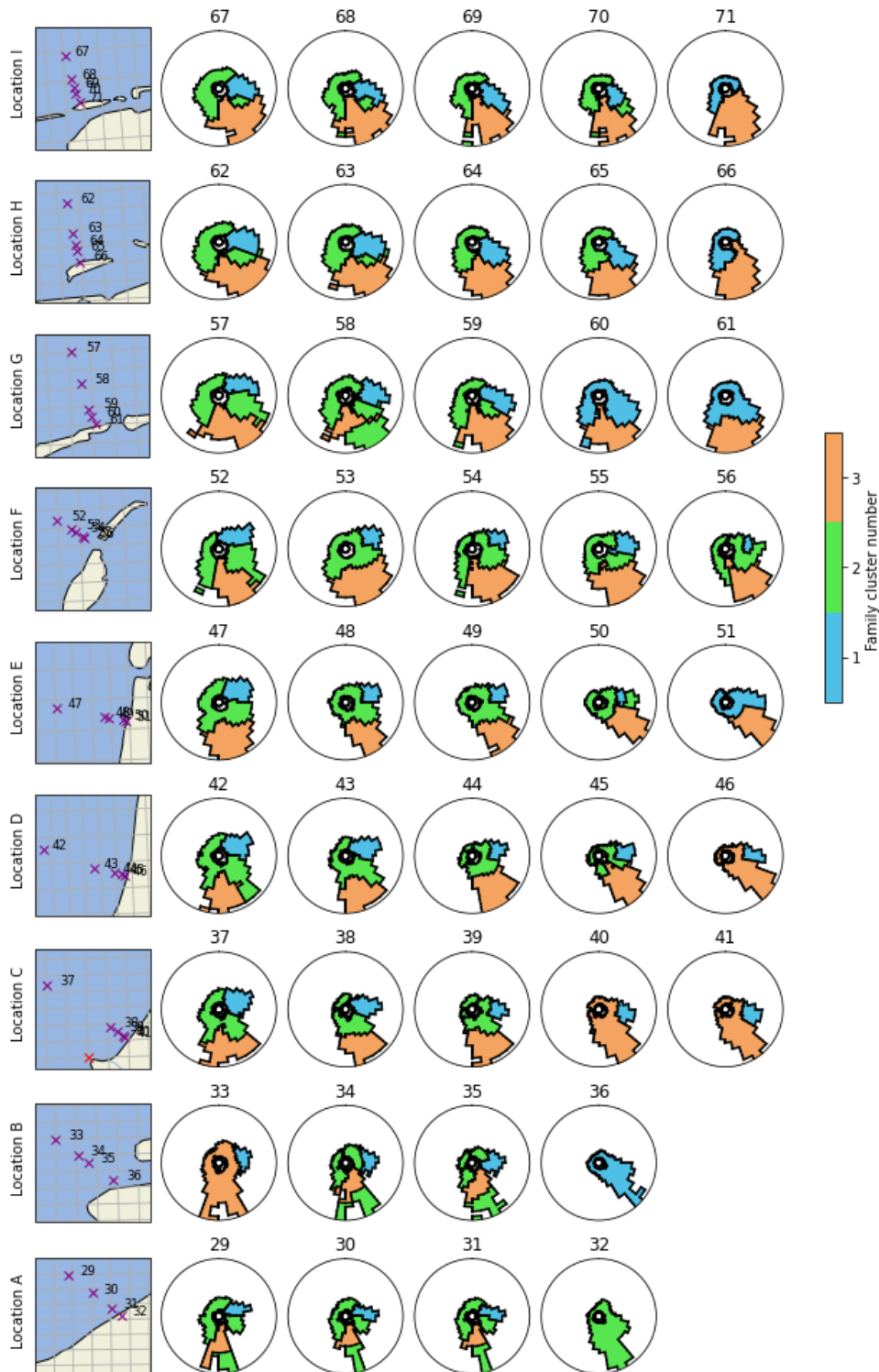
Figure 129: Wave family clusters for all the locations, where the wave families are classified into three groups.
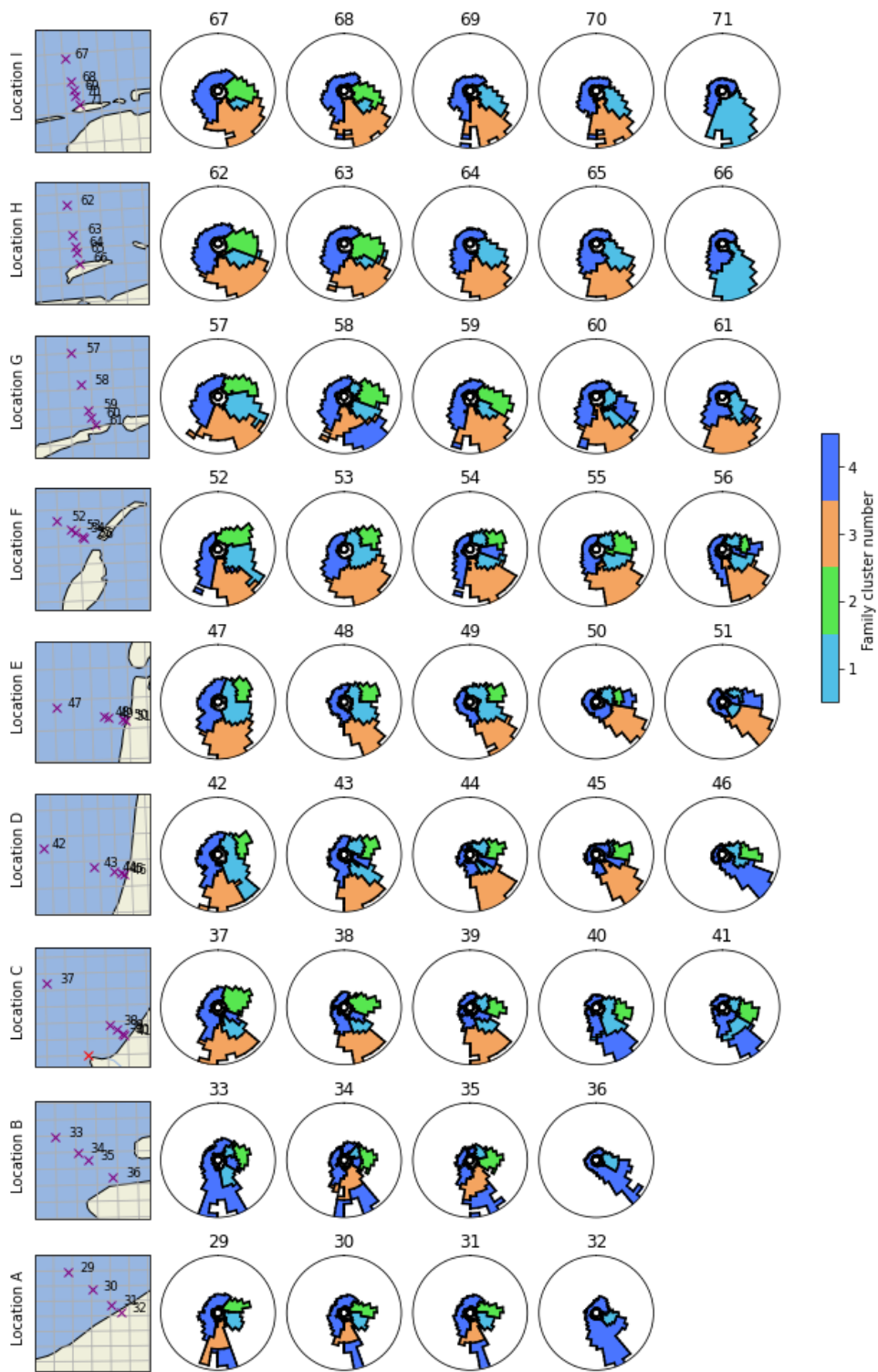
Figure 130: Wave family clusters for all the locations, where the wave families are classified into four groups.
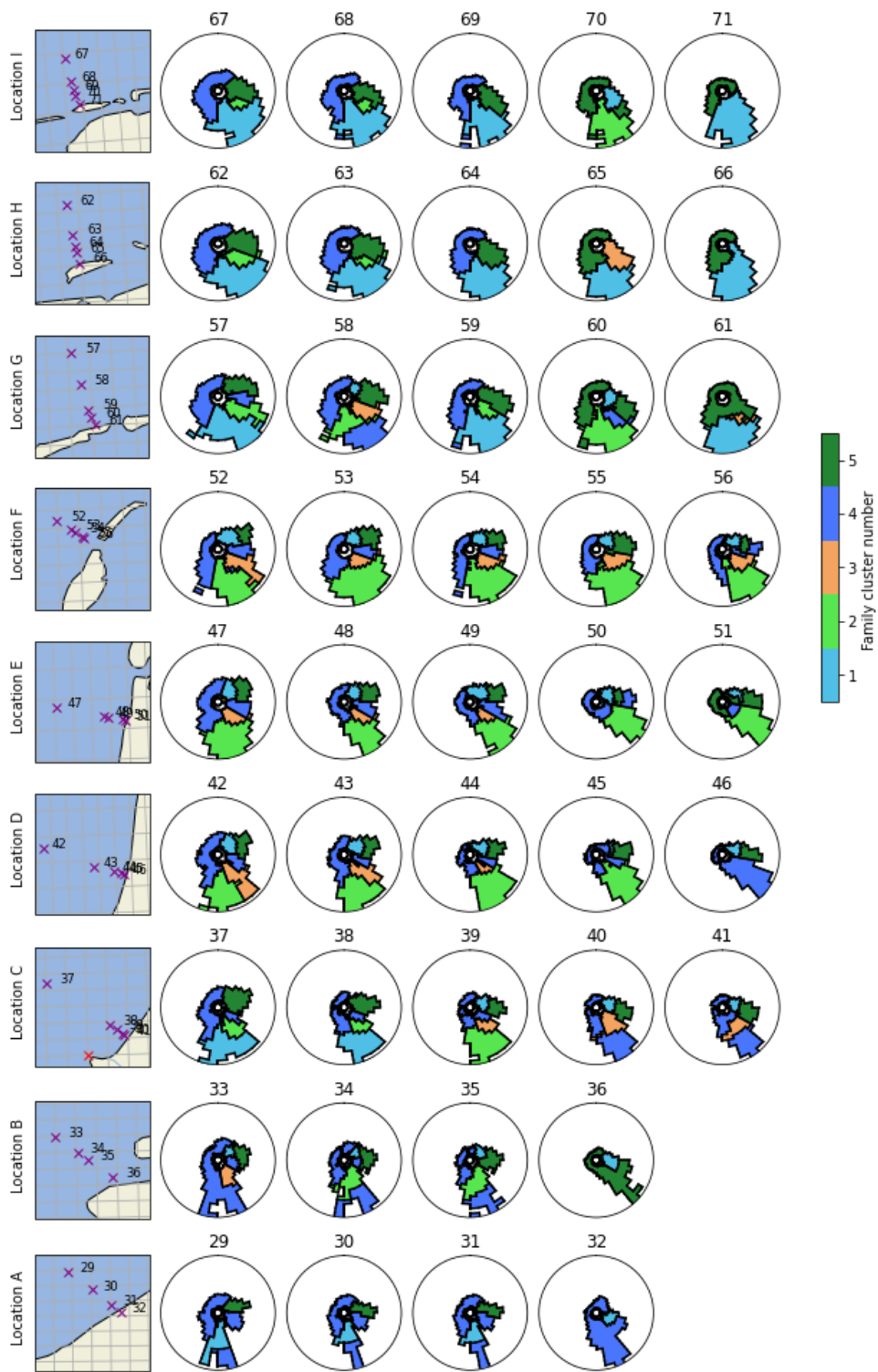
Figure 131: Wave family clusters for all the locations, where the wave families are classified into five groups.
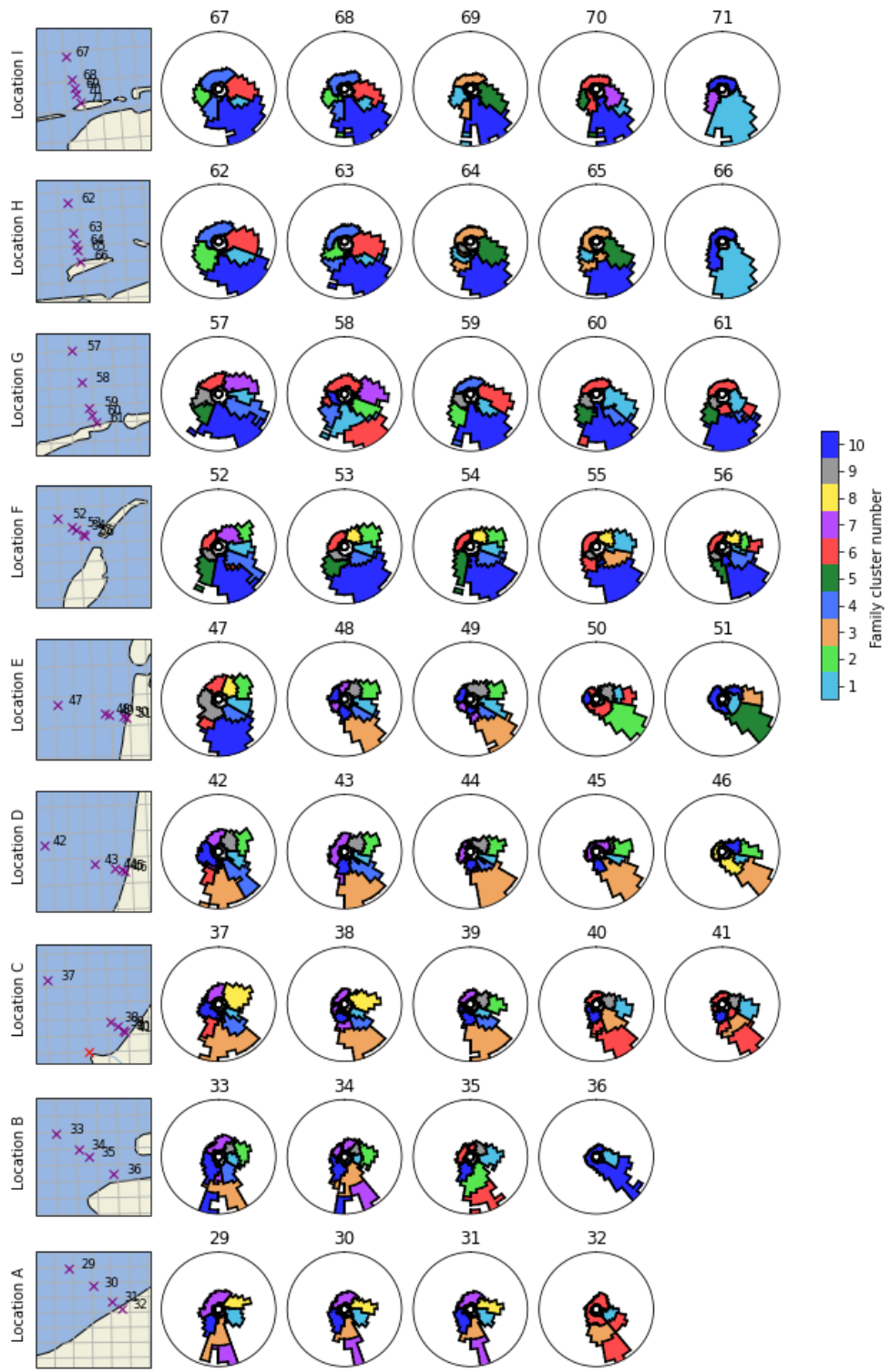
Figure 132: Wave family clusters for all the locations, where the wave families are classified into ten groups.

Appendix IV: Principal Components

The most important Principal Components are spatially depicted in this appendix, first the offshore locations and then the nearshore locations. The Principal Components show the standardized, rotated, and translated wave spectral data, from which the units are unknown. The values show the impact of the temporal value related to the Principal Component, expressed by the corresponding element in the eigenvector. Positive temporal values indicate more wave energy at the positive values in the picture below, while negative have the opposite effect. The values are scaled to the standard deviation of the related Principal Component to equalize the scales for each Principal Component.
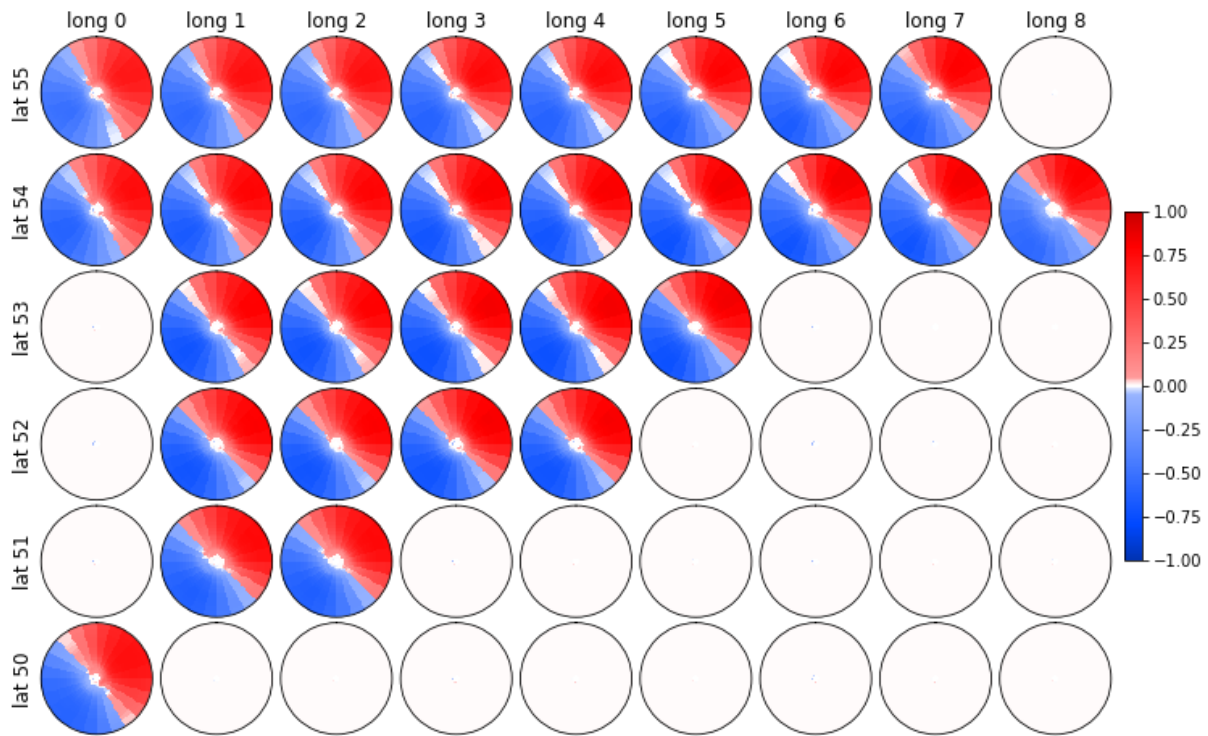
Figure 133: Principal Component 1, at the offshore locations
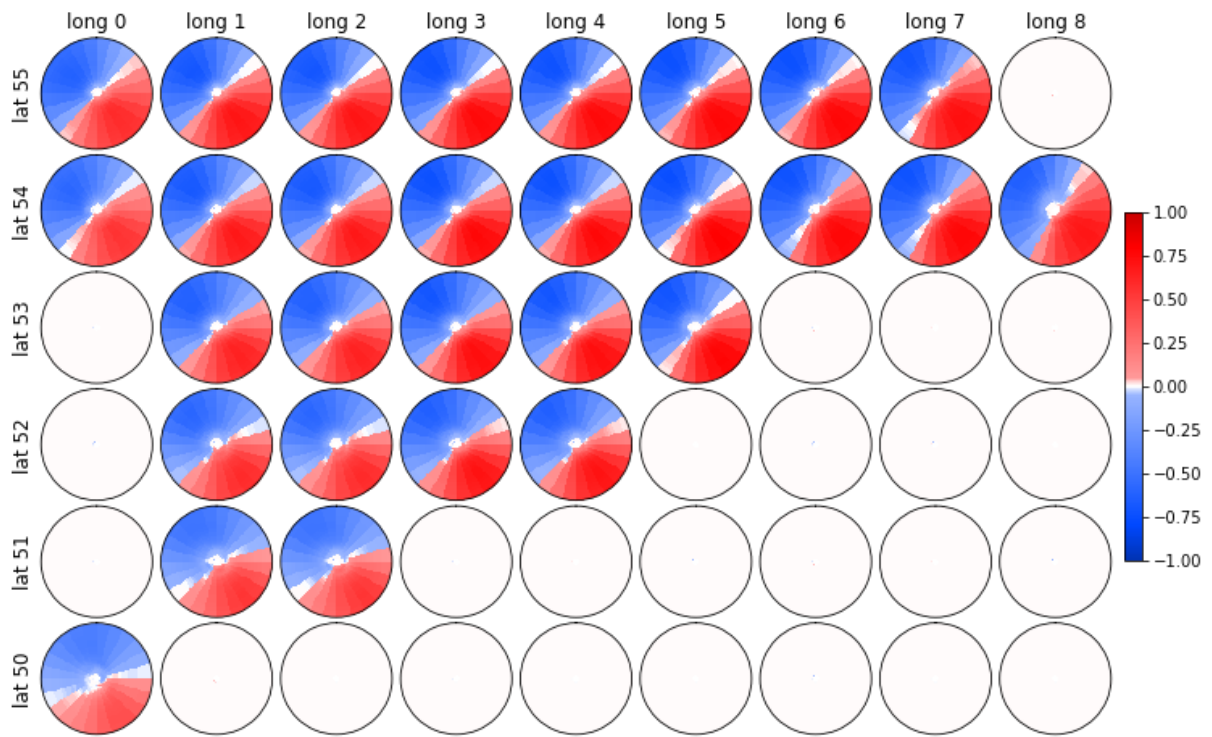
Figure 134: Principal Component 2, at the offshore locations
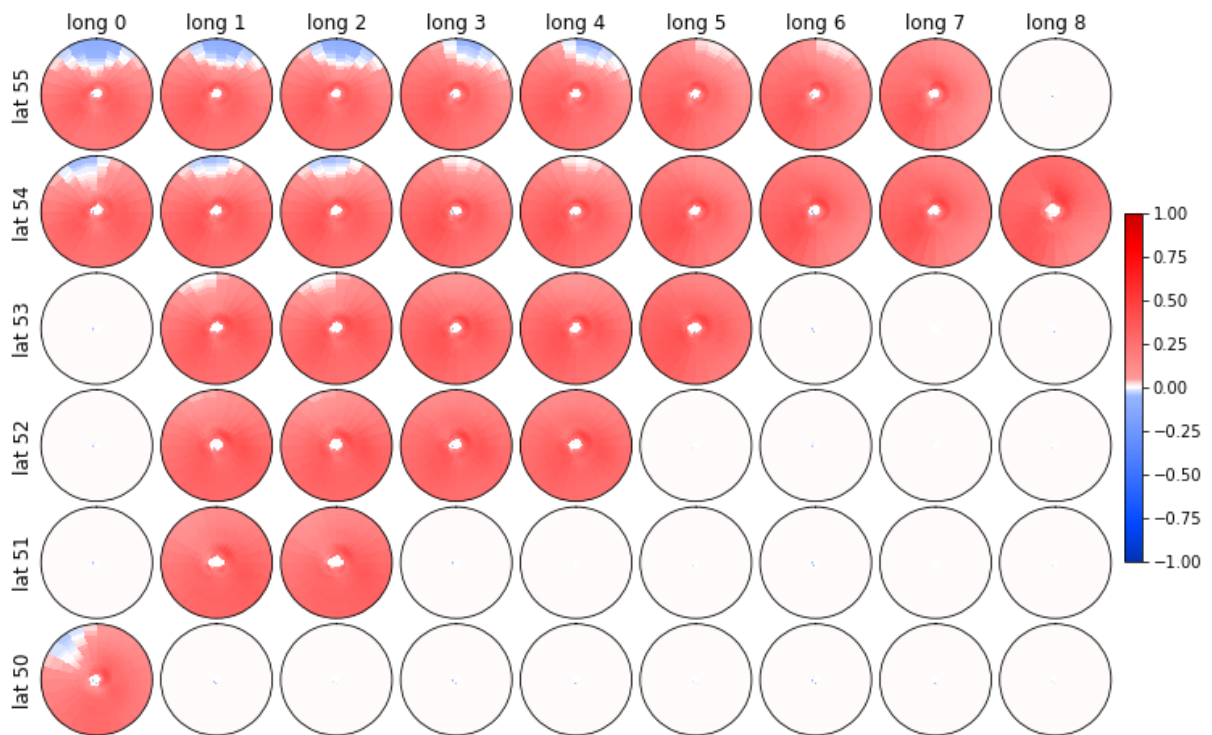
Figure 135: Principal Component 3, at the offshore locations
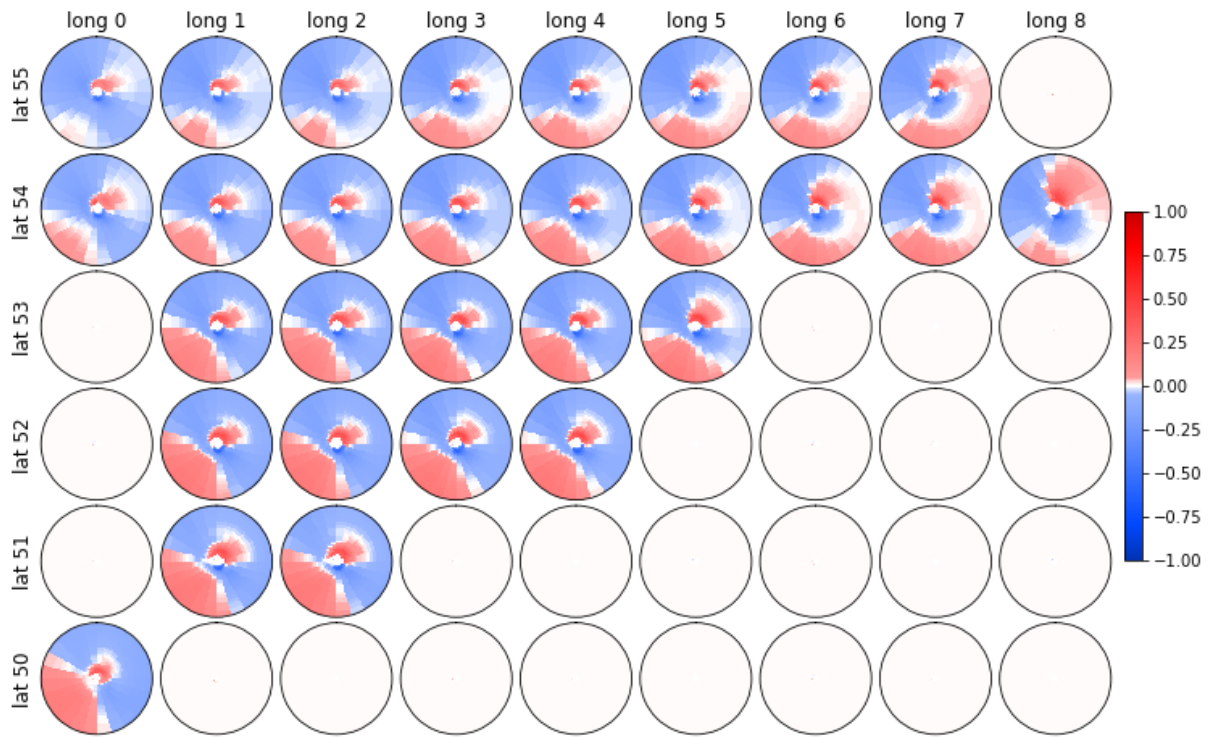
Figure 136: Principal Component 4, at the offshore location
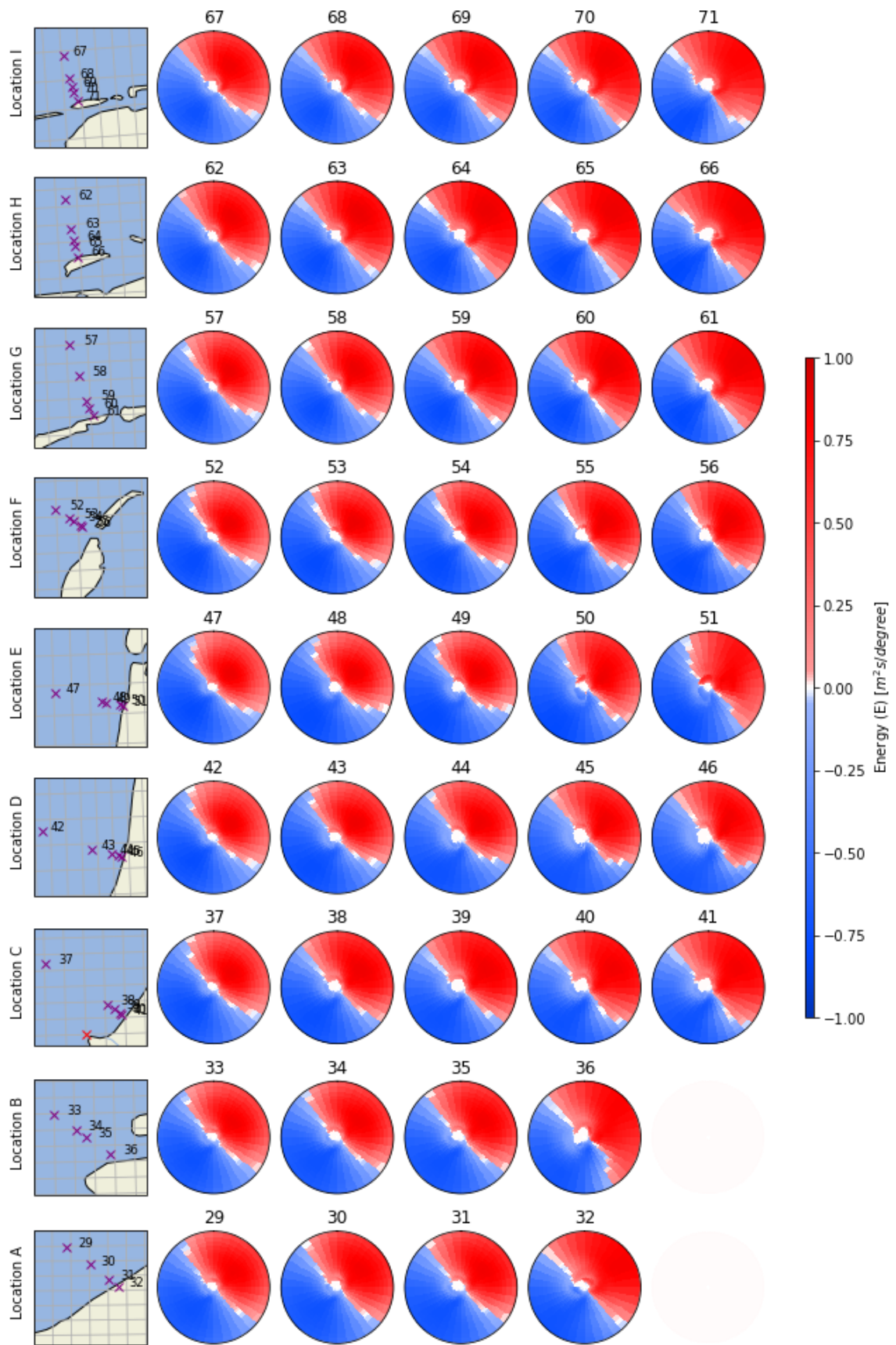
Figure 137: Principal Component 1, at the nearshore locations
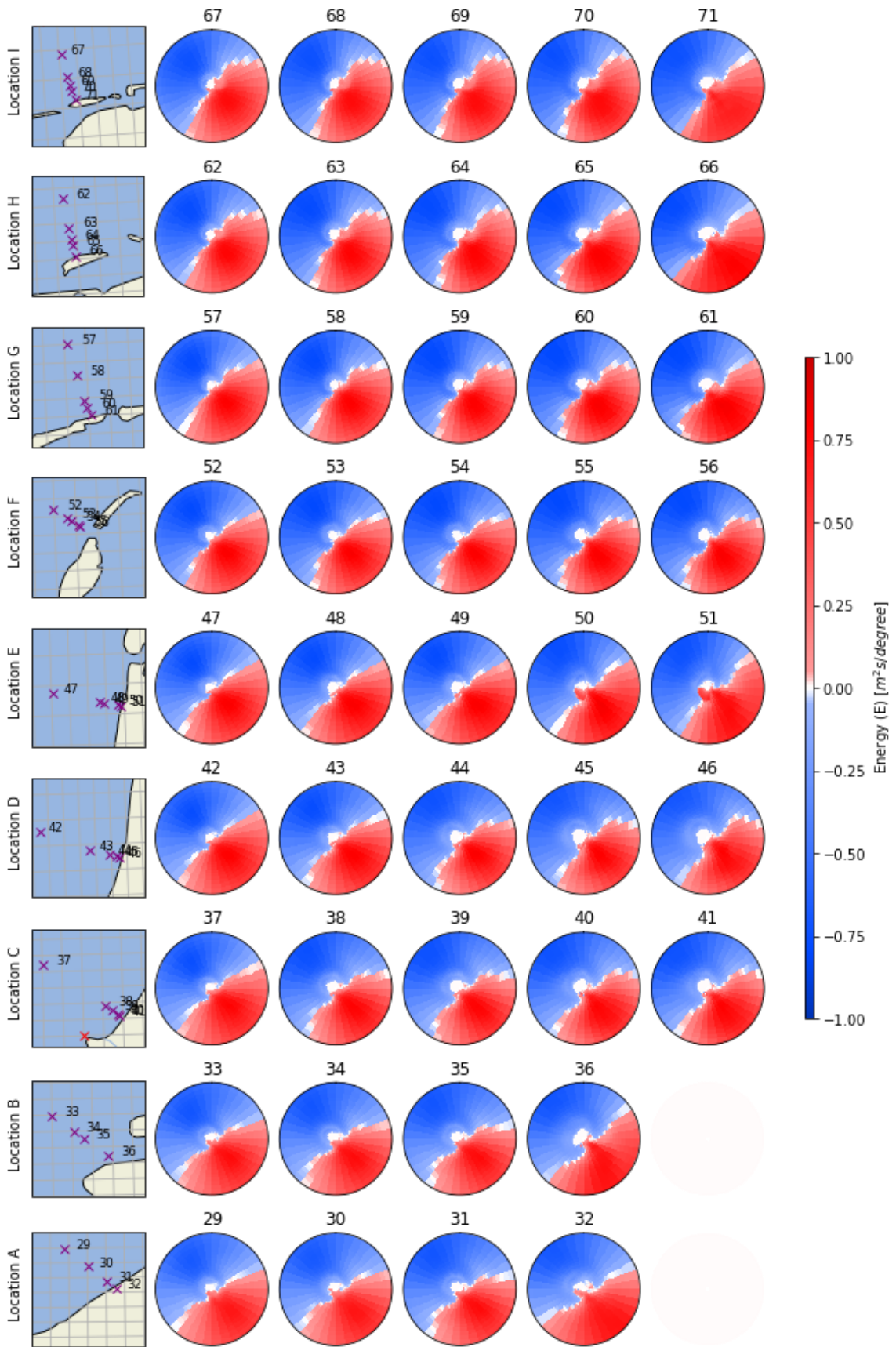
Figure 138: Principal Component 2, at the nearshore locations
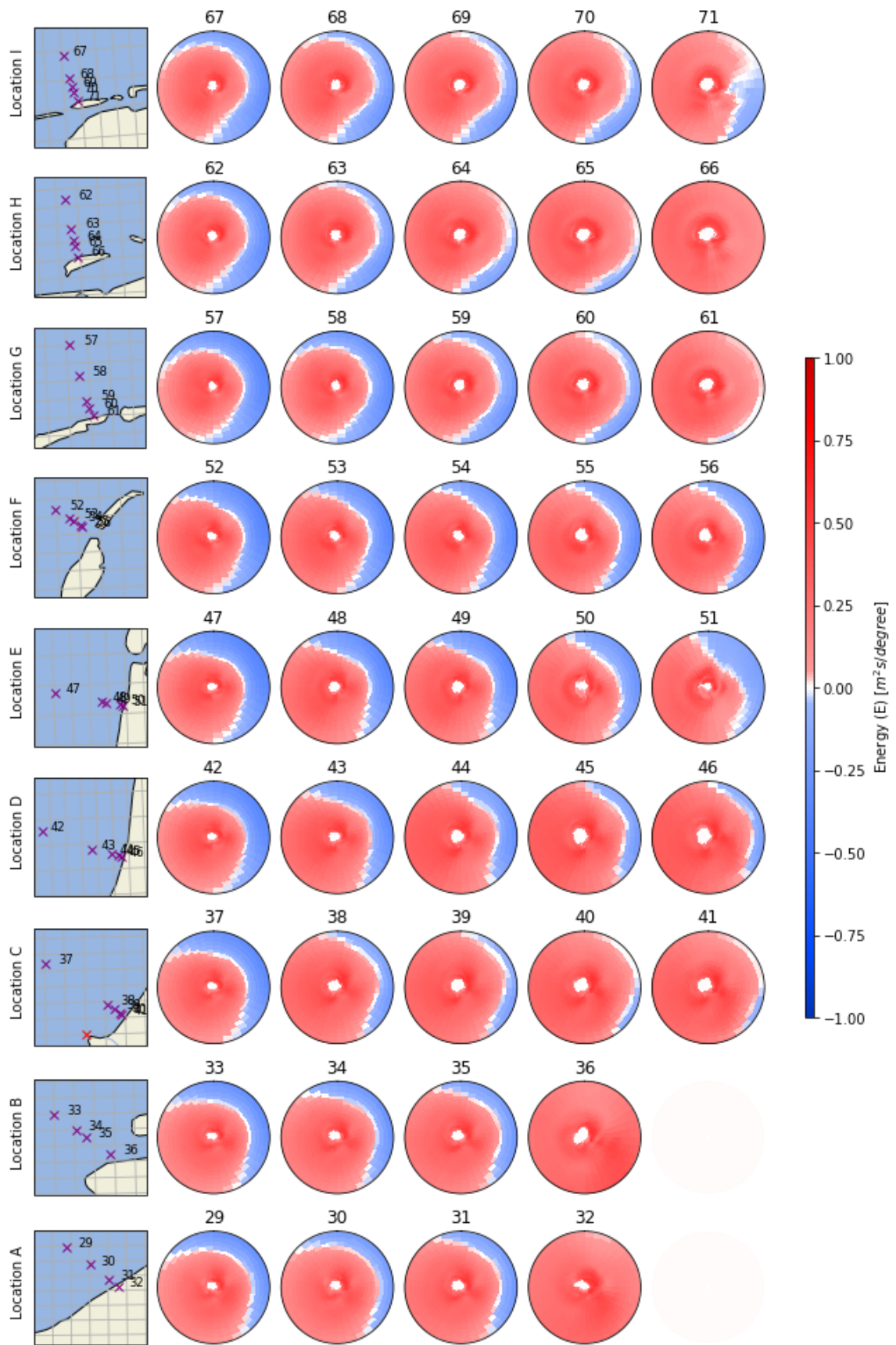
Figure 139: Principal Component 3, at the nearshore locations
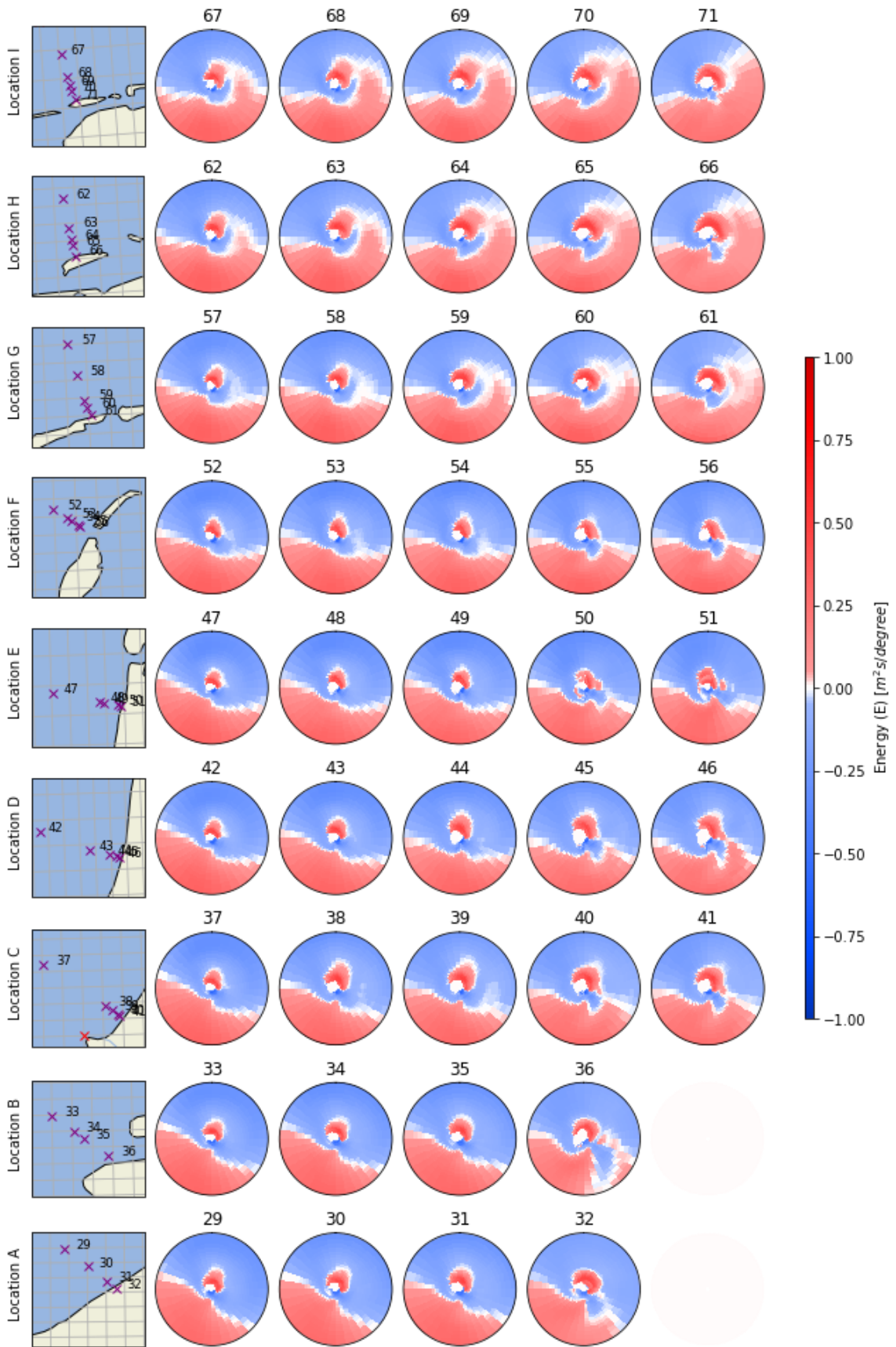
Figure 140: Principal Component 4, at the nearshore locations

Appendix V: Sea State 65 and 121 based on MDA 2000

The Sea State is a physical interpretation of the clusters; it consists of one representative frequency-directional wave spectrum at all the considered locations. This appendix shows the representative spectrum at all the locations for Sea State 65 and 121.
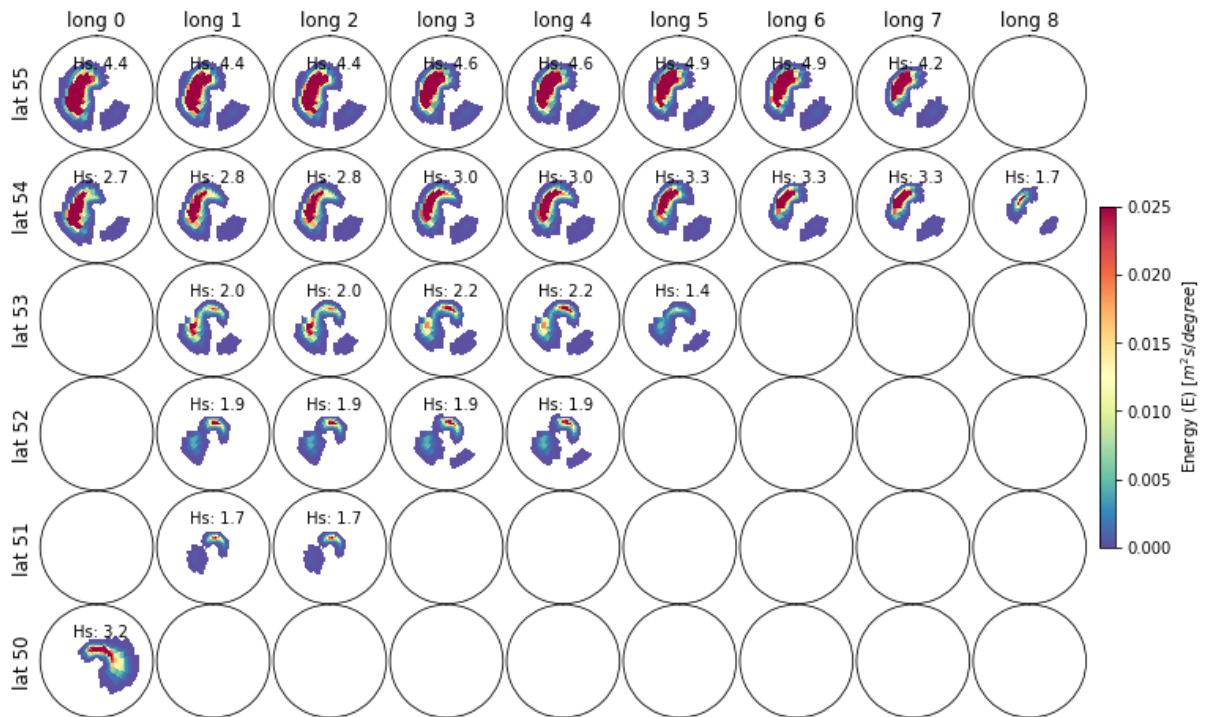
Figure 141: The representative spectrums of Sea State 65 at their offshore locations
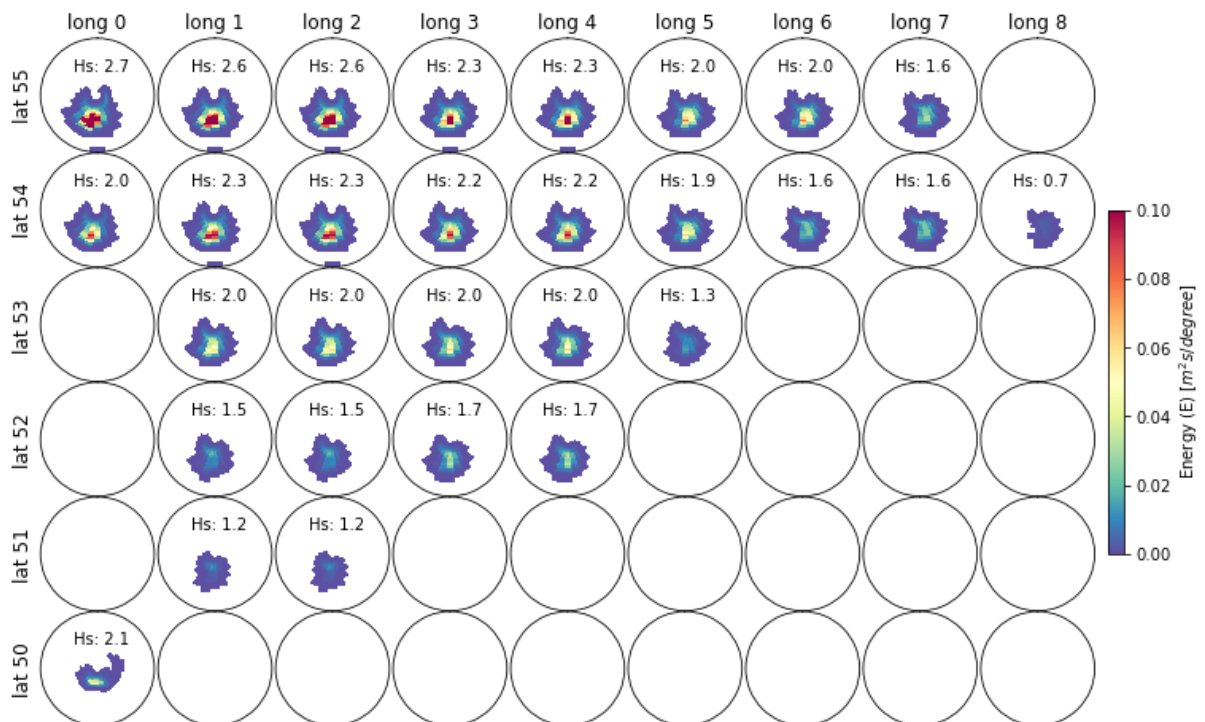
Figure 142: The representative spectrums of Sea State 121 at their offshore locations
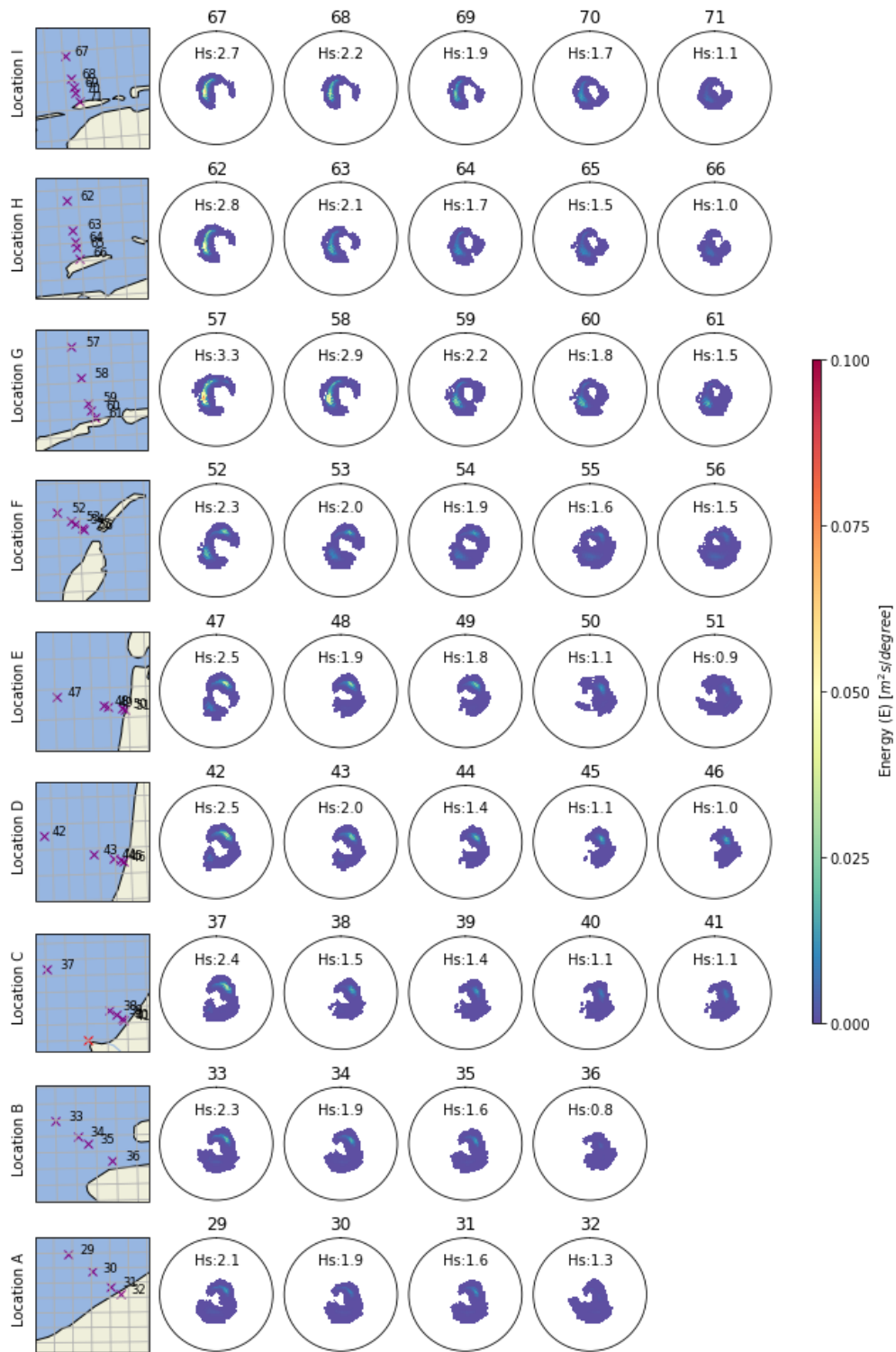
Figure 143: The representative spectrums of Sea State 65 at their nearshore locations
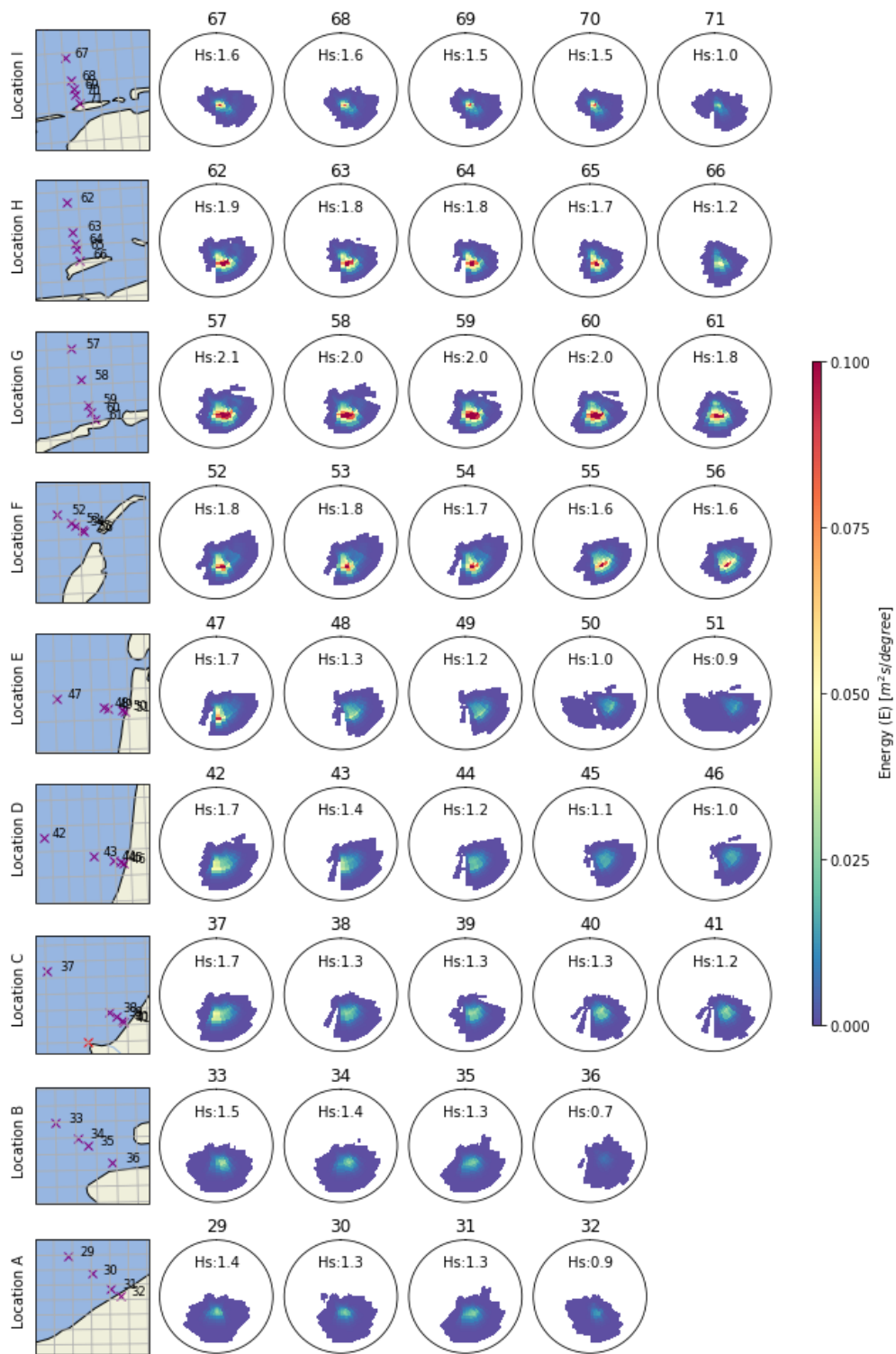
Figure 144: The representative spectrums of Sea State 121 at their nearshore locations

Appendix VI: Clusters for MDA 2000

This appendix shows the representative wave spectrums at location 42 for each cluster, which are based on the clustering operation where 2000 points are used in the formation of the groups. These 2000 points are determined with Maximum Dissimilarity Analysis and called MDA 2000. The spectrums at all the locations of a cluster form a sea state. Two exemplary sea states are depicted in appendix V.
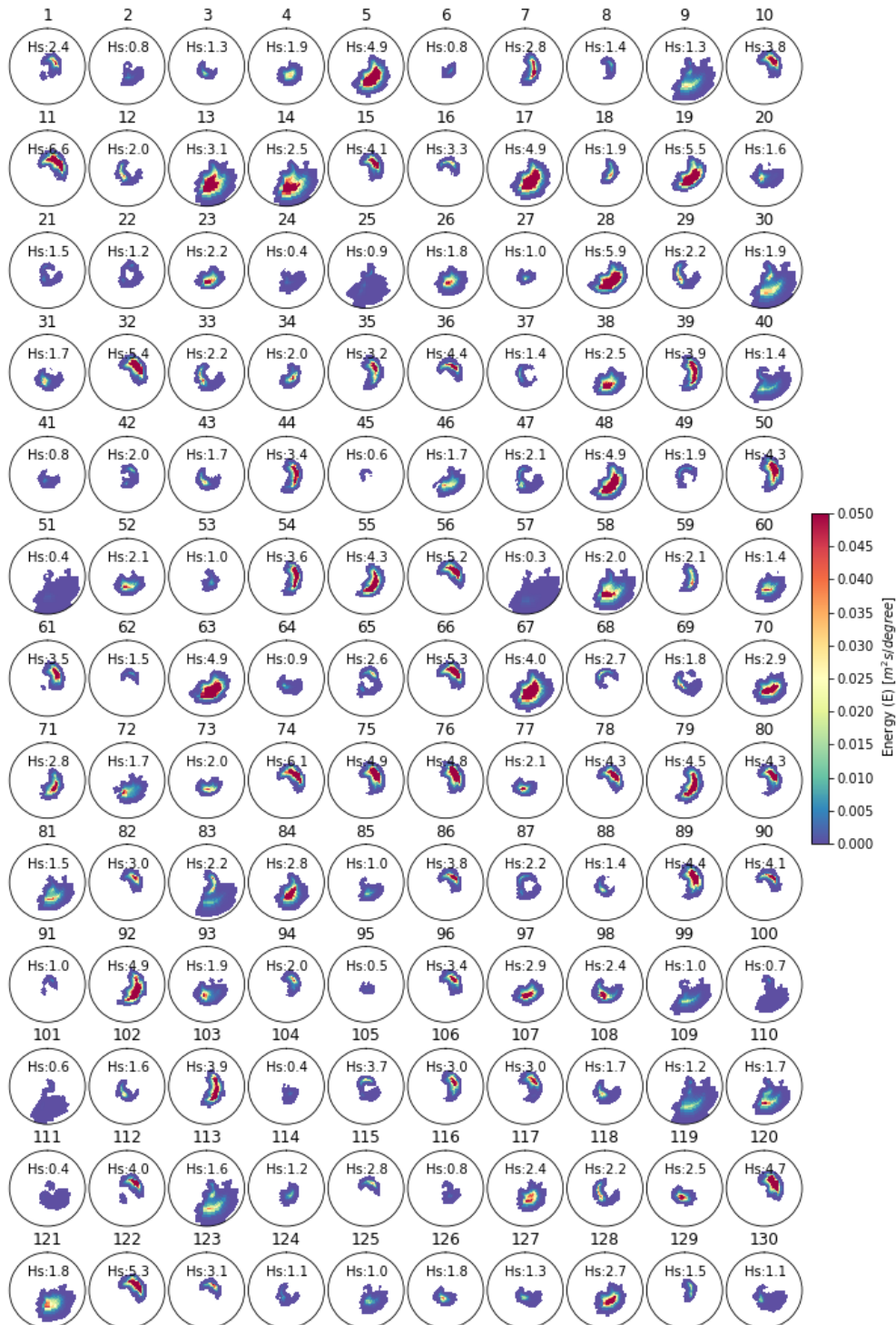
Figure 145: The representative wave spectrum at location 42 for all the Sea States that are based on the subset of 2000 points formed by Maximum Dissimilarity Analysis, called MDA 2000.

Appendix VII: Probability wave family in Wave Cluster

This appendix shows the probability for each wave cluster that waves are propagating within the boundaries of each family. High probabilities indicate that waves are propagating in that specific direction when a Sea State occurs. Following, crossing, and opposing waves can be recognized by these probabilities, as explained in chapter 5.5.3.
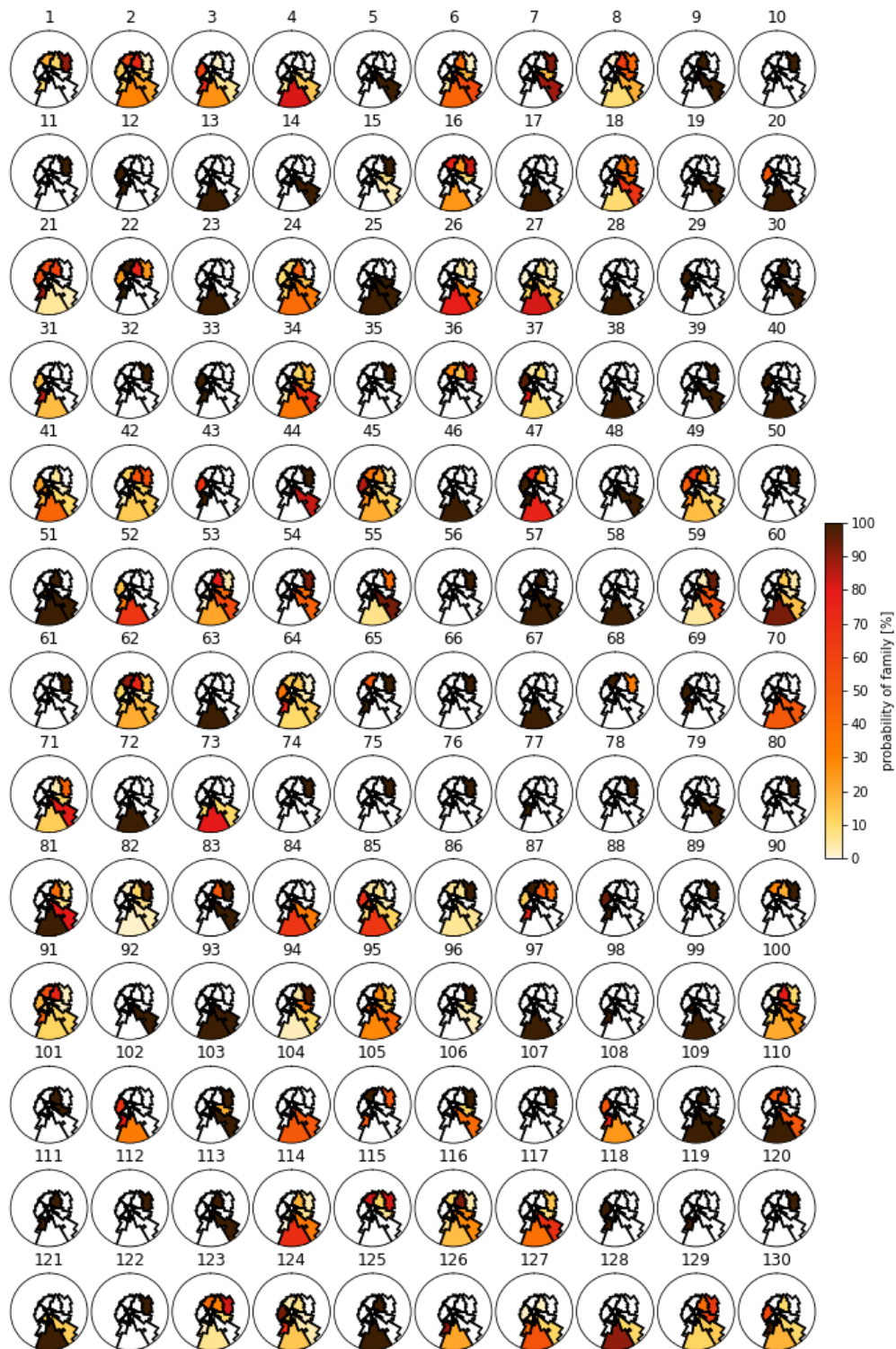
Figure 146: Probability that a wave family has energy for each Sea State, depicted in appendix VI

Appendix VII: 25 and 81 Weather Types (WT)

This appendix shows the weather types (WT) that are made by following Camus et al. (2014a). The study compared the results and implementation of 25 and 81 weather types, from which the sea level pressure is shown below. White indicates the global average sea level pressure of 1013 millibars. Red indicates a high-pressure system, with sea level pressures above the global average sea level pressure. Blue indicates a low-pressure system, where the sea level pressure is below the global average.
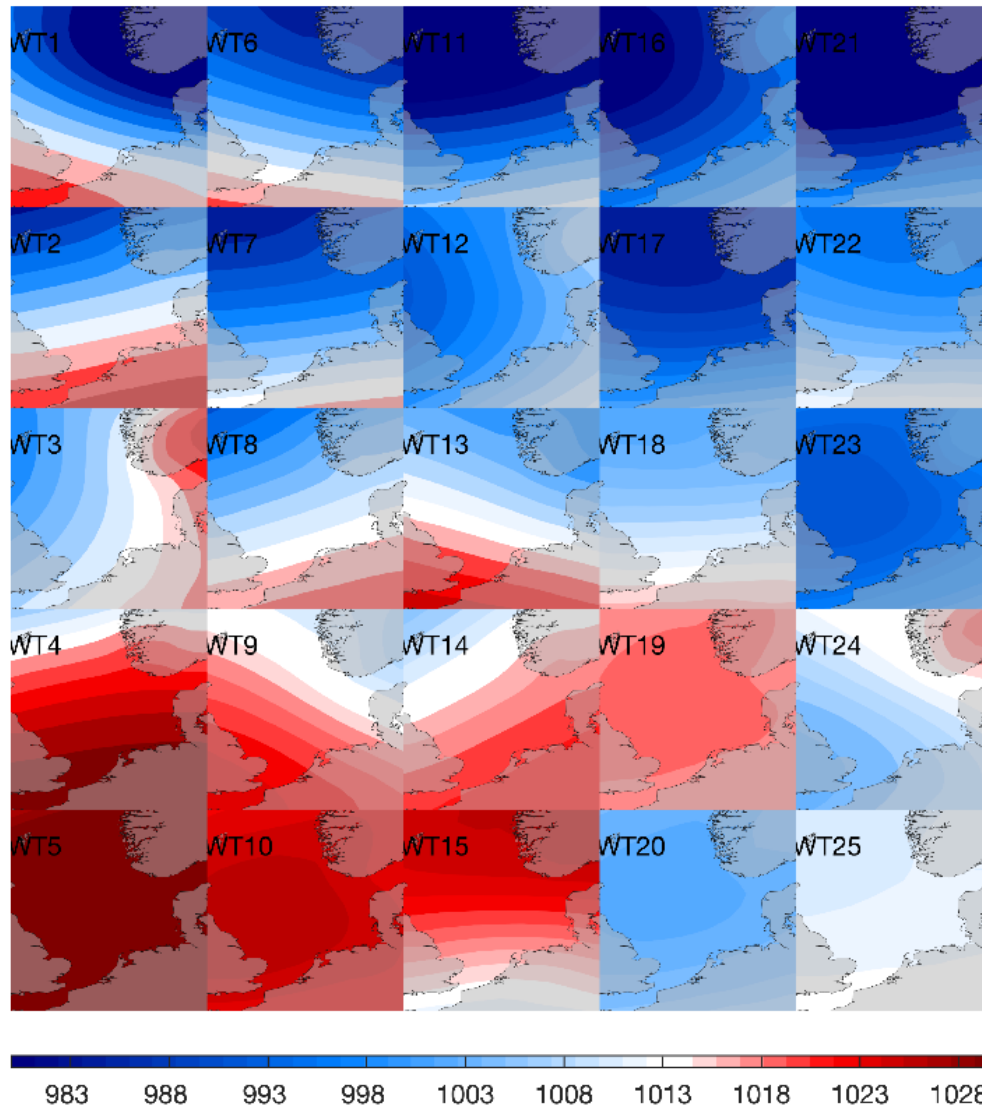
Figure 147: The outcome of clustering of sea level pressure and its gradients to 25 Weather Types (WT).
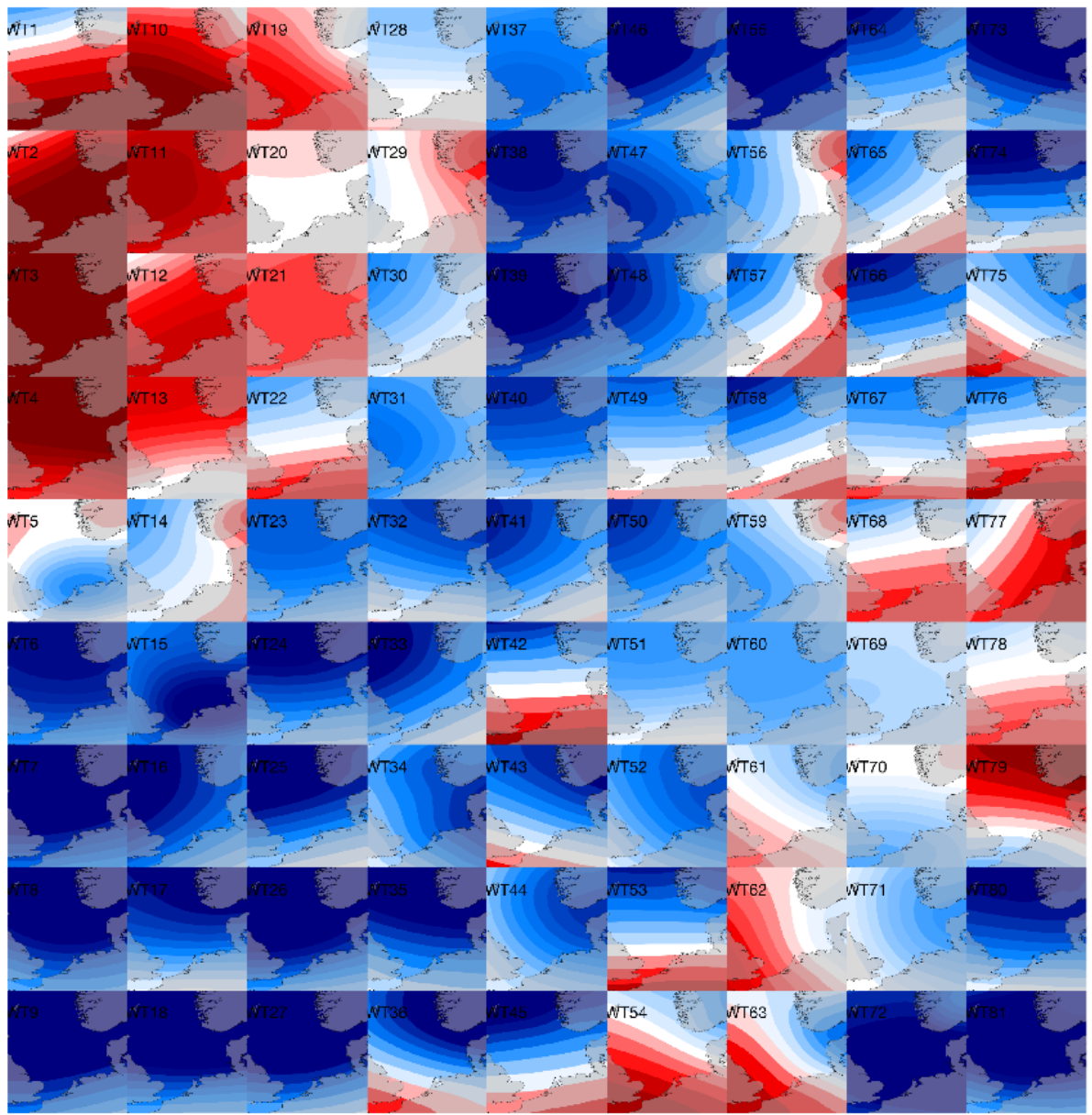
Figure 148: The outcome of clustering of sea level pressure and its gradients to 81 Weather Types (WT).

.

Appendix VIII: Correlation between 130 sea states and 81 weather types

This appendix shows the relation between Sea States and Weather Types by the probabilities that Weather Types are occurring when Sea States occur and vice versa. The interest lies mainly in the number of large probabilities and not on the specific probabilistic values.
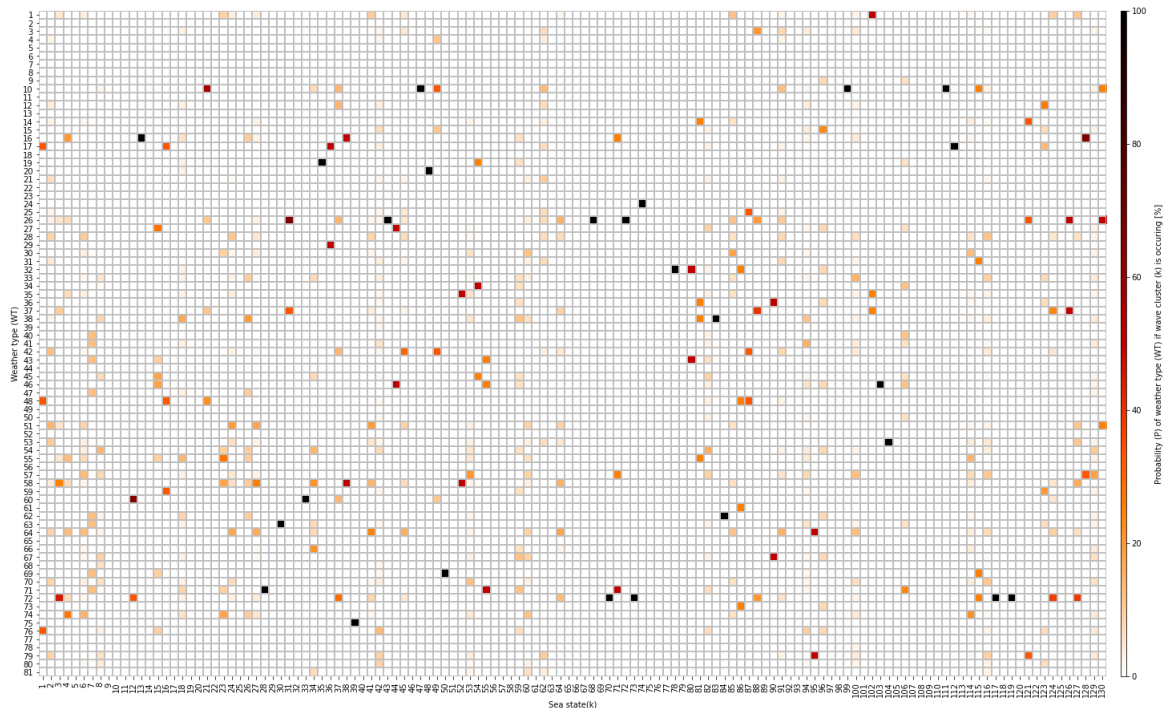

Figure 149: Probability that a specific Weather Type occurs when one of the Sea States is occurring.
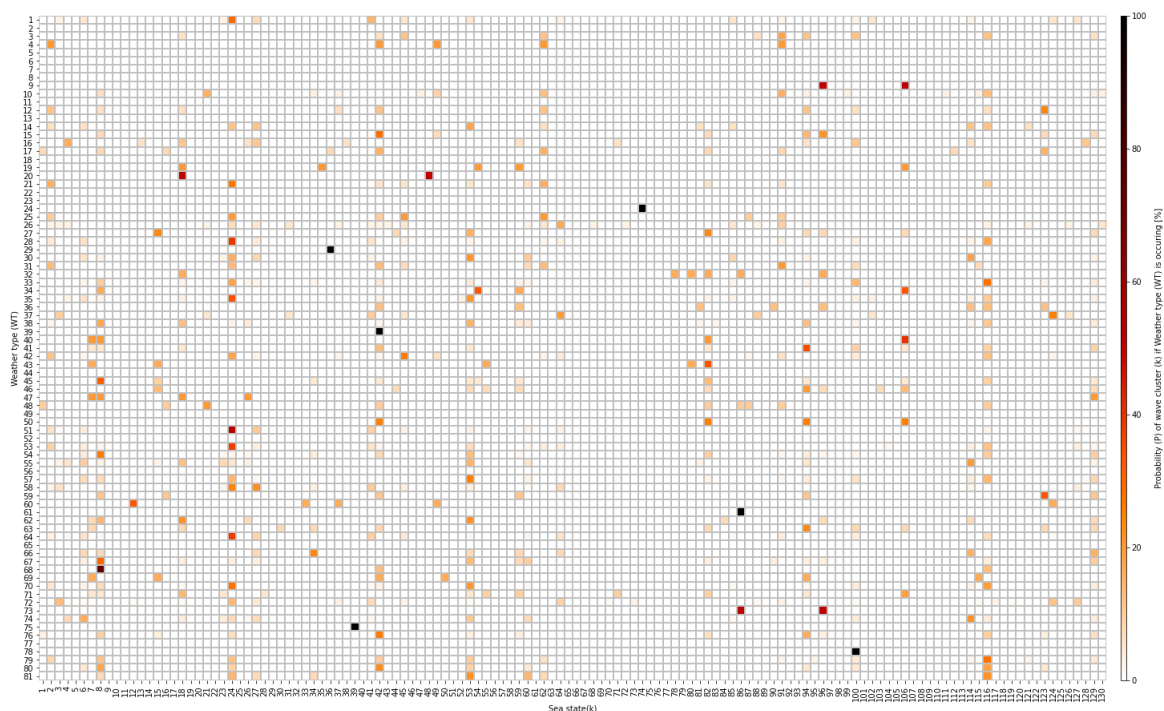
Figure 150: Probability that a specific Sea State occurs when one of the Weather Types is occurring.

Appendix IX: Energy in Wave family for 81 Weather Types at location 42.

This appendix shows the probability for each wave cluster that waves are propagating within the boundaries of each family. The wave families give insight into the wave propagation directions and the occurrence of following, crossing, and opposing waves, as explained in chapter 5.5.3.
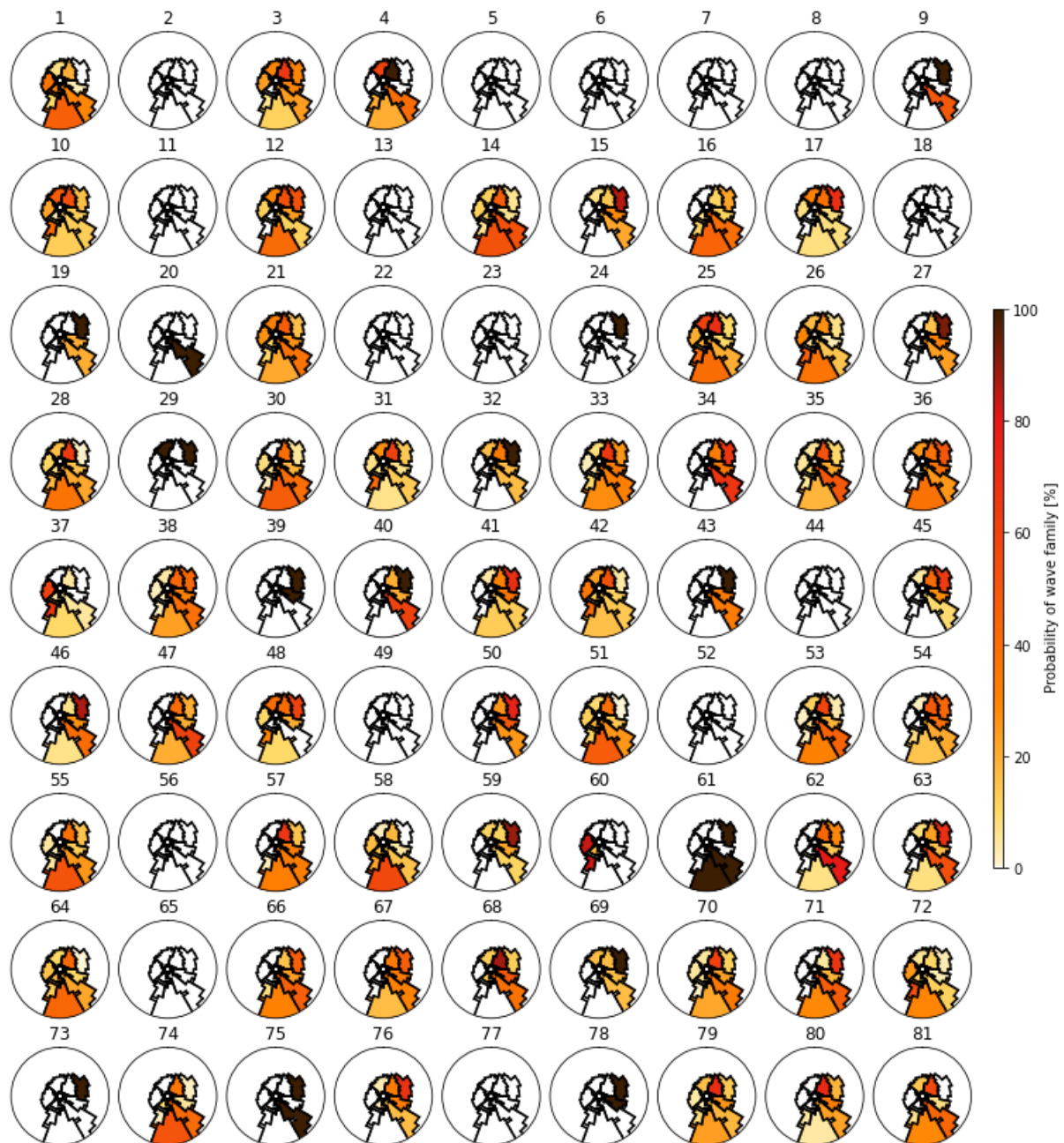

Figure 151: Probability that wave families have energy when a certain weather type occurs.

Appendix X: Wave induced bedload and suspended sediment transport

The bedload, suspended sediment, and combined sediment transport flux for various wave heights and periods is depicted in this appendix. The sediment transport formulation TRANSPOR2004 of van Rijn, with 20 vertical grid points, is used for the calculation. The following parameterization is applied: a flat bottom, a median grain size (D_{50}) of 0.25 mm, a 90% cumulative mass passing diameter (D_{90}) of 0.3 mm, a suspended sediment grain size (d_s) of 0.2 mm, and a roughness height of 5 cm related to the current (R_C) and wave (R_W).
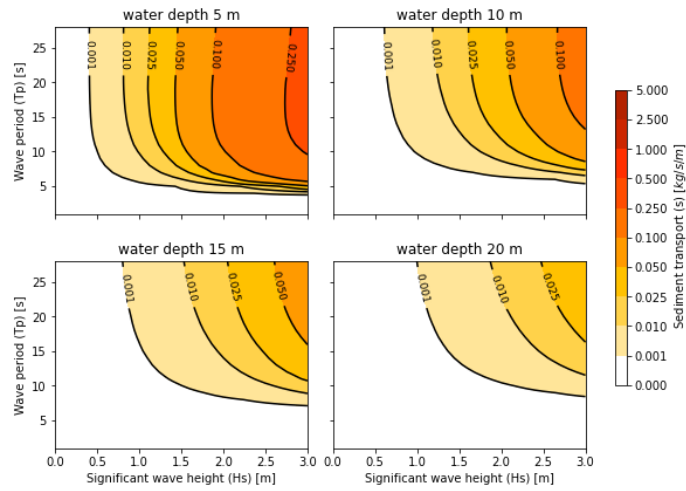

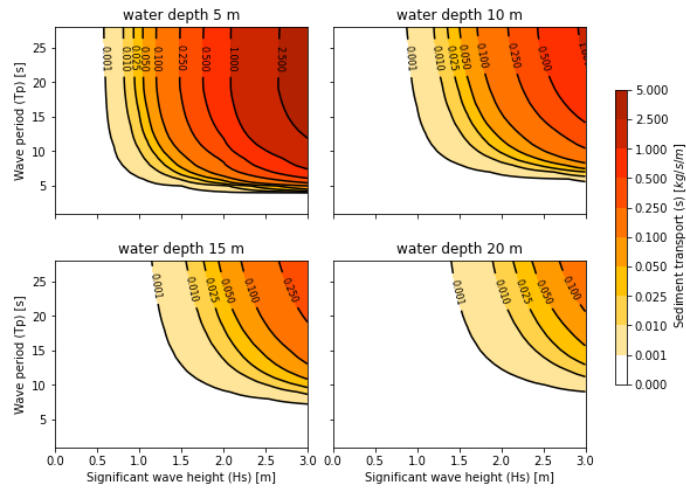*Figure 152: Bedload for various wave heights, periods, and water depths.:*

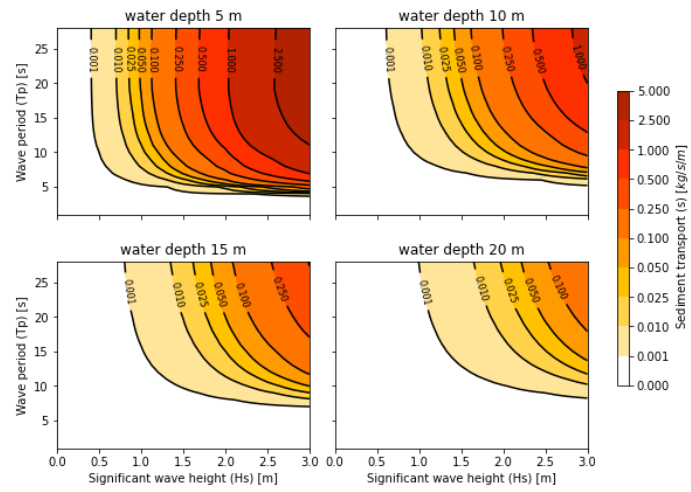*Figure 153: Suspended sediment for various wave heights, periods, and water depths.*

Figure 154: Sediment transport for various wave heights, periods, and water depths, both bedload and suspended.